MAREES TERRESTRES

BULLETIN D'INFORMATIONS

1 2 7

15 MAI 1997

Association Internationale de Géodésie

Commission des Marées Terrestres

Editeur Dr. Olivier FRANCIS
Observatoire Royal de Belgique
Avenue Circulaire 3
1180 Bruxelles

BIM 127

15 mai 1997

Preface

During the XXI General Assembly International Union of Geodesy and Geophysics (IUGG), Boulder, Col., a session on Earth Tides was held and reports about the achievements of the working groups on **'Theoretical Tidal Model'**, **'Calibration'**, and **'High Precision Tidal Data Processing'** were presented. It was decided that all the working groups should be reorganized during the Earth Tide Symposium in Brussels; thus, we were asked to organize a last working group workshop and to prepare a final report.

In the following, the reports are presented as well as (most) of the papers presented during our last meeting held in Bonn, September 16 - 19, 1996. Again, we met at the Institut für Theoretische Geodäsie, and Prof. M. Bonatz was our host.

Since there was no chairperson for the WG 'Calibration' we included a session on this topic. Our main task was to discuss our achievements within the WG's 'Theoretical Tidal Model' and 'High Precision Tidal Data Processing' and to prepare the final report including all the conclusions which were still valid, and which we want to submit to the next Earthtide symposium in Brussels.

The WG 'Theoretical Tidal Model' had to work for three tasks: First, the *definitions of the tidal parameters* were reviewed, and we agreed upon *definitions* that one should propose for a recommendation. The second task was to agree upon the *tidal model* which accounts for as many physical phenomena as possible at a precision level in agreement with the advance of the technology used for the observations. Many new computations were proposed. They incorporate Earth normal mode resonance effects, mantle inelasticity, lateral heterogeneities in the mantle and violation of hydrostatic equilibrium at the Earth's initial state. They are close to reallity because they give the right FCN resonance. Concerning the third task, we agreed upon *tidal potential developments* to be considered for precise tidal analysis.

Of course, we could not complete all the work we intended to carry through in all working groups. The reasons are mainly that new topics arose and current problems became either more clear or more complicated during the last two years. Regarding the data processing the first holds true for the topics *'Superconducting gravimeter, data format and exchange, esp. in cooperation with GGP'* and, with some reservations, for *'cooperation in the processing of tidal signals observed using space techniques'*. The last topic also contains the ocean tidal and atmospheric loading: Many new ocean tidal models need to be tested especially in remote areas in the north and the south (Arctic and Antarctic areas) as well as in mid-continental stations. Here we also have an increasing need for high precision tidal corrections for VLBI and GPS reference points, especially along the coasts of the Arctic and Antarctic oceans.

On the basis of the current research in the *'study of air pressure and hydrological effects related to tides'* as well as the *'identification and treatment of special problems of tidal recording in remote areas'* it became obvious that no simple solutions were possible. In contrary, more and extended research work is necessary. If we want to provide station corrections for air pressure explaining more than 80 % of the effects then the now available tools are not sufficient.

The tidal recording in remote areas also comprises problems which are quite unscientific, but which are cruxial if good data is needed.

In the following the final reports with the conclusions as well as the contributions to the topics of the meetings are presented.

I wish to thank M. Bonatz for his hospitality and help: Again he provided good conditions for the meetings of the members of the groups and other interested scientists. This time, in all 32 scientists from 13 countries were present. Since the working groups will be reorganized the mandate of the present WG's has ended. Therefore, also on behalf of V. Dehant I wish to thank all participants for their contributions and for their support of the successful work of these working groups. We all acknowledge the financial support from the 'Deutsche Forschungsgemeinschaft'. I thank the International Center and esp. O. Francis for publishing all the material in the Bulletin of the International Center of Earth Tides.

Gerhard Jentzsch

High Precision Tidal Data Processing - final report of the working group

by

Gerhard Jentzsch*)

1. The development of the working group

There were previous working groups which already covered parts of the topics now under consideration. The results obtained were the basis for the mandate of the running group as well as for the additional working groups on **'Theoretical Tidal Model'** and **'Calibration'**.

During the 8th International Symposium on Earth Tides in Bonn, 1977, the necessity of a working group on *'Data Analysis in Tidal Research'* was acknowledged. This group was formed under the resolution no. IV, and the first two meetings were held in Bonn in 1978 and 1979 at the Institute for Theoretical Geodesy of the University, organized by Prof. M. Bonatz. According to the task of the working group we compared up-to-date analysis methods, and we developed the first standards for the performance of tidal analyses and the output of the results (BIM, vol. 78 & 81). This, off course, had consequenses for the performance of the recording as well as for the calibration. On the other hand, the increasing resolution and stability of tidal records suggested the development of new tidal potentials as well as a tidal reference model. Therefore, this working group extended ist scope quite early to cover also the experiment and the interpretation in addition to the tidal analysis.

The third meeting was held in Warsaw, 1980, at the Polish Academy of Sciences, organized by Prof. T. Chojnicki. There, after the definition of the state of the art carried out during the first two meetings first steps towards future developments like digital recording, as well as preprocessing and automatic treatment of digital data were tried. The papers are contained in BIM, vol. 85.

Accordingly, after reporting to the 9th International Symposium on Earth Tides, New York, 1981 (Report, 1983), and the IUGG General Assembly in Hamburg, 1983, the mandate of the group was extended under the new name: *'Acquisition, Preprocessing and Analysis of Earth Tidal Data'*. The task of the group was to consider

- instrumentation and data acquisition
- preprocessing and analysis
- superconducting gravimeter
- tidal loading computation
- data bank

The next meeting was held again in Bonn, 1984. This meeting was organized by the present chairman with the help of Prof. M. Bonatz. The papers presented were published in BIM, vol. 94.

The report (Jentzsch, 1986) and the discussions at the 10th International Symposium on Earth Tides, Madrid, 1985, resulted in a new working group with the present name *'High Precision Tidal Data Processing'* (resolution no. 8). The task mentioned was to examine the consequences for tidal data processing and analysis techniques caused by the fast development of computing technology and instrumentation.

Parts of the tasks (tidal potentials) were transferred to the new working group on *'Theoretical Tidal Model'* headed by Dr. Veronique Dehant. For both groups two combined meetings were organized in Bonn in 1986 and 1988, and the results were published in BIM, vol. 99, and 104 & 105, respectively. In between, a report was prepared for the IUGG General Assembly in Vancouver, 1987 (Jentzsch, 1989).

---

*) Institut für Geowissenschaften, Friedrich-Schiller-Universität Jena, Burgweg 11, D-07749 Jena

In Helsinki, at the 11th symposium, 1989, the mandate of the group was prolonged (resolution no. 4; report: Jentzsch, 1991). The new tasks were to examine further

- time variations in tidal parameters
- meteorological and geophysical influences (environmental factors) on tidal registration, with particular emphasis on local perturbations
- superconducting gravimeter
- tidal loading computation
- data bank

The discussions concentrated now on the application of the Superconducting Gravimeter as well as on the development of standards for the acquisition and analysis of this high resolution data. Another common meeting was organized in Bonn in 1990 (published in BIM, vol. 110 & 111). During the meeting of the Permanent Commission on Earth Tides at the IUGG General Assembly in Vienna, 1991, it was decided to have a seperate working group on *'Calibration'*, headed by Dr. Bernd Richter, thus reducing the tasks of the present group. In 1992 all three working groups met again in Bonn, and the results were published in BIM, vol. 115 & 116.

At the 12th symposium in Beijing, August 1993, this working group was prolonged until the next meeting of the Permanent Commission on Earth Tides (PCET) in Boulder, 1995. On the basis of the report (Jentzsch, 1995a) with resolution no. 7 the mandate was changed now to concentrate on

- data format and exchange of SG data
- air pressure and hydrological effects related to tides,

and to identify and treat special problems of tidal recording in remote areas, and to cooperate in the processing of tidal signals observed using space techniques.

Therefore, another common meeting of the working groups took place in August/ September 1994 at the Institute for Theoretic Geodesy, University of Bonn, and again Prof. M. Bonatz was our host. The results of this meeting were published in volumes 121 & 122 of the Bulletin d'Information Mareés Terrestres.

During the meeting of the (now called) Earth Tide Commission at the IUGG General Assembly in Boulder, 1995, on the basis of the reports (e.g. Jentzsch, 1995b) it was decided that all working groups should be reorganized at the next Earth Tide Symposium in Brussels, 1997. Therefore, a final report should be prepared, and the working group had its last meeting in September 1996 again in Bonn (together with *'Theoretical Tidal Model'* and including a session on *'Calibration'*.

In the following, some of the topics discussed during our meetings are reviewed; for more details the respective papers published in BIM are the reference.

2. Achievements during the last four years

Regarding the development of the tasks of the successive working groups I refer to the respective resolutions mentioned above. Here, I only discuss the last mandate.

Following the resolution no. 7, Beijing, August 1993, the working group should continue under a changed mandate and discuss the topics

(1) data format and exchange, esp. in cooperation with GGP;
(2) study of air pressure and hydrological effects related to tides;
(3) identification and treatment of special problems of tidal recording in remote areas;
(4) cooperation in the processing of tidal signals observed using space techniques.

Within this frame some *achievements using superconducting gravimeters* and the need for a *comparison of current tidal analysis packages* were discussed as well as the *status of the data bank of the International Center for Earth Tides*.

In addition to the scientific goals of *tidal measurements in remote areas* the working group also discussed logistic and instrumental problems to name requirements for a reliable recording equipment and to ensure the stability of the calibration esp. after hard transports. These ideas have to be further developed.

The conclusions are reviewed briefly in the following:

Topic 1 was related to data recording and exchange. Here, the handling of SG data within GGP led to the recommendation to store and to exchange high rate data at intervals of e.g. 1 min, and to use the so-called PRETERNA format (Wenzel, 1994) for storage and exchange of high precision tidal data.

With regard to the establishment of the 'Global Geodynamics Project' (GGP) we strongly encouraged operators of new and existing SG stations to consider the advantages of (a) an excellent site, located away from cultural, geological and electrical noise, (b) a high-rate, precise data recording system with samples every 10 s or less at a precision of 7.5 digits for the gravity signal and 5.5 digits for the pressure, and (c) a timing accuracy of at least 10 msec, to realize the benefits of new methods of data processing and interpretation.

We intended to perform a comparison of all tidal analysis packages currently in use. Unfortunately, due to the move of the responsible person (Prof. David Crossley) this task had to be postponed. Nevertheless, we acknowledge the efforts to improve existing methods (Venedikov et al., 1995; Arnoso et al., 1997, this issue) and Wenzel (1996) to provide a realistic 'nanogal - software' for tidal data processing and analysis.

Within topic 2 the group discussed the increasing resolution and stability of tidal records with regard to the still existing problem of modelling small scale and short period air pressure effects in gravity. This resulted into the recommendation that effects of short period local air pressure variations should be studied applying a regional network of air pressure stations in addition to the local air pressure record.

Topic 3 on tidal recording in remote areas touched the problem that most ocean tidal charts due to modelling problems in Arctic areas are only valid up to 65° or 70° N and that therefore tidal gravity measurements are necessary to provide boundary conditions for the evaluation of ocean tidal models by ocean tidal loading computations. This means that tidal gravity stations close or beyond the latitude of 65° N should be established. On the other hand, on-going measurements on Greenland and in Norway show, that the problems due to the logistics as well as due to specific local conditions (e.g. power supply, disturbances caused by RADAR signals, etc.) provide boundary conditions that require specific recording equipment for this application. Dittfeld et al. (1997, this issue) discuss some of their experiences with regard to this problem.

On the other hand, in the centers of the continents still wide areas exist lacking reliable tidal information. Since tidal parameters in those areas are needed for the improvement of tidal earth models because the effect of ocean tidal loading is small, the establishment of tidal gravity stations in central Asia was recommended to achieve state of the art tidal parameters.

The last topic 4 dealt with the International Center of Earth Tides (ICET). The group recognised the fruitful and encouraging work of the International Center for the collection and exchange of tidal data and for the documentation of the development of tidal research. This work should be extended to collect all available historic earth tide data, too. Further, realizing the increasing availability of high precision and high rate data the working group recommends that the Center should develop conditions under which such high rate data can be stored and made available using modern computer networks.

Finally it was agreed that in accordance to the conclusion of the 1992 meeting of the working group the term 'quality factor' has definitely to be cancelled and replaced by the term 'internal consistency factor'.

3. Proposals to be submitted to the 13th International Symposium on Earth Tides in Brussels, July 1997

3.1 Resolutions

These resolutions are given in the appendix; below they are briefly summarized:

(1) Instrumentation

- The importance of tilt measurements for studies of local geophysical signals (especially non-tidal) is pointed out, especially in deep boreholes (< 1000 m).

- Excellent site conditions for new and existing stations with superconducting gravimeters regarding the establishment of the 'Global Geodynamics Project' are recommended.

(2) Calibration

- For *gravimeters* absolute calibration methods should be applied, e.g. inertial platforms, moving masses, state of the art absolute gravimeters.

- For *tilt and strainmeters* absolute calibration methods should be developed which are directly related to SI-units.

- Independent calibration methods should be compared to take care of systematc effects, and step response methods should be used for determining transferfunctions for amplitude and phase.

- Regarding the calibration of superconducting gravimeters the present development of an inertial gravimeter calibration system should also include a high precision portable gravimeter to facilitate in-situ calibration of SG and absolute gravimeters.

(3) Data format and analysis

- The so-called PRETERNA format (Wenzel 1994) shall be used for storage and exchange of high precision tidal data.

- For high-rate data the development of automatic processing programs for handling these data should be continued.

(4) Air pressure and hydrological effects related to tides

- The effects of short period local air pressure variations should be studied applying a regional network of air pressure stations in addition to the local air pressure record.

(5) Special problems of tidal recording in remote areas

- The establishment of gravity tidal stations close or beyond the latitude of 65° N and on the Antarctic continent is recommended.

- The establishment of tidal gravity stations in not well developed areas like central Asia is necessary to achieve state of the art tidal parameters.

(6) Cooperation in the processing of tidal signals observed using space techniques.

- VLBI and tidal gravity should cooperate regarding the determination of the FCN period and its Q - factor as well as the complex Love and Shida numbers *h* and *l* at all tidal frequencies.

- SLR and tidal gravity should cooperate regarding the validation of the mantle inelasticity effects in the tidal models which is mostly affecting the long period tides.

- Ocean tidal and atmospheric loading models should be validated by both VLBI as well as by surface gravity recordings.

- The sties of the relations of VLBI and earth tides should be extended to other space techniques e.g. GPS, SLR / LLR, too.

(7) International Center for Earth Tides

- Especially gravity tidal data (including the necessary informations, e.g. air pressure) should be sent to ICET for storage in the data bank.

- ICET should provide help for the modernization of old spring gravimeters still in use.

- We all acknowledge the successful work of

Prof. Paul Melchior

who, as a pioneer in earth tides research was a motor in the development of our field. We have deep respect for his achievements for tides in special and geosciences in general.

3.2 Future activities

All participants agreee that the system of having working group meetings inbetween the Earth Tide Symposia and the IUGG General Assemblies was very successful for the develpment of the cooperation between the different groups and, thus, successful for the progress in our scientific field. Therefore we recommend to continue this system, but to reorganize the topics in accordance with the newest developments. Topics for working groups could be

- *Ocean tidal and atmospheric loading*
- *Tidal corrections in space techniques*
- *Calibration*

These working groups should be small to be effective. We should discuss the proposal to have separate meetings of these groups and a common workshop every two years.

4. Acknowledgements

The working group on 'Data Processing in Tidal Research' was launched in 1977. Thus, my cooperation in this field covers 20 years, and I acted as a chairman over the period of the last 17 years. During this time it was possible to invite and to assemble in all more than 50 scientists from over 15 different countries in Bonn, every two years. In all, it was a time consuming but encouraging and - sometimes - also exiting job to organize these meetings and to collect the scientific outcome. At the end of this period I wish to thank all participants for their cooperation, their contributions and their patience.

Prof. Manfred Bonatz, who organized the first two meetings himself in Bonn, was always a very friendly and helpful host when we met in the Institute for Theoretical Geodesy of the University of Bonn. Prof. Tadeusz Chojnicki organized the third meeting in Warsaw in 1980. Thanks to a 'careless' organization, during this meeting the first time colleagues from both German states, from West and East Germany, could attend; because of the prolitical obstacles on such a workshop - level this was generally impossible during those days.

We all acknowledge the support of the meeting by the 'Deutsche Forschungsgemeinschaft'. The available funds enabled us to organize joint meetings of more or less all groups active in this field, and, especially, to involve colleagues from Easteuropean countries and from China.

5. References

Arnoso, J., C. de Toro, A.P. Venedikov, and R. Vieira, 1997. On the estimation of the precision of the tidal data. Bull. d'Inf. Marees Terr., this issue.

Dittfeld, H.-J., B. Engen, G. Jentzsch, P. Knudsen, F. Madsen, M. Ramatschi, K. Røthing, and P. Schwintzer, 1997. Tidal gravity measurements within the MOTIVE project. Bull. d'Inf. Marees Terr., this issue.

Jentzsch, G., 1986. Working Group on 'Acquisition, Preprocessing and Analysis of Earth Tidal Data' - report. Proc. 10th Int. Symp. Earth Tides, Madrid, 1985, Consejo Sup. de Invest. Cientificas, LI - LIV.

Jentzsch, G., 1989. Working Group on 'High Precision Tidal Data Processing' - Report. XIX General Ass. of the IUGG, Sec. GS. V, Vancouver, August 1987; IUGG Chronicle, 198, 401 - 402.

Jentzsch, G., 1991. The working group on "High Precision Tidal Data Processing" - Report. Proc. 11th Int. Symp. Earth Tides, Helsinki, 1989, Schweitzerbart, Stuttgart, 261 - 264.

Jentzsch, G., 1995a. Report of the Working Group on 'High Precision Tidal Data Processing'. Proc. 12th Int. Symp. Earth Tides, Beijing, August 1993, Science Press, Beijing, 19-24.

Jentzsch, G., 1995b. Working group on 'High Precision Tidal Data Processing' - report (abstract). XXI General Assembly Intern. Union of Geodesy and Geophysics (IUGG), Boulder, Col., p. B50.

Report, 1983. Summary of the Working Group on Data Processing in Tidal Research, Permanent Commission on Earth Tides (summerized by J.T. Kuo and prepared by G. Jentzsch). Proc. 9th Int. Symp. Earth Tides, New York, 1981,731 - 741.

Venedikov, A.P.., R. Vieira, and C. de Toro, 1995. The computer program NSV used in Madrid for tidal data processing. Bull. d'Inf. Marees Terr., 121, 9108 - 9126.

Wenzel, H.-G., 1994. PRETERNA - a preprocessor for digitally recorded tidal data. Bull. d'Inf. Marees Terr., 118, 8724 - 8734.

Wenzel, H.G., 1996. The nanogal software: Earthtide data processing package ETERNA 3.3. Bull. d'Inf. Marees Terr., 124, 9425 - 9439.

Further, I refer to the papers presented by the participants at the working group meetings, printed by the International Center, Bulletin d'Information Mareés Terrestres, volumes 78, 81, 85, 94, 99, 104 & 105, 115 & 116, 121 & 122.

6. Appendix: Proposals for resolutions to be submitted to the 13th International Symposium on Earth Tides in Brussels, July 1997

(1) Instrumentation

Recognising the importance of tilt measurements for local geophysical signals (especially non-tidal) we

encorage the further development of measuring devices for deep boreholes (< 1000 meters) to use the advantages of the high resolution tilt sensors.

Regarding the progress of the establishment of the 'Global Geodynamics Project' (GGP) this Working Group refers to earlier conclusions and strongly

recommends that operators of new and existing stations with superconducting gravimeters (SG) be encouraged to consider the advantages of

(a) an excellent site, located away from cultural, geological and electrical noise, and

(b) a high-rate, precise data recording system with samples every 10 s or less at a precision of 7.5 digits for the gravity signal and 5.5 digits for the pressure,

(c) a timing accuracy of at least 10 msec,

to realize the benefits of new methods of data processing and interpretation.

(2) Calibration

Recognising that the testing of body tide and ocean loading models requires accuracies of at least 0.2 % in amplitude and at least 0.1° in phase the *working group of Calibration*

recommends that for *gravimeters*

this should be realized applying absolute calibration methods, e.g. inertial platforms, moving masses, state of the art absolute gravimeters;

that for *tilt and strainmeters*

absolute calibration methods should be developed which are directly related to SI-units.

Furtheron, independent calibration methods should be compared to take care of systematc effects, and step response methods should be used for determining phase- and transferfunctions.

Recognising the need to calibrate superconducting gravimeters, we

recommend that the present development of an inertial gravimeter calibration system be encouraged to include a high precision portable gravimeter to facilitate on-situ calibration of SG and absolute gravimeters.

(3) Data format and analysis

Recognising the increase of the precision of recording gravimeters, the need to store and to exchange high rate data at intervals of e.g. 1 min, and that the so-called International Format for exchange of hourly tidal data cannot fulfill this need, the Working Group of High Precision Tidal Data Processing

recommends that the so-called PRETERNA format (Wenzel 1994) shall be used for storage and exchange of high precision tidal data.

Recognising the neccessity of recording high-rate data in order to extend the spectrum to higher frequencies and to improve the signal-to-noise ratio in the tidal bands we
recommend to continue the development of automatic processing programs for handling these data.

(4) Air pressure and hydrological effects related to tides

Referring to the increasing resolution and stability of tidal records and the still existing problem of modelling small scale and short period air pressure effects in gravity we
recommend that effects of short period local air pressure variations should be studied applying a regional network of air pressure stations in addition to the local air pressure record.

(5) Special problems of tidal recording in remote areas

Realizing that most ocean tidal charts due to modelling problems in Arctic areas are only valid up to 65° to 70° North and that in Antarctic areas large ice shelfs cause similar problems, and
recognizing that tidal gravity measurements provide boundary conditions for the evaluation of ocean tidal models by ocean tidal loading computations we
recommend the establishment of gravity tidal stations close or beyond the latitude of 65° N and on the Antarctic continent.

Recognizing that in the centers of the continents still wide areas exist lacking reliable tidal information and
regarding that tidal parameters in those areas are needed for the improvement of tidal earth models because the effect of ocean tidal loading is small we
encourage the establishment of tidal gravity stations in not well developed areas like central Asia to achieve state of the art tidal parameters.

(6) Cooperation in the processing of tidal signals observed using space techniques.

Realizing the progress achieved in the determination of tidal parameters from space geodetic techniques such as VLBI, SLR, GPS, and
recognizing the complementary character of the information derived from space geodetic techniques with respect to gravity recordings, we
encourage a close cooperation of groups involved in space geodesy and tidal gravity studies regarding the determination of tidal deformation parameters, e.g. the FCN period and its Q - factor as well as the complex Love and Shida numbers h and l at all tidal frequencies.

Recognizing the influences of Earth tidal deformation on the Earth rotation parameters determined by VLBI, and
realizing the effects of ocean and atmospheric loading on both types of measurements we
recommend that ocean tidal and atmospheric loading models should be validated by VLBI as well as by surface gravity recordings.

Realizing the potential of modern space techniques other than VLBI (e.g. GPS, SLR / LLR, ...) we
encourage to include these methods into the investigations of tidal signals.

(7) International Center for Earth Tides

Recognising that still many groups do not make there data available to the ICET data bank, and **realising** that already some records were lost without a copy at the Center we
recommend that esp. gravity tidal data (including the necessary informations, e.g. air pressure) should be sent to ICET for storage in the data bank.

Recognising the existens of many old spring gravimeters esp. in East-Europe and the possibility of their use by recording in these countries we
ask the ICET to provide help for the modernization of these gravimeters.

Finally, all the participants of the Working Group meetings greatly acknowledge the successful work of

Prof. Paul Melchior

who, as a pioneer in earth tides research was a motor in the development of our field. We have deep respect for his achievements for tides in special and geosciences in general.

REPORT OF THE WG ON THEORETICAL TIDAL MODEL

V. Dehant
Royal observatory of Belgium

Preface:

This report is a draft-report of what will be sent to the President of the Earth Tide Commission, Prof. H-G. Wenzel, and what will be presented at the next Earth Tide Symposium in Brussels in July. Comments and corrections should be sent rapidly to me by e-mail at V.Dehant@oma.be

1. Concerning the definitions of the tidal parameters

- The definition of the tidal gravimetric factor used by Wahr (1981) is different with respect to the definition used by the ICET.

- Space geodesists usually use Wahr's (1981) definitions for the tidal parameters as the station tidal displacements (used for instance for tidal corrections of VLBI stations) or as the tidal contributions to the geopotential.

- For gravimetric tides, it is generally admitted that the ICET definition must be used, so that the Wahr-Dehant model can be used for the tidal gravimetric factor. The definition proposed by Mathews et al. (1995) is very interesting when considering the degree two potential only. But there is no gain when considering the degrees 3 and 4 in addition.

- For space geodesy, because only a few degree 3 tides in the frequency domain are necessary to achieve the mm level in the tidal displacements and because this effect can be computed easily in the time domain from one nominal value of the degree 3 Love number and from the station position and the Moon and the Sun positions, it has been proposed to use Mathews et al.'s (1995) definition.
  In addition, because one generally uses precise ephemerides of time dependent positions of the Moon and Sun, the expressions of the Earth response for degree 2 have been given in the time domain with only a few corrections at particular frequencies. The time domain expressions account for the latitude dependence of the Love numbers (due to the Earth's rotation and the Earth's flattening). The second step frequency dependent corrections account for the effects of the frequency dependence of the Love numbers. This frequency dependence is either due to Earth's inelasticity (only important at long period tides) or due to a resonance induced by normal modes (for diurnal tides). A subroutine has been done for users as mentioned in the IERS conventions.

- The difficulty of defining Love numbers or tidal factors for an ellipsoidal Earth has been pointed out because it is no more possible to define the Earth's response with only one parameter as it was the case for a spherical Earth. It is particularly the case for strain as well as for tilt, for which there must be different Love numbers in different directions.

- It has also been pointed out that it is impossible to define a transfer function for strain because there is no strain in a rigid Earth (this was already the case for the spherical Earth).

2. Concerning the seismic model used for computing the Earth tide transfer function.

The 1066A model of Gilbert and Dziewonski (1975) should certainly be replaced by the PREM model of Dziewonski and Anderson (1981). The small effects of lateral heterogeneities with respect to that model on the Love numbers show that it is not necessary to consider corrections to PREM, except for the flattening profile of the equal density surfaces, of the equipotential surfaces and of the rheological properties inside the Earth.

We must also account for the change in the top layer of the mantle and of the surface layer which is an ocean in PREM and which should be replaced, for instance, by constraining the Earth's mass and mean moment of inertia.

In addition, the WG points out that:

(1) (PREM + hydrostatic equilibrium) does not give a core flattening in agreement with the observed Free Core Nutation (FCN) period,

(2) (PREM + hydrostatic equilibrium) does not give a global Earth dynamical flattening in agreement with the one deduced from the observed precession,

(3) On the one hand, there exists a non-hydrostatic geoid, and on the other hand, the seismologists observe lateral heterogeneities with respect to the hydrostatic model of the Earth's interior. So, we know that the Earth is not in hydrostatic equilibrium.

Solutions have been proposed to these problems:

(1) to consider a parameterization (semi-analytical method) with the core flattening deduced from the observed FCN period and the dynamical flattening deduced from the observed precession constant (as done in Mathews et al., 1995)

(2) to integrate numerically inside a new Earth model considering violation of hydrostatic equilibrium and having the right core flattening and the right global Earth dynamical flattening in its initial state (as done in Dehant and Defraigne, 1996)

3. Concerning the Earth tidal transfer functions

There are five kinds of computation which are characterized here below.

(1) Authors:	Wahr, Dehant
Kind of method:	numerical integration of a truncated system of equations (truncation at the first order in the flattening) accounting for Earth's rotation and flattening, starting from an hydrostatical rotating Earth obeying Clairaut's equation in its initial state.
Tool:	generalized spherical harmonics
Characteristics:	totally coupled system of max. 22 differential eqs. (3 S-modes: 18 eqs.; 2 T-modes: 4 eqs.) solved into two steps:

(1) a super-truncated system with 1 S-mode (6 eqs.) and 2 T-modes (2x4 eqs.)
(2) two systems for the 2 remaining S-modes (2x6 eqs.)

Advantages: solution for both the tidal deformations and the forced nutations;
treatment of the resonances induced by the Earth's normal modes, in particular of the liquid core resonance (resonances from 6 seismic modes, CW, FCN and TOM in the diurnal band, resonances from the Axial-Spin-Modes in the long period band).

Disadvantages: complicated formalism, large numerical effort; probably too complicate to extend for lateral heterogeneities at other degrees and orders than the (2,0) (i.e. the flattening); geophysical parameters taken from the input model PREM not all in agreement with the observations.

(2) Author: Li
Kind of method: small parameter perturbations (only the first order applied)
Tool: generalized spherical harmonics
Characteristics: partly coupled system, one mode solved after the other (6 eqs. for each S-mode and 2 eqs. for each T-mode)
Advantages: same coefficient matrix for each system as in the spherically symmetric case; convenient also for modeling complicated large scale inhomogeneities.
Disadvantages: at present only solution for tidal deformations, and no resonance effect to the Earth's normal modes.

(3) Author: Wang
Kind of method: first-order perturbation method based on the variational principle
Tool: normalized spherical harmonics for scalar and vector fields
Characteristics: totally uncoupled system, separate determination for each perturbation component
Advantages: simple formalism, small numerical effort because only the kernel functions for a spherically symmetric starting Earth model need to be determined, and they can be determined once for all the computations; convenient also for modeling complicated large-scale lateral inhomogeneities.
Disadvantages: at present only solution for tidal deformations, and no resonance effect to the Earth's normal modes.

(4) Authors: Mathews, Buffett, Shapiro
Kind of method: small parameter perturbations (only the first order applied) and additional treatment by a semi-analytical method for the frequency dependence induced by the resonance in the diurnal band (FCN, FICN, CW).
Equation of motion is for the deformation part of the displacement field, wherein the forcing includes terms arising from the nutational motion. Deviation from the spherical Earth's solution is also governed by spherical Earth equations with effects of rotation and ellipticity entering true terms in the forcing and in the boundary conditions. These terms depend on the solution of the unperturbed problems.
Tool: classical unnormalized spherical harmonics for scalar and vector fields
Characteristics: partly coupled system, one mode solved after the other

(6 eqs. for each S-mode and 2 eqs. for each T-mode)

Advantages: same ordinary differential system as in the spherically symmetric case for each step of the successive determinations; treatment of the normal mode resonances with parameters of which the computed values from PREM can be adjusted by values deduced from different kinds of observations.

Disadvantages: at present only solution for tidal deformations

(5) Authors: Dehant, Defraigne

Kind of method: . first step: numerical integration of the equations of convection in a steady state spherical Earth (newtonian inner core, inviscid fluid outer core, and newtonian mantle) in order to compute the displacements of the boundaries and the eulerian potential due to the flow associated with mantle mass anomalies; these mass anomalies are derived from seismic tomography data. The model includes phase transitions inside the mantle. From this model one gets the new equal-density surfaces, the new equal-rheological-property surfaces and the new equi-potential surfaces, different from hydrostatic equilibrium and which do not coincide.
. second step: numerical integration of the tidal deformation equations; integration of a truncated system of equations (truncation at the first order in the flattening) accounting for Earth's rotation and flattening, starting from a rotating Earth which includes degree 2, order 0 density lateral heterogeneities in its initial state resulting from convection (violation of hydrostatic equilibrium). The initial positions of the boundaries, the initial gravity, and the initial potential are given by the output of the first step.

Tool: generalized spherical harmonics

Characteristics: for the second step, totally coupled system of max. 22 differential eqs. (3 S-modes: 18 eqs.; 2 T-modes: 8 eqs.) solved into two steps:
(1) a super-truncated system with 1 S-mode (6 eqs.) and 2 T-modes (2x4 eqs.)
(2) two systems for the 2 remaining S-modes (2x6 eqs.)

Advantages: solution for both the tidal deformations and the forced nutations;
treatment of the resonances induced by the Earth's normal modes, in particular of the liquid core resonance (resonances from 6 seismic modes, CW, FCN and TOM in the diurnal band, resonances from the Axial-Spin-Modes in the long period band),
core flattening (and thus the FCN) and global Earth flattening identical to the observed values.

Disadvantages: complicated formalism, large numerical effort, probably too complicate to extend for other degrees and orders in lateral heterogeneities than the (2,0) (i.e. the flattening).

A benchmark model based on PREM has been built. Because PREM last layer is an oceanic layer, its two last layers have been replaced by one of which the density conserves the total mass of the Earth and the mean moment of inertia has been built. The numerical results of the different method can be compared outside of the diurnal band where only (1), (4) and (5) have a frequency dependence due to the Earth normal mode resonance. This comparison has shown that (1) and (3) were very close together for the

tidal gravimetric factor while (3) and (4) were very close together for the tidal displacement and the tidal eulerian potential. Note that (5) for the benchmark PREM model is similar to (1). The results are compared for M2 and O1 in the Table just below.

So that for the tidal station displacement (choice between (3) and (4)) we would recommand (4), because (2) is ignoring the frequency dependence.

And for the tidal gravimetric factor (choice between (1) or (5) and (2)), we would recommend (1) or (5), because (3) is ignoring the resonance again. Note that (5) is very recent and is not yet published; but, if one wants to have a FCN at the observed period, (5) should be better than (1).

4. Concerning the tidal potential

- For the treatment of superconducting gravimeter data and of some very precise gravimeter data, the precision of the tide generating potentials should be better than 5 nanogals in the time domain.

- To that aim, at least the order five for the Moon and three for the Sun in the tidal potential must be considered; one must also account for the Earth's flattening, the Earth's nutations, the lunar inequality; the additional direct and indirect planetary perturbations must be considered for the same reason. Additional arguments (like planetary arguments) of the tidal potential development are thus necessary.

- The effects of the lunar inequality and the indirect effects of the planets are included (all together and without separation) in the ephemerides used for the development of TGP; if identification of these effects are wanted they must be identified in the spectrum, knowing the frequencies of the arguments involved in the harmonic representation. The only difference between the spectral method and the analytical method is that in the ephemerides used by an analytical method, those effects have been added separately.

- The effects of the nutations in obliquity and in longitude are included separately in both the spectral method and the analytical method. In the spectral method, these effects are accounted for by using a change of reference frame approach (the nutation matrix is used). In the analytical method, they are accounted for as a second order effect (2d order approximation method) and they appear separately in the solution.

- The truncation level of theoretical tidal potential should be in agreement with the required precision.

- The only two potentials which could obey to these requirements are Hartmann and Wenzel (1995) and Roosbeek (1996). These two potentials use different methods (spectral method/analytical method) which have their advantages and inconvenients.

- For the validation of tidal potentials in the time domain, it is necessary to use an ephemeris tide which should be more accurate than the tidal potentials and which should be independent of the potentials (not based on the same ephemeris).

- For the validation of tidal potentials in the frequency domain, observations of amplitudes of related phenomena can be used; the observed nutation amplitudes, for instance, can be used to validate the

diurnal tesseral part of the tidal generating potential.
If one starts from recent Moon, Sun and planet ephemerides to compute a TGP, one may not validate the obtained TGP with an ephemeris tide derived from the same ephemerides as those used for the TGP.
If one starts from analytical theories expressing the positions of the Moon, Sun and planets, one may not validate the obtained TGP with an ephemeris tide (or any other phenomena) derived from the used analytical ephemerides.

- Considerations about the separation of tidal frequencies in the case of a spectral approach:
The spectral method used to build a TGP is applied on recent observations of the relative positions of Moon, Earth, and Sun (as the DExxx series) and of which the time interval covered is not sufficient to separate two tidal waves with close frequencies. It is currently not possible to compute the TGP precisely enough and over a time interval long enough to separate two tidal waves with very close frequencies using only the frequency information provided by a FFT. However, using the phase information this statement becomes obsolete (at least for the luni-solar waves). Indeed, knowing a priori approximatively the value of the frequency, knowing a priori the observed phase, and knowing a priori the phases of the arguments involved in the possible combinations to obtain the observed frequency, it is possible to separate mathematically two waves with close frequencies.
For instance this is the case for two tidal wave frequencies separated by 2*ps (ps is the mean longitude of the perihelion which has a very long period). However, one can not do the same thing for the planetary direct and indirect effects because in that case, one does not have a sine (or cosine) component only, but one has both a sine and a cosine component. The phase information mixed then the phase of the arguments with the phase of the effect.

- Considerations about the separation of tidal frequencies in the case of an analytical approach:
While the argument ps appears in the recent Celestial Mechanics theories for the motion of the Moon around the Earth (Chapront and Chapront-Touze's (1987) ephemerides), it does not appear in Bretagnon and Francou's (1987) ephemerides for the Sun. So, Roosbeek has taken the Keplerian approach in order to identify the tidal waves of the Sun-Earth system from those induced by considering the planets in addition. The waves involving a non-zero ps argument are thus taken from the Keplerian approach, while the other waves are taken from Bretagnon and Francou's ephemerides. After some tests, Roosbeek has shown that Bretagnon and Francou's ephemerides are not more accurate than the Keplerian approach for the corresponding part.

- The previous discussion has leaded us also to the following remark:
Even for 100 years around J2000 you would not see any change in the tidal force due to the time-variation of ps (its period is about 20 940 years). This has leaded us to the fundamental question: Is the ps argument really necessary? In favour of keeping it, you would have: (1) there is a nomenclature used for the tidal waves and a notation using Doodson's numbers which would no more be valid. But this would not really embarrass you because the last Doodson number would be 5 for all the waves and one could still use the same names for the tidal waves as before, knowing that the frequencies could be different by a certain number times ps. In addition, in favour of keeping it, you would also have: (2) dropping ps would add out-of-phase components in the developments for the Moon and the Sun also. In favour of exploding the waves containing ps as argument, one must consider that keeping ps or

"dropping" (in the sense mentioned just before) ps would not change the results for the tides.
This remark is only valid for tides. It is not valid for applications which would need precise computations of frequencies.

- From a comparison with an ephemeris tide in the time domain, the spectral method starting from recent ephemerides gives the best results; the Hartmann and Wenzel (1995) tidal potential is the only tidal potential development at the nanogal level.

- From a comparison with observed precession/nutations in the frequency domain, the analytical method gives the best results; the Roosbeek (1996) tidal potential is the only one giving the right nutation series and the right precession.

- The time scale used in the computations of tides from tidal potentials should be well defined (UT, UT1, or UTC).

References:

Bretagnon P. and Francou G., 1987, "Planetary theories in rectangular and spherical variables. VSOP 87 solutions.", Astron. Astrophys., 202, pp 309-315.

Chapront J. and Chapront-Touze M., 1987, "ELP 2000-85: Une solution du mouvement de la lune couvrant la periode historique.", Notes scientifiques et techniques du Bureau des Longitudes, SO21.

Dehant V., 1987a, "Integration of the gravitational motion equations for an elliptical uniformly rotating Earth with an inelastic mantle.", Phys. Earth planet. Inter., 49, pp 242-258.

Dehant V., 1987b, "Tidal parameters for an inelastic Earth.", Phys. Earth planet. Inter., 49, pp 97-116.

Dehant V. and Ducarme B., 1987, "Comparison between the observed and the computed tidal gravimetric factor.", Phys. Earth planet. Inter., 49, pp 192-212.

Dehant V. and Defraigne P., 1996, "Body tides for an ellipsoidal rotating and convective Earth.", in preparation.

Hartmann T. and Wenzel H.G., 1994, "Catalogue of the earth tide generating potential due to planets.", Bulletin d'informations Mares Terrestres, 118, 8847-8880.

Hartmann T. and Wenzel H.-G., 1995, "The HW95 tidal potential catalogue.", Geophys. Res. Lett., 22, 24, pp 9278-9301.

Li Guojing and Hsu H.T., 1991, "The tidal modeling theory with a lateral inhomogeneous, inelastic mantle.", 11th Int. Symp. on 'Earth Tides', Helsinki, Finland, August 1989, ed. J. Kakkuri, E. Schweizerbart'sche Verlagsbuchhandlung, Stuttgart.

Mathews P.M., B.A. Buffett, and I.I. Shapiro, 1995, "Love numbers for a rotating spheroidal Earth: New definitions and numerical values.", Geophys. Res. Lett., 22, pp 579-582.

McCarthy D.D., 1996, "IERS Conventions.", IERS Technical Note 21.

Roosbeek F., 1996, "RATGP95: A harmonic development of the tide generating potential using an analytical method.", Geophys. J. Int., 126, pp 197-204.

Wahr J.M., 1981, "Body tides on an elliptical, rotating, elastic and oceanless Earth.", Geophys. J. R. astron. Soc., 64, pp 677--703.

Wang Rongjiang, 1991, "Tidal deformations of a rotating, spherically asymmetric, visco-elastic and laterally heterogeneous Earth.", Ph. D. Thesis, Univ. of Kiel, Peter Lang Publ., Frankfurt am Main, Bern, New York, Paris, 139 pp.

Wang R., 1994, "Effect of rotation and ellipticity on Earth tides.", Geophys. J. Int., 117, pp 562-565.

Working standards concerning the definitions of the tidal parameters

- Considering the definitions used for tidal analysis,

we define the tidal gravimetric factor (delta) at the station as the Earth's transfer function (a coefficient in the frequency domain) between the body tide signal measured at the station by a gravimeter and the amplitude of the vertical component of the gradient of the external tidal potential at the station position;

we define the tidal tilt as the deflection at the station of the instantaneous gravity vector with respect to the local normal to the deformed surface, in a direction defined by an azimuthal angle.
It can be expressed in function of tilts in west-east direction and in north-south direction. These tilts are, in turn, expressed as transfer functions between the non-rigid Earth tilts in these directions and the corresponding rigid Earth results;

we define the tidal strain on the ellipsoid as the derivatives at the station of the deformations along the local vertical (vertical strain) and along an horizontal direction defined by an azimuthal angle (horizontal strain); horizontal strain is expressed in function of the derivatives at the station of the deformations along the north-south, east-west and north-east directions. The theoretical tidal strains should be scaled by the external tidal potential at the station position divided by the gravity and by the radius at that point;

The effect of the elevation of the station must not be considered here, except for particularly high elevation stations (above 1km) for which it is advised to correct the observation using the following formula:
delta(r + H) = delta(r) + [-4h + 15k/2] H/r
with h = 0.6, k = 0.3

- Considering the definitions used in space geodesy,

we do not define one unique Love number h but rather a set of Love numbers h in the radial direction as coefficients in the expression of the Earth's transfer function in the frequency domain between the tidal displacement at the station along the radius and the geoid tide at the Earth equatorial radius (potential at the equatorial radius divided by gravity there);

we do not define one unique Shida number l but rather two sets of Shida

numbers, one set in each of the two different directions orthogonal to the radius, the east-west direction and the north-south direction; they are defined as coefficients in the expression of the Earth's transfer function in the frequency domain between the transverse tidal displacement in these two directions and the spherical harmonic coefficient of the corresponding geoid tide at the equatorial radius (spherical harmonic coefficient of the potential at the equatorial radius divided by gravity there);

we do not define one unique Love number k but rather a set of Love numbers k as coefficients in the expression of the Earth's transfer function in the frequency domain between the free-space potential associated with the mass redistribution due to the tides and the external tidal potential at the equatorial radius; this transfer function accounts for the radial dependence of the free potential outside the Earth.

- For space geodesy as for tidal analysis, the ellipsoid in use in these definitions corresponds to the equilibrium state of a hydrostatically prestressed Earth. Any other Earth's reference ellipsoid would not change the results.

- Comments:
  ----

1. Tidal parameters are called here Love numbers or Shida numbers because this is the way they have been called in the spherical Earth case; in the ellipsoidal Earth case, one has latitude dependent and longitude dependent functions; similarly, there is not only one number for the tidal gravimetric factor but rather a set of dimensionless numbers involved together with latitude and longitude dependent functions; in addition the free space potential depend on the radius, while each element in the set of k Love numbers is radially independent.

2. Because of the conventions of the scientists measuring effectively the parameters, the definitions used in the frame of tidal analysis are separated from those used in space geodesy. Indeed, the first ones are usually expressed (if possible and if not too complicated) as a transfer function in the physical sense of the word, i.e. a ratio of the non-rigid Earth tidal response to the rigid Earth response, for an external tidal forcing (except for the strains which do not exist in the case of a rigid Earth). On the other hand, in space geodesy, one usually expresses the response in function of the external potential and using a scaling factor. In both cases dimensionless numbers have been defined.

3. Concerning tilts, it was not possible to express the NS and WE tilts as transfer functions with respect to the same external forcing because this forcing is different in the two directions. On the other hand, for a spherical Earth as well as for an ellipsoidal Earth, the forcing acting in these horizontal directions correspond (1) in the North-South direction, to the force acting in the direction perpendicular to the normal, along the meridian and towards the South, and (2) in the West-East direction, to the force acting in the direction perpendicular to the normal, along the parallel and towards the East.

These definitions are proposed because there are already tilt data reduced by using the expression of the force at the station position in these two directions as expressed in the resolution.

The convention for the sign is that the tilt should be positive northward and eastward, and that the azimuthal angle should be taken, as do the

geodesists, from North eastward.

Tilts at the same latitude and in the same azimuthal direction on the Earth surface should be similar.
While the latitude dependent functions for the tidal gravimetric factors are rather simple, they are on the contrary more complicated for the tilts.

4. Concerning strains, it is impossible to express them as a transfer function between a non-rigid Earth and a rigid Earth because there is no strain in a rigid Earth. So, in order to obtain them from a tidal potential we must define them by scaling them by the tidal potential. Because the observations are scaled by the same scaling factor as for the tilts, we continue to define them in the same way.

The convention is that the strain should be positive in the direction of the force and that the azimuthal angle is to be taken, as do the geodesists, from North eastward; in this case the formula for getting the strain (strain_A) in any azimuthal angle (A) from the strain in the North-South direction (strain_NS), the strain in the East-West direction (strain_EW), and the strain in the North-East direction (strain_NE) is:

$$strain\_A = Strain\_NS \cos^2(A) + strain\_EW \sin^2(A) + \sin(2A)\ strain\_NE$$

Note that the formula presented in Melchior (1967, pp 67) suppose that the azimuthal angle (A') is taken from South eastward and the strain_NE is replaced by a strain in the North-West direction (strain_NW). So that:

$$strain\_A' = strain\_NS \cos^2(A') + strain\_EW \sin^2(A') + \sin(2A')\ strain\_NW$$

5. Concerning h and l, we have defined the vertical displacement and horizontal displacements as used in geodesy, scaling them by a factor independent of the latitude.
In space geodesy, one does not use transfer functions but rather the values of the displacements themselves. They compute them from the theoretical values of the Love numbers and the external tidal potential.

These Love numbers must be scaled by the gravity in order to be dimensionless.

For reasons of simplicity, it is better to avoid any latitude dependence of the scaling factor which can be computed at the equatorial radius or at the mean radius, because most tide generating potentials are given with respect to a Doodson constant expressed either at the mean radius or at the equatorial radius. But because the equatorial radius is one of the fundamental astronomical constants, it has been use in the above definitions.

Working standards for the computations of the tidal parameters

Considering

- that the seismological models for the mean rheological properties inside the Earth as well as for lateral heterogeneities will be more and more precise with elapsing time,

- that the astronomical constants are changing with time and are already available from a file by the FTP-anonymous system at the IERS (International Earth Rotation Service).

. that the theoreticians put more and more physics in their models,

. that the Free Core Nutation (FCN) period needs to be known very precisely for tides and consequently that its value computed from an Earth in hydrostatic equilibrium is too far from its observed value as deduced from tide and nutation observations (434 sidereal days in inertial space),

we do not recommend any specific model but rather propose

. that the ICET (International Centre for Earth Tides) prepares a printed material with some working standards based on the up-to-date values of the tidal Love numbers as defined here above for tidal analysis, computed from the most recent geophysical parameters,

. and that the IERS (International Earth Rotation Service) does the same for space geodesists by means of the publication of the Standards or Conventions clearly expressing the tidal parameters and their numerical values for space geodesists,

. these working standards being upgraded from time to time.

Working Standards for the tide generating potential.

Recognizing advances that have been made in determining precise tidal potentials,

we recommend that the user choose the potential most suited to the level of accuracy required.
As determined by this working group, the published potentials and their accuracy are:

Author	Doodson	Cart-wright et al.	Bulles-feld	Tamura	Xi	Hartmann and Wenzel	Roosbeek
Date of publication	1922	1971-1973	1985	1987	1989	1995	1996
Number of waves	378	505	656	1200	2934	12935	6499
Precision in time domain [nanogal]	104	38	24	8	6	0.1	2
Precision in frequ. domain [nanogal]	1.4	0.6	0.3	0.1	0.1	0.002	0.03
Ephemeris used	Brn /Kepler	EJC /Meeus	EJC /?	DE118 /LE62	EJC /Meeus	DE200 /LE200	Brt /Chp
Constant used	Mixed	IAU 1964	IAU 1976	MERIT 1983	MERIT 1983	IERS 1992	IERS 1996

Method	AM	SM	SM	SM	AM	SM	AM
Truncation level of computation	10^-4	4.10^-5	3.10^-5	10^-5 and 5.10^-6	10^-6	1 - 10^-8 D1	10^-7
Number of digits given	5	5	5	6	6	10	8

AM means Analytical Method and SM means Spectral method.

D1 is the Doodson constant.

Brn is written for Brown (1905) (for the Moon); EJC for Eckert et al. (1954) (for the Moon); Brt is written for Bretagnon and Francou (1987) (for the Moon); Chp for Chapront and Chapront-Touze (1987) (for the Sun and planets).

Note that the potential must be computed using the algorithm as provided by the author, without substitution of coefficients of terms.

Comments:
---

1. We consider, at the present time, that the most accurate time-domain representation, suitable for tidal gravity, is provided by Hartmann and Wenzel (1995) (Which provide us with the most accurate potential based on a spectral method), and the most accurate frequency-domain representation, suitable for astronomical nutations, is provided by Roosbeek (1996) (most accurate potential based on an analytical method).

2. By "spectral method" we mean that the tide generating potential is based on a spectral analysis applied on recent ephemerides as the DExxx series. For instance, Hartmann and Wenzel (1995) development is based on DE203 from JPL. This method has limitations on the frequency separation.

   By "analytical method" we mean that the tide generating potential is based on analytical developments starting from ephemerides given by a theory of celestial mechanics in which the integration constants are derived from the observations. For instance, Roosbeek (1996) development is based on VSOP87 of Bretagnon and Francou (1987) and ELP87 of Chapront and Chapront-Touze (1987). On the contrary to the spectral method, it will be difficult to go one order further down in the computation because such an analytical development would be very heavy to handle.

References.

Bretagnon P. and Francou G., 1987, "Planetary theories in rectangular and spherical variables. VSOP 87 solutions.", Astron. Astrophys., 202, pp 309-315.

Brown W.E., 1905, "Theory of the motion of the Moon.", Memoires of the Royal Astronomical Society, London, 57, no. 2, pp 136-141.

Bullesfeld F.-J., 1985, "Ein Beitrag zur harmonischen Darstellung des gezeitenerzeugenden Potentials.", Deutsche Geodatische Kommission, Reihe C, 314, Munchen.

Cartwright D.E. and Tayler R.J., 1971, "New computations of the tide generating potential.", The Geophysical Journal of the Royal Astronomical Society, 23, no. 1, Oxford.

Cartwright D.E. and Edden C.A., 1973, "Corrected tables of tidal harmonics.", The Geophysical Journal of the Royal Astronomical Society, 33, no. 3, Oxford.

Chapront J. and Chapront-Touze M., 1987, "ELP 2000-85: Une solution du mouvement de la lune couvrant la periode historique.", Notes scientifiques et techniques du Bureau des Longitudes, SO21.

Doodson A.T., 1922, "The harmonic development of the tide generating potential.", Proceedings of the Royal Society (London), Series A, 100, pp 306-328. Reprint in International Hydrographic Revue, 31, no. 1, Monaco 1954.

Eckert W.J., Jones R. and Clark H.K., 1954, "Improved lunar ephemeris 1952-1959.", 283-363 US Govt. Print. Off., Washington D.C.

Hartmann T. and Wenzel H.-G., 1995, "Catalogue HW95 of the tide generating potential.", Bulletin d'informations Marees Terrestres, 123, pp 9278-9301, Bruxelles.

Hartmann T. and Wenzel H.-G., 1995, "The HW95 tidal potential catalogue.", Geophys. Res. Lett., 22, 24, pp 9278-9301.

McCarthy D.D., 1992, "IERS Standards.", IERS Technical Note 13.

McCarthy D.D., 1996, "IERS Conventions.", IERS Technical Note 21.

Meeus J., 1962, "Table of Moon and Sun.", Kesselberg Sterrenwacht, Kessel-Lo, Belgium.

MERIT Standards, US Naval Observatory, no 167.

Roosbeek F., 1996, "RATGP95: A harmonic development of the tide generating potential using an analytical method.", Geophys. J. Int., 126, pp 197-204.

Tamura Y., 1987, "A harmonic development of the tide-generating potential.", Bulletin d'informations Mares Terrestres, 99, pp 6813-6855.

Xi Q.W., 1989, "The precision of the development of the tidal generating potential and some explanatory notes.", Bulletin d'informations Marees Terrestres, 105, pp 7396-7404.

Recurrence relations of the surface spherical harmonics for development of the tidal generating potential in the near future

Xi Qinwen

(Center for Analysis and Prediction, State Seismological Bureau, Beijing, China, 100036)

Abstract

A fully normalized associated Legendre function has been defined by author for the development of the tide generating potential, and a set of recurrence relations of the surface spherical harmonica has been deduced from the recurrence relations of the Legendre function and the Chebyshev polynomial. According to that the programs for development of the tide generating potential have been developed, so the running time is decreased to 8 minutes and 34 seconds from 15 days.

Author recognize that the fully normalized associated Legendre function has taken an effect of the normalization, so It is not necessary to adopt the Doodson normalization, even if one has to use that , it is also not necessary to adopt a decimal value, integer values approximating to that are enough. Author approve of that the fully normalized associated Legendre function may be used instead of the Doodson normalization. Using the recurrence relations will make the expression of the tide potential simple and standard.

In this paper some impotent problems on high precision tidal data processing has been discussed. A mistake due to recalculating the Doodson constant is pointed. The identity of the reference system of the celestial body and the station is discussed also.

Key words Development of tide generating potential, recurrence relations, spherical harmonics, normalization, celestial body.

As it is known that the tidal generating potential due to a celestial body can be expressed as follows :

$$V=\frac{fM}{R}\sum_{n=2}^{\infty}\left(\frac{\rho}{R}\right)^{n}P_n\left(\cos\vartheta\right) \tag{1}$$

Here, we discuss only the tidal generating potential due to a celestial body, the effect of the Earth's flattening on the tidal generating potential is ignored. By using the addition theorem of the spherical harmonics

$$P_n\left(\cos\vartheta\right)=\sum_{m=0}^{n}\frac{1}{2n+1}\overline{P}_n^m\left(\cos\theta\right)\overline{P}_n^m\left(\sin\delta\right)\cos\left(ml\right) \tag{2}$$

where ϑ is the geocentric zenith distance of a celestial body generating tides, θ is the colatitude of the station, δ is the declination of the celestial body, and

$$\overline{P}_n^m\left(x\right)=\sqrt{\left(2n+1\right)\frac{\left(n-m\right)!}{\left(n+m\right)!}\left(2-\delta_m\right)}\;P_n^m\left(x\right) \tag{3}$$

is the fully normalized associated Legendre function, with

$$\delta_m=\begin{cases}1 & for \quad m=0\\ 0 & for \quad m\neq 0\end{cases}$$

therefore, the expression (1) can be written as follows

$$V = \frac{fM}{R}\sum_{n=2}^{\infty}\left(\frac{\rho}{R}\right)^n \sum_{m=0}^{n}\frac{1}{2n+1}\overline{P}_n^m(\cos\theta)\overline{P}_n^m(\sin\delta)\cos(ml) \tag{4}$$

We have found that in expression (4), actually, the last two terms just constitute a fully normalized surface spherical harmonic, it can be as follows

$$Y_n^m(\delta,l) = \overline{P}_n^m(\sin\delta)\cos(ml) \tag{5}$$

in which the term $\cos(ml)$ is another form for the expression of Chebyshev polynomial, it means

$$T_m(\cos l) = \cos(ml)$$

Therefore

$$Y_n^m(\delta,l) = \overline{P}_n^m(\sin\delta)T_m(\cos l) \tag{6}$$

the the expression (4) can be rewritten as follows

$$V = \frac{fM}{R}\sum_{n=2}^{\infty}\left(\frac{\rho}{R}\right)^n \sum_{m=2}^{n}\frac{1}{2n+1}\overline{P}_n^m(\cos\theta)Y_n^m(\delta,l) \tag{7}$$

which is the basis for the development of the tidal generating potential. By the recurrence relation of Chebyshev polynomial

$$T_m(x) = 2xT_{m-1}(x) - T_{m-2}(x)$$

and the fully associated Legendre function, one can obtain the recurrence relations of the fully normalized surface spherical harmonics

$$\left.\begin{aligned}
&Y_0^0 = 1; \qquad Y_1^0 = \sqrt{3}\sin\delta; \qquad Y_1^1 = \sqrt{3}\cos\delta\cos l = \sqrt{3}\cos\zeta \\
&Y_n^{n-1} = \sqrt{\frac{2n+1}{3}}Y_1^0 Y_{n-1}^{n-1} \\
&Y_n^n = \sqrt{\frac{2(2n+1)}{3n}}Y_1^1 Y_{n-1}^{n-1} - \sqrt{\frac{(2n+1)(2n-1)}{4n(n-1)}}\kappa\cos^2\delta\, Y_{n-2}^{n-2} \\
&Y_n^m = \sqrt{\frac{(2n+1)(2n-1)}{3(n-m)(n+m)}}Y_1^0 Y_{n-1}^m - \sqrt{\frac{(2n+1)(n+m-1)(n-m-1)}{(2n-3)(n+m)(n-m)}}Y_{n-2}^m
\end{aligned}\right\} \tag{8}$$

with

$$\kappa = \begin{cases} 2 & for \quad n = 2 \\ 1 & for \quad n \neq 2 \end{cases}$$

$$\left.\begin{aligned}
&\sin\delta = \sin\varepsilon\cos\beta\sin\lambda + \cos\varepsilon\sin\beta \\
&\cos\zeta = \cos\beta\cos\lambda\cos\Theta + (\cos\varepsilon\cos\beta\sin\lambda - \sin\varepsilon\sin\beta)\sin\Theta \\
&\Theta = \tau + s - 180^\circ
\end{aligned}\right\} \tag{9}$$

We rewrite the expression (7) as follows

$$V = \frac{3}{4}fM\left(\frac{a}{c}\right)^3\frac{1}{a}\sum_{n=2}^{\infty}\left(\frac{\rho}{a}\right)^n\sum_{m=0}^{n}\overline{P}_n^m(\cos\theta)\left[\frac{4}{3(2n+1)}\left(\frac{c}{R}\right)^{n+1}\left(\frac{a}{c}\right)^{n-2}Y_n^m(\delta,l)\right]$$

$$= D\sum_{n=2}^{\infty}\left(\frac{\rho}{a}\right)^n\sum_{m=0}^{n}\overline{P}_n^m(\cos\theta)\left[\frac{4}{3(2n+1)}\left(\frac{c}{R}\right)^{n+1}\left(\frac{a}{c}\right)^{n-2}Y_n^m(\delta,l)\right] \tag{10}$$

where c is the approximate value of the R, a is the semi-major axis of the Earth's Ellipsoid, and

$$D=\frac{3}{4}fM\left(\frac{a}{c}\right)^3\frac{1}{a}=\frac{3}{4}fE\frac{M}{E}\left(\frac{a}{c}\right)^3\frac{1}{a} \tag{11}$$

is a new definition for the Doodson constant (Xi,1989).

The terms in the brackets of the expression (10) are really what we have to develop.

We decide to adopt a form like the expression (10) for a new tidal potential, mainly because:

1) We appreciate Hartmman and Wenzel's (1995) position and practice without using the approach of the Doodson normalization. The fully normalized surface spherical harmonics have been adopted by us directly. The maximum of absolute values of these harmonics are not greater than 3.5, most of them are about 2, in fact, it has taken an effect of the normalization, this is an advantage of adopting the fully normalized associated spherical harmonics. Even if one has to use the Doodson normalization, for which it is not necessary to adopt a decimal value, an integer values approximating to that are enough.

2) To keep the form of the Doodson constant does not take the custom separate and may not make the coefficients of the tidal waves to be too large as putting the constant into the developed part. From the modern viewpoint, the Doodson constant and the normalization and his numerical code method are still an original view.

3) In the brackets of the expression (10), the absolute value of the term $Y_n^m(\delta,l)$ is not greater than 3.5, so the order of the magnitude of the product $\frac{4}{3(2n+1)}\left(\frac{a}{c}\right)^{n-2}$ generally indicates the order of the magnitude of the tide waves corresponding to their degree n. The value of the product is 4.6×10^{-6} for $n=5$ and 7.6×10^{-8} for n=6. It could be used to determine the significant digits for the tide waves of degree n.

4) In the expression (7), a and c do not appear, this indicates that the tidal generating potential is independent of the value of them. The expression (10) is identical with the expression (7), although the former includes a and c, which are the introduced constants for an identical transformation and may not change the identical character. In other words, if we give the values of a and c, then the Doodson constant corresponding to them will be fixed. In the expression (10), a and c included in the Doodson constant can be always canceled by those in the term $\left(\frac{\rho}{a}\right)^n$ and in the brackets. Therefore, any approximate values of a and c, in principle, could be used and regarded as errorless. The thing is that when we calculate the term $\left(\frac{\rho}{a}\right)^n$, the same value of a must be adopted as it has been used in the development. In this way one need not consider the change of the real semi-major axis of the Earth's Ellipsoid. The change of the Doodson constant depends only on the geocentric gravitational constant fM for a given tidal potential. Therefore, there has been a mistake due to recalculating the Doodson constant when one compared different

potentials. This is just as a Chinese saying: one draw a snake and add feet to it. The recalculation will increase the errors in the process of the comparison and computation.

5) The results of such a development can be easily transformed to the form with the Doodson normalization. It will make the comparison of different potentials to be convenient.

From Y_n^n in the expression (8), we can see that: the first part on the right will generate the tide waves of order n and $n-2$; the second part on that includes only the tide waves of order $n-2$. If the tide waves of order $n-2$ can not be fully canceled by each other due to the truncation errors, it will generate so called "pseudo-waves".

Considering the expression (2) we can see that:

1) In the expression (2), as the positions of the station and the celestial body are exchangeable, the influence of their errors on the tidal generating potential (or tidal generating force) are identical, so one must give them with the same accuracy by the requirement. For example, if the required accuracy for the celestial coordinates is 0.02", correspondingly, the station coordinates must also be provided with the accuracy of 0.02". In view of the limited accuracy to obtain the deflection of the vertical, at the accuracy level of 1^{ngal}, the required accuracy for the station coordinates is in very harsh terms and can probably not be achieved.

2) The coordinates of the celestial body and the station must be in a same reference system. Hartmann and Wenzel have converted celestial coordinates to a terrestrial geocentric system, which would be a quasi conventional terrestrial system. The World Geodetic System 1984 (WGS-84) is orientated the requirement to the station within our accuracy, the WGS-84 is a conventional terrestrial system (CTS).

References

Xi Qinwen (1989): The precision of the development of the tidal generating potential and some explanatory notes. BIM 105, 7396-7404, Bruxelles, 1989.

Hartmman,T. and Wenzel, H.-G. (1995): The HW95 tidal potential catalogue. Geophysical Research Letters, 22, No.24,1995.

NEW RESULTS IN LABORATORY CALIBRATION OF GRAVIMETERS

VARGA PETER

Geodetic and Geophysical Research Institute of the Hungarian Academy of Sciences (Sopron, P.O.B. 5., H-9401 Hungary)

The calibration device developed for LaCoste-Romberg (LCR) gravimeters, *(Varga, 1989)* were mounted in the Geodynamical Observatory of the Eötvös Loránd Geophysical Institute of Hungary. The equipment generates gravity variations of about 112 microgal with the use of a suspended cylindrical ring. The mass of the ring raised aud lowered over the gravimeter has a mass of 3200 kg. The first experimental results obtained in 1991 show that the LCR instruments can be calibrated using this device with an accuracy 0.2 per cent on better *(Varga et al., 1991; Csapó et al., 1991)*. Later on the calibration device was automated and got a computer regulation. This development of course not increased the accuracy of the equipment but alloved to carry out more experiments as earlier and allows to introduce statistical methods in the study of the calibration parameters of the gravimeters. A complete report of the calibration procedures carried out with the heavy mass experiment was published by *Varga et al. in 1995.*

A calibration system based on the same principle was described by *Achilli et al., 1995.* This experiment was set up for calibration of the GWR superconducting gravimeters with the use of a ring with a mass of 273 kg. The generated gravity variation (6.7 microgal) in principle allows, due to the instrumental sensitivity of the order of 0.001 microgal, a calibration accuracy of 0.15 per cent. In the practice the calibration factor has been determined with a precision of about 0.3 per cent.

The calibration of the LCR instruments carried out so far in Budapest shows high inner accuracy (0.1–0.2 microgal), *(Varga et al., 1995, Meurers, 1996)* and allows to increase the reliability of the gravity earth tidal data because the most important error source of these observations lies in the imperfect calibration.

It was also shown by the experiments carried out at Geodynamical Observatory Budapest that the deviation of the large-scale Airy-type gravitational constant from the gravitational constant obtained in a laboratory is at most 10^3. This device, in case of reached by us calibration accuracy of (0.1–0.2) per cent, can be used to solve different problems of gravimetry important in the study of the Earth tides as well:

- possible non-linearity of the gravimeters *(Götze et al., 1983; Becker, 1984)* and to detect small instrumental imperfectunesses *(Meurers, 1996)*;

- a calibration of tidal gravimeters is necessary with an accuracy of 0.1 per cent to prove the latitude dependence of earth tidal parameters and to discoven mantle heterogeneities on the basis os gravimetric tidal records.

To perform high quality calibrations numerous error sources must be investigated. These are described in detail in *Varga et al., 1995; Varga 1996.* They are among others the gravimetric effect of air pressure variation, the accurate position determination of the ring and its magnetic effect, the temporal variation of the digital voltmeter constant used to record the gravimeter output.

According to the experience accumulated during the operation with the calibration device developed by us it was concluded that the most serious error sources are the instrumental drift together with the earth tidal effect and the microseismis noise. The danger caused by these error sources is connected with the fact that they generate sistematic deviations which can not be easily removed with the use of common statistical technics. *Meurers (1996)* found for example in case of LCR D-9 a difference in calibration factors obtained on calibration lines and those which resulted from the experiments caried out in the underground laboratory of the Observatory in Budapest. Of course this daviation can be specific for the investigated LCR D-9 becouse until present similar phenomena, were not detected in case of other gravimeters, but it is also possible that this deviation is due to systematic influences during the heavy mass experiment. Such a systematic effect can be produced by, the microseismic noise, which is from time to time fairly high at the Geodynamical observatory Budapest.

Instrumental drift and gravity tide effect

For the Geodynamical Observatory Budapest on the basis of earth tidal observations carried out there the earth tidal parameters δ and κ are known with high accuracy. For example the comparison campaign with the Askania GS-15 of the TU Prague proved that the reliability of the amplitude ratios (δ) of the Observatory, based on the record of BN-07 first of all, for main constituents is (0.1-0.2) per cent *(Table 1.)*

The influence of Earth tides was removed from the calibration data with the use of the Cartwright-Tajlor-Edden development and with the δ and κ values determined from gravity records carried out in the Geodynamical Observatory Budapest. Of course this procedure has problems at the 10^{-1} microgal level needed for 10^{-1} per cent calibration accuracy, because the tidal parameters are known with sufficient accuracy only for the few biggest

Table I. Gravity earth tide parameters determined for the Geodynamical Observatory Budapest (A) and results obtained with the GS-15 No 228 of the TU Prague (B)

Epoch	A		B	
	1988-1992		1988-1989	
	δ	κ	δ	κ
Diurnal waves				
O_1	1.1515	+0.1°	1.1496	+0.1°
K_1	1.1378	-0.1°	1.1362	0.0°
Semi-diurnal waves				
M_2	1.1813	-0.6°	1.1823	-0.8°
S_2	1.1764	+0.5°	1.1855	-0.5°

tidal waves. The residual of the lunisolar effect can be removed from the observation data together with the instrumental drift.

The accurate removal of the drift is one of the most important problems in the laboratory calibration procedures. For this purpose the following condition was supposed: the gravity effect of the ring on the gravimeter is always the same at a given ring position and therefore the measured gravity difference at this point is the drift. The tidal and atmospheric effects must be removed of course before the determination of the drift curve. By the repeated up and down movements of the ring an accurate drift curve can be obtained which allows to exclude this effect with the reliability of 0.1 microgal or even better.

Microseismic noise

The microseismic noise are generated by atmospheric and oceanic sources. They were recorded at the Geodynamical Observatory Budapest with an Askania gravimeter. It was found, that the microseismic activity has seasonal character and its level is rather high. The amplitude of the noise is between 5 and 30 microgal and its period is between 5 and 10s. What is very unfavourable for the calibration procedure: the observed microseisms undergo systematic beating with period from 1 to 5 min. It seems that this phenomenon is the most remarkable error source of the gravimetric measurements at the Geodynamical Observatory Budapest. The corresponding ravity variations range from 1–2 microgal to 10–30 microgal. The gravity amplitude values generated by microseisms can be used qualitatively only because the linearity of the used for recording the seismicity Askania instru-

ment was not proved at the microseismic frequency band. Of course the influence of the microseismic activity can be reduced significantly by increasing the number of observations. In this way the influence of the seismic noise can be redeced to 0.2 % even in case of a single calibration procedure *(Table 2)*. Of course calibrations should be performed at times of low microseismic noise level.

Table II. Root mean square (rms) error values in microgal relative to the expected theoretical variation of the gravity *(Varga et al., 1995)*

Number of observations	rms error values
6	0.47 (0.40 %)
12	0.41 (0.36 %)
40	0.29 (0.25 %)
50	0.25 (0.22 %)
70	0.25 (0.22 %)

The influence of microseisms is important problem becouse the need of very accurate determination of the extrema. To determine them, it is necessary to introduce adjustment calculations. This can be the least square method (the L_2 norm) in case of Gaussian error (noise) distribution. In the observations of the gravity during the calibration procedure a number of outliers-passibly due to the long-periodic (1–5 minutes) beating of the microseisms — were detected which can not be handled with the commonly used beast square method. For the adjustment calculations instead of least squares possibly the robust estimation method must be used *(Somogyi et al., 1993)*.

On the basis of experience accumulated until now, the calibration device equipped with a heavy cylindrical ring is one of the most reliable method of laboratory calibration of gravimeters. Its accuracy (at present 0.2 per cent) can be further reduced. For this purpose

- more sensitive instruments are needed (e.g. superconducting gravimeters)

- if the construction of new superconducting gravimeters allows an effective way to increase the gravity effect is the reduction of the inner diameter of the ring used in the calibration device. If the inner diameter of the ring is reduced from 30 cm to 20 or to 15 cm the corresponding gravity effect generated by the ring of the mass 3200 kg will be ± 89 or ± 118 microgal instead of ± 56 microgal.

- the problem of accurate removal of the instrumental drift is of first order importance. For this purpose new statistical processing methods — like the robust estimates — are also needed

- the influence of the microseismic noise can be reduced either with an appropriate antiseismic isolation or with a special feed-back system. In the future a place with reduced — relative to Geodynamical Observatory Budapest — seismic noise must be selected. This way a calibration accuracy of 0.1 per cent or even better can be reached.

References

Varga P., 1989. Laboratory calibration of gravimeters. Österr. Beiträge zur Meteorol. Geophys., 2, 111-121

Varga P., 1996. Laboratory gravimetry. Laboratory calibration of gravimeters and problems related to the gravitational constant. Österr. Beiträge zur Meteoral. Geophys., 14, 79-90

Varga P., Csapó G., Becker M., Groten E., 1991. Laboratory calibration of LCR type gravimeters. XX^{th} General Assembly IUGG, Vienna 1991

Csapó G., Varga P., 1991. Some problems of the calibration of recording gravimeters. Bull. d'Inf. Marrées Terrestres, 110, 7960-7964

Varga P., Hajósy A., Csapó G., 1995. Laboratory calibration of LaCoste-Romberg type gravimeters by using a heavy cylindrical ring. Geophys. J. Int., 120, 745-757

Achilli V., Baldi P., Casula G., Errani M., Focardi S., Guerzoni M., Palmonary F., Raginu G., 1995. A calibration system for superconducting ravimeters. Bull. Géodésique, 69, 73-80

Meurers B., 1996: Comparison of feedback calibration methods - Results from LCR D-9. Österr. Beiträge zur Meteoral. Geophys., 14, 235-248

Götze H. J., Meurers B., 1983. Some results of calibration factor determination of LaCoste-Romberg gravimeters (Model D.). J. Geophys., 52, 136-139

Becker M., 1984. Analyse von hochpräzisen schwere messungen. Deut. Geod. Komm. C, 294, 1-99

Somogyi J., Závoti J., 1993. Robust estimation with interactively reweighted least-square method. Acta Geod. Geoph. Mont. Hung., 28, 2-4, 465-490.

NEW SHORT BASE STRAINMETERS AT THE HUNGARIAN GEODYNAMICAL OBSERVATORIES

Varga P., Geodetic and Geophysical Research Institute of the Hungarian Academy of Sciences, Sopron, Hungary
Varga T., Eötvös Loránd Geophysical Institute of Hungary, Budapest Hungary
Latinina L.A., Institute of Seismology of the United Institute of the Physics of the Earth, Russian Academy of Sciences, Moscow, Russia

The network of strainmeter stations of the Pannonian Basin consists at this time six stations (Beregovo I, Beregovo II, Budapest, Pécs, Sopron, Vyhné) and operates eight quartz tube strainmeters. At all stations regular (daily) local calibrations are carried out for a fast recognition of possible defects in the records, systematic intercalibration is organised with a mobile calibration device developed by Mentes (1993). To avoid later uncertainties all steps of maintenance and data processing in case of all stations are carried out in the same way as far as possible and similar computer programms are in use. The strainmeter network of the Pannonian Basin is described in detail in Varga et al., 1994.

The importance of strainmeters in earth tide research lies in fact that the Love number combinations determined from deformation measurements are more sensitive to inner structure of the Earth as other methods and the resonance effect at the diurnal frequency band more pronounced as in case of gravimetric or pendulum measurements. This is so inspite of the low calibration accuracy of strainmeters which is (2–4) percent. The residual noise spectrum of the data shows a 0.3–0.7 nano-strain noise in the frequency band of semi-diurnal waves and somewhat higher in case of diurnal waves. The analysis of records shows that the used by us strainmeters have a resolution 10^{-10}

which are of the order of 10^{-8}. The quartz tube strainmeters have low long-term annual drift. It is of the order (1–10) micrometer per year.

The other field in which the strainmeter data can be used effectively is the study of the recent geological processes in the environment of the instruments and also in regional scale. This is so in spite of the cavity and topography effects deforming the observation results. At present the modern methods of space geodesy are effectively used to study the horizontal recent crustal displacements. The resolution of the GPS measurements is 10^{-7} at a 100 km base, while the annual rate of tectonical deformations is typically 10^{-7}. Similar accuracy can be achieved with the SLR. On the other hand the strainmeters — as it was mentioned above — offers $10^{-10} - 10^{-11}$ resolution at (1–100) m base. Evidently it can be useful to combine the regional SLR and GPS deformation data with the informations gathered from short base strainmeter records.

The problem what limits the use of strainmeters both in tidal and recent tectonical research is connected with the extensive dimension of the strainmeters. For the recently used instruments big underground galeries are needed where the observations are relative expensive and the conditions of long-term stability of the recording only hardly can be satisfied.

To overcome this last problem short base strainmeter was developped at the Geodetic and Geophysical Research Institute (Sopron), and tested at the Geodynamical Observatory Budapest (Eötvös Loránd Geophysical Institute of Hungary) in close cooperation with colleagues from the Institute of Physics of the Earth of the Russian Academy of Sciences (Moscow). The experiments with short base mirocextensometer were carried out in a galery of the Budapest Geodynamical Observatory parallel to the 21.3 m long quartz tube strainmeter (Fig. 1) accross a geological fault (Fig. 2). First — some years ago — a short base strainmeter with mechanical read out was installed (see the upper device shown on Fig. 2). After the detailed study of this device a new version of the microextensometer equipped with capacitive transducer was designed by Mentes (1994) and mounted (see the lower device shown on Fig. 2) in February 1996. The device in 1.2 m long, it is fixed to the rocks mechanically. After a period of stabilization the registrations were started in the second half of April 1996. A one month long, record (22.04.1996–27.05.1996) obtained by the short

base strainmeter is shown on Fig. 3. To give an impression on the recorded curve a peace of the analogous record is shown on Fig. 4, where M denotes the curve recorded with the short-base strainmeter, while I denotes the curve obtained with the parallel, 21 m long strainmeter and II shows the curve of the 13 m long strainmeter. It can be concluded that the microextensometer M has much stronger instrumental drift as the long base devices I and II installed long time ago. The energy spectrum of the record of the microextensometer (Fig. 5) shows significant peaks at the diurnal and semi-diurnal frequency bands. It can be concluded, that the record of the short-base instruments has a rather high instrumental and/or environmental noise. The wavelet transform of the record obtained with the microstrainmeter (Fig. 6) shows how big was the variation in the spectral content of the observed data between 22.04.1996 and 27.05.1996.

It can be concluded that the microstrainmeter after a period of stabilization (February–April, 1996) started to record the earth tides and was characterised with an acceptable amount of the drift and external noise. Probably this instrument shall give useful informations on earth tides and recent tectonical movements. It can be easily installed and need not extended galeries.

Acknowledgement. The development of the short base strainmeter was supported by the Hungarian Sciences Fund OTKA (Projekt No. T014896).

Authors express their thank to Dr. J. Závoti for his help in calculation of the wavelet transform of the record obtained with the microstrainmeter.

References

Mentes Gy., 1993. Mareés Terrestres, Bull. d'Information, 115, 8467–8471.

Mentes Gy., 1994. Acta Geod. Geoph. Hung., 29(1–2), 161–177.

Varga P., Varga T., 1994. Acta Geod. Geoph. Hung., 29(1–2), 57–80.

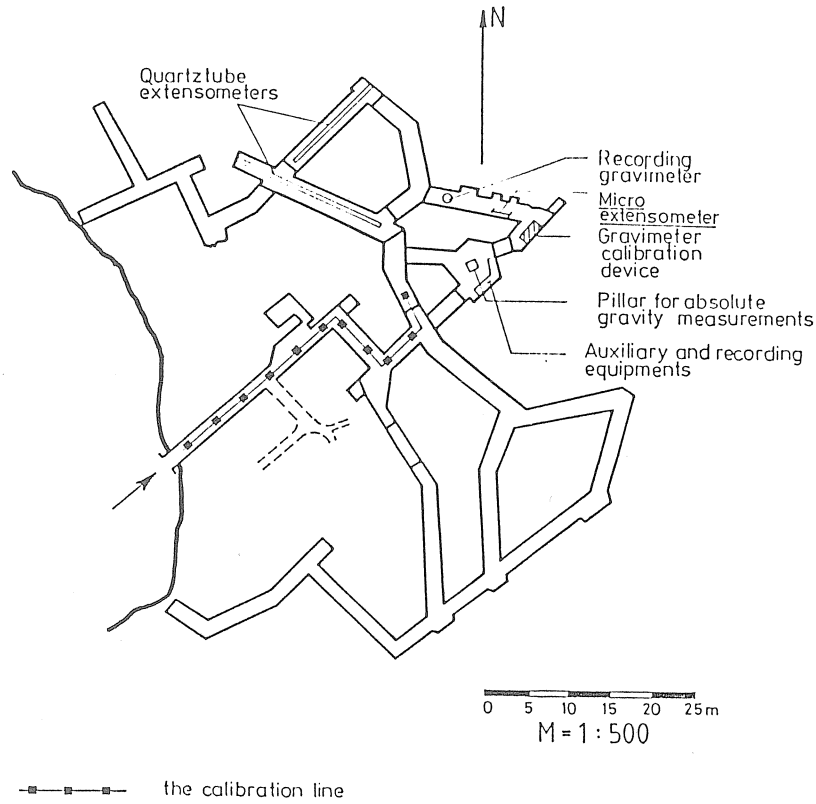

Fig. 1. Geodynamical Observatory Budapest

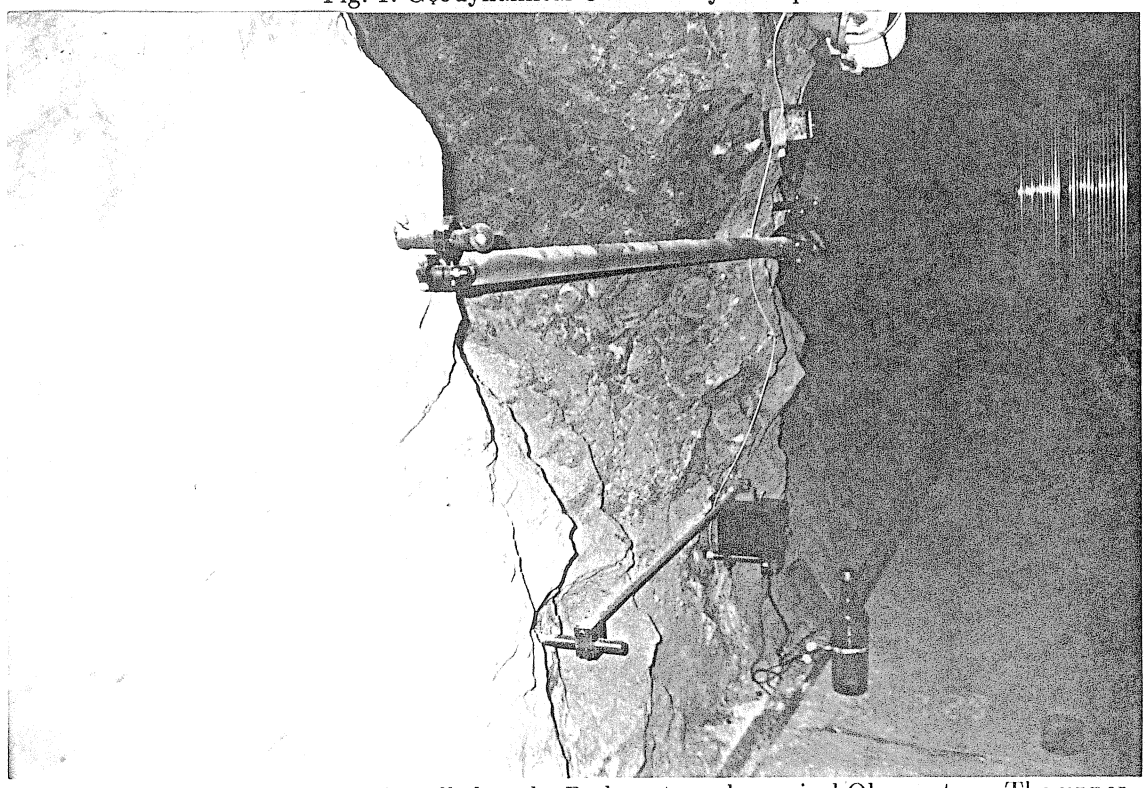

Fig. 2. Microextensometers installed at the Budapest geodynamical Observatory. The upper device is equipped with a mechanical read-out device, the lower instrument installed in February 1996 and is equipped with capacitive transducer

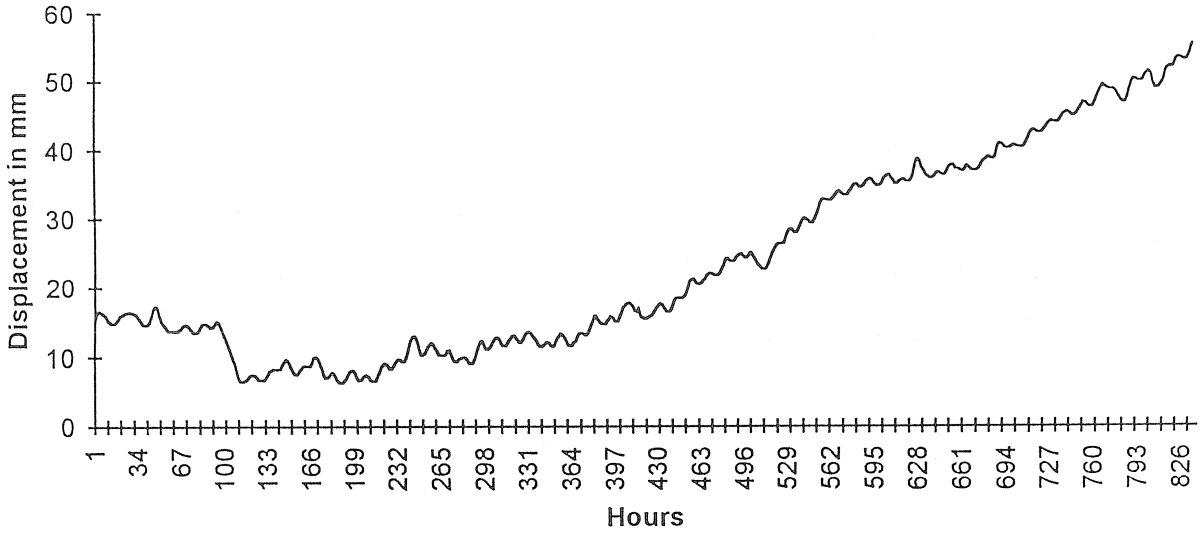

Fig. 3. Record of the short base strainmeter obtained from 22.04.1996 to 27.05.1996

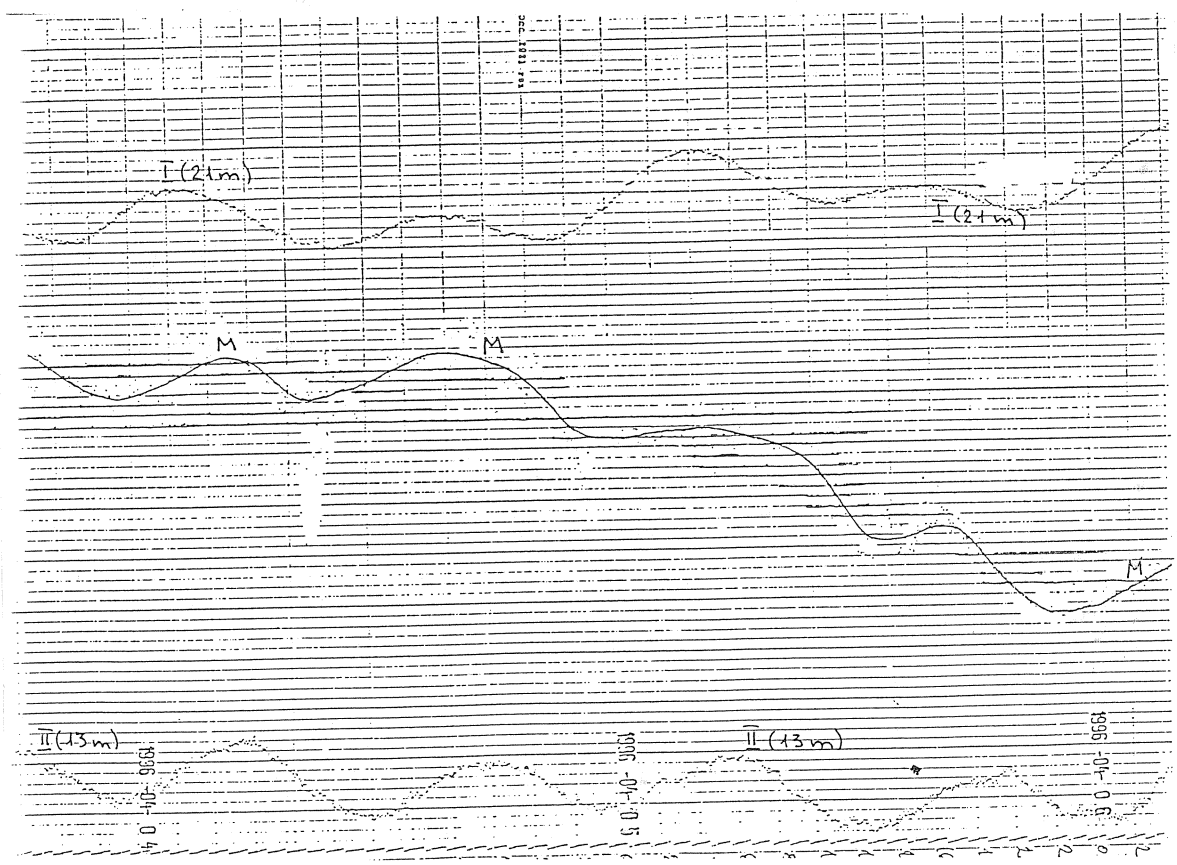

Fig. 4. Analogous strainmeter record observed between 04.04.1996 and 06.04.1996

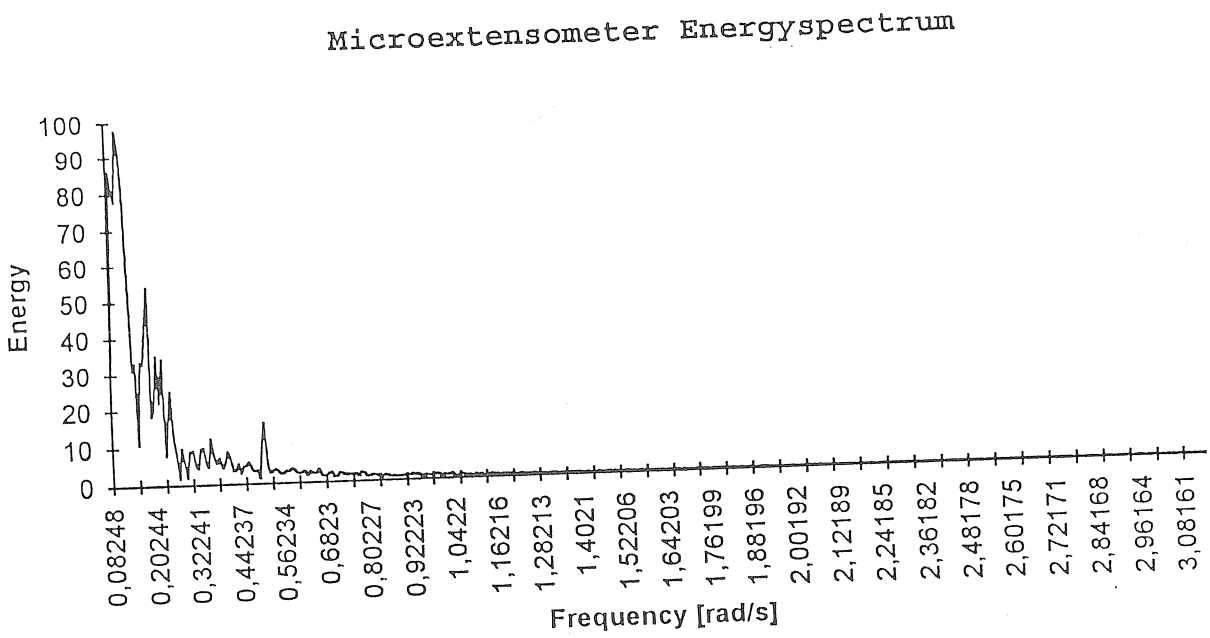

Fig. 5. Energy spectrum of the record obtained with short base strainmeter

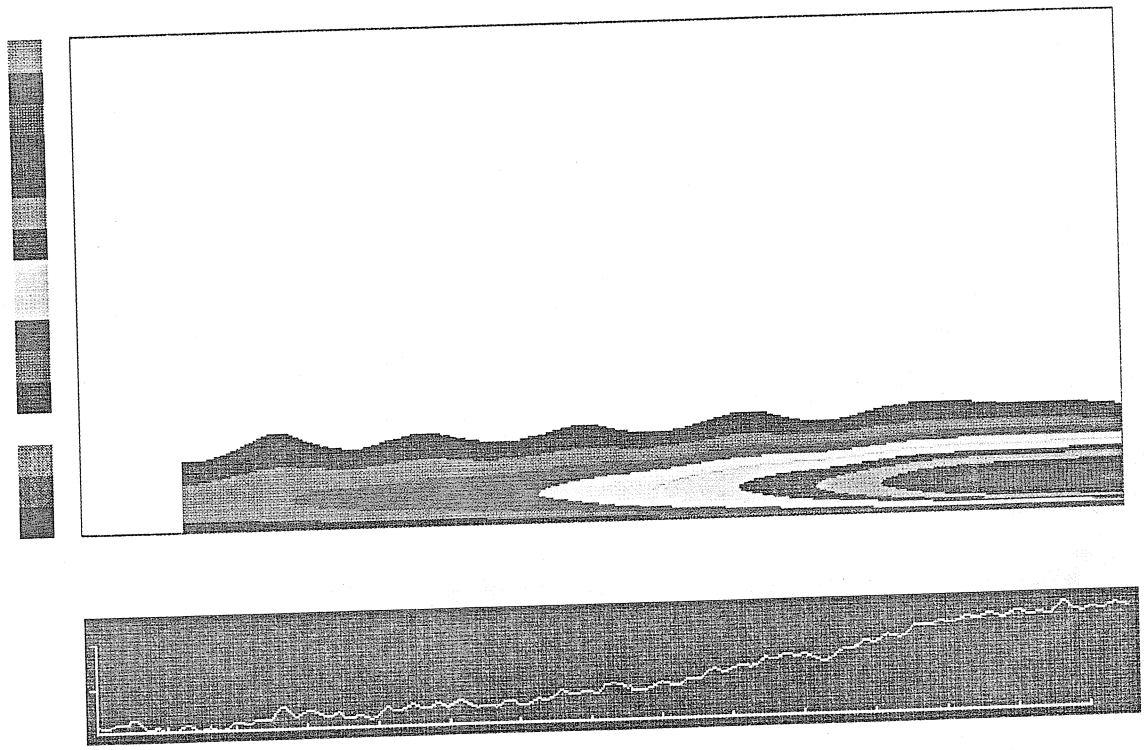

Fig. 6. Wavelet transformation of the record obtained with the microextensometer

First results of the extensometric measurements in South Hungary

Gyula Mentes
Geodetic and Geophysical Research Institute of the Hungarian Academy of Sciences, H-9400 Sopron, Csatkai E. u. 6-8, Hungary

and

Zsolt Berta
Mecsekurán Ore Mining Ltd., H-7614 Pécs, P.O.B. 65., Hungary

Abstract

In the frame of a cooperation between the Mecsekurán Ore Mining Ltd. and the Geodetic and Geophysical Research Institute of the Hungarian Academy of Sciences a quartz tube extensometer was installed for local and global geodynamical deformation measurements in the uranium mine in Pécs, in the southern-middle part of Hungary. In the paper the recording site, the construction of the extensometer are described and the results obtained in the period 1993-1995 are given.

1. Introduction

Investigation of the Earth crust deformation is of great interest for studying recent geodynamical processes. For this reason several extensometric stations were established in the Pannonian Basin and on its margin (Fig.1.) in the frame of scientific cooperations between Hungary (Geodetic and Geophysical Research Institute of the Hungarian Academy of Sciences) and the neighbouring countries (Czech Republic, Slovakia, Ukraine). The map shows the azimuths, the lengths and the sensors of the extensometers, too. All instruments were installed for geodynamical purposes but the one in Pécs placed in the uranium mine was developed for studying the local, spontaneous deformations and movements to solve environmental and mining safety problems beside geodynamical measurements.

The uranium mining activity started in the Mecsek mountain nearby the city of Pécs in 1956. Since that time 18 million m^3 of rock have been mined out, enormous waste rock piles and tailing ponds have been produced and the depth of mining exceeded 1000 m. The mining processes have a tremendous effect both on the natural and the human environment. To study and manage the aftermath of these influences a monitoring system was established and continuously developed in the surface and underground area of the uranium mine.

The monitoring system consisting of geodetic, geodynamical, hydrogeological and radiological measurements makes possible the complex geodynamical interpretation of data obtained by the high sensitive quartz tube extensometer. The main elements of the monitoring system which can be used for correction of the extensometric measurements and for investigation of geodynamical phenomena are:

1. Regular geodetic measurements for controlling the subsidence of the undermined field,
2. A multichannel seismological station with sensors on the surface and in the underground area for controlling the spontaneous geodynamical events (rockfalls, stress replacements, etc.),
3. Continuous measurement of the temporal variation of air pressure, temperature, radon concentration in the mine,
4. Measurement of groundwater-level changes in several observation wells drilled around the mining area.

The extensometric station in Pécs is the only one in the Pannonian basin where a complex set of the additional parameters is measured therefore the behaviour of the extensometer due to the variation of the different parameters can be also very well tested.

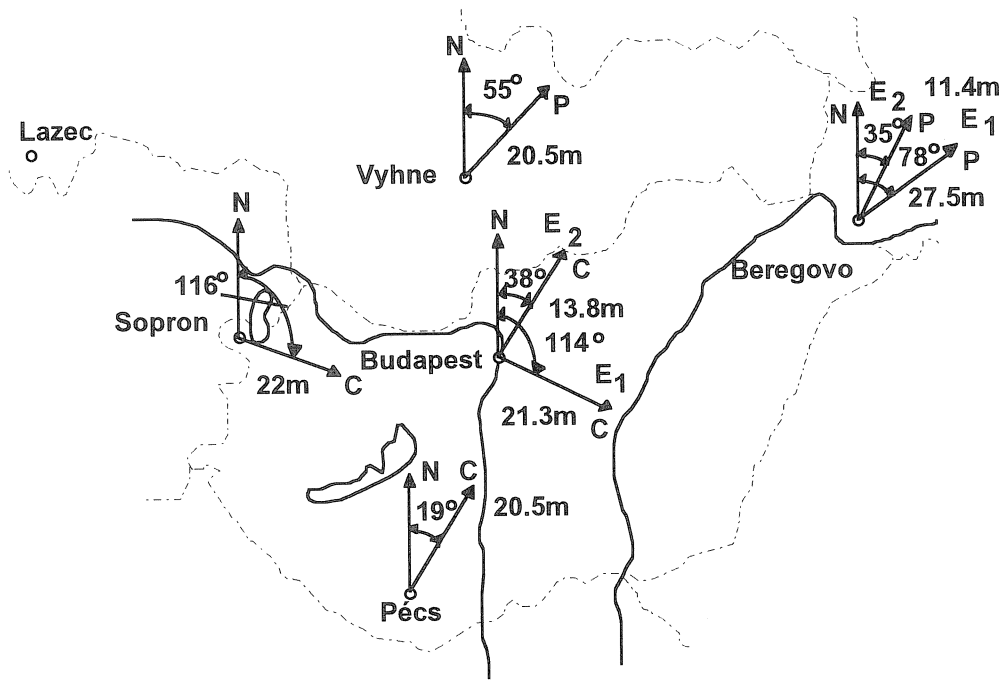

Fig. 1. The extensometric network in the Pannonian Basin. C=extensometer with capacitive transducer, P=extensometer with photo recorder, N=North

2. The construction of the extensometric station and the quartz tube extensometer

The extensometer is placed in a depth of 1050 m from the surface far away from the still working region of the uranium mine. A short blind working was excavated from an unused main transporting tunnel of the mine for the instrument. The blind working is separated and thermally insulated from the major opening where the air ventillation system is working by sluice-gates and plastic foam bulkheads (Fig. 2.). This ensures an annual temperature stability of 0.5 °C and the monthly variation of the temperature is less than 0.1°C in the extensometer room. The variation of the temperature at the instrument does not depend on the working of the ventillation system because of the triple thermal insulation and the low heat-flow through the rock. The temperature at the instrument is 41°C.

The construction of the quartz tube extensometer installed in Pécs similarly to the other instruments in the Pannonian basin is based on the principle developed by Latynina and Karmaleeva (1978). The extensometer is made of 2-2.5 m long quartz tubes which have a diameter of 45 mm and a wall thickness of about 2-3 mm. The linear thermal extension coefficient of the quartz tubes is $0.45 \cdot 10^{-6}$. The individual tube pieces are assembled by means of two-component resin and muffles made of quartz tubes which have a greater diameter (46-49 mm) than the long ones to be attached. The one end of the extensometer is attached to the rock by means of a stainless steal bolt and the other end holds the moving plate of the capacitive transducer. The standing plates of the transducer are fixed to the rock. The attached quartz tubes are suspended on very fine wires connected to supports making possible the levelling of the quartz tube (Fig. 3).

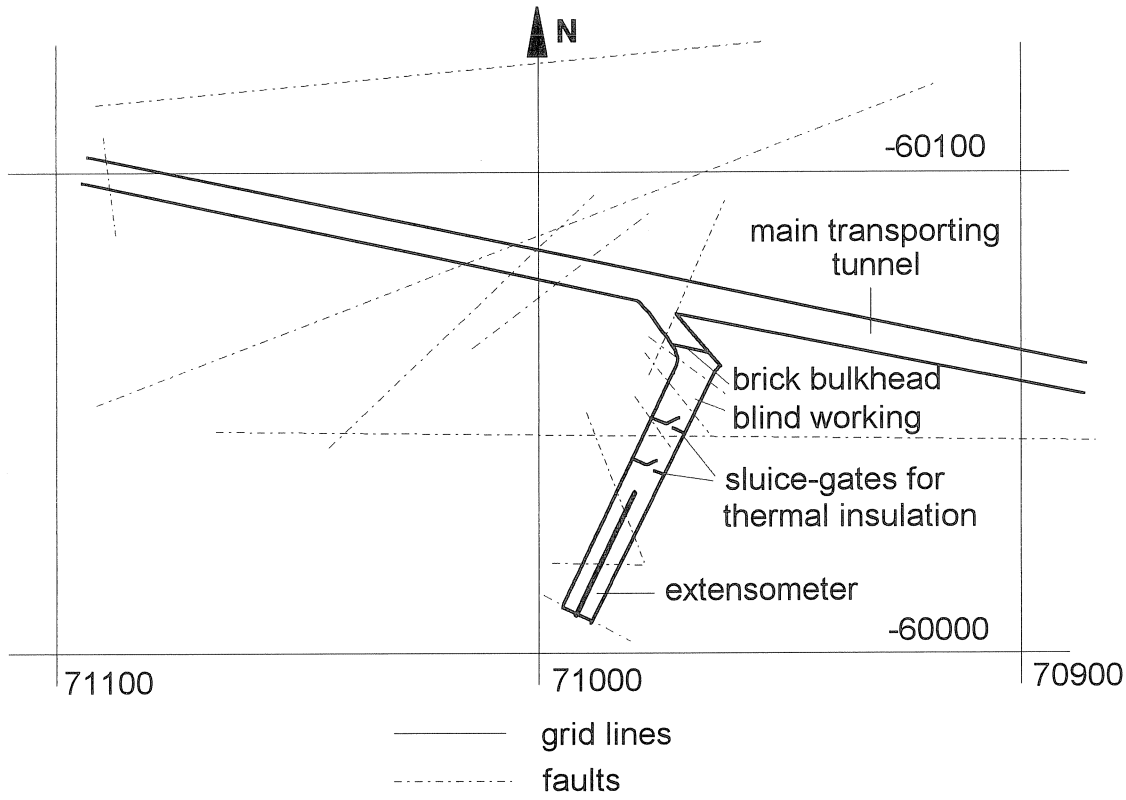

Fig.2. The recording place of the extensometer in a depth of 1050 m in the mine. The coordinates are given in system HDR.

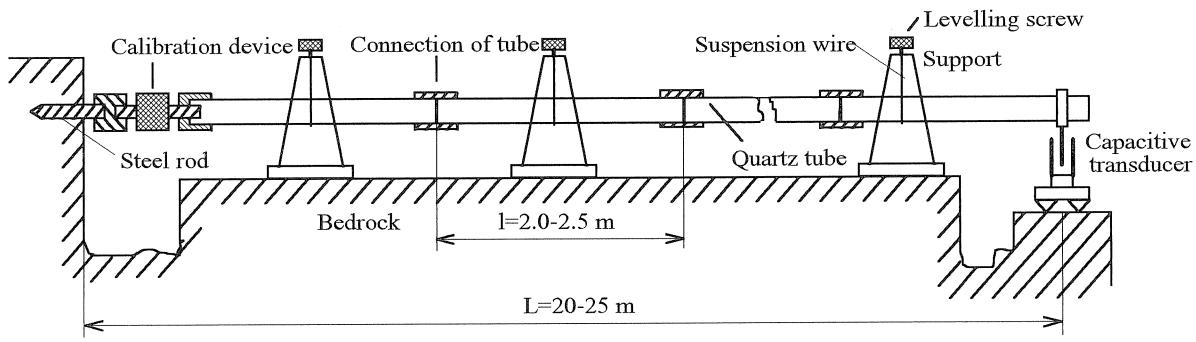

Fig. 3. The principal construction of the long quartz tube extensometers

The capacitive transducer is a differential condenser which is connected in a capacitive bridge the output signal of which is amplified by a carrier-frequency amplifier. The output signal of this amplifier is both analogous and digitally recorded.

For regular controlling the stability and the sensitivity of the extensometer a special crapaudine was developed and built into the extensometer between the bolt fastened into the rock and the quartz tube (Fig. 3). The crapaudine was tested by means of a laser interferometer before the installation. Its linearity is better than 1 per cent and it gives a constant displacement of 4.6 nm/Hgcm. The sensitivity of the extensometer determined by the crapaudine from the regular daily calibrations has been constant since the installation and its value is 1.15 nm/mV.

The construction of the quartz tube extensometers, the principle of the capacitive transducer, the methods and problems of the calibration are described in more details by Mentes (1991, 1993, 1994a, 1994b, 1995a, 1995b)

3. Results of the continuous measurements between 1993 and 1995

The extensometer was installed in May 1992. In this year and the beginning of the next one the drift of the extensometer was very high and therefore there were a lot of gaps in the obtained data. One of the causes of the high drift at the very beginning of the recording could be the warming up of the rock after closing the recording room by the sluice-gates. Another reason was the deformation of the rock after cutting the recording gallery. Maybe the movements of the rock due to the numerous small faults in the surroundings of the recording room hindered the consolidation of the rock and the extensometer. Otherwise the recording conditions were unchanged during the studied time interval. Even the short breaks of the ventillation in the major opening caused no measurable temperature variations in the recording room and remarkable signal changes at the extensometer.

Figures 4-6 show the measured deformation in the time interval 1993-1995. The positive slope of the curve means an extension and the negative one a contraction in the direction of the extensometer which have an azimuth of 19°. From the hourly recorded data daily averages were calculated and plotted in the Figures.

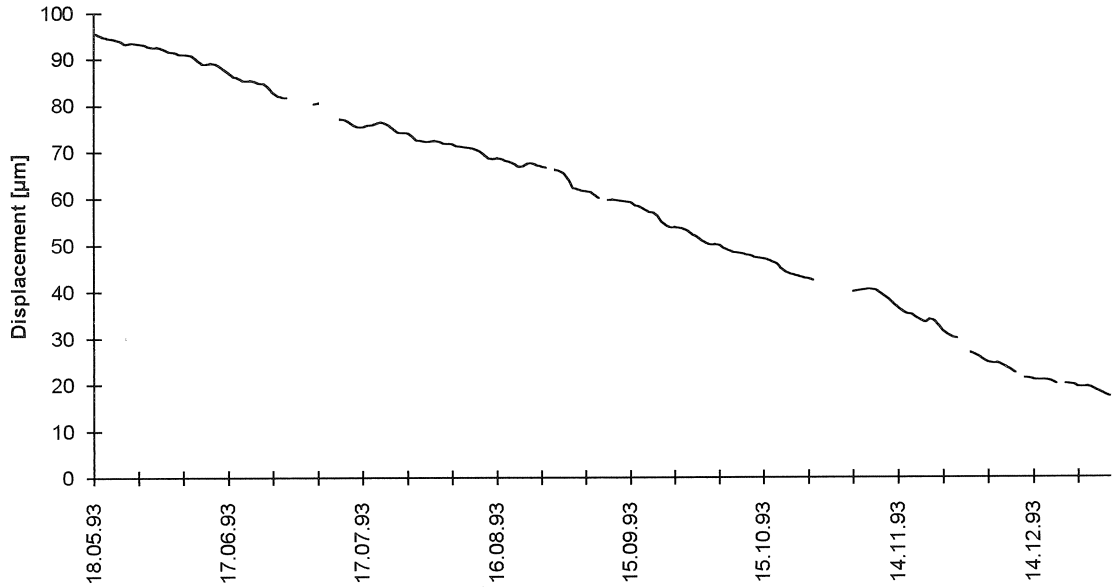

Fig. 4. Deformation measured by the quartz tube extensometer in Pécs in 1993

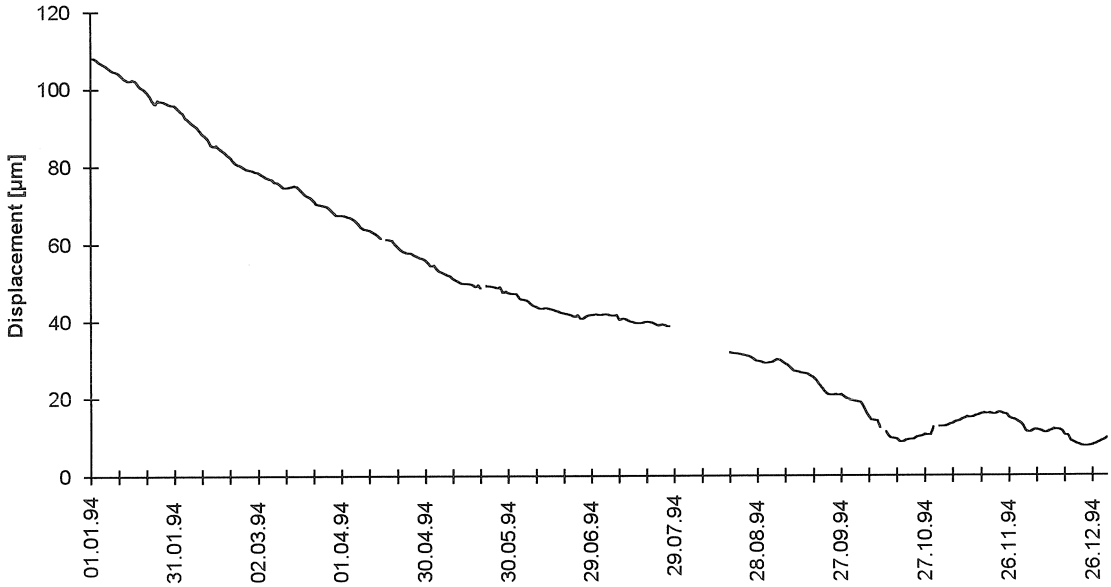

Fig. 5. Deformation measured by the quartz tube extensometer in Pécs in 1994

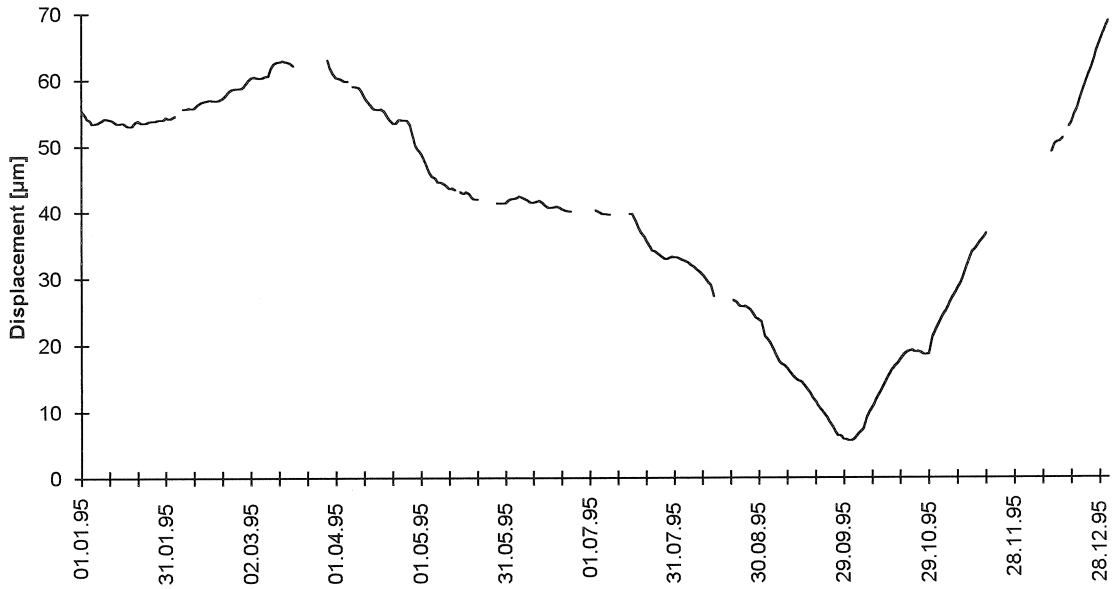

Fig. 6. Deformation measured by the quartz tube extensometer in Pécs in 1995

The annual rates of the contraction determined from the measured data are:

in 1993: -80 µm/year,
in 1994: -96 µm/year,
in 1995: -37 µm/year (average value).

Since the end of the year the rate of the contraction has become slower and in the first half of the year 1995 an extension was measured for a short time and in the second half of the year the direction of the displacement turned over suddenly into extension of high rate. The reason of this change is not yet known. Maybe it is due to the consolidation of the recording place or due to changes in the mining activity. But the extension agrees with the results of other geophysical investigations showing an extension with a direction of maximum of W-NW in the southern part of Hungary (Dövényi and Horváth, 1990).

We need a much longer data record to obtain satisfying results and to investigate the influence of the cave deformation, the instrumental drift, the small cracks and faults, and the changes of the surface topography of the mining area. For this reason a lot of additional measurements of other geophysical parameters are also available as mentioned earlier.

References

Latynina, L. A., Karmaleeva, R. A. 1978: Deformographic measurements, Nauka, Moscow, (in Russian).

Dövényi, P., Horváth F.1990: Determination of contemporary crustal stress regime in Hungary, Acta Geod. Geoph. Mont. Hung., 25/3-4/, pp. 257-388.

Mentes, Gy. 1991: Installation of a quartz tube extensometer at the Sopron Observatory, Marees Terrestres Bulletin D'informations, Bruxelles, 110, 7936-7939.

Mentes, Gy. 1993: Sort remarks concerning the calibration of quartz tube extensometers, Marees Terrestres Bulletin D'informations, Bruxelles, No. 115, pp. 8467-8471.

Mentes, Gy. 1994a: Instruments for Precise Determination of Horizontal Deformations in the Pannonian Basin, Acta Geod. Geoph. Mont. Hung.,29/1-2/, pp. 161-177.

Mentes, Gy. 1994b: Automation of Geodynamical Observations, Acta Geod. Geoph. Mont. Hung., 29/3-4/ pp. 421-438.

Mentes, Gy. 1995a: High Precision Calibration of Quartz Tube Extensometers. Proceedings of the Twelfth International Symposium on Earth Tides (Ed. H. T. Hsu), Science Press, Beijing, New York, pp. 209-214.

Mentes, Gy. 1995b: In-situ calibration of quartz tube extensometers, Marees Terrestres Bulletin D'informations, Bruxelles, No. 121, pp. 9070-9075.

Meeting of the Working Group on High Precision Tidal Data Processing
Bonn, September 16-19, 1996

SIMULTANEOUS TIDAL OBSERVATIONS USING TWO VARIANTS OF THE MODERNIZED GS-11 GRAVIMETER: "BN" (BONATZ) AND "R" (DITTFELD-NEUMEYER)

Tadeusz CHOJNICKI

Space Research Centre, Polish Academy of Sciences
Bartycka 18A, 00-716 Warsaw

A b s t r a c t

Two simultaneous annual series of Earth tides observations were analysed, performed from June 1992 till June 1993 at the Warsaw station using two reconstructed Askania gravimeter Gs-11: no. 110 (BN-17) and no. 112 (112/R). In order to compare the value of the improvements, both instrument were used in the identical conditions. For calculations the classical method of analysis based on the least-squares technique was used.

Since June 1992 the Warsaw station [Chojnicki, 1984] [Żarnowiecki, 1975] has been equipped with two gravimeters: Askania Gs-11 no. 110 reconstructed by prof. M. Bonatz and named BN-17 [Bonatz, 1973, 1977], [Wilmes, 1975], and Askania Gs-11 no. 112 reconstructed by dr. H.-J. Dittfeld and dr. J. Neumeyer and named 112/R [Dittfeld et al., 1985]. Both gravimeters were installed in the identical conditions in a common thermostated box (capacity about 15 m^3), on the neighbouring pillars. The observations using these two gravimeters were performed since June 1992 till June 1993.

The analysis of observations was performed by the classical method based on the least-squares principle [Chojnicki, 1977]. In order to avoid an influence of the calibration method of either instrument, the results were calibrated using model (i. e. the most probable) values of amplitude factors of O1 and M2 waves for Warsaw, presented in Table 1.

Table 1. Model values of observed amplitude factors at the Warsaw station.

Wave	Amplitude factor
O1	1.15568
P1	1.15413
K1	1.13848
N2	1.17545
M2	1.18485
S2	1.17932

The formula used for the calculation of the calibration coefficient K was:

$$K = \frac{1}{2}\left[(\delta[\mathrm{O1}]_O/\delta[\mathrm{O1}]_M + \delta[\mathrm{M2}]_O/\delta[\mathrm{M2}]_M\right] \qquad (1)$$

where the subscript O denotes the observed value and the subscript M - the model one.

The results of analysis of observations for the gravimeter BN-17 are presented in Table 2 and those for the gravimeter 112/R in Table 3.

In order to compare the quality of results obtained with either instrument, the following parameters were considered (listed in the Table 4):

- a mean square error m_o of one-hour observation after adjustment;
- mean square errors M_1 and M_2 of observations in diurnal and semidiurnal band, respectively;
- a difference dm_{cv} between m_{oc} and m_{ov}, i. e. between mean square errors of observations calibrated with constant and variable calibration coefficient, respectively;
- a relative error e_{M4} of M4-wave;
- an amplitude factor of S1-wave;
- an inverse of the relative error e_{S4} of S4-wave;
- standard deviations m_{sen} and m_{ins} of temperature sensitive (P1, K1, S2), and insensiitive (O1, N2, M2) amplitude factors, respectively, calculated in relation to model values, taking into consideration weights proportional to amplitude of wave.

The column "Remarks" in Table 4 presents quality features characterized by the listet parameter values.

Table 2. Results of analysis of observations performed with the gravimeter BN-17.

```
WYROWNANIE KONCOWE - FINAL ADJUSTMENT                                  CHOJNICKI METHOD

KONCOWE WYNIKI OBLICZEN - OCENA DOKLADNOSCI NA PODSTAWIE RESIDUUM
FINAL RESULTS OF COMPUTATIONS - ESTIMATION OF ACCURACY BASED ON RESIDUAL
 .00001993 1 1 0 0  10001111    52.23   -21.01  110      .00              981.245

STATION 0905 WARSZAWA                VERTICAL COMPONENT                      POLAND

52 14 N          21 01 E          H 110 M          P  4 M           D 260 KM
THE UNDERGROUND OF THE PALACE OF CULTURE                        QUATERNARY SANDS
ZAKLAD GEODEZJI PLANETARNEJ CBK PAN          T.CHOJNICKI
GRAVIMETER   BN-17 (ASKANIA GS-11  NO 110)
CALIBRATION - MODEL OF O1 AND M2 IN WARSAW - WITHOUT REGARD TO TIME VARIATIONS
INSTALLATION    T.CHOJNICKI / M. BONATZ / S.GADOMSKI
OPERATION    T.CHOJNICKI / M. GADOMSKI

LEAST SQUARE ANALYSIS IN CLASSICAL MANNER (CHOJNICKI)
FILTRATION OF OBSERVATIONS / FILTER  51/  833
POTENTIAL CARTWRIGHT-EDDEN-(DOODSON) / COMPLETE EXPANSION
COMPUTATION - ZAKLAD GEODEZJI PLANETARNEJ CBK PAN - WARSZAWA - PC IBM/T 386

92 6  317-92 8 26 8/92 8 29 8-9210 16 3/9210 2112-9210 2317/9210 3010-9211  923
9211 1310-9211 26 7/9212  3 0-93 1  6 0/93 1 1412-93 1 28 4/93 2  411-93 2 15 8
93 2 2012-93 3  5 2/93 3 12 1-93 3 18 7/93 3 2519-93 6 2020

TOTAL NUMBER OF DAYS    382          7726  READINGS

    WAVE GROUP     ESTIM.AMPL.  AMPLITUDE FACTOR   PHASE DIFFERENCE   RESIDUALS
ARGUMENT  N SYMBOL VALUE R.M.S.   VALUE    R.M.S.    VALUE   R.M.S.   AMPL. PHASE

105.-139. 65  Q1   6.34   .13   1.16750   .02413     1.715   1.183    .19   77.9
143.-149. 26  O1  34.66   .14   1.15204   .00473     -.028    .236    .22 -175.6
152.-158. 22  M1   3.28   .12   1.16145   .04373     .577    2.155    .03   77.0
161.-163. 10  P1  17.30   .15   1.16292   .01009    4.726    .497    1.43   86.8
164.-164.  3  S1   4.55   .14  19.60492   .61117   70.102   1.789    4.46   73.3
165.-168. 20  K1  49.02   .14   1.17085   .00333     .519    .163    1.46   17.7
172.-177. 22  J1   2.66   .13   1.13977   .05588    1.882   2.807    .10   120.6
181.-1E3. 37  OO1  1.23   .10   1.16156   .09714    -.149   4.795    .00  -72.5
207.-23X. 41  2N2  1.09   .04   1.18342   .04136    4.002   2.002    .08   76.1
243.-248. 24  N2   6.37   .05   1.19169   .00848    1.134    .408    .21   36.9
252.-258. 26  M2  33.88   .05   1.18859   .00169     .464    .081    .86   18.7
262.-267. 17  L2    .63   .03   1.22613   .06443    2.808   3.010    .05   42.9
271.-274.  9  S2  16.99   .05   1.22800   .00368     .853    .171    .97   15.1
275.-2X5. 38  K2   3.95   .05   1.16647   .01383     .153    .679    .02   26.1
327.-375. 17  M3    .34   .02   1.06880   .07718    1.127   4.138    .01   86.6
382.-382.  1  S3    .20   .03   2.00227   .26582   24.615   7.607
455.-455.  1  M4    .04   .02    .38227   .17011 -102.153  25.485
491.-491.  1  S4    .14   .02   1.35282   .16709    8.004   7.079

R.M.S.ERROR M-ZERO      2.0934   MICROGAL

R.M.S.ERROR FOR BANDS    D   8.6452   SD   2.9752   TD   1.8472   QD   1.1645

O1/K1     .9839          1-O1/1-K1     .8899          M2/O1    1.0317

REFERENCE EPOCH    1993  1  1   .00       JULIAN DATE  2448988.50
```

Table 3. Results of analysis of observations performed with the gravimeter 112/R.

WYROWNANIE KONCOWE - FINAL ADJUSTMENT CHOJNICKI METHOD

KONCOWE WYNIKI OBLICZEN - OCENA DOKLADNOSCI NA PODSTAWIE RESIDUUM
FINAL RESULTS OF COMPUTATIONS - ESTIMATION OF ACCURACY BASED ON RESIDUAL
.00001993 1 1 0 0 10001111 52.23 -21.01 110 .00 981.245

STATION 9905 WARSZAWA VERTICAL COMPONENT POLAND

52 14 N 21 01 E H 110 M P 4 M D 260 KM
THE UNDERGROUND OF THE PALACE OF CULTURE QUATERNARY SANDS
ZAKLAD GEODEZJI PLANETARNEJ CBK PAN T.CHOJNICKI
GRAVIMETER ASKANIA GS-11 NO 112/R
CALIBRATION - MODEL OF O1 AND M2 IN WARSAW - WITHOUT REGARD TO TIME VARIATIONS
INSTALLATION T.CHOJNICKI / H.-J. DITTFELD / S.GADOMSKI
OPERATION T.CHOJNICKI / M.GADOMSKI

LEAST SQUARE ANALYSIS IN CLASSICAL MANNER (CHOJNICKI)
FILTRATION OF OBSERVATIONS / FILTER 51/ 833
POTENTIAL CARTWRIGHT-EDDEN-(DOODSON) / COMPLETE EXPANSION
COMPUTATION - ZAKLAD GEODEZJI PLANETARNEJ CBK PAN - WARSZAWA - PC IBM/T 386

92 6 6 9-92 8 610/92 8 14 7-92 8 26 8/92 9 214-9210 1515/9210 2112-9210 2222
9210 3010-9211 8 7/9211 1310-9211 26 7/9212 212-9212 321/9212 911-9212 11 4
9212 1711-93 1 1410/93 1 1910-93 4 1113/93 4 17 9-93 6 2020

TOTAL NUMBER OF DAYS 379 7617 READINGS

WAVE GROUP ARGUMENT	N	SYMBOL	ESTIM.AMPL. VALUE	R.M.S.	AMPLITUDE FACTOR VALUE	R.M.S.	PHASE DIFFERENCE VALUE	R.M.S.	RESIDUALS AMPL.	PHASE
105.-139.	65	Q1	6.29	.12	1.15718	.02273	-1.176	1.125	.13	-96.2
143.-149.	26	O1	34.84	.14	1.15784	.00455	-.054	.225	.05	-143.3
152.-158.	22	M1	3.08	.12	1.09175	.04109	.308	2.156	.19	175.0
161.-163.	10	P1	16.92	.14	1.13680	.00964	-2.514	.485	.79	-109.8
164.-164.	3	S1	1.90	.14	8.19941	.58406	-85.841	4.089	1.90	-93.9
165.-168.	20	K1	47.32	.13	1.13027	.00318	-.509	.162	.52	-126.3
172.-177.	22	J1	2.92	.12	1.25386	.05322	-1.142	2.431	.22	-15.2
181.-1E3.	37	OO1	1.22	.10	1.15360	.09149	.323	4.541	.01	137.2
207.-23X.	41	2N2	1.08	.05	1.16452	.05676	.344	2.792	.01	57.8
243.-248.	24	N2	6.29	.06	1.17595	.01199	.385	.584	.09	26.6
252.-258.	26	M2	33.71	.07	1.18260	.00241	.329	.117	.67	16.8
262.-267.	17	L2	.54	.05	1.05651	.09019	2.035	4.894	.06	160.2
271.-274.	9	S2	16.27	.07	1.17624	.00523	-.493	.255	.26	-32.1
275.-2X5.	38	K2	4.12	.07	1.21684	.01975	-.391	.930	.19	-8.3
327.-375.	17	M3	.36	.03	1.12623	.09340	-9.018	4.748	.06	-75.7
382.-382.	1	S3	.28	.03	2.80440	.32376	70.777	6.613		
455.-455.	1	M4	.01	.02	.08090	.23433	-60.516	165.955		
491.-491.	1	S4	.06	.02	.59594	.23020	19.834	22.131		

R.M.S.ERROR M-ZERO 2.2281 MIKROGAL

R.M.S.ERROR FOR BANDS D 8.2244 SD 4.2261 TD 2.2318 QD 1.5930

O1/K1 1.0244 1-O1/1-K1 1.2116 M2/O1 1.0214

REFERENCE EPOCH 1993 1 1 .00 JULIAN DATE 2448988.50

Some estimation results given in Table 4 are graphicaly presented in Fig. 1 (deviations from model values) and in Fig. 2 (stability of the calibration coefficient). Calibration curves given in Fig. 2 were calculated by the method presented at the meeting of Working Group "Data Processing in Tidal Research" in Bonn - October 1984 [Chojnicki, 1985].

Table 4. Parameters for quality estimation of the results.

Parameter	Value		Remarks
	BN-17	112/R	
m_o	2.09 *ugal*	2.23 *ugal*	measurement accuracy
M_1	8.65 *ugal*	8.22 *ugal*	
M_2	2.98 *ugal*	4.23 *ugal*	
dm_{cv}	0.03 *ugal*	0.26 *ugal*	calibration stability
e_{M4}	0.44	2.90	
a.f. S1	19.60	8.20	temperature insensivity
$1/e_{S4}$	8.10	2.59	
m_{sen}	0.033	0.010	
m_{ins}	0.006	0.002	measurement accuracy

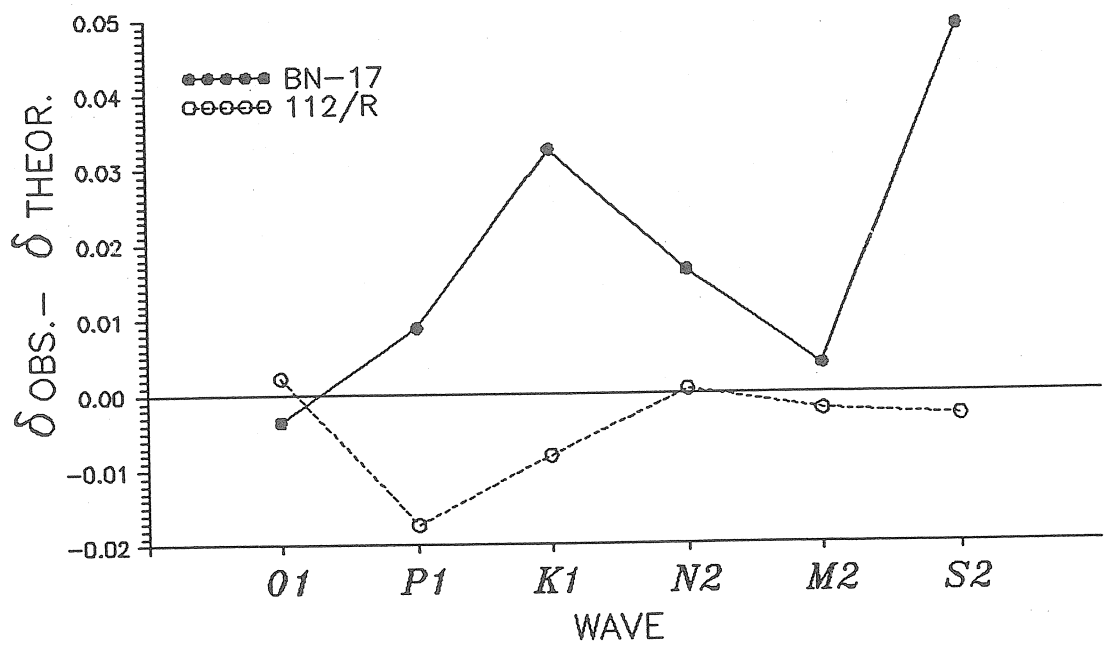

Fig. 1. Deviations of amplitude factors from model values

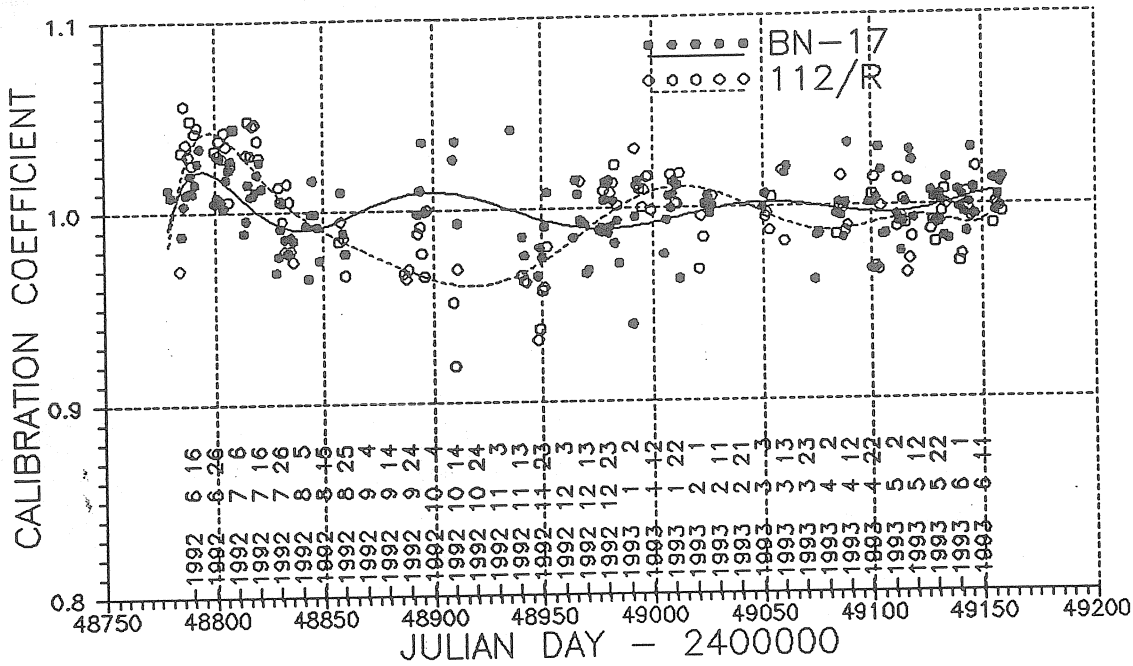

Fig. 2. Stability of calibration

In Table 4 smaller values of parameters indicate better results of the given quality features in "Remarks". Based on this table and Figs. 1 and 2, it may be concluded that the value of reconstruction in both types of the gravimeter is similar. However, are two features distinguish these types of the gravimeter: BN-17 seems to be more temperature sensitive [Wenzel. 1975] then 112/R, but its calibration coefficient is slightly more stable than that of 112/R.

Fig. 1 shows that for gravimeter BN-17 amplitude factors of temperature-sensitive waves are on increase while the ones for the 112/R are on decrease. Opposite signs of temperature influence in both ravimeters are also confirmed by the fact that the difference between phase lags obtained for S1-waves from both instrument is about 180^{o} (exactly $156^{o} \pm 4^{o}.5$, s. Table 2 and 3).

It cannot be excluded that some of the presented differences between the two gravimetersare partially due to an inherently different spring system of each gravimeter and not to the modification, or that before modification the technical state of gravimeter no. 110 (i. e. now BN-17) was worse than that of no. 112 (i. e. now 112/R).

References

Bonatz M., 1973, *Gezeiten registrierungen mit einem auf kapazitiven Abgriff umgerüsteten Askania-Gravimeter Gs-12,* Mitt. Inst. f. Theor. Geod. no. 22, Bonn.

Bonatz M., 1977, *Experiences and results from 20 transformed Askania-Gravimeters,* Proceed. of the 8th International Symposium on Earth Tides, Bonn, September 1977, 165-175.

Chojnicki T., 1977, *Sur l'analyse des observations de marees terrestres,* Ann. Geophys., 33, 1/2, 157-160.

Chojnicki T., 1984, *Results of gravimetric observations of Earth tides in 1980 - 1982 at the Warszawa station no. 0905,* Publs. Inst. Geophys. Pol. Acad. Sc., F-11 (173), 3-77.

Chojnicki T., 1985, *Determination of the shape of the calibration curve,* Bull. d'Inform. de Marées Terrestres, 94, 6312-6320.

Dittfeld H.-J., Neumeyer J., Schwahn W., 1985, *Recent developments at the Gravimetric Observatory Potsdam,* Proceed. of the 10th International Symposium on Earth Tides, Madrid, September 1985, 43-50.

Wenzel H.G., 1975, *Stability of temperature in a transformed Askania-Gravimeter,* XVI IUGG General Assembly, Grenoble 1975.

Wilmes H., 1975, *Systematische Fehler beim kapazitiven Abgriff BN,* Beiträge zur Erdgezeitenforschung, Veröff. Deutsche Geod. Komm., Reihe B, Heft 211, München.

Żarnowiecki W., 1975, *Observation stations for Earth tides in Poland,* Publs. Inst. Geophys. Pol. Acad. Sc., 94, 69-75.

ON THE ESTIMATION OF THE PRECISION OF THE TIDAL DATA.

J. Arnoso[1)], C. de Toro[1)], A.P. Venedikov[1,2,3)], R.Vieira[1)]

[1)] Instituto de Astronomia y Geodesia, Madrid
[2)] Geoforschungszentrum, Potsdam
[3)] Geophysical Institute, Sofia.

1. Introduction.

One of the impacts of the analysis method MV66 (Venedikov, 1966, Melchior et al., 1968, Melchior, 1981) on the tidal investigations was a new estimation of the precision. Somewhat surprisingly, it has been shown, through MV66, that the precision is considerably lower (up to 10 times) than it has been earlier estimated (Lecolazet, 1958). MV66 has also shown that the precision is frequency dependent, lower for low frequencies, i.e. the D tides, and higher for the high frequencies, i.e. the SD and TD tides.

The estimates of Lecolazet (1958) have been obtained under the implicit assumption that the noise is WN (white noise). Actually, the noise, mainly due to meteorological influences, is a correlated or coloured noise (CN), having different power at different frequencies. This has been taken into account by MV66 due to which we have got a less optimistic but more realistic knowledge of the precision.

The method of Chojnicki (1973) has initially estimated the precision under the same assumption for a WN. The result was (Wenzel, 1976a,b, 1977) an overestimated (too high) precision. In this relation Wenzel has suggested a method for a more realistic frequency dependent estimation of the precision based on a Fourier analysis of the residuals. This way of estimation has been applied by Chojnicki (1978) as well as by the ETERNA program (Wenzel, 1994a,b).

Finally, all methods mentioned above, including the new versions of MV66 (Ducarme, 1975, Venedikov et al, 1995), provide similar estimates of the precision. In our opinion, the estimates of Chojnicki and Wenzel have not a good enough theoretical motivation. Nevertheless, they can be accepted as realistic, as far as they remain very close to the estimates of MV66.

In (Toro et al., 1993, here and further referred as DAD, the name of the corresponding computer program) has been developed a method for direct analysis of hourly tidal data. Unlike Chojnicki and MV66, as well as the usual applications of ETERNA, DAD is proceeding an analysis of hourly data without any filtration.

The theoretical advantage of a direct analysis is clear - it is always recommendable the MLS (Method of the Least Squares) to be applied on original data. Another one is that the direct processing allows the computation of residuals at any time, including in real time. The latter is allowing, in principle, to look for anomalies in real time, which can be precursors of earthquakes and volcanos. It is also allowing a prediction in real time of both the tidal signal and the drift. This can be interesting for ocean tide prediction in situations of strong winds and changes of the air pressure.

If filtered data are analysed, using filters of length n, we are not able to compute residuals at n/2 or (n-1)/2 points before and after every gap. Still more important deficiency of the filtered data is that the computation of the residuals should stop n/2 hours before the end of the record, i.e. this cannot be done in real time. Since the drift is eliminated, a prediction including the drift is not available. All this gives serious advantages of DAD.

In the same time, since the covariance matrix of the data is not known, DAD has been obliged to apply the false hypothesis of WN, thus providing too low MSD (mean square deviations) compared to the realistic MSD of the methods mentioned above.

In a recent development of DAD we have included 3 ways of estimation of the precision without the assumption of a WN, which will be discussed in the following Sections. Some comparisons are made with MV66 and ETERNA, the latter being a generalization of the method of Chojnicki. Unfortunately, out of our attention is the interesting Japanese analysis method (Tamura et al. 1991, Ishiguro et al., 1983).

2. The problem of the estimation of the precision when there is a CN.

In Figure 1.a. is given a sample of 800 points of a simulated Gaussian WN w_t, $t = 1,2,...n$ with $Var(w_t) = \sigma^2 = 1$. This series has been created in order to make experiments with it as a noise of n = *18000* hourly tidal data.

In Figure 1.b. is given the spectrum of the whole series of w_t, i.e. w_t in the frequency domain. The spectrum is represented by the quantity

(1) $S(\omega) = h(\omega)(n/4)½ = [p(\omega)(n/2)]^{½}$ for $\omega = \omega_j = 2\pi j/n$, $j = 0, 1, 2, \ldots n/2$.

Here $h(\omega)$ is the amplitude and $p(\omega)$ is the power of the noise w_t at frequency ω (here and further under "frequency" we understand angular frequency or velocity).

Obviously, $h(\omega)$ and $p(\omega)$, as well as $S(\omega)$, are characteristics of the effect of the noise at frequency ω. In this sense, the spectrum in Figure 1.b. shows that the effect of w_t is, approximately, one and the same at all frequencies w. This is also a demonstration of the well known fact that the WN has theoretically one and the same power over all frequencies.

More generally, the effect of any kind of noise w_t at frequency ω, can be characterized by

(2) $$L(\omega) = [E(S^2(\omega))]^{½}$$

which can be considered as a theoretical level of the noise at frequency ω.

If w_t is a WN, it can be shown that

(3) $$L^2(\omega) = Var(w_t) = \sigma^2 = 1$$

i.e. w_t or, generally, a WN, has a constant variance in both time and frequency domains.

We shall simplify the real picture of the theoretical tidal spectrum by supposing that some of the ω_j defined by (1) are the tidal frequencies. Then any application of the MLS, making the assumption of a WN, will estimate the variance σ^2, respectively the standard σ, by the MSD s computed through

(4) s^2 = the mean of $S^2(\omega_j)$ for all non-tidal frequencies ω_j.

From Figure 1.b. is easy to state that we shall certainly get, in this way, a reasonable MSD, very close to $s = 1$.

In Figure 2.a. is given a sample of a simulated correlated stationary noise CN z_t, $t = 1,2,...n = 18000$ and, in Figure 2.b., the spectrum $S(\omega)$ of z_t, defined in the same way as above

for w_t. The CN z_t is obtained as MA process using 18047 values of the simulated WN w_t. Namely, z_t is computed through

(5) $z_t = f_0 w_t + f_1 w_{t-1} + ... + f_{47} w_{t-47}$ where $f_\tau = c(48 - \tau)(3\cos 15^0\tau + \cos 30^0\tau)$,

c being a normalizing coefficient such that

(6) $$Var(z_t) = Var(w_t) = \sigma^2 = 1.$$

Unlike (3), now

(7) $$L^2(\omega) = E(S^2(\omega)) = r^2(\omega)\sigma^2 .$$

where $r(\omega)$ is the response of the filter f_τ defined in (5) and $\sigma^2 = 1$.

Now we have a frequency dependent theoretical level of the noise represented by Figure 2.c. Both $L(\omega)$ and $S(\omega)$ show an accumulation of energy (or power) at the D domain (around $\omega = 15^0$) as well as at the SD domain (around $\omega = 30^0$), like the noise of the real tidal data. In this case we have a constant variance in the time domain, like in the case of the WN, but a variable variance in the frequency domain.

Let us suppose that such a CN is processed by the MLS as a WN, i.e. the precision is estimated according to (4). Due to the theorem of Parseval we shall get an MSD approximately equal to $s = 1$. Obviously, with respect to the higher level of the noise at the D and SD domains, an MSD $s = 1$ is too low.

3. Estimation of the precision by DAD using noisy waves.

We would get reasonable MSD if they are frequency dependent and computed using

(8) $s^2(D)$ = *mean of* $S^2(\omega)$ *for non-tidal* ω *in the D domain, near* 15^0
$s^2(SD)$ = *mean of* $S^2(\omega)$ *for non-tidal* ω *in the SD domain, near* 30^0
$s^2(TD)$ = *mean of* $S^2(\omega)$ *for non-tidal* ω *in the TD domain, near* 45^0
$s^2(LP)$ = *mean of* $S^2(\omega)$ *for non-tidal* ω *in the LP domain, under* 15^0

instead of (4).

As known and shown in Figure 3, the tidal spectrum is a line spectrum. The lines are concentrated in some bands, which are the basis to create the tidal groups used by MV66, as well as by other methods of analysis. Between the bands are intervals with non-tidal frequencies at which theoretically and practically the tidal signal has zero power. Hence, the power which can be observed at these frequencies is entirely due to the noise. If we can estimate this power, through it we can estimate the precision according to (8).

Following this idea DAD can deal, during the analysis, with a set of waves called NW (noisy waves). The frequencies of the NW are selected between the tidal bands as shown in Figure 3. The NW have unknown amplitudes and phases, estimated together with the parameters of the tidal waves.

Generally, the computation scheme is the following.

Let the observation equations used by the analysis, without any NW, are $\boldsymbol{Ax} = \boldsymbol{y}$, where $\boldsymbol{y}$ is a vector of observations, $\boldsymbol{A}$ is a known matrix and $\boldsymbol{x}$ is a vector of unknowns. This means that $\boldsymbol{Ax}$ is representing the tidal signal and, in DAD, the drift. If the NW are to be considered, the observation equations become

(9) $$Ax + Bu = y$$

where Bu represents, say, k NW, u being composed by $2k$ elements related with unknown amplitudes and phases of these waves.

DAD determines the estimates of x according to the initial equations $Ax = y$, through $x = (A^TA)A^{-1}\ y$. Thus the tidal parameters are obtained unaffected by the NW. This is important because the inclusion of Bu can make (A^TA) less stable.

Then B, as well as u are transformed in the following way

(10) $$C = (B - A\ (A^TA)^{-1}\ A^TB)T \quad and \quad v = T^{-1}u$$

where T is an upper triangular matrix such that $C^TC = I$ (identity matrix). After that we get the MLS estimates of v through

(11) $$v = C^Ty.$$

It is essential that Cv is a vector orthogonal to A, having $2k$ degrees of freedom. Due to this, the quantity

(12) $$s^2 = (Cv)^T(Cv)/2k = (\ v^Tv)/2k$$

is an estimate of the variance of the data y, i.e. s is an MSD, having 2k degrees of freedom.

In DAD the term Bu is actually

(13) $$Bu = B_0u_0 + B_1u_1 + B_2u_2$$

where the subscript l of B_lu is l 0, 1 or 2 corresponding to the NW in the LP, D and SD domains. Through v_l, using (12), we get different estimates at the LP, D and SD frequencies. Special estimation for the TD domain is not made. At these frequencies is accepted that the MSD obtained under the conception of WN are good enough.

4. Estimation of the precision by DAD through analysis of residuals.

This option is similar to the estimation of the precision used by ETERNA. After the analysis the hourly residuals are submitted to a Fourier analysis. From the power of the residuals at one or another frequency domain we get corresponding frequency dependent MSD. As far as the residuals are free of tidal signals, this technique can be considered as a variant to apply the expressions (8).

We do not dispose by details about the procedure used by ETERNA, especially how it proceeds when the data have gaps.

In DAD, since the data have almost always gaps, we have developed a simple algorithm for Fourier analysis of such data, without interpolations. This was an easy task because we are interested only in the power at very few frequencies ω, mainly at $\omega = 15^0, 30^0$ and 45^0.

The data are subdivided into intervals of length m hours, where m is a multiple of 24, e.g. $m = 48$. The intervals are without overlapping, without gaps in the intervals. If there are some gaps, they remain between the corresponding intervals.

The non-zero Fourier frequencies corresponding to intervals of length m are

(14) $\omega_j = 180^0 j/n,\ j = 1, 2, \ldots n/2,$

e.g., for $m = 48,$

$\omega_j = 7.5^0, 15.0^0, 22.5^0, 30.0^0, 37.5^0, 45.0^0, \ldots 180^0.$

Since m is multiple of 24, the set of ω_j will always include the D, SD and TD frequencies

(15) $\omega = 15.0^0, 30.0^0,$ *and* $45^0.$

We shall denote by $S(D)$, $S(SD)$ and $S(TD)$ the values of $S(\omega)$ defined by (1) corresponding to the frequencies (15).

DAD computes $S(D)$, $S(SD)$ and $S(TD)$ for every interval, then

(16) $s^2(D) =$ *mean of* $S^2(D)$ *for all intervals*
$s^2(SD) =$ *mean of* $S^2(SD)$ *for all intervals*
$s^2(TD) =$ *mean of* $S^2(TD)$ *for all intervals.*

The quantities s thus obtained are accepted as MSD corresponding to the D, SD and TD tidal domains. For frequencies higher than TD the MSD at TD is accepted.

If $m = 24$, the MSD for the LP is accepted to be equal to $s(D)$. If $m > 24$, then MSD is obtained as s above but corresponding to the frequency $\omega = 7.5^0$.

5. A more simple but more correct estimation of the precision.

The above Sections 3 and 4, as well as the technique applied by Chojnicki and Wenzel, show that the processing of hourly data needs special sophisticated methods for estimation of the precision which can never be equivalent to a correct MLS estimation. In the same time we dispose by correctly defined MLS estimations of the precision made by MV66, justified by a huge experimentation.

In this relation, DAD is also applying a third way of estimation of the precision which, we believe, can be recommended to all methods of tidal analysis. It consists in the following stages.

(i) The data are processed by MV66, e.g. by the program NSV (Venedikov et al., 1995) which provides the MSD at the main tidal frequency domains.

(ii) The data are processed by DAD, the precision of the tidal parameters being estimated using the MSD provided by the stage (I).

6. Some results using model data.

In Tables 1 and 2 are given the MSD (estimation of the standard s) obtained using various methods and variants of analysis.

The variants used are:

DADNW: method DAD using noisy waves (Section 3);
DADFA: method DAD using Fourier analysis of residuals (Section 4);
ET49, ET51, ET239: method ETERNA using filters of length 49, 51 and 239 respectively;
V36, V40, V44, V48, V52: MV66, using filters of length 36, 40, 44, 48, 52 respectively.

Generally, it seems that all results are satisfactory. An exception is the case ET49 which provides too high values for the D frequency for both cases of WN and CN. Another exception is the case V36 which has too low values in the case of the CN in Table 2.

Acknowledgments

The work of one of the authors (Venedikov) on this paper has been supported mainly by the Consejo Superior de Investigaciones Cientificas of Spain and partly by the GeoForschungsZentrum Potsdam.

References:

(BIM = Bulletin d'Information des Marees Terrestres, editeur P.Melchior)

Chojnicki, T., 1973. Ein verfahren zur Erdgezeitenanalyse in Anlehnung an das Prinzip der kleinsten Quadrate, Mitt. Inst. Theor. Geodaesie Univ. Bonn, Nr 15.

Chojnicki, T., 1978: Supplementary precision estimation of results of tidal data adjustment, BIM 78, 4670-4675.

Ducarme, B., 1975: The computation procedures at the International Center for Earth tides, BIM 72, 4156-4181.

Ishiguro, M., Akaike, H.,Ooe, M., & Nakai, S., 1983. A Bayesian approach to the analysis of Earth tides, Proc. 9th Int. Symp. Earth Tides, New York 1981, Schweizerbart'sche Verlangsbuchhandlung, Stutgart, 283-292.

Lecolazet, R., 1958: L'influence des erreurs accidentelles dans l'analyse harmonique. Obs. R. Belg., Comm. 142, S. Geoph. 47.

Melchior, P., 1978, sec. edition 1981: The tides of the planet Earth, Pergamon press, Oxford, Chapter 7, 161-191.

Melchior, P., Venedikov,A.P.,1968: Derivation of the wave M3 (8 279) from the periodic tidal deformations of the Earth. Physics Earth Plan. Interiors, vol. 1, 363-372.

Schueller, K., 1977, Tidal analysis by the Hybrid Least Squares frequency domain convolution method, 8th Int. Symp. Earth Tides, Bonn.

Tamura, Y., Sato, T., Ooe, M., & Ishiguro, M., 1991. A procedure for tidal analysis with a Bayesian information criterion, Geophys. J. Int., 104, 507-516.

Toro C. de, Venedikov A.P., Vieira R., 1993: A new method for Earth tide data analysis. BIM, 116, 8557-8586.

Venedikov,A.P.,1966: Une methode d'analyse des Marees terrestres a partir d'enregistrements de longueurs arbitraires, Acad. Royal de Belgique, Bull. Cl. Sci., 5e S., t. LIII, fasc. 3, Communications de l'Observatoire Royal de Belgique, S. Geoph. No 71. 463-485.

Venedikov, A.P., Vieira, R., Toro, C. de, 1995: The computer program NSV used in Madrid for tidal data processing. BIM 121, 9108-9126.

Wenzel, H.-G., 1976a: Some remarks to the analysis method of Chojnicki. BIM 73, 4187-4191.

Wenzel, H.-G., 1976b: Zur Genaugkeit von gravimetrischen Erdgezeiten - beobachtungen. Wissenschaftlichen Arbeiten der Lehrsttuele ftr Geodaesie, Photogravimetrie und Kartographie, Technishen Universitaet Hannover, 67.

Wenzel, H.-G., 1977: Estimation of accuracy for the earth tide analysis results, BIM 76, 4427-4445.

Wenzel, H.-G., 1994a: Earth tide analysis package ETERNA 3.0., BIM 118, 8719-8721.

Wenzel, H.-G., 1994b: ETERNA - an Earth tide analysis program package for the personal computer, preprint, submitted to Bulletin Geodesique, January 1994.

Table 1. Estimation of the precision of the white noise w_t (Figure 1)

Tidal species		D	SD	TD	QD
Theoretical level of the noise		1.00	1.00	1.00	1.00

programs	variants				
DD	DADNW	1.06	1.03	1.06	
	DADFA	1.00	0.99	1.01	0.97
ETERNA	ET49	1.20	1.07	0.99	1.20
	ET51	0.98	1.02	1.00	1.16
	ET239	1.03	1.07	0.96	1.18
NSV	V48	1.00	1.00	1.02	1.00
	V36	1.01	1.04	1.04	1.01
	V40	0.99	1.00	1.00	0.99
	V44	0.98	1.00	1.03	1.04
	V46	0.99	0.98	1.00	1.04

Table 2. Estimation of the precision of the stationary noise z_t (Figure 2)

Tidal species		D	SD	TD	QD
Theoretical level of the noise		3.08 - 3.99	0.93 - 1.81	0.65 - 0.84	0.47 - 0.52

programs	variants				
DD	DADNW	2.63	1.31	0.78	
	DADFA	3.26	1.54	0.80	0.52
ETERNA	ET49	4.50	1.58	0.70	0.57
	ET51	3.68	1.49	0.71	0.55
	ET239	3.86	1.55	0.69	0.56
NSV	V48	3.30	1.45	0.77	0.51
	V36	2.90	1.10	0.64	0.47
	V40	3.13	1.45	0.73	0.47
	V44	3.25	1.43	0.79	0.52
	V46	3.35	1.52	0.73	0.47

Figure 1.a. Sample of simulated Gaussian white noise (time domain)

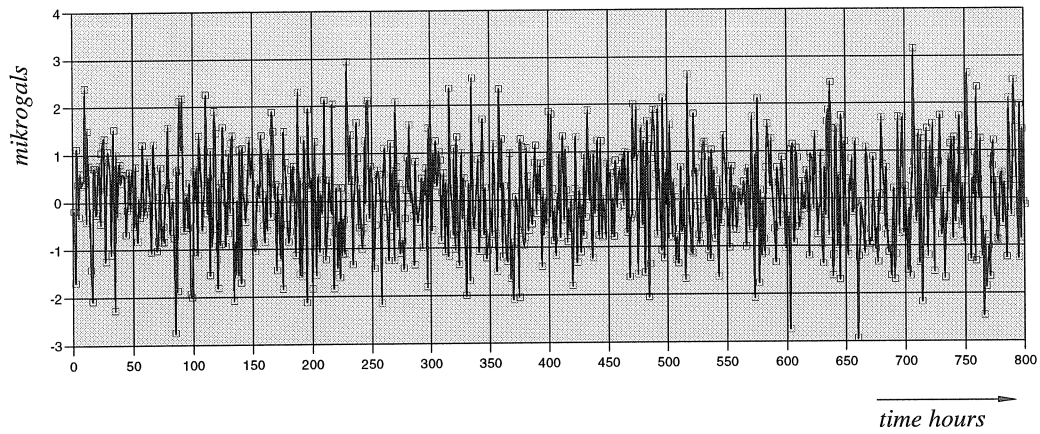

Figure 1.b. Energy spectrum of the simulated white noise (frequency domain)

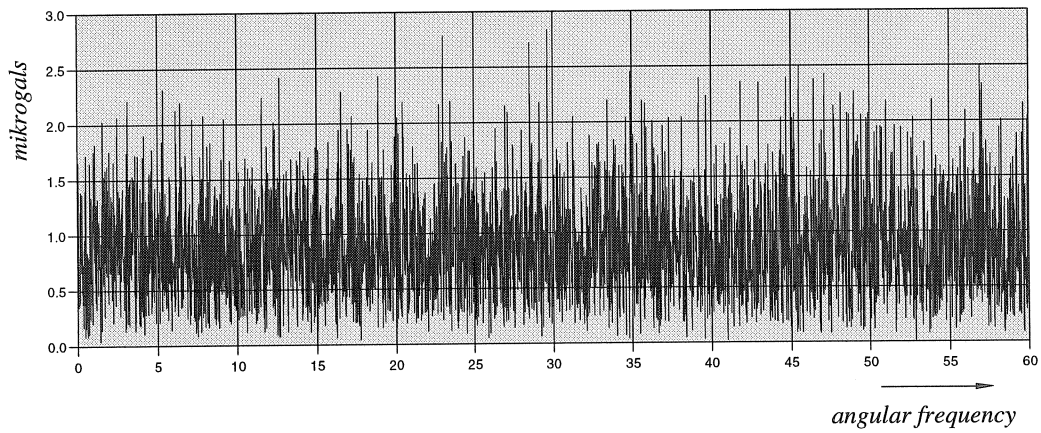

Figure 2.a. Simulated correlated Gaussian noise obtained as an MA process

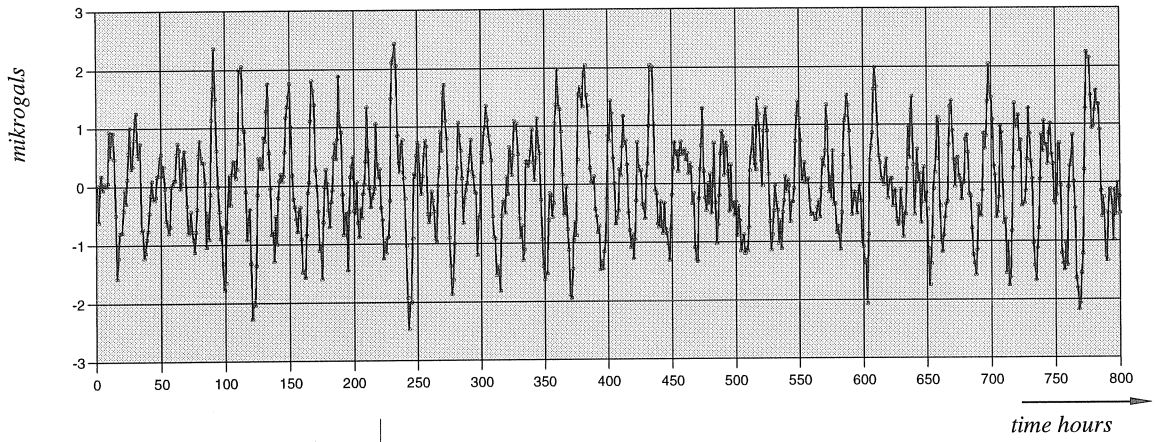

Figure 2.b. Energy spectrum of the correlated noise

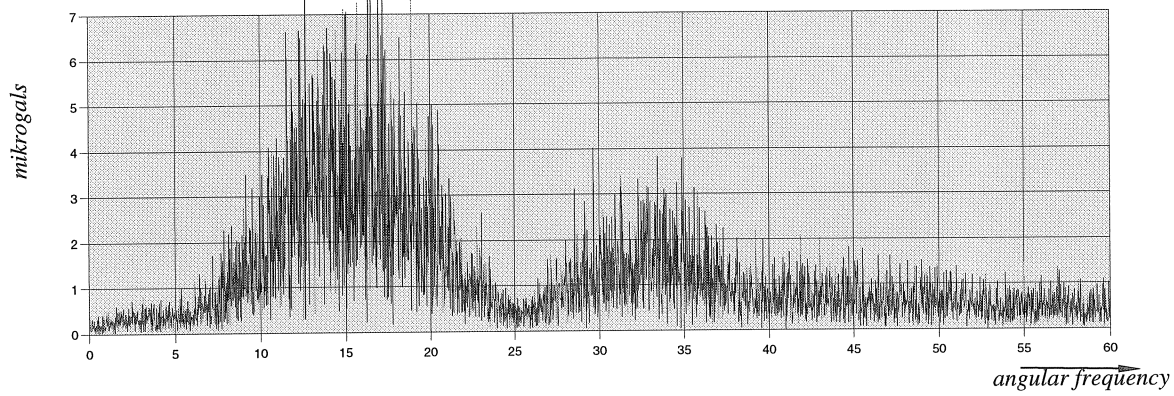

Figure 2.c. Response of the filter used or theoretical level of the noise

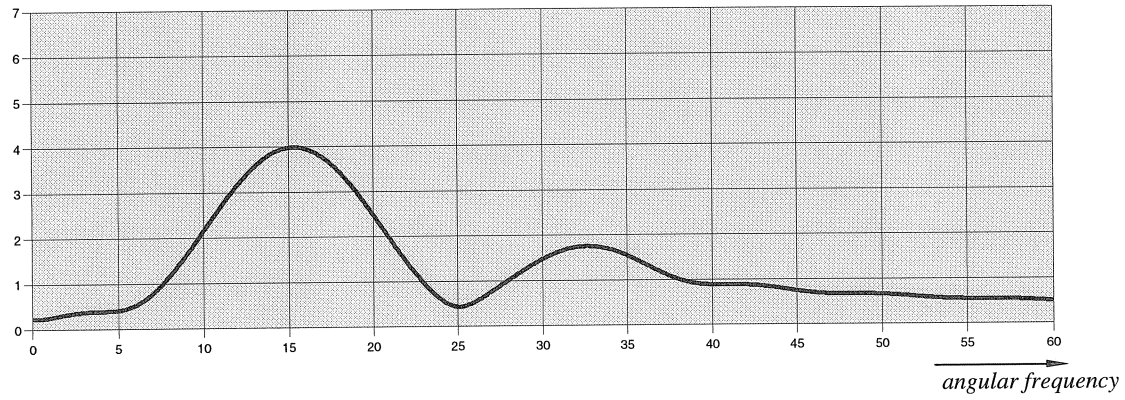

Figure 3. Tidal spectrum and distribution of the noisy waves NW used for the estimation of the precision

Long period (LP) tides

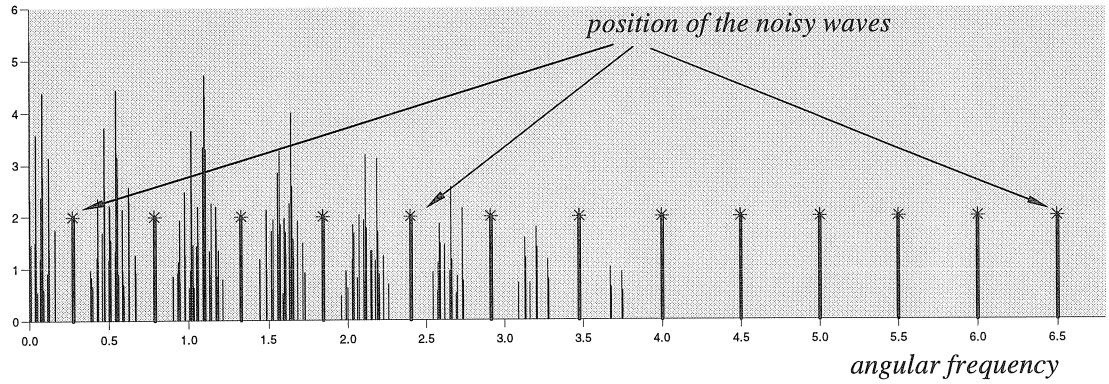

Diurnal (D) tides

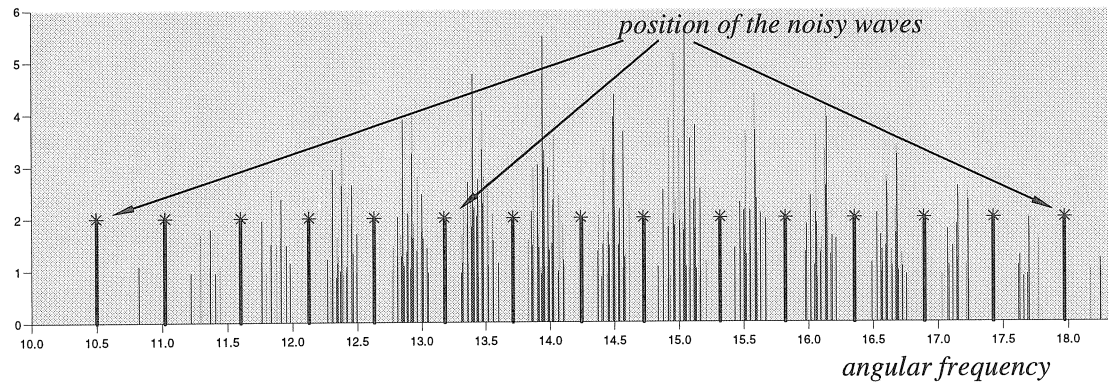

Semidiurnal (SD) tides

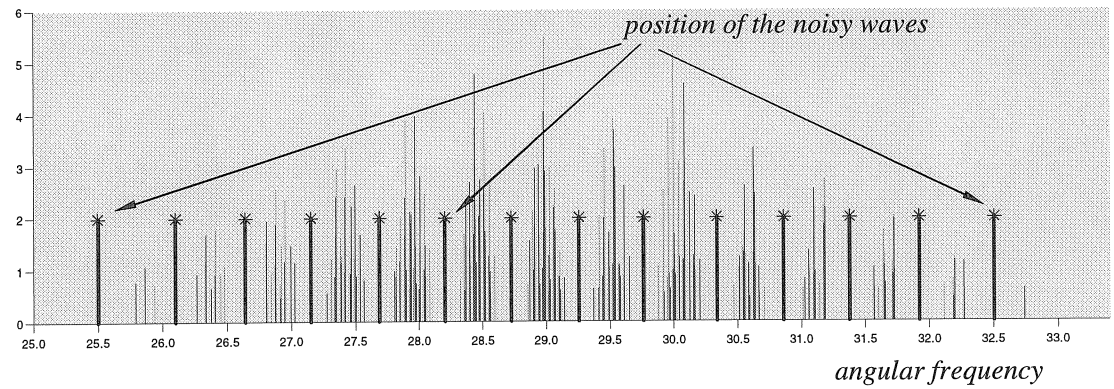

Tidal Influences on VLBI

Harald Schuh
Deutsches Geodätisches Forschungsinstitut (DGFI), Abt. I
Marstallplatz 8, 80539 München, Germany, (schuh@dgfi.badw-muenchen.de)

Rüdiger Haas
Geodätisches Institut der Universität Bonn (GIUB)
Nußallee 17, 53115 Bonn, Germany, (haas@uni-bonn.de)

Abstract The paper gives an overview about all effects related to the tides which have to be taken into account in modern space geodetic techniques. Solid Earth tides and ocean tides cause deformations of the Earth and influence the Earth's rotation. Corresponding to the precision of VLBI measurements a very high accuracy of the tidal models is required to avoid apparent diurnal signals in the results. Parameters of ocean loading models and of atmospheric loading models can be determined significantly by VLBI. The results generally confirm the existing theoretical models but also give some indications for deficiencies of the current global models at some locations on the Earth.

1 Introduction

The tides due to gravitational attraction of the Sun and the Moon cause deformations of the solid Earth and influence the Earth rotation parameters (ERPs). In 1989, SCHUH specified all effects related to the tides which have to be taken into account in today's high precision geodetic observing techniques, such as Very Long Baseline Interferometry (VLBI), Global Positioning System (GPS), Satellite Laser Ranging (SLR), Lunar Laser Ranging (LLR) and others. This paper will give an overview about the 'state of the art' of tidal modelling in modern space techniques, and the models applied in VLBI data analysis will be presented. Over the last decade the precision of the VLBI delay measurements has been increased at least by the factor 2 and is by far better than the accuracy of the models used for VLBI data analysis. Thus, refined models for the tidal influences had to be implemented into the VLBI data analysis software. This has been done to reduce the postfit residuals and – even more important if tidal displacements are considered – to avoid a propagation of errors of the tidal models into the Earth rotation parameters. Today, these parameters can be determined by VLBI with a high, i.e. subdaily, resolution. Finally, it will be shown that from VLBI data, parameters of the tidal and loading models can be determined and be used to validate and/or to improve the theoretical models.

2 Influences of the tides on deformation and rotation of the Earth

In the following chapter, a brief overview will be given about all tidal influences which have to be considered when analyzing modern space geodetic data. Deformations of the Earth which occur either during an observing session or between two observation periods change the geometry of the station network. Variations of the Earth rotation parameters influence the orientation of the network with respect to the quasi-inertial reference system of extragalactic radio sources. It will be shown which tidal influences are considered in one of the most prominent VLBI software packages, the CALC/SOLVE data analysis system [MA, 1990].

2.1 Solid Earth tides

The theoretical model for the displacements due to the solid Earth tides is described by HAAS and SCHUH [this issue, 1997]. The present standard version of the CALC/SOLVE VLBI software follows the International Earth Rotation Service (IERS) Standards [MCCARTHY, 1992] that recommend a simplified version of a theoretical model for an elastic Earth by WAHR [1981]. The IERS 1992 model

includes only second degree tides. The frequency dependence of the solid Earth tides due to the Free Core Nutation (FCN) resonance is taken into account for the K_1-tide for the radial displacements. However, the tangential displacements are not corrected for frequency dependence. There are several other tidal waves close to the FCN resonance for which the IERS Standards [1992] do not include frequency dependent second degree Love and Shida numbers h_{21} and l_{21}. In a recent paper [HAAS and SCHUH, 1996] it was shown that the differences between a more complete frequency dependent solid Earth tide model (43 additional diurnal terms, radial and tangential) and the model of the IERS Standards [1992] amount to $\pm$ 5 mm and cannot be neglected any more in present space geodetic data analysis.

New harmonic developments of the tide generating potential published by TAMURA [1987], HARTMANN and WENZEL [1995], ROOSBEEK [1996] consider the contributions of the Moon and the Sun up to a degree higher than two. Indirect planetary effects and direct planetary effects are also accounted for. There are very small differences for the tidal station displacements of less than $\pm$ 0.03 mm, depending on the choice of the harmonic expansions of the tidal potential to account for the frequency dependence of the Love and Shida numbers. Small shifts in the FCN period by a few days will only marginally influence the modeled tidal station displacements.

The solid Earth tides also influence the rotation of the Earth. Variations of the Earth's rotation caused by the tidal deformation of the polar moment of inertia have been theoretically derived by several authors, e.g. WOOLARD [1959], YODER et al. [1981]. The periods and phases of the fluctuations of Universal Time (UT1) are well determined by the motions of the Moon and the Sun, but the amplitudes are less certain because of the imperfections in the model for the tidal deformations of the liquid core and the oceans and because of the probable inelasticity of the Earth's mantle. The CALC/SOLVE VLBI software contains the model by YODER et al. [1981].

2.2 Ocean tides and ocean loading

As a secondary tidal effect the solid Earth is deformed – mainly elastically – under the load exerted on the Earth's crust by the oceanic tides. The observable components of the deformational response, e.g. the displacements of surface points, are subsumed under the term 'ocean tidal loading effects'. The uplift or subsidence of the Earth due to ocean tidal loading is generally of the order of a few centimeters. However, for stations near coastlines or on islands the size of the effect can be one order of magnitude larger. In geophysical models the deformation of the terrain, i.e. the displacement of the station is a function of the ocean tide heights, the areal shape and depth of the oceans, and the rheology of the oceanic and continental lithosphere between the loading masses and the station on the solid Earth. The general statements concerning ocean loading models which were given by SCHUH [1989] are still valid. A recent computation of ocean loading parameters by SCHERNECK [1995] is based on new ocean tide maps obtained by LE PROVOST et al. [1994] from a finite element ocean tide model. The present CALC/SOLVE VLBI software contains the model by SCHERNECK [1991], which is based on the SCHWIDERSKI [1979] tidal maps for the eleven dominant ocean tide components.

Oceanic tides and ocean currents cause also variations of the Earth rotation parameters due to the asymmetric distribution of the oceans. These fluctuations in Earth rotation are qualitatively different from the ones caused by solid Earth tides. Hydrodynamical models of the dominant ocean tides have been evaluated first by BROSCHE et al. [1989] to determine the angular momentum of the oceans. The oceanic tidal angular momentum (OTAM) consists of two parts: the first part due to relative motions of the water represented by tidal currents and the second part due to the changing tensor of inertia connected with the tidal height variations. Both contributions and their sum can be represented by a sinusoidal wave in dependence on the total phase. The polar component of OTAM excites variations of UT1, the equatorial components of OTAM cause periodic polar motion. Theoretical models of the latter have been published by WÜNSCH and SEILER [1992] and by SEILER and WÜNSCH [1995]. In the last years several authors used VLBI data to compute 'empirical' models for the periodic variations

of UT1 and of polar motion due to the ocean tides. A recent paper by CHAO et al. [1996] gives an overview about the different existing models for the diurnal and semidiurnal variations of the Earth rotation parameters.

2.3 Atmospheric tides and atmospheric loading

Air pressure lows and highs (cyclones and anticyclones) can be regarded as time dependent loading on the Earth's surface. According to their geometry they generate large-scale deformation fields with some hundred up to some thousand kilometers wavelength. Due to the velocity of the passing (anti-) cyclones, the periods of the loading function are between a few days and some weeks. There is also a diurnal pressure variation corresponding to the solar S_1 tide, resonances with other diurnal tides and an annual period of the global air pressure distribution. Such air pressure anomalies can cause vertical displacements in the centimeter range and horizontal displacements in the millimeter range. Theoretical studies have been published by RABBEL and ZSCHAU [1985], RABBEL and SCHUH [1986], VANDAM and WAHR [1987] and MANABE et al. [1991]. An atmospheric loading model is not included in the standard version of the CALC/SOLVE VLBI software.

The atmospheric excitation of the Earth's rotation is a well known effect since many years and has been investigated by several authors. Very comprehensive overviews were given by EUBANKS [1993] and DICKEY [1993].

2.4 Tidal corrections in the IERS Conventions (1996)

The new IERS Conventions [MCCARTHY, 1996] contain several improved models for the tidal corrections compared to the former IERS Standards [MCCARTHY, 1992]. This includes tidal effects on the geopotential needed for satellite techniques which have not been covered in this paper. It is recommended to implement the new or modified models in all software packages used for space geodetic techniques when highest accuracies are required.

3 Improved deformation models for VLBI data analysis

In a detailed study by HAAS [1996], improved models for the deformation due to solid Earth tides and due to oceanic and atmospheric loading were introduced into the CALC/SOLVE VLBI software. For the solid Earth tides and for ocean loading these models agree or are very similar to those given in the new IERS Conventions [1996]. Solid Earth tides were modeled using the harmonic expansion of the tide generating potential by TAMURA [1987] and the resonance model for Love and Shida numbers by WAHR [1981]. The FCN resonance period was set to 434 days, a value determined empirically by gravity analyses [DEFRAIGNE et al., 1994]. The frequency dependence was applied for radial and tangential components, and third degree tides were considered, too. For ocean loading the model SCHERNECK [1995] was taken, i.e. based on the ocean tide model by LE PROVOST [1994], and additionally to the 11 model tides ocean loading contributions for 308 interpolated tides were computed using admittance functions and the harmonic expansion of the tide generating potential by TAMURA [1987]. For the site dependent pressure responses a model was applied which considers the diurnal pressure variations with respect to the daily mean and the annual pressure variations with respect to the annual mean. The amplitudes of local and mean annual atmospheric pressure variations can easily be obtained from VLBI experiments. With the refined deformation models the standard deviation of a usual VLBI solution was reduced by up to 12 %. Even more important is the periodic signal in the differences "old"-"new" of 3-hourly Earth rotation parameters (x_p, y_p, UT1-UTC). "Old" means the results of a VLBI solution using the standard CALC/SOLVE package based on the old IERS standards [1992]. "New" means the results of a similar VLBI solution carried out with a new version of CALC/SOLVE which contains the refined models. As an example figure 1 shows the differences

"old"-"new" for the pole components. There is a clear diurnal period in the differences, i.e. in former VLBI solutions, errors of the models for tidal corrections propagated into the ERPs.

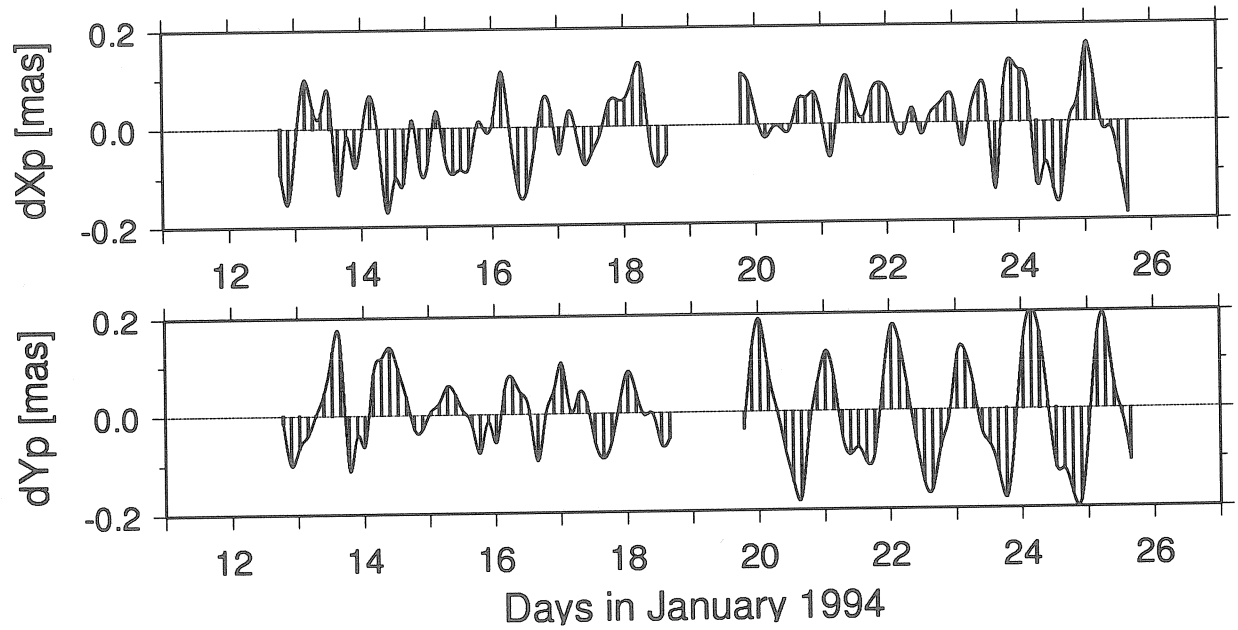

Figure 1: Differences "old"-"new" for 3-hourly pole components x_p and y_p. In both components, differences with diurnal and semidiurnal periods are clearly visible.

4 Tidal and loading parameters determined by VLBI

Several parameters of the solid Earth tide model could be determined with unprecedented accuracy by VLBI as shown in the paper of HAAS and SCHUH [this issue, 1997]. This offers the chance to validate or to improve the theoretical tidal model not only by gravity measurements but also by modern space techniques. It will be demonstrated below that from VLBI data also parameters of the ocean loading model and of the atmospheric loading model can be estimated.

4.1 Ocean loading parameters

In all ocean loading models the time dependent displacement vector $\Delta_O X_i$ in the local Up-East-North coordinate system (i=1, 2, 3) can be computed as a sum of the contributions of n individual ocean tides T where φ is the corresponding astronomical argument. The amplitudes A_{iT} and the Greenwich phase lag Φ_{iT} of each tidal component T are determined from global ocean tide models and loading Green's functions. The well-known frequencies and astronomical arguments of the four dominant semidiurnal tides (M_2, S_2, N_2, K_2) and the four dominant diurnal tides (K_1, O_1, P_1, Q_1) were used to calculate partial derivatives which were entered in a least squares analysis with the CALC/SOLVE VLBI data analysis software package.

$$\Delta_O X_i(t) = \sum_{T=1}^{n} A_{iT} \cos(\varphi_T(t) - \Phi_{iT}) \qquad (1)$$

About 725,000 VLBI delay observables obtained by different international VLBI networks from 1979 to 1995 (which is about 50 % of all geodetic VLBI data presently available) were combined for a 'batch solution'. In the batch solution station positions and velocities, radio source positions, daily Earth orientation parameters (i.e. x_p, y_p, UT1 and nutation corrections $d\psi$, $d\epsilon$), clock and atmosphere parameters and additionally eight loading amplitudes and eight phases were estimated for each of the VLBI stations Onsala (Schweden), Wettzell (Germany), Hartebeesthoek (South Africa), Fort Davis (Texas, USA), Gilcreek (Alaska, USA), Mojave (California, USA), Richmond (Florida, USA) and Westford (Massachusetts, USA). These are those radio telescopes which contributed most

of the observations to the global database. For all other stations and also for the smaller ocean tides, the loading parameters of the model SCHERNECK-SCHWIDERSKI [1991] or of the model SCHERNECK-LE PROVOST [1995] were entered. For both versions in comparison to a reference solution without loading parameters the square sum of the delay residuals reduces by 1527 ps^2, or by 3380 ps^2 respectively, for the additonal 128 degrees of freedom. The significance level of the improvement by the new solution is better than 99 %. As an example table 1 gives the ocean loading amplitudes and phases for Wettzell. Columns 1 and 2 contain the theoretical values computed by SCHERNECK [1991], based either on the SCHWIDERSKI [1979] ocean tide maps or on the ocean tide model by LE PROVOST [1994]. Our estimates from the VLBI solution and their scaled standard deviations are listed in columns 3, 4. The standard deviations from the least squares fit were scaled independently of the tidal frequencies, and they represent an inner accuracy, which is usually too optimistic by a factor 2-3. The results of the only similar VLBI solution published so far by SOVERS [1994] are given in column 5.

Table 1: Model values and VLBI estimates of ocean loading amplitudes A and phases P for Wettzell: 1 Model SCHERNECK-SCHWIDERSKI [1991], 2 Model SCHERNECK-LE PROVOST [1995], 3 VLBI estimates (this paper) based on a priori model SCHERNECK-SCHWIDERSKI, 4 VLBI estimates (this paper) based on a priori model SCHERNECK-LE PROVOST, 5 VLBI estimates by SOVERS [1994]

Wettzell	Tide		Model values M-a 1	Model values M-b 2	VLBI estimates V-a 3	VLBI estimates V-b 4	VLBI estimates V-c 5
	M_2	A [mm]	4,94	4,60	5,91 ± 0,31	6,30 ± 0,31	4,37 ± 0,4
		P [°]	291,0	289,1	287,2 ± 2,9	279,1 ± 2,7	306,9 ± 5,2
	S_2	A [mm]	1,43	1,60	1,49 ± 0,30	1,70 ± 0,30	0,73 ± 0,4
		P [°]	321,9	319,7	321,2 ± 11,7	316,9 ± 10,3	306,0 ± 31,5
	N_2	A [mm]	1,04	0,99	1,00 ± 0,31	1,03 ± 0,31	0,71 ± 0,5
		P [°]	273,1	269,0	311,1 ± 18,0	303,2 ± 17,5	264,9 ± 32,6
	K_2	A [mm]	0,34	0,44	2,12 ± 0,32	2,20 ± 0,32	0,72 ± 0,5
		P [°]	324,1	314,9	333,2 ± 8,4	332,1 ± 8,1	290,3 ± 39,7
	K_1	A [mm]	1,82	1,88	3,93 ± 0,41	3,69 ± 0,41	6,84 ± 0,7
		P [°]	301,7	303,7	211,4 ± 6,1	211,1 ± 6,5	354,1 ± 5,9
	O_1	A [mm]	0,77	1,06	2,84 ± 0,40	2,74 ± 0,40	1,65 ± 0,6
		P [°]	258,9	268,5	349,0 ± 7,9	352,3 ± 8,2	194,0 ± 20,8
	P_1	A [mm]	0,56	0,63	2,66 ± 0,40	2,70 ± 0,39	5,47 ± 0,6
		P [°]	300,3	299,8	132,2 ± 8,5	132,5 ± 8,4	170,2 ± 6,3
	Q_1	A [mm]	0,04	0,05	1,53 ± 0,40	1,50 ± 0,40	2,2 ± 0,7
		P [°]	247,8	251,5	82,6 ± 14,8	84,3 ± 15,1	118,5 ± 18,2

The results of the VLBI solution agree for all stations rather well with both of the models for the semidiurnal tides M_2, S_2 and N_2. The differences are usually less than 20 % of the amplitudes themselves and the phases agree within their double standard deviations. As a typical example, figure 2 shows the M_2 tidal loading amplitudes and phases at four VLBI stations. For the K_2 ocean tide, the loading parameters determined by VLBI are rather different from the theoretical models. This also holds for the diurnal tides K_1, O_1, P_1, Q_1. At almost all of the VLBI stations, the VLBI amplitudes exceed the theoretical amplitudes by the factor 1,5 - 4. It is still unclear, whether those amplitudes are underestimated in the theoretical models. Future VLBI solutions with a larger database, i.e. with more data covering a longer time span, will contribute to the validation of theoretical models. In the present study, the fit was slightly better, when the ocean loading model based on the ocean tide model LE PROVOST [1994] was used. As can be seen in figure 3, at some of the eight VLBI stations the standard deviations of the M_2 ocean loading phases based on the LE PROVOST [1994] ocean tide model are smaller than the ones based on the SCHWIDERSKI [1979] model. This trend is not always so clear for the other tides, however.

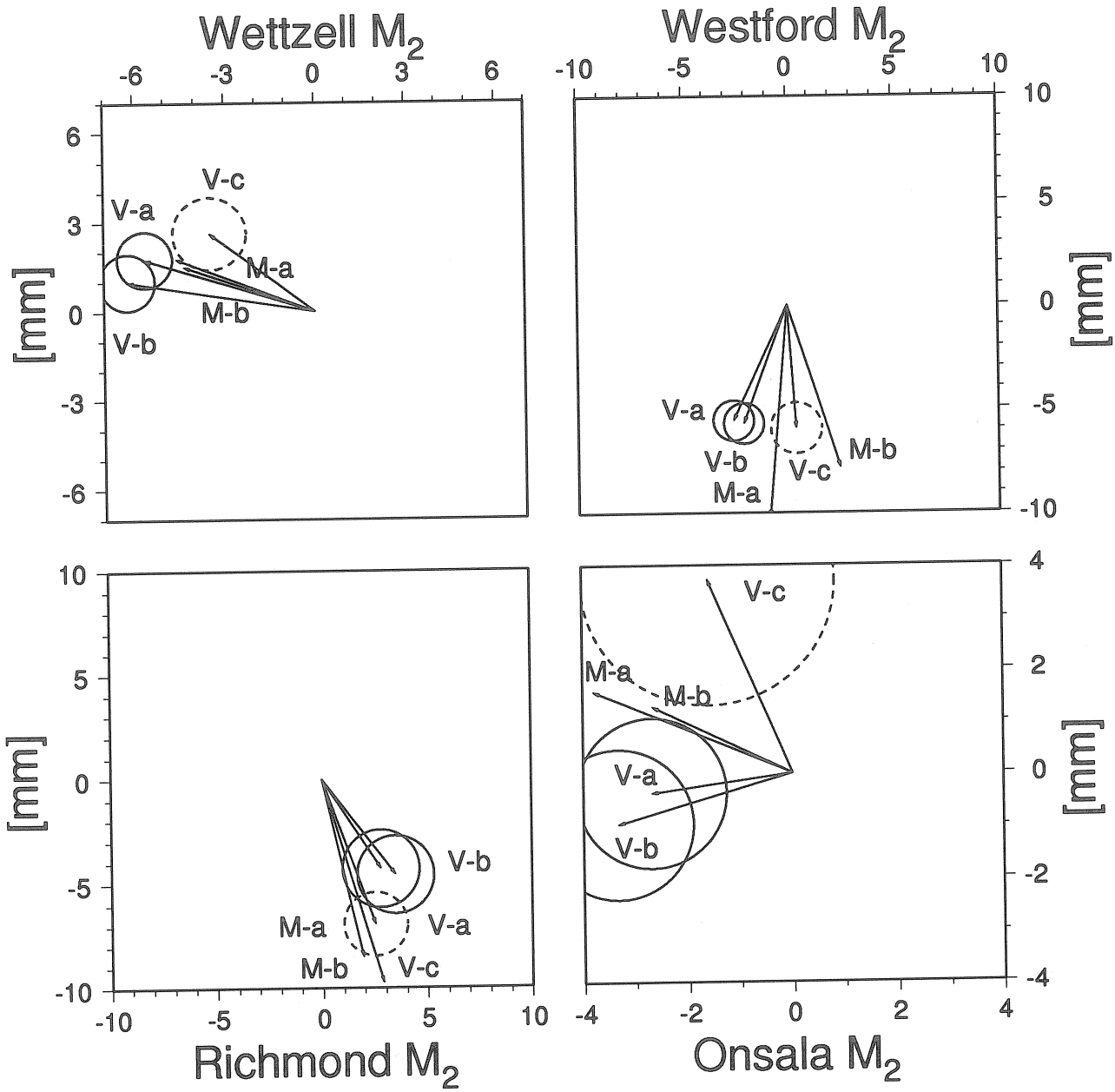

Figure 2: Model values and VLBI estimates of loading amplitudes and phases of the ocean tide M_2 for Wettzell (Germany), Westford (Massachusetts, USA), Richmond (Florida, USA) and Onsala (Sweden): Arrows without error ellipses show model values and are marked by M-a (model SCHERNECK-SCHWIDERSKI [1991]) and M-b (model SCHERNECK-LE PROVOST [1995]). Arrows with error ellpises in solid lines show the VLBI estimates of this paper and are marked with V-a (VLBI estimates based on the a priori model Scherneck-Schwiderski) and V-b (VLBI estimates based on the a priori model Scherneck-Le Provost). Arrows with error ellipses in broken lines show the VLBI estimates of SOVERS [1994] and are marked with V-c.

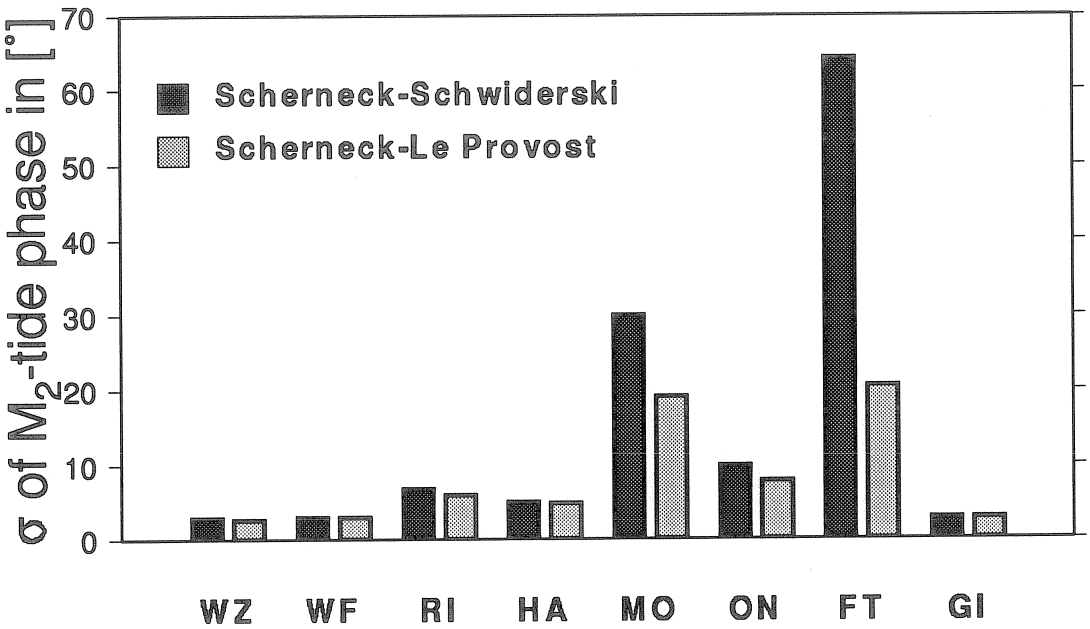

Figure 3: Standard deviations of the M_2 ocean tide loading phases. Dark columns show the standard deviations which are obtained with the SCHERNECK-SCHWIDERSKI model, light columns show the standard deviations which are obtained with the SCHERNECK-LE PROVOST model. Stations: Wettzell (WZ), Westford (WF), Richmond (RI), Hartebeesthoek (HA), Mojave (MO), Onsala (ON), Ft.Davis (FT), Gilcreek (GI)

4.2 Atmospheric loading parameters

The application of atmospheric loading corrections to the VLBI data significantly influences the results, i.e. baseline components and post-fit residuals. We also have solved for the atmospheric loading coefficients by a VLBI global solution. Loading coefficients for the 14 VLBI stations which contributed most of the observations to the whole database were determined according to the model by MANABE et al. [1991] (see equation 2). This model describes the radial component $\Delta_A X_1$ of the station displacement vector due to atmospheric pressure as a function of the time dependent local pressure $p(t)$ and a mean pressure $\bar{p}$ by a dimensionless pressure loading coefficient α_p. Discontinuities of the pressure distribution can be generated at coastlines due to the static response of the sea (inverted barometer hypothesis, IBH), i.e. for ocean areas the pressure contribution has to be set to zero due to the static response of the water masses. The validitiy of the inverted barometer hypothesis was also tested by VLBI, i.e. the VLBI results were compared with both, the parameters given by MANABE et al. (1991) for the IBH and those given for the non-inverted barometer hypothesis (NIBH).

$$\Delta_A X_1(t) \quad = \quad \alpha_p(p(t) - \bar{p}) \tag{2}$$

The results for the atmospheric loading coefficient α_p are shown in table 2 and figure 4. Columns 1 and 2 in table 2 give the model values by MANABE et al [1991] using the IBH or the NIBH, column 3 contains our results and column 4 the results by MACMILLAN and GIPSON [1994] which were also obtained from VLBI. In general the theoretical model by MANABE et al. [1991] is confirmed, but there are significant anomalies for some stations, e.g. for Onsala (Sweden).

The cross correlation coefficients r(x,y) between the theoretical atmospheric loading parameters x_i of MANABE et al. [1991] and the empirical results y_i obtained by VLBI were computed with equation 3. In this equation, w_i are the weights of the results y_i. Table 3 lists the cross correlation coefficients.

$$r(x,y) \quad = \quad \frac{\sum_{i=1}^{n}(x_i \cdot (w_i \cdot y_i))}{\sqrt{(\sum_{i=1}^{n} x_i^2 \cdot \sum_{i=1}^{n}(w_i \cdot y_i)^2)}} \tag{3}$$

Table 2: Model parameters and VLBI estimates of atmospheric loading coefficients α_p, stations near the coast are marked by C, stations far from the coast by I. Columns 1 and 2 show model parameters by MANABE et al. [1991], column 3 contains the VLBI results presented in this paper and column 4 shows the VLBI results by MACMILLAN and GIPSON [1994]

Station		MANABE et al. IBH [mm/hPa] 1	MANABE et al. NIBH [mm/hPa] 2	VLBI estimate (this paper) [mm/hPa] 3	MACMILLAN and GIPSON [mm/hPa] 4
Algopark	I	-0,435	-0,453	-0,45 ± 0,19	-0,44 ± 0,36
Greenbank	I	-0,479	-0,528	-0,68 ± 0,17	-0,17 ± 0,12
FD-VLBA	I	-	-	-0,50 ± 0,14	-
Ft.Davis	I	-0,532	-0,547	-0,61 ± 0,16	-0,44 ± 0,17
Gilcreek	I	-0,432	-0,536	-0,42 ± 0,03	-0,35 ± 0,04
Hartebeesthoek	I	-0,540	-0,644	-0,09 ± 0,30	-0,16 ± 0,20
Mojave	I	-0,457	-0,542	-0,17 ± 0,11	-0,30 ± 0,09
Pietown	I	-	-	-0,28 ± 0,15	-
Wettzell	I	-0,442	-0,523	-0,56 ± 0,04	-0,53 ± 0,05
Haystack	C	-0,369	-0,458	-0,40 ± 0,27	-0,58 ± 0,12
Matera	C	-	-	-0,45 ± 0,14	-
Medicina	C	-0,431	-0,563	-0,43 ± 0,17	-
Onsala	C	-0,254	-0,517	-0,05 ± 0,04	-0,16 ± 0,07
Westford	C	-0,366	-0,454	-0,48 ± 0,03	-0,43 ± 0,04

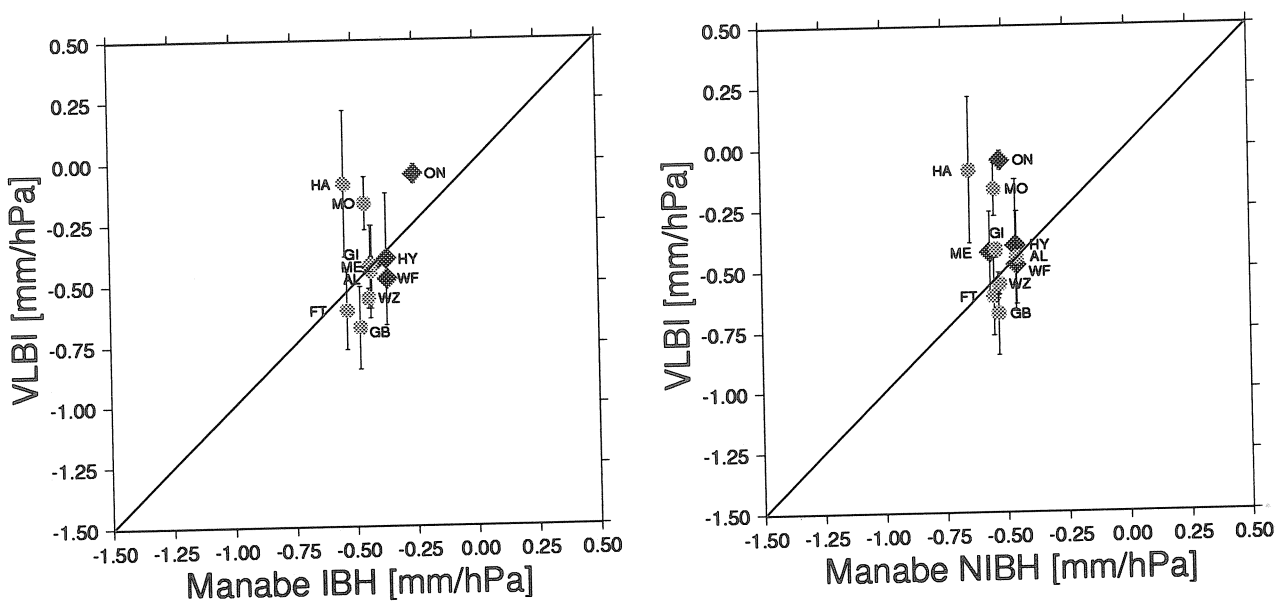

Figure 4: Scatter plots of model parameters and VLBI estimates of atmospheric loading coefficients for the station: Algopark (AL), Greenbank (GR), Ft.Davis (FT), Gilcreek (GI), Hartebeesthoek (HA), Mojave (MO), Wettzell (WZ), Haystack (HY), Medicina (ME), Onsala (ON) and Westford (WF), (circles = stations in the inland, diamonds = stations at the coast)

Table 3: Cross correlation coefficients between model parameters and VLBI estimates of atmospheric loading coefficients.

	IBH	NIBH
a) all stations regarded	0.86	0.84
b) only the stations near the coast regarded	0.85	0.85
c) only the stations far from the coast regarded	0.87	0.81

There is a small tendency that the IBH fits slightly better with the VLBI data than the NIBH. Using all stations for which atmospheric loading coefficients have been determined, the correlation coefficient is 0.86 for the IBH and 0.84 for the NIBH. If we take only those stations which are closer than 500 km to the coast, the correlation is 0.87 for IBH and 0.81 for NIBH, respectively. For the other stations which are far from the coast, there is no difference between the correlation coefficients for IBH and NIBH: both are 0.85.

It can be seen form figure 4 that the VLBI results agree with theory within their error bars for all stations except Hartebeesthoek (South Africa), Mojave (California, USA) and Onsala (Sweden). The antennae of Hartebeesthoek and Mojave could be influenced by local effects which counteract to atmospheric loading. Moreover, both stations only took part in few observations of the whole database and their atmospheric loading parameters got large errors. The atmospheric loading parameter of Onsala was determined to -0.05 ± 0.04. Thus, it received a very small error, but completely disagrees with theory. The Onsala telescope is located very close to the coast and is largely surrounded by water, which – assuming the IBH – reduces the atmospheric loading effect. Furthermore, the telescope is built directly on bedrock and may show a rather unusual response to air pressure variations.

5 Conclusion

Insufficient models for the solid Earth deformation and for ocean and atmospheric loading cause an apparent diurnal signal in the Earth rotation parameters which are determined by VLBI. Thus, it is absolutely necessary to implement refined models of these effects, e.g those given by the new IERS Conventions [1996], in the analysis software of space geodetic observations.

Today, VLBI data can also be used to solve for parameters of the models for the solid Earth tides, ocean loading and atmospheric loading. This will allow to validate or to improve the existing models. Concerning the loading problem, in the future we may even be able to infer parameters for regional structures of the top layers of the Earth's crust from inverse solutions. The consideration of other exogenic surface deformations as caused by long-term variations of the sea level and of the groundwater level and by ice or snow loading should be envisaged, too.

References

[1] Brosche P., U. Seiler, J. Sündermann, J. Wünsch: *Periodic changes in Earth's rotation due to oceanic tides*, Astron. Astrophys. 220, 318-320, 1989

[2] Chao B. F., R. D. Ray, J. M. Gipson, G. D. Egbert, C. Ma: *Diurnal/semidiurnal polar motion excited by oceanic tidal angular momentum*, J. Geophys. Res., Vol. 101, No. B9, 20151-20163, 1996

[3] Defraigne P., V. Dehant, J. Hinderer: *Stacking gravity tide measurements and nutation observations in order to determine the complex eigenfrequency of the Nearly Diurnal Free Wobble*, J. Geophys. Res., Vol. 99, NO. B5, 9203-9213, 1994, with an corretion in J. Geophys. Res., Vol. 100, No. B2, 2041-2042, 1995

[4] Dickey J. O.: *Atmospheric Excitation of the Earth's Rotation: Progress and Prospects via Space Geodesy*, Contributions of Space Geodesy to Geodynamics: Earth Dynamics, Geodynamics Series, Vol. 24, 55-70, AGU, 1993

[5] Eubanks T. M.: *Variations in the Orientation of the Earth*, Contributions of Space Geodesy to Geodynamics: Earth Dynamics, Geodynamics Series, Vol. 24, 1-54, AGU, 1993

[6] Haas R., H. Schuh: *Determination of frequency dependent Love and Shida numbers from VLBI data*, Geophys. Res. Lett., Vol. 23, No. 12, 1509-1512, 1996

[7] Haas R.: *Untersuchungen zu Erddeformationsmodellen für die Auswertung von geodätischen VLBI-Messungen*, Ph.D. thesis, University of Bonn, 1996

[8] Haas R., H. Schuh: *Determination of tidal parameters by VLBI*, Bull. d'Inform. Marées Terr., this issue

[9] Hartmann T., H.-G. Wenzel: *Catalogue HW95 of the tidal potential*, Bull. d'Inform. Marées Terr., Vol. 123, 9278-9301, 1995

[10] Le Provost C., M. L. Genco, F. Lyard, P. Vincent, P. Canceil: *Spectroscopy of the world ocean tides from a finite element hydrological model*, J. Geophys. Res., Vol. 99, 24777-24797, 1994

[11] Ma C., J. M. Sauber, L. J. Bell, T. A. Clark, D. Gordon, W. E. Himwich: *Measurement of horizontal motions in Alaska using very long baseline interferometry*, J. Geophys. Res., Vol. 95, No. B13, 21991-22011, 1990

[12] MacMillan D. S., J. M. Gipson: *Atmospheric pressure loading parameters from very long baseline interferometry observation*, J. Geophys. Res., Vol. 99, No. B9, 18081-18087, 1994

[13] Manabe S., T. Stao, S. Sakai, K. Yokoyama: *Atmospheric loading effect on VLBI observations*, Proceedings of the AGU Chapman Conference on Geodetic VLBI: Monitoring Global Change, 111-122, NOAA Technical Report NOS 137 NGS 49, U.S. Departement of Commerce, NOAA/NOS, Rockville, MD, 1991

[14] McCarthy D. D. (ed.): *IERS Standards*, IERS Technical Note 13, Observatoire de Paris, 1992

[15] McCarthy D. D. (ed.): *IERS Conventions*, IERS Technical Note 21, Observatoire de Paris, 1996

[16] Rabbel W., J. Zschau: *Static deformations and gravity changes at the earth's surface due to atmospheric loading*, J. Geophys., 56, 81-99, 1985

[17] Rabbel W., H. Schuh: *The influence of atmospheric loading on VLBI-experiments*, J. Geophys., 59, 164-170, 1986

[18] Roosbeek F.: *RATGP95: a harmonic development of the tide-generating potential using an analytical method*, Geophys. J. Int., Vol. 126, No. 1, pp. 197-204, 1996

[19] Scherneck H. G.: *A parameterized Solid Earth Tide Model and Ocean Tide Loading Effects for Global Geodetic Baseline Measurements*, Geophys. J. Int., 106, 677-694, 1991

[20] Scherneck H. G.: *Comparing loading effects due to recent ocean tide models*, presented at the IERS Workshop 1995, Paris

[21] Schuh H.: *Tidal influences on VLBI observations*, Bull. d'Inform. Marées Terr., Vol. 105, 7495-7501, 1989

[22] Schwiderski E. W.: *Detailed Ocean Tide Models of (N_2, M_2, S_2, K_2) and (K_1, P_1, O_1, Q_1), including an atlas of tidal charts and maps*, presented at the XVIIth IUGG General Assembly, Canberra, 1979

[23] Seiler U., J. Wünsch: *A refined model for the influence of the ocean tides on UT1 and polar motion*, Astron. Nachr. 316/6, 419-423, 1995

[24] Sovers O. J.: *Vertical ocean loading amplitudes from VLBI measurements*, J. Geophys. Res., Vol. 21, No. 5, 357-360, 1994

[25] Tamura Y.: *A harmonic development of the tide-generating potential*, Bull. d'Inform. Marées Terr., Vol. 99, 6813-6855, 1987

[26] VanDam T. M., J. M. Wahr: *Deformations of the Earth's surface due to atmospheric loading, effects on gravity and baseline measurements*, J. Geophys. Res., , Vol. 92, 1281-1286, 1987

[27] Wahr J. M.: *Body tides on an elliptical, rotating, elastic and oceanless earth*, Geophys. J. R. Astron. Soc., 64, 677-703, 1981

[28] Wessels P., W. H. F. Smith: *Free software helps map and display data*, EOS Trans. Amer. Geophys. U., Vol. 55, 293-305, 1991

[29] Woolard E.W.: *Inequalities in mean solar time from the tidal variations in the rotation of the earth*, Astron. J., 64, 140-142, 1959

[30] Wünsch J., U. Seiler: *Theoretical amplitudes and phases of the periodic polar motion terms caused by ocean tides*, Astron. Astrophys. 266, 581-587, 1992

[31] Yoder C. F., J. G. Williams, M. E. Parke: *Tidal Variations of Earth Rotation*, J. Geophys. Res., 86, 881-891, 1981

Determination of Tidal Parameters from VLBI

Rüdiger Haas
Geodätisches Institut der Universität Bonn (GIUB)
Nußallee 17, 53115 Bonn, Germany, (haas@uni-bonn.de)

Harald Schuh
Deutsches Geodätisches Forschungsinstitut (DGFI), Abt. I
Marstallplatz 8, 80539 München, Germany, (schuh@dgfi.badw-muenchen.de)

Abstract We determined second degree and third degree Love and Shida numbers of the solid Earth tide model from VLBI data. The results for the different parts of the tidal spectrum (long-period, diurnal, semi-diurnal) were published by HAAS AND SCHUH [1996] and are here discussed in some more detail. They are slightly different for the various frequency bands and a clear resonance in the tidal deformation can be seen around the Free Core Nutation [FCN]. In a more general approach complex Love and Shida numbers are used. This corresponds to a phase lag of the tidal deformation due to anelasticity of the Earth. Imaginary parts of the Love numbers h_{21} and l_{21} were computed for the strongest semidiurnal and diurnal tides. Finally, the complex eigenfrequency of the FCN resonance was determined, with a FCN period of 430 $\pm$ 22 days in the celestial reference frame and a quality factor Q of 1400 ($1000 < Q < 2100$). This direct determination of Q based on tidal deformations measured by VLBI agrees rather well with superconducting gravimeter measurements but disagrees with former analyses of VLBI nutation data.

1 Introduction

Theoretical models for the solid Earth tides predict a frequency dependence of the tidal deformation in the diurnal frequency band. This is expressed by frequency dependent second degree Love and Shida numbers h_{21} and l_{21}. Due to anelastic dispersion in the Earth's mantle the tidal deformation lags behind the tide generating potential. This can be expressed by complex Love and Shida numbers. We will present Love and Shida numbers for individual tides and also parameters which describe the resonance of the tidal deformation in the diurnal frequency band. VLBI least squares analyses were performed for the case of an elastic Earth and also by solving for imaginary parts of the Love and Shida numbers, corresponding to an anelastic Earth. The VLBI measurements permit the determination of these parameters independently from other hypotheses using a direct estimation approach.

2 Theoretical solid Earth tide model

Each theoretical model of the solid Earth tides consists of two parts. The first part is the tide generating potential due to the gravitational attraction of the solar system bodies. The second part is the so-called Earth's transfer function, which describes how the Earth's shape changes as a response to variations of the tide generating potential. It is parameterized by the Love number h for the radial displacements, the Shida number l for the tangential displacements and the Love number k for the free space potential induced by the tides.

In the most trivial case of a non-rotating, spheroidal and elastic Earth the topocentric tidal displacement of a station with spheroidal coordinates (ϕ, λ, r) is described by equations (1) to (3) which contain constant Love and Shida numbers. In these equations Δ_U, Δ_E, Δ_N are the tidal displacements in topocentric Up, East and North direction, respectively. The tide generating potential is denoted by W, g is the gravity at the station considered

$$\Delta_U = h \cdot \frac{W}{g} \tag{1}$$

$$\Delta_E = l \cdot \frac{\partial W}{\partial \lambda} \cdot \frac{1}{g \cdot \cos(\phi)} \tag{2}$$

$$\Delta_N = l \cdot \frac{\partial W}{\partial \phi} \cdot \frac{1}{g} \tag{3}$$

and ϕ and λ are the latitude and longitude of the station.

The relationship between the tide generating potential and the tidal displacements becomes more complicated if we consider the Earth's shape, its structure, its material properties and its rotation. The Love and Shida numbers are not constant values anymore but become frequency and latitude dependent. Due to the different directions of the rotation axis of the Earth's fluid core and the rotation axis of the Earth's mantle, the Earth has a normal mode called the Free Core Nutation [FCN] with an eigenfrequency in the diurnal frequency band. This mode is resonantly excited by the second degree, first order tidal potential, so that the solid Earth tides in that period range are strongly frequency dependent. This can be expressed by frequency dependent Love and Shida numbers. WAHR [1981] determined transfer functions for an elliptical, rotating, elastic and oceanless Earth and published the Love and Shida numbers for individual tides.

$$\Delta_U = \sum_{n=1}^{n_{max}} \sum_{m=0}^{n} \sum_{T} h_{nm}(\omega_T) \cdot \frac{W_{nmT}}{g} \tag{4}$$

$$\Delta_E = \sum_{n=1}^{n_{max}} \sum_{m=0}^{n} \sum_{T} l_{nm}(\omega_T) \cdot \frac{\partial W_{nmT}}{\partial \lambda} \cdot \frac{1}{g \cdot \cos(\phi)} \tag{5}$$

$$\Delta_N = \sum_{n=1}^{n_{max}} \sum_{m=0}^{n} \sum_{T} l_{nm}(\omega_T) \cdot \frac{\partial W_{nmT}}{\partial \phi} \cdot \frac{1}{g} \tag{6}$$

Using a harmonic expansion of the tide generating potential equations (1) to (3) can be substituted by equations (4) to (6). In equations (4) to (6) $h_{nm}(\omega_T)$ and $l_{nm}(\omega_T)$ are the Love and Shida number of a tide T of degree n and order m with frequency ω_T. Each tide T contributes by W_{nmT} to the total tide generating potential. For the Love and Shida numbers of the second degree diurnal tides Wahr gives the resonance formulas (7) and (8). In these equations ω_T, ω_{O_1} and ω_{FCN} are the frequencies of each specific tide T, of the tide O_1 and of the FCN, respectively, and h_{RS} and l_{RS} are resonance strength factors.

$$h_{21}(\omega_T) = h_{21}(\omega_{O_1}) + h_{\mathrm{RS}} \cdot \frac{\omega_T - \omega_{O_1}}{\omega_{\mathrm{FCN}} - \omega_T} \tag{7}$$

$$l_{21}(\omega_T) = l_{21}(\omega_{O_1}) + l_{\mathrm{RS}} \cdot \frac{\omega_T - \omega_{O_1}}{\omega_{\mathrm{FCN}} - \omega_T} \tag{8}$$

In Wahr's model based on the seismic Earth model 1066A by Gilbert and Dziewonski the period of the FCN is 461 sidereal days in the celestial reference frame.

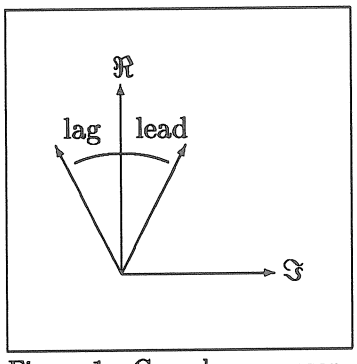

Figure 1.: Complex representation: $\Re$ is the real part (in-phase), $\Im$ is the imaginary part (out-of-phase)

Anelasticity of the Earth's mantle causes a lag of the tidal deformation with respect to the tide generating potential [e.g. WAHR AND BERGEN, 1986]. This can be described by complex transfer functions whose imaginary parts represent the out-of-phase tidal response (see figure 1). In this general approach the real Love and Shida numbers in equations (4) to (6) have to be replaced by complex Love and Shida numbers. The resonance parameters in equations (7) and (8) become complex, too. A complex eigenfrequency of the FCN ($\omega_{\mathrm{FCN}} = \Re(\omega_{\mathrm{FCN}}) + i\,\Im(\omega_{\mathrm{FCN}})$) allows to determine the 'quality factor' Q, which describes the damping of the resonance. It can be calculated from the real and the imaginary part of the eigenfrequency:

$$Q = \frac{\Re(\omega_{\mathrm{FCN}})}{2 \cdot \Im(\omega_{\mathrm{FCN}})} \tag{9}$$

3 Estimation of Love and Shida numbers for individual tides

First we solved directly for frequency dependent Love and Shida numbers of individual tides from VLBI data. The harmonic expansion of the tide generating potential by TAMURA [1987] was used to calculate partial derivatives for the main diurnal tides which were entered in a least squares analysis with the CALC/SOLVE VLBI data analysis software package. Taking any other of the present tidal potential models yields almost identical results.

About 725,000 VLBI delay observables observed in different international VLBI networks from 1979 to 1996 (which is about 50 % of all geodetic VLBI data presently available) were combined for a batch

solution. In such a solution, 'global parameters', which are common to all VLBI experiments, as well as 'arc-parameters', which belong to individual VLBI experiments only are estimated together. Apart from minor differences, the models used in the CALC/SOLVE software package agree with those recommended by the IERS Standards [1992]. This includes corrections due to ocean tide loading computed according to SCHERNECK [1991].

3.1 Elastic Earth

If we consider the Earth being elastic, equations (4) to (6) are used for the determination of Love and Shida numbers for individual tides from VLBI data. In a batch solution the station positions and velocities, radio source positions, daily Earth orientation parameters (i.e. pole position x_p, y_p, Universal Time UT1 and nutation corrections $\delta\psi$, $\delta\epsilon$), clock and atmosphere parameters and additionally 12 discrete values of h_{21} and 12 discrete values of l_{21} for the main diurnal tides were estimated. The Love and Shida numbers of the tide S_1 were fixed to their theoretical values because the tide S_1 is a strong atmospherical tide as well.

Table 1: Estimates of frequency dependent Love and Shida numbers h_{21}, l_{21}

Tide	Doodson number	Love number h_{21}		Shida number l_{21}		
		Wahr	This paper	Wahr	This paper	
Q_1	135.655	0.603	0.560 ± 0.012	0.084	0.074 ± 0.003	[/]
O_1	145.555	0.603	0.606 ± 0.002	0.084	0.082 ± 0.001	[/]
M_1	155.655	0.600	0.435 ± 0.030	0.084	0.069 ± 0.008	[/]
π_1	162.556	0.587	0.623 ± 0.090	0.085	0.108 ± 0.022	[/]
P_1	163.555	0.581	0.574 ± 0.005	0.085	0.085 ± 0.001	[/]
K_1	165.555	0.520	0.496 ± 0.002	0.087	0.086 ± 0.001	[/]
K_1'	165.565	0.514	0.458 ± 0.014	0.087	0.054 ± 0.005	[/]
ψ_1	166.554	0.937	-0.136 ± 0.228	0.074	-0.428 ± 0.056	[/]
ϕ_1	167.555	0.662	0.702 ± 0.121	0.082	0.094 ± 0.030	[/]
θ_1	173.655	0.612	0.934 ± 0.158	0.084	0.080 ± 0.039	[/]
J_1	175.455	0.611	0.538 ± 0.031	0.084	0.075 ± 0.008	[/]
OO_1	185.455	0.608	0.555 ± 0.054	0.084	0.074 ± 0.013	[/]

Table 1 gives the estimates for h_{21} and l_{21} and their scaled standard deviations in comparison with values published by WAHR [1981]. The standard deviations obtained from the least squares fit are scaled independently of the tidal frequencies and represent an inner accuracy, which is usually too optimistic by a factor 2-3. The correlation coefficients between the estimated tidal parameters were investigated, too. The maximum correlations are about 0.6 and they were obtained between Love and Shida numbers of the same tide. In VLBI the baseline vectors are measured which contain both radial and tangential motions of the two stations involved. Thus, each measurement contains information on h and l. All other correlation coefficients, i.e. between Love and Shida numbers of different tides, are very small, i.e. less than 0.18, 72 % of them are ≤ 0.05.

In figures 2 and 3 the solid lines show the theoretical model of Wahr in the diurnal frequency band with an FCN period of 461 sidereal days. Love and Shida numbers estimated from VLBI are plotted by discrete points, and the error bars show the scaled standard deviations. The estimates of h_{21} and l_{21} of those tides with a strong tidal potential (e.g. Q_1, O_1, P_1, K_1) have small error bars and they lie close to the theoretical values. The tide M_1 is the only tide for which h_{21} shows a discrepancy from theory larger than three times the formal error. This confirms analyses of gravimetric data which usually show for M_1 differences between observations and theory [e.g. MELCHIOR et al., 1996] probably due to interactions between Earth tides and ocean tides. The resonance close to the FCN can be seen very clearly not only for the K_1 tide but also for the smaller terms nearby. It is notable that from VLBI data good estimates of the Shida numbers are obtained corresponding to tangential tidal

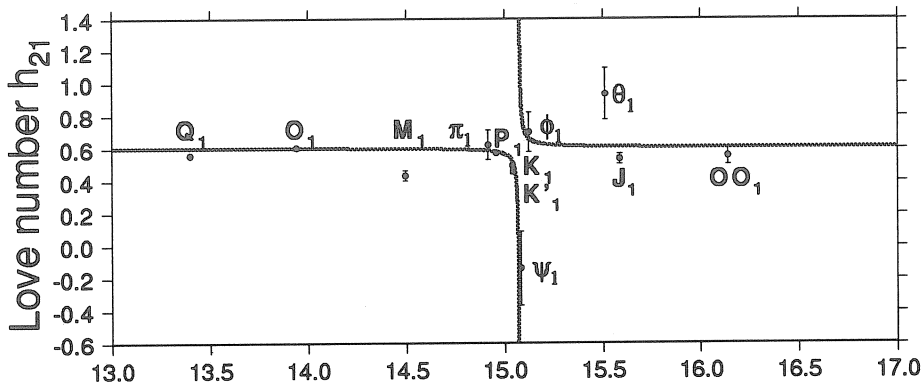

Figure 2: Estimates of frequency dependent Love numbers h_{21} and Wahr's theoretical model (solid line).

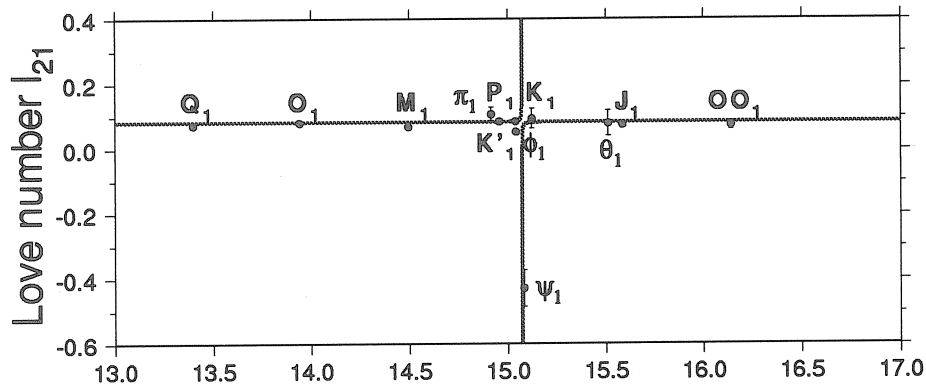

Figure 3: Estimates of frequency dependent Love numbers l_{21} and Wahr's theoretical model (solid line).

displacements which are much smaller than the radial displacements. The results for h_{21} and l_{21} of tides with a weak tidal potential show larger discrepancies from the theoretical values than the strong tides. However, these differences are always less than twice the formal error except for ψ_1 which for h is on the 'wrong part' of the resonance curve: the VLBI result is $h(\psi_1) = -0.136 \pm 0.228$ whereas it is 0.934 in Wahr's theory. As to the large standard deviation of the Love number of that weak tide close to the FCN resonance, it is open whether the determination by VLBI can be regarded as significant. Anyway, this first attempt to determine h_{21} and l_{21} for individual diurnal tides directly from VLBI data is successful and shows a rather good agreement with Wahr's theoretical model.

3.2 Anelastic Earth

Based on the same VLBI data which were used in the previous chapter for determining real Love and Shida numbers, i.e. the elastic case, we solved now for real and also for imaginary components of the main diurnal and semidiurnal tides. Theoretical values of the real and imaginary parts due to anelasticity are given in the new IERS Conventions [McCarthy, 1996] for the main tides. Our results are shown in the last columns of tables 2 and 3, again with their scaled standard deviations, and they are compared with theoretical values taken from the IERS Conventions. For h the results of the VLBI global solution are also compared to other empirical determinations published recently [Mitrovica et al., 1994, Ray et al., 1995].

Table 2: Theoretical values and estimates of frequency dependent and complex Love numbers h, real parts are denoted by $\Re$, imaginary parts by $\Im$, all values are dimensionless

Tide	Theory		Mitrovica et al., 1994		Ray et al., 1995		This paper	
	$\Re$	$\Im$	$\Re$	$\Im$	$\Re$	$\Im$	$\Re$	$\Im$
Q_1	0.603	−0.002		-		-	0.559 ± 0.012	$+0.046 \pm 0.012$
O_1	0.603	−0.002	0.618 ± 0.007	-0.010 ± 0.007	0.594	-0.004 ± 0.013	0.612 ± 0.002	-0.017 ± 0.002
M_1	0.600	−0.002		-		-	0.422 ± 0.031	$+0.086 \pm 0.031$
π_1	0.588	−0.002		-		-	0.484 ± 0.093	$+0.098 \pm 0.093$
P_1	0.582	−0.002	0.56 ± 0.02	$+0.010 \pm 0.010$		-	0.567 ± 0.005	$+0.002 \pm 0.005$
K_1	0.523	−0.003	0.50 ± 0.01	-0.010 ± 0.009	0.512	-0.006 ± 0.012	0.512 ± 0.003	-0.003 ± 0.003
K_1'	0.518	−0.003	0.53 ± 0.06	-0.03 ± 0.060		-	0.429 ± 0.019	-0.156 ± 0.019
ψ_1	1.053	−0.002	0.8 ± 0.6	-0.6 ± 0.5		-	-0.277 ± 0.234	$+0.150 \pm 0.234$
ϕ_1	0.664	−0.002	0.5 ± 0.4	$+0.2 \pm 0.3$		-	0.764 ± 0.126	-0.583 ± 0.126
θ_1		-		-		-	0.705 ± 0.161	-0.321 ± 0.161
J_1		-		-		-	0.542 ± 0.031	$+0.036 \pm 0.031$
OO_1		-		-		-	0.495 ± 0.054	-0.034 ± 0.054
N_2	0.603	−0.002		-	0.626	$+0.015 \pm 0.044$	0.615 ± 0.006	$+0.034 \pm 0.006$
M_2	0.603	−0.002		-	0.613	-0.000 ± 0.007	0.600 ± 0.001	-0.002 ± 0.001
S_2	0.603	−0.002		-		-	0.592 ± 0.002	$+0.010 \pm 0.002$
K_2	0.603	−0.002		-		-	0.641 ± 0.010	-0.015 ± 0.010

Table 3: Theoretical values and estimates of frequency dependent and complex Shida numbers l, real parts are denoted by $\Re$, imaginary parts by $\Im$, all values are dimensionless

Tide	Theory		This paper	
	$\Re$	$\Im$	$\Re$	$\Im$
Q_1	0.085	−0.001	0.076±0.003	+0.016±0.003
O_1	0.085	−0.001	0.083±0.001	−0.001±0.001
M_1	0.085	−0.001	0.072±0.008	−0.033±0.008
π_1	0.085	−0.001	0.054±0.023	+0.008±0.023
P_1	0.086	−0.001	0.083±0.001	+0.001±0.001
K_1	0.087	−0.001	0.090±0.001	+0.002±0.001
K_1'	0.087	−0.001	0.060±0.006	−0.036±0.006
ψ_1	0.071	−0.001	−0.460±0.058	+0.234±0.059
ϕ_1	0.083	−0.001	0.081±0.031	−0.106±0.031
θ_1		-	0.047±0.040	−0.180±0.040
J_1		-	0.076±0.008	+0.003±0.008
OO_1		-	0.058±0.013	−0.014±0.013
N_2	0.085	−0.001	0.091±0.001	+0.011±0.001
M_2	0.085	−0.001	0.088±0.001	+0.007±0.001
S_2	0.085	−0.001	0.084±0.001	+0.008±0.001
N_2	0.085	−0.001	0.091±0.002	−0.011±0.002

In contrast to our direct solution the first reference [MITROVICA et al., 1994] used an indirect, i.e. a two step approach via radial displacements determined by VLBI and the results of the second reference [RAY et al., 1995] are based on satellite altimetry and ocean tidal measurements. The approach described in this paper allows the direct determination of complex Love and Shida numbers and is more precise than any previous attempt. However, only some of our results for the imaginary parts differ significantly from zero, some of them are 6-10 times larger than their standard deviations. In the range of the FCN resonance large imaginary parts are obtained, which in the case of h for two tides (K_1', ϕ_1) exceed their fourfold standard deviations. Further investigations have to follow, whether dissipation processes exist within the Earth. That could cause larger phase lags than those predicted so far. There are also several tides for which the VLBI solution yielded positive imaginary parts which is senseless from a theoretical point of view. However, almost all of those positive imaginary parts are in the range of their standard deviations and therefore cannot be treated as significant.

4 Estimation of resonance parameters for the tidal deformation

The next idea was to estimate the five parameters of a frequency dependent model for the diurnal tides, i.e. to solve for $h_{21}(\omega_{O_1})$, $l_{21}(\omega_{O_1})$, h_{RS}, l_{RS}, ω_{FCN} in equations (7) and (8). Again, the harmonic expansion of the tide generating potential by Tamura was used to calculate partial derivatives. The same VLBI data as described in the previous section were used to run batch solutions.

4.1 Elastic Earth

We started again with an elastic Earth. Those five resonance parameters mentioned above were solved for as well as h_{20}, l_{20} for the long-period part, h_{22}, l_{22} for the semidiurnal part of the second degree tidal spectrum and h_3, l_3 for the third degree part of the tidal spectrum. Equations (7) and (8) are not linear with respect to ω_{FCN} and therefore a sufficient number of iterations had to be carried out to obtain final results. Figure 4 shows the result for the FCN resonance period as obtained after each iteration. Having started with Wahr's theoretical value of 461 sidereal days, the FCN period converges at 426,3 days. Table 4 gives the final results for the 11 parameters and their standard deviations after 12 iterations of the least squares fit.

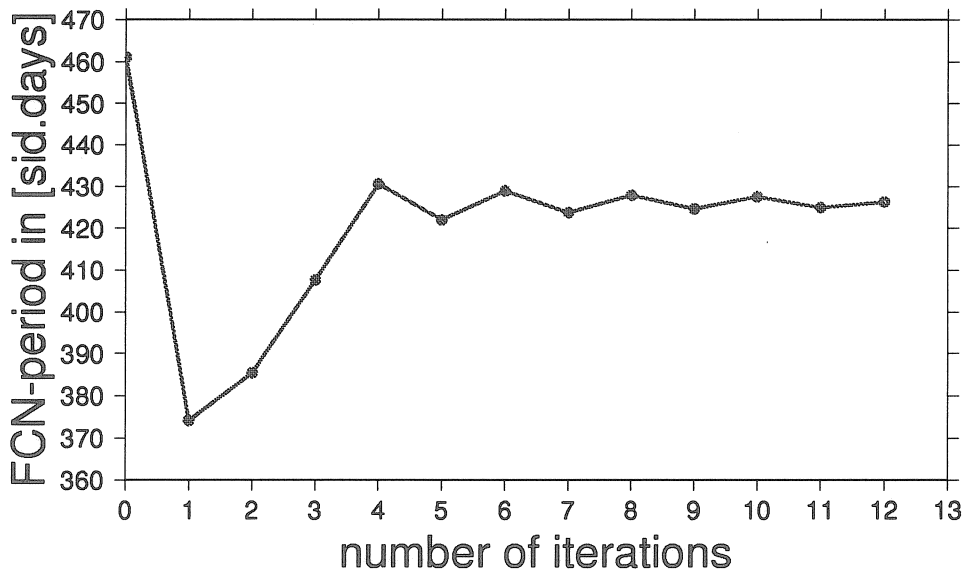

Figure 4: Iteration process, FCN-period derived from the estimated FCN-frequency

Table 4: Estimates of resonance parameters in the diurnal frequency band and h_{20}, l_{20}, h_{22}, l_{22}, h_3 and l_3 compared with theoretical values published by WAHR [1981].

	VLBI analysis, this paper			Wahr [1981]	
second degree, long periods					
h_{20}	0.559	±	0.012	0.606	[/]
l_{20}	0.094	±	0.003	0.0840	[/]
second degree, diurnal periods					
$h_{21}(\omega_{O_1})$	0.598	±	0.002	0.603	[/]
$l_{21}(\omega_{O_1})$	0.080	±	0.0005	0.0842	[/]
h_{RS}	−0.00162	±	0.00016	−0.00246	[/]
l_{RS}	0.00011	±	0.00003	0.0000781	[/]
ω_{FCN}	1.002346	±	0.00011	1.002171	[cycles/sid.day]
P_{FCN}	426.3	±	20.3	460.5	[sid.days]
second degree, semidiurnal periods					
h_{22}	0.600	±	0.001	0.609	[/]
l_{22}	0.0875	±	0.0001	0.0852	[/]
third degree, all periods					
h_3	0.281	±	0.048	0.291	[/]
l_3	0.0151	±	0.0048	0.0149	[/]

Table 5 contains the correlation coefficients between the estimated resonance parameters. The strongest correlation with 0.80 was obtained between the FCN frequency ω_{FCN} and the resonance strength factor h_{RS}. Correlations between the five resonance parameters and the six parameters of the other parts of the tidal band are less than 0.04. The estimates of h_{20}, l_{20} are correlated by 0.62, those of h_{22}, l_{22} by 0.21 and those of h_3, l_3 by 0.15. All other correlations, i.e. between the parameters of different parts of the tidal spectrum, are less than or equal to 0.03.

Table 5: Correlation coefficients between the estimates of the resonance parameters, dimensionless

	h_{RS}	$l_{21}(\omega_{O_1})$	l_{RS}	ω_{FCN}
$h_{21}(\omega_{O_1})$	0.48	0.57	0.36	0.02
h_{RS}		0.27	0.26	0.80
$l_{21}(\omega_{O_1})$			0.64	0.01
l_{RS}				0.12

Figures 5 and 6 show the diurnal frequency band: the clear resonance at a period of 426 sidereal days can be seen in comparison to the resonance period of 461 sidereal days in Wahr's theoretical model. The latter is plotted by thin lines in figures 5 and 6 while the thick lines represent our results including the error ranges of the five-parameter model.

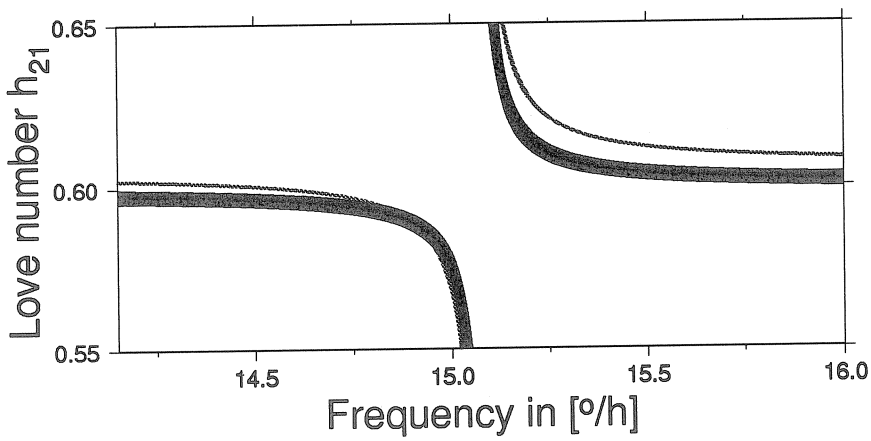

Figure 5: Estimates of resonance model parameters for Love numbers h_{21} including the error ranges (thick lines) and Wahr's theoretical model (thin lines).

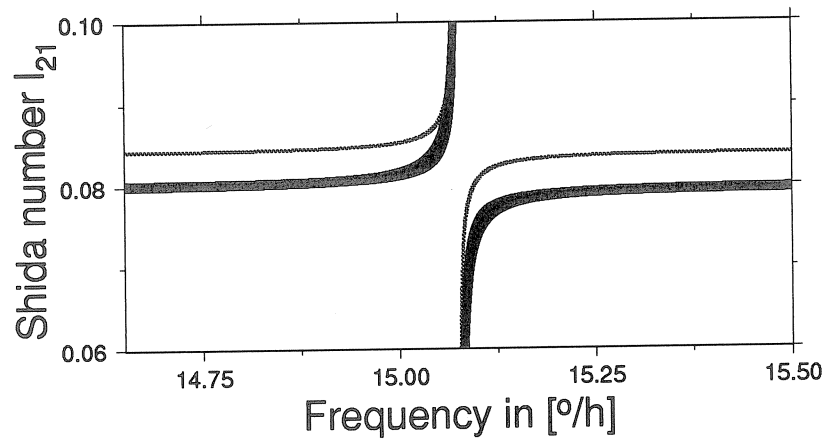

Figure 6: Estimates of resonance model parameters for Love numbers l_{21} including the error ranges (thick lines) and Wahr's theoretical model (thin lines).

4.2 Anelastic Earth

The parameters which represent the FCN resonance in the second degree diurnal tides, i.e. the resonance strength factors h_{RS}, l_{RS} and the FCN frequency ω_{FCN} in equations (7) and (8) can be treated as complex parameters, too. This allows to determine the complex eigenfrequency ω_{FCN} and the quality factor Q as defined at the end of section 2. The results from the direct determination of the resonance parameters via tidal defomations contained in VLBI measurements are shown in table 6. Table 7 gives the correlation coefficients between the estimated complex resonance parameters. The strongest correlations were obtained between the FCN frequency ω_{FCN} and the resonance strength factor h_{RS}: 0.83 between the real parts and 0.91 between the imaginary parts of these parameters.

The FCN period was 430.1 ± 21.6 days and the quality factor Q was determined to 1400 ($1000 < Q < 2100$). This is not far from many similar analyses of tidal gravimetric measurements (e.g. DEFRAIGNE et al., 1994, 1995, FLORSCH et al., 1994) which yielded results for Q usually between 2000 and 3000. However, a completely different approach for the determination of Q based on nutation data observed by VLBI gave a considerably higher Q of 31000 ($24000 < Q < 42800$) (DEFRAIGNE et al., 1994, 1995). The reason for this discrepancy has to be investigated.

Table 6: Estimates of complex resonance parameters in the diurnal frequency band, real parts are denoted by $\Re$, imaginary parts by $\Im$

	$\Re$	$\Im$	
$h_{21}(\omega_{O_1})$	0.598 ± 0.002	-	[/]
h_{RS}	−0.00162 ± 0.00016	0.00001 ± 0.00015	[/]
$l_{21}(\omega_{O_1})$	0.080 ± 0.0005	-	[/]
l_{RS}	0.00012 ± 0.00003	−0.00011 ± 0.00002	[/]
ω_{FCN}	1.00232 ± 0.00012	0.00036 ± 0.00012	[cycles/sid.day]
P_{FCN}	430.1 ± 21.6		[sid.days]

Table 7: Correlation coefficients between the estimates of the complex resonance parameters, real parts are denoted by $\Re$, imaginary parts by $\Im$, all values are dimensionless

	$\Re(h_{RS})$	$\Im(h_{RS})$	$l_{21}(\omega_{O_1})$	$\Re(l_{RS})$	$\Im(l_{RS})$	$\Re(\omega_{FCN})$	$\Im(\omega_{FCN})$
$h_{21}(\omega_{O_1})$	0.451	0.010	0.569	0.352	0.021	0.030	0.034
$\Re(h_{RS})$		0.003	0.247	0.212	0.002	0.829	0.003
$\Im(h_{RS})$			0.018	0.019	0.148	0.001	0.908
$l_{21}(\omega_{O_1})$				0.635	0.038	0.005	0.003
$\Re(l_{RS})$					0.074	0.132	0.001
$\Im(l_{RS})$						0.002	0.147
$\Re(\omega_{FCN})$							0.005

5 Discussion and Conclusions

The results show that VLBI data provide valuable information for the independent and direct determination of frequency dependent Love and Shida numbers in the long-period, diurnal and semidiurnal tidal ranges. We started for the case of an elastic Earth. Corresponding to the frequency dependence of second degree Love and Shida numbers we obtained an FCN period of 426 ± 20 sidereal days in the celestial reference frame. An FCN period shorter than that given by Wahr was already derived from nutation observations and gravity tide measurements [e.g. DEFRAIGNE et al., 1994, 1995]. In spite of this agreement with other recent investigations the large standard deviation of the FCN period

should be noted which is probably due to the strong correlation with the FCN resonance strength. Additionally to the different resonance period, both h_{21} and l_{21} curves are slightly shifted in the total level with respect to the theoretical model. The second degree Love numbers h_{2m} determined from VLBI are in all frequency bands smaller than those given by theory. The largest difference between theoretical models and our results was obtained for the long-period Love number h_{20} which is only 0.559 ± 0.012 in the VLBI solution. For the second degree Shida numbers l_{2m} no such obvious trend can be seen in our results. It is remarkable that even third degree Love and Shida numbers h_3, l_3 could be determined in good agreement with theoretical models within their error ranges.

In two further VLBI solutions presented in this paper we considered an anelastic Earth, i.e. also imaginary parts of the Love and Shida numbers for the most prominent tides were estimated, some of them differing significantly from zero. A phase lag between the tide generating potential and the tidal deformation can be expressed by complex Love and Shida numbers. The complex eigenfrequency ω_{FCN} of the FCN was determined with an FCN period of 430 ± 22 sidereal days and a quality factor Q of 1400 ($1000 < Q < 2100$). Both results agree well with analyses of tidal data sets, but for Q they disagree with former analyses of nutation data observed by VLBI.

References

[1] Defraigne, P., V. Dehant, and J. Hinderer: *Stacking gravity tide measurements and nutation observations in order to determine the complex eigenfrequency of the Nearly Diurnal Free Wobble*, J. Geophys. Res., Vol. 99, No. B5, 9203-9213, 1994, with a correction in J. Geophys. Res., Vol. 100, No. B2, 2041-2042, 1995

[2] Florsch, N., F. Chambat, J. Hinderer and H. Legros: *A simple method to retrieve the complex eigenfrequency of the Earth's nearly diurnal-free wobble; application to the Strasbourg superconducting gravimeter data*, Geophys. J. Int., 116, 53-63, 1994

[3] Haas, R. and H. Schuh: *Determination of frequency dependent Love and Shida numbers from VLBI data*, Geophys. Res. Lett., Vol. 23, No. 12, 1509-1512, 1996

[4] McCarthy, D. D. (ed.): *IERS Standards*, IERS Technical Note 13, Observatoire de Paris, 1992

[5] McCarthy, D. D. (ed.): *IERS Conventions*, IERS Technical Note 21, Observatoire de Paris, 1996

[6] Melchior, P., B. Ducarme, O. Francis: *The response of the Earth to tidal body forces described by second- and third-degree spherical harmonics as derived from a 12 year series of measurements with the superconducting gravimeter GWR/T3 in Brussels*, Phys. of the Earth and Planet. Int., 93, 223-238, 1996

[7] Mitrovica, J. X., J. L. Davis, P. M. Mathews and I. I. Shapiro: *Determination of tidal h Love number parameters in the diurnal band using an extensive VLBI data set*, Geophys. Res. Lett., Vol. 21 No. 8, 705-708, 1994

[8] Ray, R. D., S. Bettadpur, R. J. Eanes and E. J. O. Schrama: *Geometrical determination of the Love number h_2 at four tidal frequencies*, Geophys. Res. Lett., Vol. 22, No. 16, 2175-2178, 1995

[9] Scherneck, H. G.: *A parameterized Solid Earth Tide Model and Ocean Tide Loading Effects for Global Geodetic Baseline Measurements*, Geophys. J. Int., 106, 677-694, 1991

[10] Tamura, Y.: *A harmonic development of the tide-generating potential*, Bulletin d'Information Marées Terrestres, Vol. 99, 6813-6855, 1987

[11] Wahr, J. M.: *Body tides on an elliptical, rotating, elastic and oceanless earth*, Geophys. J. R. Astron. Soc., 64, 677-703, 1981

[12] Wahr, J. M. and Z. Bergen: *The effect of mantle anelasticity on nutations, earth tides, and tidal variations in rotation rate*, Geophys. J. R. Astron. Soc., 87, 633-668, 1986

[13] Wessels, P. and W. H. F. Smith: *Free software helps map and display data*, EOS Trans. Amer. Geophys. U., Vol. 55, 293-305, 1991

High sampling rate data acquisition system for GWR superconducting gravimeter C021

Michel Van Camp

Observatoire Royal de Belgique, Avenue Circulaire, 3, B-1180 Bruxelles, Belgium,
e-mail: Michel.VanCamp@oma.be

Abstract

A data acquisition system is connected on the "*Gravity Signal*" output of the GWR Superconducting Gravimeter C021 installed in Membach (east of Belgium). The data acquisition system consists in a DCF-controlled card provided with an analog/digital converter. In order to study the Earth's free oscillations, the chosen sampling rate is 1 Hz. Analysis of an important earthquake and comparison with 3 others gravimeters are presented. This data acquisition system gives also an information on the phase shift induced by the filter of the "*Tide*" output. For that purpose, we perform an ETERNA tidal analysis on data from "*Gravity Signal*" output, which is compared with the results obtained with the "*Tide*" output.

1. Introduction

GWR-cryogenic gravimeters are provided with different outputs. Usually data acquisition systems are connected on "*Tide*" or "*High Resolution Gravity Signal*" outputs. These are provided with a 1 minute lowpass filter. We present here a data acquisition system that is connected on the "*Gravity Signal*" output provided with a 1 s lowpass filter.

As the Global Geodynamics Project (GGP Newsletter #2, 1996) plans explicitly to study Earth's free oscillations with superconducting gravimeters, we connected in December 1995 a high sampling rate data acquisition system on the "*Gravity Signal*" output of the superconducting gravimeter C021. We do not use the "*mode*" output of C021 that consists in an analog bandpass filter flat from about 1 to 50 cycles per hour with a gain of 20. This filter was designed for operation on the IDA network but gives a not well known phase shift. In this paper we present the different data acquisition systems connected on C021, then we compare them. It gives an opportunity to evaluate the phase shift induced by the "*Tide*" output traditionally used by tidal acquisition systems.

On 17 February 1996, an important earthquake (ms = 8.0) happened in the Irian Jaya region giving a first opportunity to test the high sampling rate data acquisition system. We present here a first comparison with other instruments: superconducting gravimeters T018 and C025 and La Coste-Romberg gravimeter ET-19.

2. The data acquisition systems

The sensing unit of a superconducting gravimeter consists in a sphere that levitates in a magnetic field. Any displacements of this sphere are detected, preamplificated and integrated. Then the signal is sent back to a feedback coil, which holds the sphere at its null position. The magnitude of the current through the feedback coil provides measurements of changes in the gravitational forces. Four different outputs give this signal (Figure 1):

1. the "*Gravity Signal*" output, lowpass filtered ($T_{cutoff} \approx 1$ s);
2. the "*Tide*" output, lowpass filtered ($T_{cutoff} \approx 72$ s);
3. the "*High Resolution Gravity Signal*" output, lowpass filtered ($T_{cutoff} \approx 40$ s), not used on C021;
4. the "*Mode*" output, lowpass filtered (1 min. $< T_{cutoff} <$ 1h), not used on C021.

A Keithley 2000 6.5 digits voltmeter, guided by a PC, reads the output "*Tide*" two times per second. This sampling rate is guided by DCF. Then a numerical anti-aliasing least squares filter (Bloomfield,1976) (T_{cutoff} = 20s, length = 239) is applied and data are resampled every 10 s. Note that for security, this system "*Tide*" is double. The tide peak-to-peak amplitude is about 3 V, 6.5 digits are equivalent to 5 10^6 points, so 1 point is equivalent to about 6 10^{-4} nm/s^2

The output "*Gravity Signal*" is read by a card developed at the Royal Observatory by the Seismological Section. This card includes a 18 bits analog/digital converter with an oversampling rate of 200 Hz guided by a DCF-controlled quartz. A digital filter decimates those oversampled data to 25 Hz. Then a PC redecimates data to 1 Hz with a least squares filter (T_{cutoff} = 5 s, length = 249 data). To avoid over-voltage from the gravimeter output we placed a divider bridge (ratio 1:11) before the card. The tide peak-to-peak amplitude is about 3 V / 11, 18 bits are equivalent to 262144 points, so 1 point is equivalent to about 1.15 10^{-2} nm/s.

The high sampling rate was chosen in order to study Earth's free oscillations as it allows a better frequency resolution than 10 s or 1 min. data. Furthermore, the higher cutoff frequency of the output "*Gravity Signal*" prevents attenuation of normal modes frequencies.

3. Data preprocessing, tidal analysis and time lag

The "*Grav. Sig.*" data acquisition system provides an independent measurement and processing of gravitational changes. Moreover, we have a control of the long term behaviour of the instrument (it could eliminate systematic effects that data acquisition systems could produce). System "*Grav. Sig.*" gives also an information on the phase lag of the "*Tide*" filter as shown below.

Before data preprocessing with PRETERNA, we decimated data from system "*Grav. Sig.*" to 1 data / 10 s (LSQ anti-aliasing filter, T cutoff = 50 s, length = 239) in order to compare them with data from system "*Tide*". Data from both systems are corrected for pressure effects with an admittance of -3.58 nm s^{-2} hPa^{-1}. Then we performed an ETERNA tidal analysis (Wenzel, 1996). Table 1 shows amplitude factors and phases for the main diurnal (O_1, K_1) and semi-diurnal waves (M_2, S_2).

Table 1. Tidal analysis by ETERNA on 112.13 days (from: 1996.01.24 00h00 UTC to: 1996.05.15 02h00 UTC). For system "Tide" phases values are calculated with 30 s phase lag while values in parentheses are calculated with a 35.10 s phase lag

	System TIDE				System Gravity Signal			
	Amplitude	*Stdv.*	Phase [*deg.*]	*Stdv.*	Amplitude	*Stdv.*	Phase [*deg.*]	*Stdv.*
O_1	**1.15103**	***0.00025***	**0.0717** (0.0914)	***0.0145***	**1.15110**	***0.00022***	**0.0917**	***0.0129***
K_1	**1.13956**	***0.00019***	**0.2704** (0.2917)	***0.0106***	**1.13955**	***0.00016***	**0.2899**	***0.0094***
M_2	**1.18998**	***0.00008***	**2.4049** (2.4460)	***0.0046***	**1.18998**	***0.00008***	**2.4475**	***0.0046***
S_2	**1.19527**	***0.00016***	**0.7153** (0.7579)	***0.0096***	**1.19513**	***0.00016***	**0.7569**	***0.0097***

Standard deviation of weight unit:

0.732 nm/s² (0.733 nm/s²)	0.733 nm/s²

Comparisons between phases obtained from system "*Tide*" and "*Gravity Signal*" show a difference of about 5 seconds, as shown in Table 2. In fact, up to now the "*Tide*" output time lag was supposed to be 30 s, but this tidal analysis shows that a value of 35.10 s is more correct. So we performed a new analysis with this time lag that gives new phase values written in Table 1 in parentheses. The 35.10 s time lag agrees with the time lag determined by Wenzel (Francis *et al.*, 1997) using the step response method. Note that these 35.10 s reflects just the time lag between "*Tide*" and "*Gravity Signal*" outputs, not the total time lag as the feedback integrator and the "*Gravity Signal*" filter produce a time lag too (about 3.5 s), determined by Wenzel.

Table 2. Difference between phases of "*Tide*" and "*Gravity Signal*" (G.S.) outputs for waves O_1, K_1, M_2, S_2. Differences before and after addition of a 5.10 s time lag for system "*Tide*".

	Phase lag = 30 s		Phase lag = 35.10 s	
	Phase (G.S.)- Phase (Tide) (degrees)	Phase (G.S.)-Phase (Tide) (seconds)	Phase (G. S.)- Phase (Tide) (degrees)	Phase (G. S.)-Phase (Tide) (seconds)
O_1	**0.0200**	**5.164**	**0.0003**	**0.077**
K_1	**0.0195**	**4.693**	**-0.0018**	**-0.433**
M_2	**0.0426**	**5.291**	**0.0015**	**0.186**
S_2	**0.0416**	**4.992**	**-0.0010**	**-0.12**

4. Comparison of residues

Residues are obtained, by subtracting from the hourly data, a tidal signal calculated using the amplitudes factors and phases obtained from the tidal analysis of the original data themselves. To correct for air pressure effect, we subtract the locally recorded atmospheric pressure signal from the gravity record using a barometric admittance adjusted by least squares by ETERNA. The admittance is -3.35 ± 0.02 nm s^{-2} hPa^{-1} for system *"Grav. Sig."* and 3.34 ± 0.02 nm s^{-2} hPa^{-1} for system *"Tide"*. We see on Figure 2 that residues from both systems are very similar. Note that comparison with absolute gravimeter (Francis *et al.*, 1996) indicates that the observed trend is not due to instrumental drift.

On Figure 3 we plot the difference between residues of systems *"Tide"* and *"Grav. Sig."*. Remaining spikes and jumps are bigger than 2 nm/s² and are due to maintenance or earthquakes. Step 1 (1996.02.13) is due to a change in the gravimeter electronics grounding, step 2 (1996.03.04) is due to a change in the characteristics of the *"Grav. Sig."* antialiasing filter (cutoff frequency of 0.2 Hz in place of 0.5 Hz). After the second step the curve returns to the same level than before the first step: this is by chance. Three other small steps (step 3, 4 & 5) occur on March, 21, April 03 and 13, 1996, due to some tests on the gravimeter electronics. Steps 1, 4 & 5 appear on both systems (this is too small to be seen on Figure 2) but correction factors are different, step 3 appears only clearly on system *"Tide"*; that is the reason why steps occur also after difference between residues. This stresses the problem of step correction, different for each system: step 1 is due to a real difference between systems, explained by the grounding problem, but steps 3 & 4 are mainly due to "human factor" as data from each system are processed by two different persons. Anyway the effect remains quite small.

5. Earth's free oscillations

On 17 February 1996, at 05h59m33s UTC, a 8.0 ms Earthquake occurred in Irian Jaya, Indonesia (western part of New Guinea, 0.5° N, 135.8° E). It gave the opportunity to test the performances of C021 for seismic free oscillations frequencies. Analyses are performed after 09h00 UTC in order to avoid saturation due to first body-wave and Rayleigh-wave arrivals.

First we performed a cross spectrum analysis between the *"Tide"* and the *"Gravity Signal"* output; for this purpose data from system *"Grav. Sig."* were decimated to 1 data / 10 s. A theoretical tidal signal is computed from the tidal potential development of Tamura (Tamura, 1987) and subtracted from the original data of both systems. In order to avoid any long period residuals, data were then high-passed (LSQ filter, T cutoff = 3600 s, length = 499). Results of cross spectrum analysis using a Parzen window are shown in Figure 4. The cross spectrum gives a nice opportunity to visualize the time lag between filters *"Tide"* and *"Gravity signal"*. Fitting by least squares a straight line through the phases, the following relationship appears: *phase lag = -14864 frequency + 8.14.* Table 3 shows lags for some periods. Values determined by Wenzel (Francis *et al.*, 1997) using sine waves injected in the feedback coil are also shown for comparison. Remember that this last method gives the total gravimeter phase lag, filter *"Tide"* included.

Table 3. Phase lags for different periods. Lags between *"Tide"* and *"Gravity Signal"* outputs are in the first column. Lags induced by *"Tide"* filter and all the instrument are in the second column.

Period	Phase (Grav. Sig.) - Phase (Tide)	Phase (Tide) given by sine waves
50 s	40 s	45 s
100 s	39 s	42 s
200 s	37 s	39 s
500 s	30 s	38.2 s

For Periods greater than 200 s results from cross spectrum are too small, as in tidal band we should have about 35 s. This shows the limit of cross spectral analysis to determine phase lags. It is mainly due to lack of signal below 500 s.

Then we performed spectral analysis with data from instruments C021 (Membach, *"Gravity Signal"* output), C025 (Vienna, *"High Resolution Gravity Signal"* output), T018 (Potsdam, *"Mode"* output) and LCR-ET-19 (Schiltach, *"Tide"* output). LCR-ET-19 gravimeter results are interesting. Indeed, Richter (Richter *et al.*, 1995) showed in a compared study between seismometers STS-1, STS-2, superconducting gravimeter SG-102 and gravimeter LCR-ET-19 that LCR-ET-19 and STS-1 instruments give the best results in the free oscillations frequency band.

As LCR-ET-19 and T018 sampling rate is 1 data / 5 s, C025 and C021 data were decimated after lowpass filtering (T cutoff = 16 s, length = 239). Then data are high-passed but no theoretical tide was removed. On Figures 5, 6, 7 & 8 we see amplitude spectra for C021, C025, T018 and ET-19 instruments. Spectra are calculated with 65536 data using a Parzen window. Dashed lines indicate modes' frequencies as given by Widmer (Widmer, 1991). Results from ET-19 are the best ones, those from Potsdam the noisiest; it is certainly due to the proximity of T018 to the city.

The Irian Jaya event was not the best one for mode excitation (Widmer, personal communication, 1996), so we plan to study more thoroughly free oscillations with cryogenic gravimeters in the near future.

6. Conclusions

The high sampling rate data acquisition system connected to the output *"Gravity Signal"* gives very good results in the tidal band and allows us to confirm the long term behavior of the superconducting gravimeter C021. Furthermore this high sampling rate data acquisition system gives an evaluation of the time lag induced by the *"Tide"* filter. The C021 instrument seems also to be a good broad band seismometer but this needs to be confirmed.

Acknowledgment

I thank Dr. B. Ducarme, Dr. O. Francis and M. Hendrickx for their fruitful discussions. Dr. Francis and M. Hendrickx are also acknowledged for the maintenance of the SG gravimeter C021 and the *"Tide"* data. I am very grateful to M. Snissaert, A. Somerhausen and Dr. M. Van Ruymbeke who helped me to fit the *"Grav. Sig."* data acquisition system. I am indebted to Dr. B. Meurers, Dr. J. Neumeyer and Dr. W. Zürn who kindly gave data from their systems. This work was supported by the "Fonds pour la Formation à la Recherche dans l'Industrie et l'Agriculture".

References

- Bloomfield, P., Fourier analysis of times series: an introduction, *John Wiley & Son,* 1976.

- Francis, O., Ducarme, B., Van Ruymbeke M., One year of registration with the C021 cryogenic gravimeter at the Membach station (Belgium), *submitted to the proceedings of the Tokyo meeting,* October 1996.

- Francis, O., Van Camp, M., Schott, P., Wenzel, H.-G., Instrumental transfer function determination for cryogenic gravimeter GWR C021 at station Membach, *paper to be presented at the XXIIIth International Symposium of Earth Tides,* Bruxelles, July 22-24, 1997.

- GGP Newsletter # 2, *edited by D. Crossley and J. Hinderer*, November 16, 1996.

- Richter, B., Wenzel, H.-G., Zürn, W., Klopping, F., From Chandler wobble to free oscillations: comparison of cryogenic gravimeters and other instruments in a wide period range, *Phys. Earth Planet. Inter.,* **91**, 131-148, 1995.

- Tamura, Y., A harmonic development of tide-generating potential, *Bull. Inf. Marées Terrestres,* **99**, 6813-6855, 1987.

- Wenzel, H.-G., The nanogal software: Earth tide data processing package: ETERNA 3.3, *Bull. Inf. Marées Terrestres,* **124,** 9425-9439, 1996.

- Widmer, R., The large-scale structure of the deep Earth as constrained by free oscillation observations, *Ph-D Thesis,* University of California, San Diego, 1991.

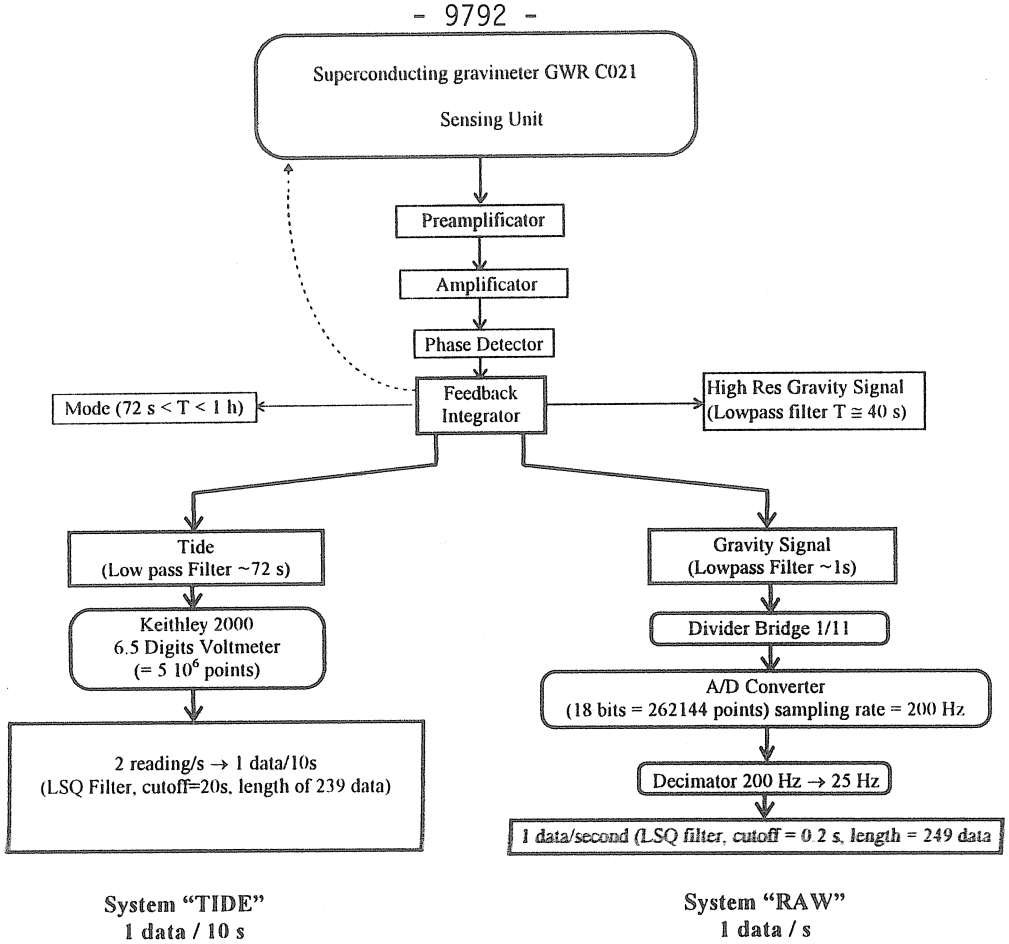

Figure 1. Gravimeter electronics and data acquisition systems of the C021 cryogenic gravimeter. Outputs "Mode" and "High Res Gravity Signal" are not used.

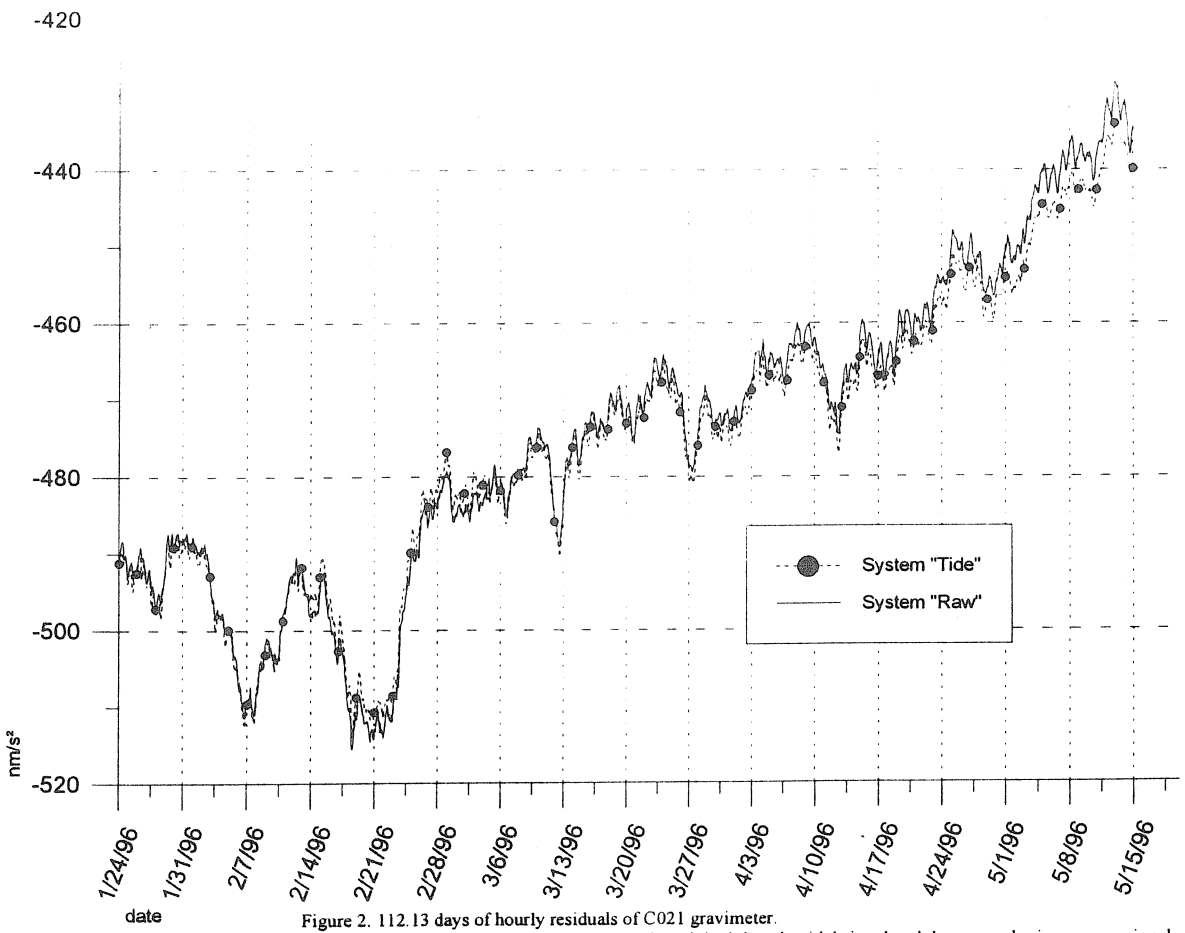

Figure 2. 112.13 days of hourly residuals of C021 gravimeter.
These data are obtained by subtracting from the original data the tidal signal and the atmospheric pressure signal.

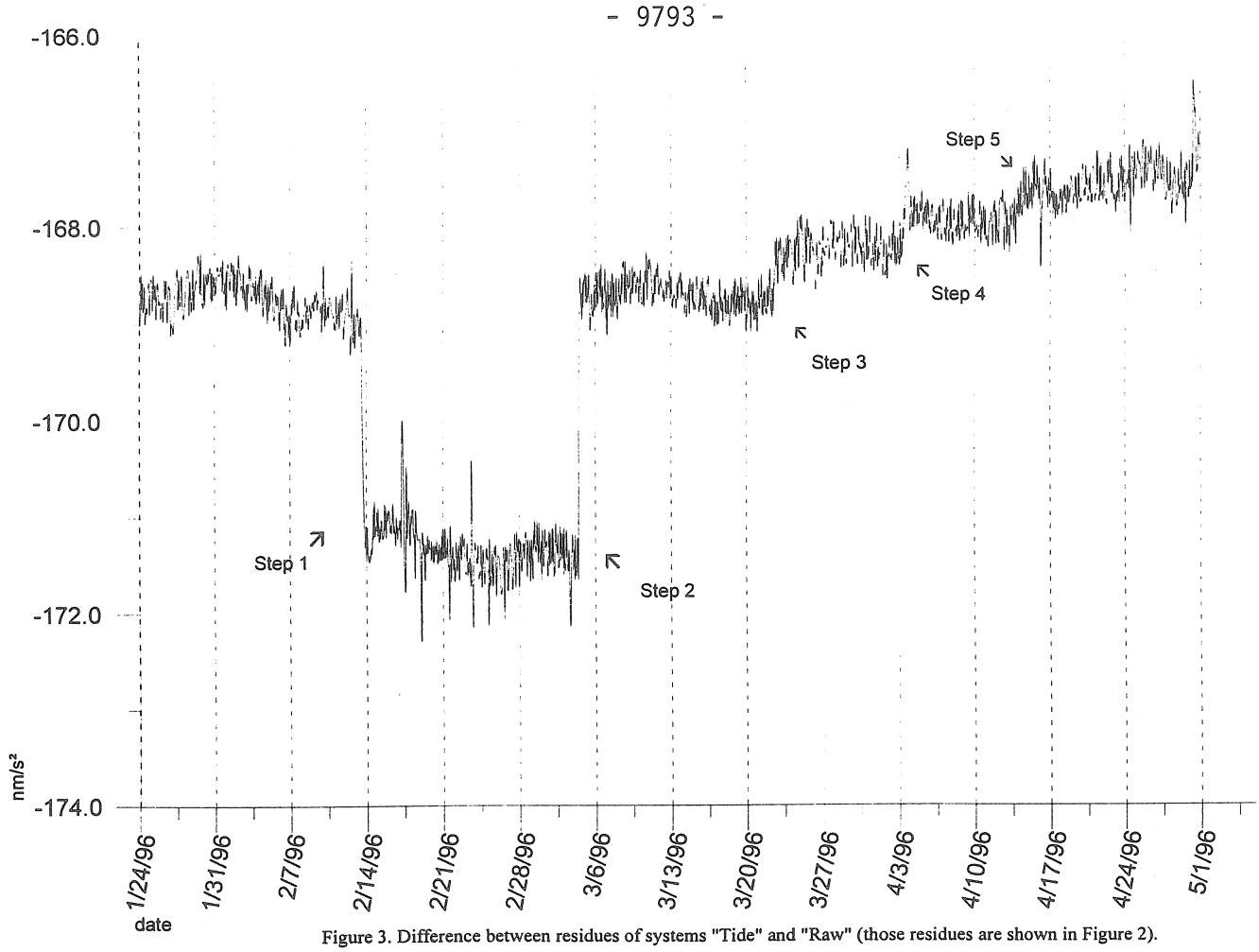

Figure 3. Difference between residues of systems "Tide" and "Raw" (those residues are shown in Figure 2).

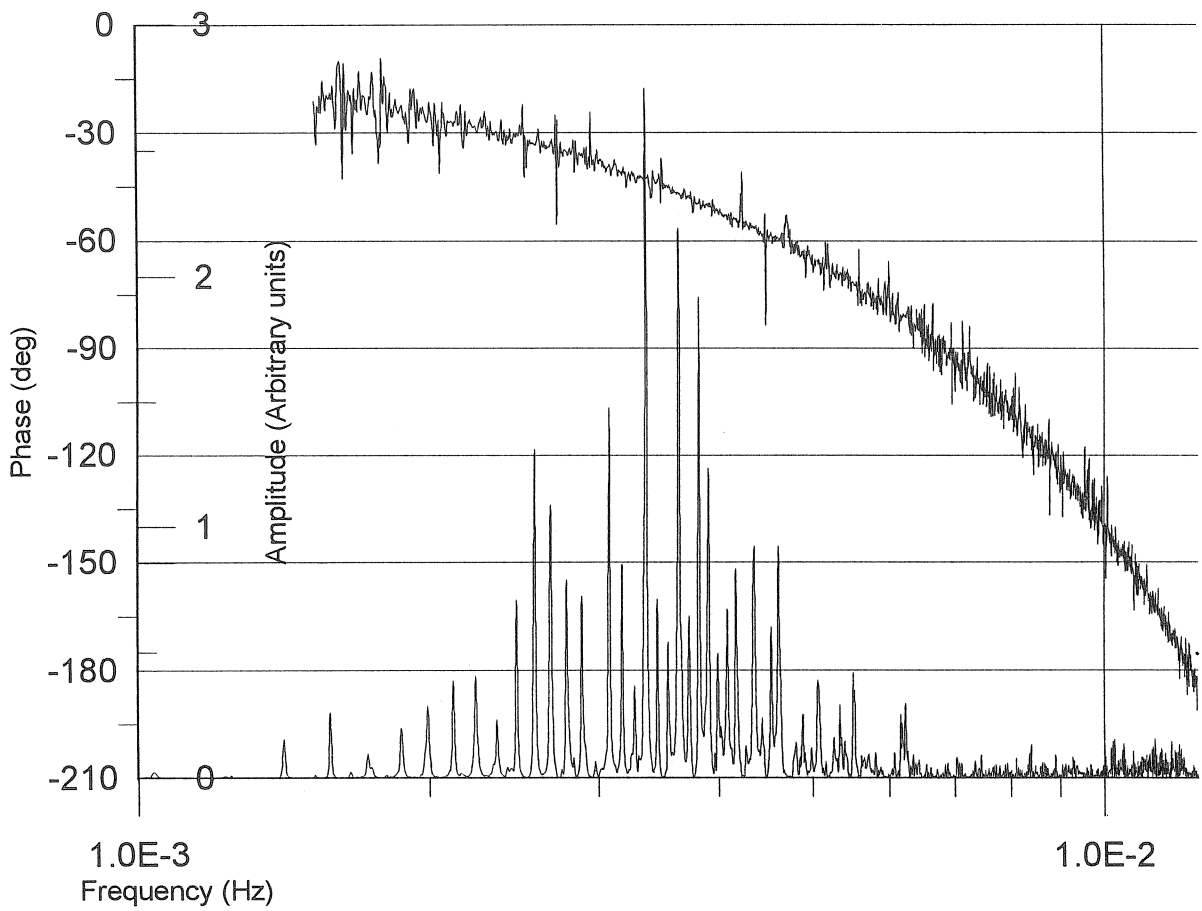

Figure 4 : Irian Jaya earthquake (17 Feb. 1996). Cross spectrum between "tide" and "gravity signal" output. Sampling rate : 1 data / 10 s. Data from 17/02/1996 09h04m00s to 19/02/1996 23h55m50s.

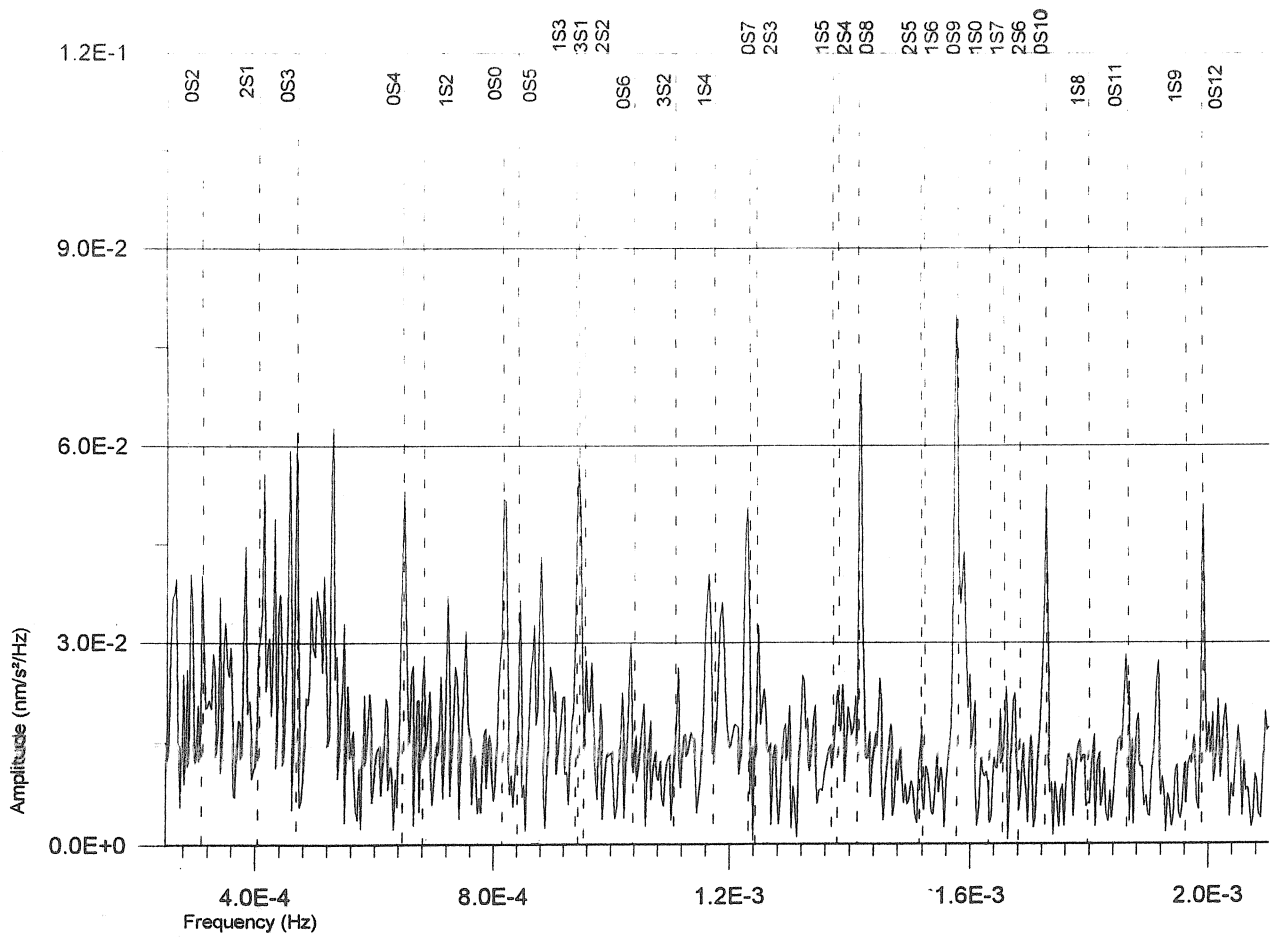

Figure 5. Gravimeter C021 gravity signal output. Amplitude spectrum from 3 to about 94 h after the Irian Jaya earthquake, of 17 February 1996. Vertical dashed lines indicate theoretical degenerate eigenfrequencies given by Widmer (Widmer, 1991).

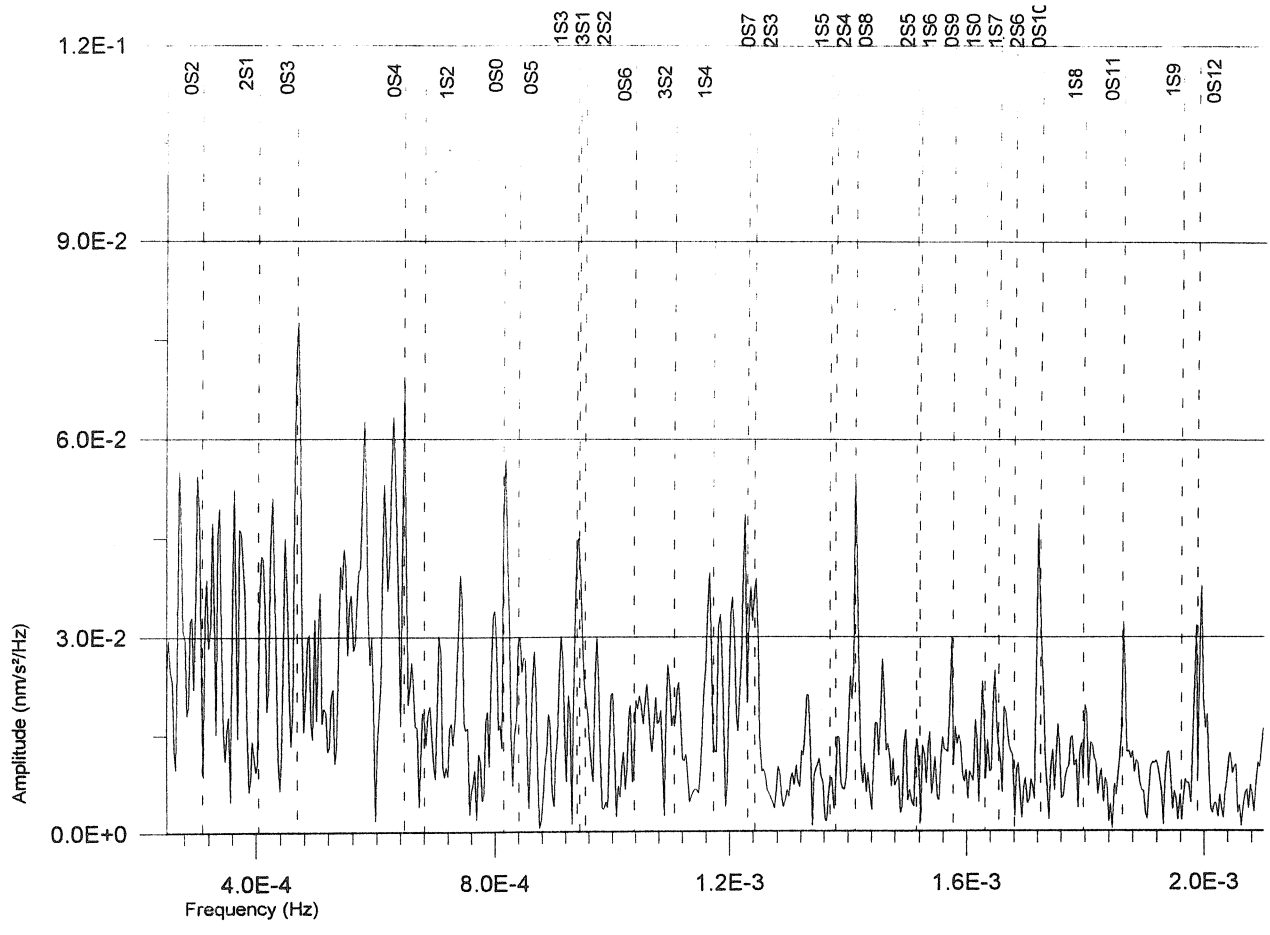

Figure 6. Gravimeter C025 high. res. grav. signal output. Amplitude spectrum from 3 to about 94 h after the Irian Jaya earthquake, of 17 February 1996. Vertical dashed lines indicate theoretical degenerate eigenfrequencies given by Widmer (Widmer, 1991).

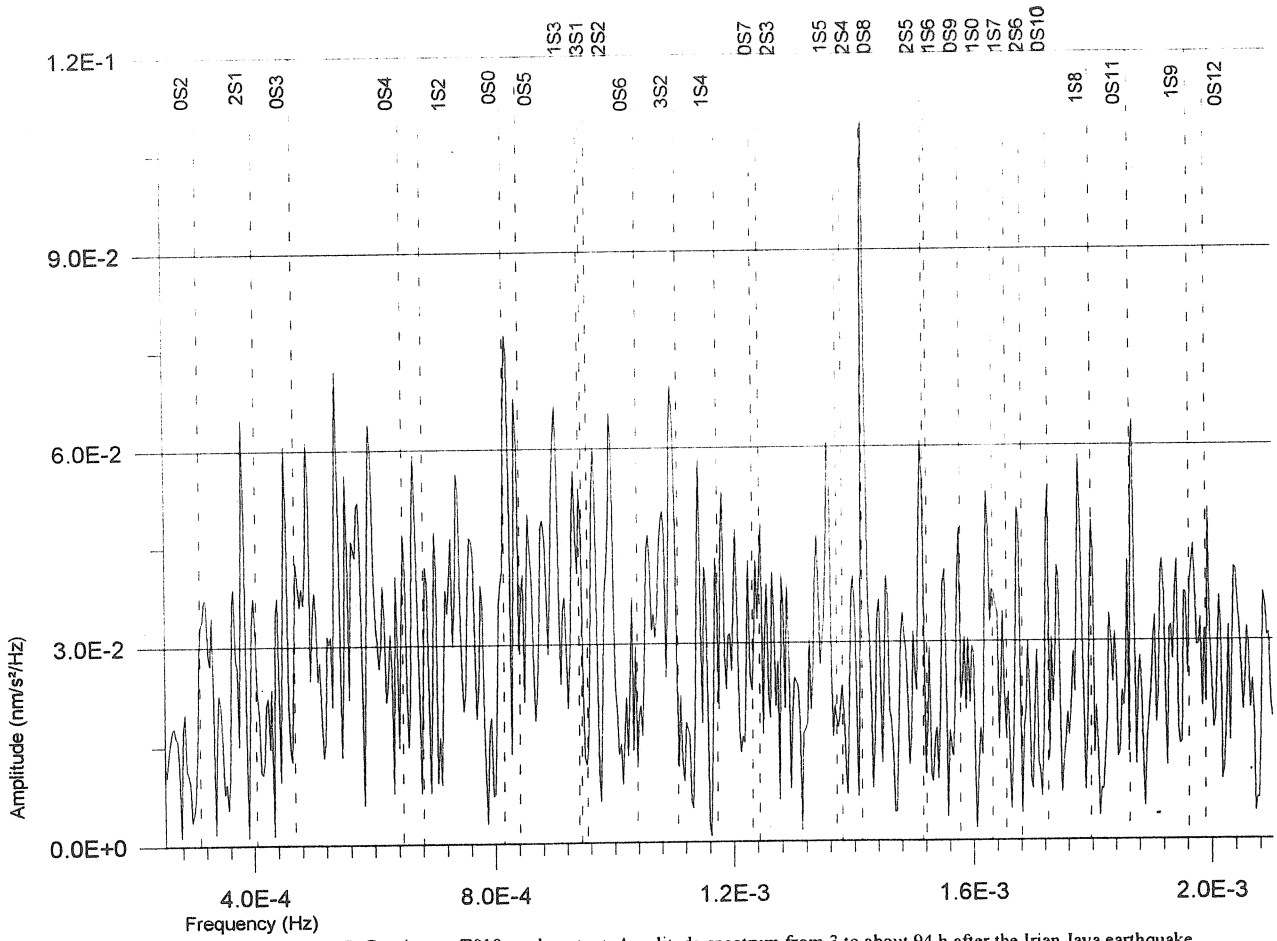

Figure 7. Gravimeter T018 mode output. Amplitude spectrum from 3 to about 94 h after the Irian Jaya earthquake, of 17 February 1996. Vertical dashed lines indicate theoretical degenerate eigenfrequencies given by Widmer (Widmer, 1991).

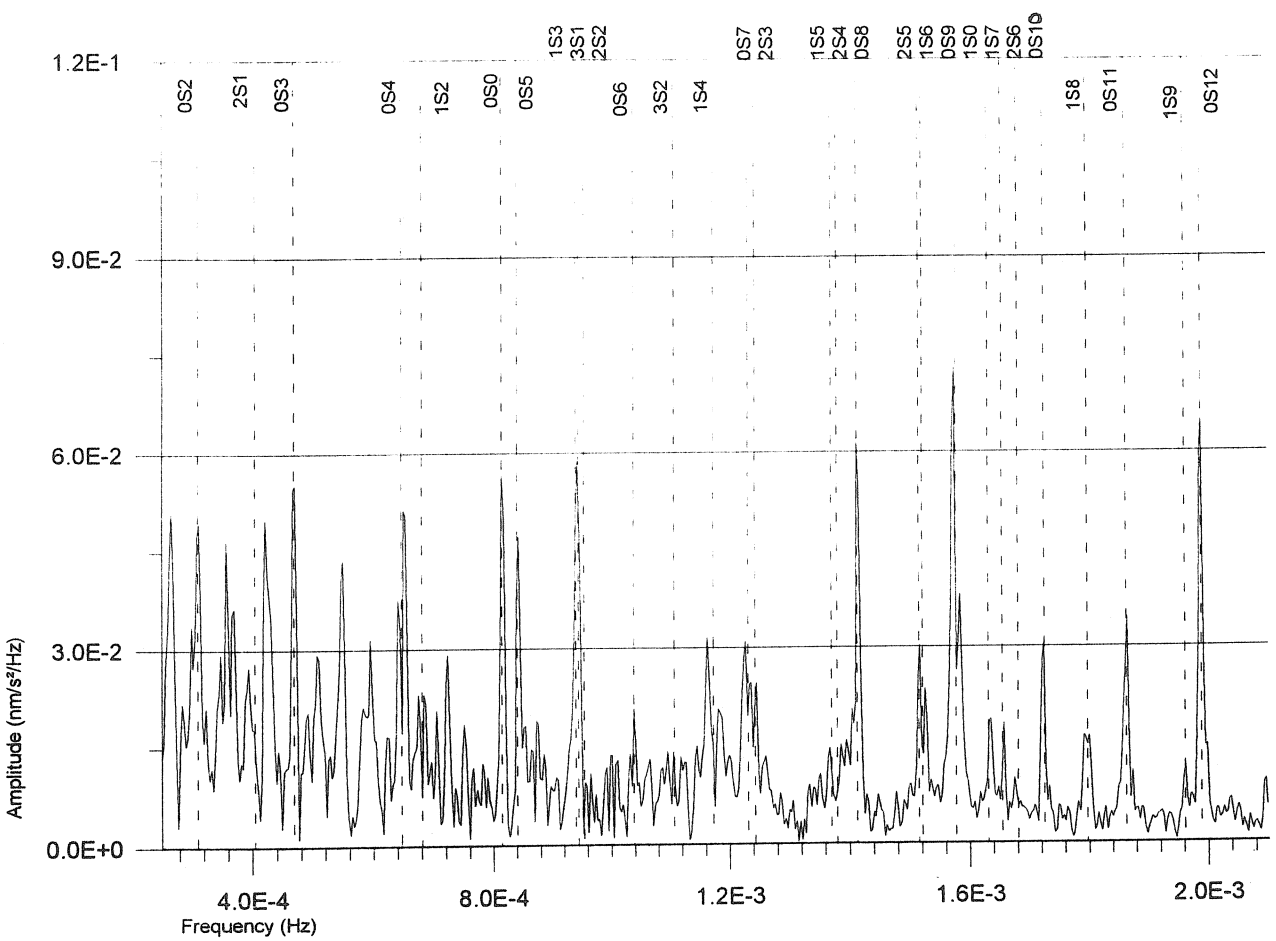

Figure 8. Gravimeter LCR ET-19 tide output. Amplitude spectrum from 3 to about 94 h after the Irian Jaya earthquake, of 17 February 1996. Vertical dashed lines indicate theoretical degenerate eigenfrequencies given by Widmer (Widmer, 1991).

Longtime behaviour of superconducting gravimeters derived from observed time series

Martina Harnisch, Günter Harnisch
Institut für Angewandte Geodäsie, Außenstelle Potsdam
Michendorfer Chaussee 23, PF 600808, D-14408 Potsdam

Summary

Basing on data of the superconducting gravimeters TT60 (Wettzell, 1989 - 1995) and SG103 (Bad Homburg, 1993 - 1995, Wettzell 1996), it is demonstrated that the linear part as well as the exponential initial run of the instrumental drift may vary considerably. These variations occur not only between different instruments but also between different observation periods of one and the same gravimeter. During the preprocessing of data series greatest care has to be taken on the elimination of steps, frequently occuring in the recordings of superconducting gravimeters. In order to avoid serious falsifications, only greater steps should be eliminatited. An exact threshold can not be given generally. The data of the TT60 yield a gravimetric factor of $\delta_{Chandler} = 1.16$ for the Chandler wobble of the polar motion.

1. Introduction

When the first superconducting gravimeters were developed in the early seventies, it was expected that their low instrumental drift would support investigations on long-term phenomena. Indeed B. RICHTER could derive the gravitational effect of polar motions from a time series of nearly three years recorded with the gravimeter TT40 at Bad Homburg [1]. But not each of the later experiments with different instruments at different sites in the world was similarly successful.

Two years ago we presented a paper concerning the processing of data from the gravimeters SGB (UCSD) and TT40 (IfAG), recorded 1989 - 1991 at Miami [4]. Especially the exponential constituent of the instrumental drift and the role of steps were discussed. In the following we continue this discussion basing on data of the gravimeter TT60, recorded 1989 - 1995 at Wettzell. After some disappointing initial results it was the long time span of this series which encouraged us to continue this troublesome job very carefully. In addition to the satisfactory final result (from our point of view) also some methodical aspects may be of common interest.

The installation and the maintenance of the gravimeters were done by B. RICHTER and P. WOLF (both IfAG, Frankfurt a.M.). The job of the authors was only the processing of the recorded data.

2. Technical aspects of the instrumental drift

The instrumental drift is a mixture of numerous components with a variety of sources. WARBURTON & BRINTON gave a detailed survey of the possible mechanisms of the drift behaviour of superconducting gravimeters [2]. From this compilation it is easy to understand that the instrumental drift may have different values and different signs, depending on the contribution of the single components (fig. 1). But no explanation can be given for drift rates in the order of 200 µGal/year as it shows the gravimeter SG103 installed in april 1996 at Wettzell (replacing the elder TT60).

Between 1993 and 1995 the SG103 recorded at Bad Homburg. During this time it showed a linear drift of about +20 µGal/year. After the transportation to Wettzell the drift was about -180 µGal/year (fig. 2). Reinitialization and demagnetization, done in september 1996, could not reduce the very large drift rate.

3. The restkurve as a tool to derive the instrumental drift from observed data

In order to derive long-term and aperiodic phenomena we use the residuals which remain after "all known influences" (e.g. tides, environmental influences) have been subtracted from the observed gravity variations. They are distinguished from the residuals of adjustment procedures using the german word

"restkurve". The number of eliminated influences may vary during the processing procedure. They may also include the effect under investigation (e.g. the influence of polar motion), which later may be added again. In this case the subtraction acts as a "saving procedure" of the respective component.

Drift Source	Drift Direction	Drift Upper Limit (4 Week Test)
Helium Leaks		
Sphere Chamber	↓	< 1 μGal/year
Vacuum Can	↑	<< 1 μGal/year
Initialization Procedure		
Cooldown Procedure	?	
Temperature Annealing	?	
Adjustment of Magnetic Gradient	?	
Magnets - Current Decay		< 5 μGal/year
Lower	↓	
Upper	↑	
Guard Coils	↓*	
Temperature	↓ ↑	< 6 μGal/year
Capacitance Bridge	↓ ↑	< 12 μGal/year
Tilt	↓*	< 1 μGal/year
Sphere		
Flux Motion	↓ ↑	
Gas Adsorption	↓	
	↑	

* - if gravimeter was set up properly ↓ - sphere down ↑ - sphere up

Fig. 1: Possible Drift Mechanisms (after WARBURTON & BRINTON [2])

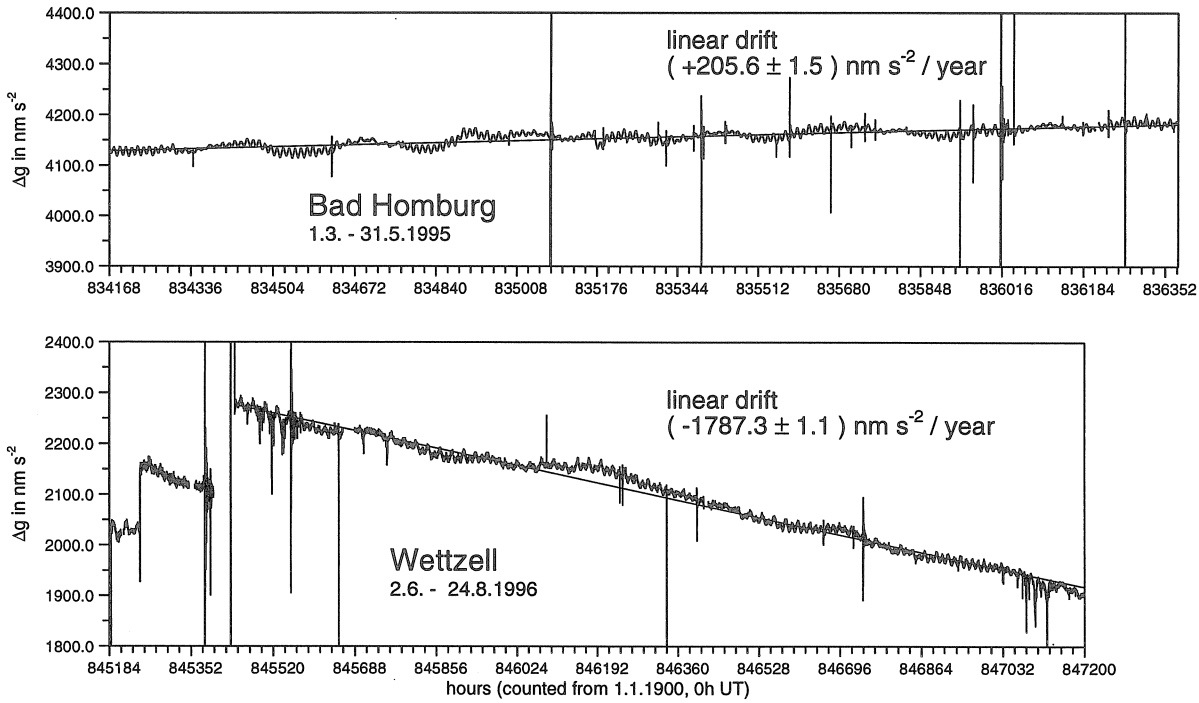

Fig. 2: Restkurven of Gravimeter SG103 (theoretical tides and air pressure influence subtracted)

3.1. Influence of steps

Obviously superconducting gravimeters have a tendency to sudden shifts of the measured values. Such steps occur more frequently than in the records of spring gravimeters and should be considered down to some nm s^{-2} [3]. Steps should be monitored using data with a time resolution as high as possible.

Long-term effects are very difficult to detect in the residuals of a time series. They are easily covered by falsifications of the restkurve. Therefore we tried to correct especially the steps very carefully and as completely as possible.

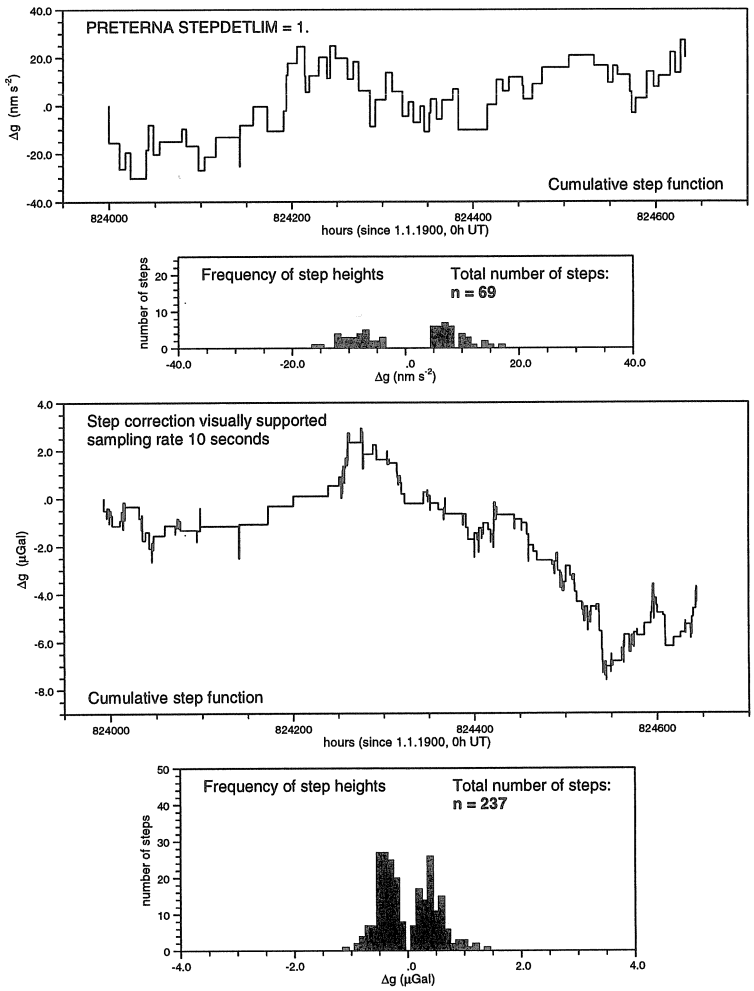

Fig. 3: Step statistics TT60, Wettzell. Cumulative step function and frequency distribution of steps

In the lower half of fig. 3 the result of a visually supported inspection of 10-s-data is shown. The processed section covers a time span of 4 weeks. 237 steps could be detected down to 1 nm s^{-2}. Obviously the gap in the middle of the frequency diagram is caused by steps, which are hidden by the noise and therefore could not be detected. One can only hope that these undetectable steps extinguish each other and in this way don't falsify the restkurve.

In the upper half the same data were processed using the PRETERNA program with a threshold of 1 nm s^{-2}. For this purpose the data must at first be decimated to equidistant 1-min-values. Alltogether 69 steps were found down to 4 nm s^{-2}.

Looking on the cumulative step functions, their different tendencies are shocking. But this is not all! A third processing with PRETERNA setting another threshold would give a third version of the cumulative

step function, and nobody is able to decide what version is the right one. A possible explanation for these discrepancies may be an asymmetric distribution of upward and downward directed steps of different amount (as can also be seen from the synthetic example, fig. 5, 6).

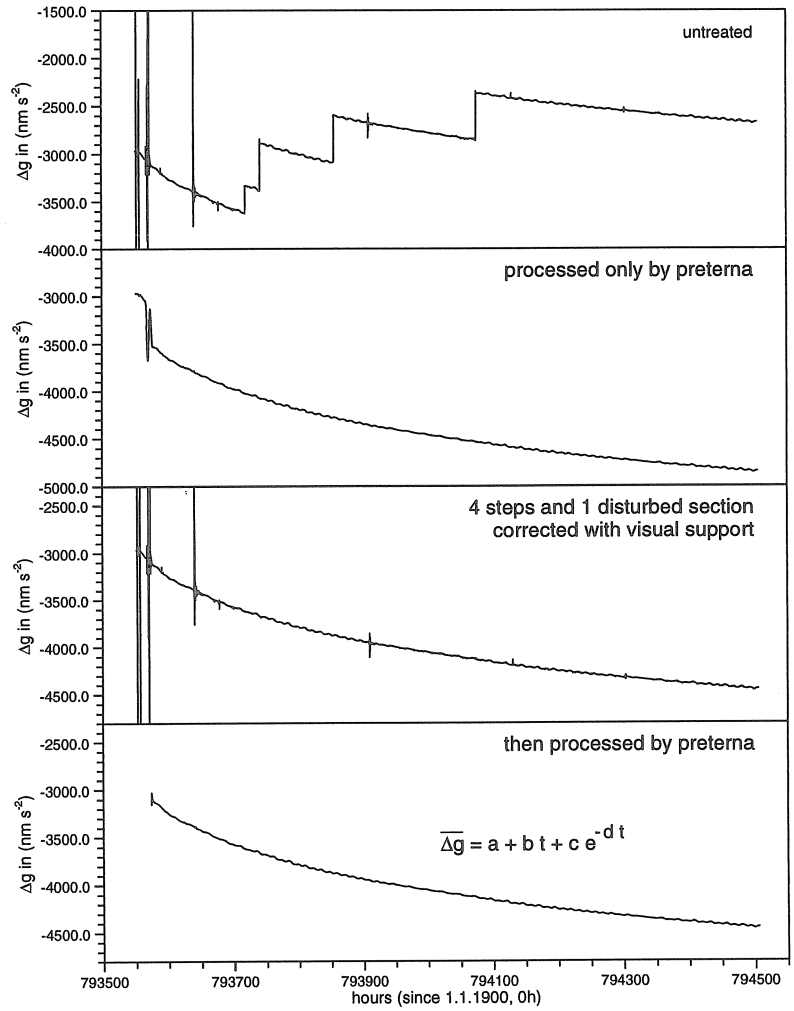

Fig. 4: Disturbed section of a restkurve, demonstrating several steps of the preprocessing

3.2. Exponential constituents of the instrumental drift (initial run)

After the gravimeter was set up at a new place or different greater maintenance activities (e.g. reinitialization), an additional exponential constituent may arise, which superimposes the normal more or less linear drift. Figure 4 shows an example from practice (TT60, Wettzell). The exponential constituent may be eliminated using a drift model with linear and exponential terms:

$$\Delta g = a + b\,t + c\,\exp(-d\,t).$$

This function is fitted to the restkurve. The coefficients are estimated by an iterative procedure. The simple model enables a high approximation accuracy of exponential constituents. Discrepancies may arise in the initial part. In such cases the first few values may be rejected or a second exponential function may be fitted. In both cases the loss of data is less than it would be if the whole exponentially influenced part was cut off. In this way the exponential drift model helps to shorten the unavoidable gaps.

If the restkurve is broken in many small sections, which are short compared with the characteristic time scale of the effect under investigation, it is very important at first to subtract (save) the interesting effect

(e.g. polar motion) as good as possible using all available preliminary informations. Otherwise the effect would be eliminated together with the drift in the single sections.

In the TT60 data (Wettzell 1989 - 1995) a total of 7 sections with exponential constituents were found. The decay times (decay to about 10% of the initial value of the disturbation) varied between 1 week and 4 weeks. Earlier investigations of the data of other gravimeters, e.g. the gravimeters TT40 and SGB, installed 1989 - 1991 at Miami, showed decay times of about 30 days (TT40, Jan.-Feb.1991), 15 days (SGB, April 1990), and 5 days (SGB, August 1990) [4]. Obviously the decay times depend on the installation conditions, and they are not characteristic parameters of every single instrument.

3.3. Linear part

After having subtracted the exponential constituents (only the pure exponential function, without the linear part of the drift model) the remaining part of the restkurve should be a more or less straight line. An example is given below in connection with the discussion of the TT60 series, recorded 1989 - 1995 at Wettzell. It becomes evident that each section may have its own value of the linear drift. This value varies considerably for several parts of the restkurve of one gravimeter at one and the same place. There are no defined links between the single sections which would us enable to fit the single parts to an overall drift model covering the total time span. That is why the interesting effects at first must be saved as it was described in context with the exponential constituent of the restkurve. Only long-term series with uninterrupted sections longer than the characteristic time scale of the interesting effects give the chance to study long-term phenomena without depending on apriori informations or tricks.

4. Synthetic example of instrumental drift and some experiments with the PRETERNA program

A synthetic drift model was compiled including steps of 10 and 50 nm s^{-2}, a linear drift of -178 nm s^{-2}/year and a noise of 10 nm s^{-2} (standard deviation), in order to demonstrate the influence of steps on the restkurve and on the results of preprocessing. The total length of this synthetic series is 14 days, the sampling rate 1 min (fig. 5). From this simple example it can clearly be seen that the noise hids the small steps on the backward side of the bulges. If we decide not to consider the ramps of several hours as steps, a systematic drift of the cumulative step function and as a consequence a systematic falsification of the restkurve would arise.

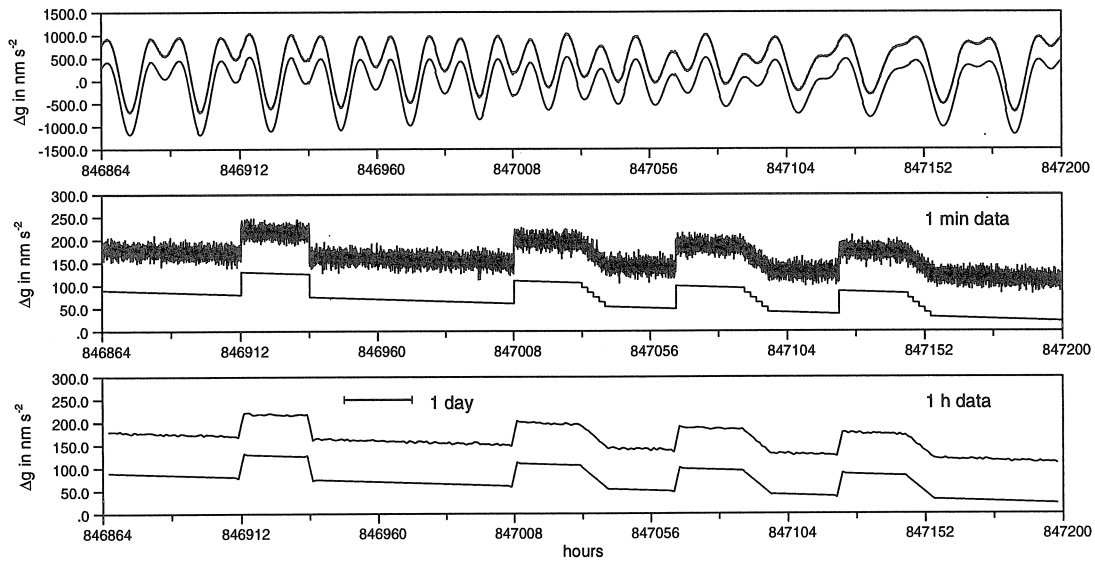

Fig. 5: Synthetic drift model: steps 10 and 50 nm s^{-2}, linear drift -178 nm s^{-2}/year, noise 10 nm s^{-2}. Above: Synthetic observations. Middle: restkurve, sampling rate 1 min. Below: the same restkurve decimated to hourly values. Upper curves with noise, lower curves without noise.

In the undermost part of the figure the same drift model is shown, but with data decimated to hourly values. In this case the cascades of small steps on the rear of the bulges are transformed into a single ramp. The consequence is the same as in the case of the 1 min data.

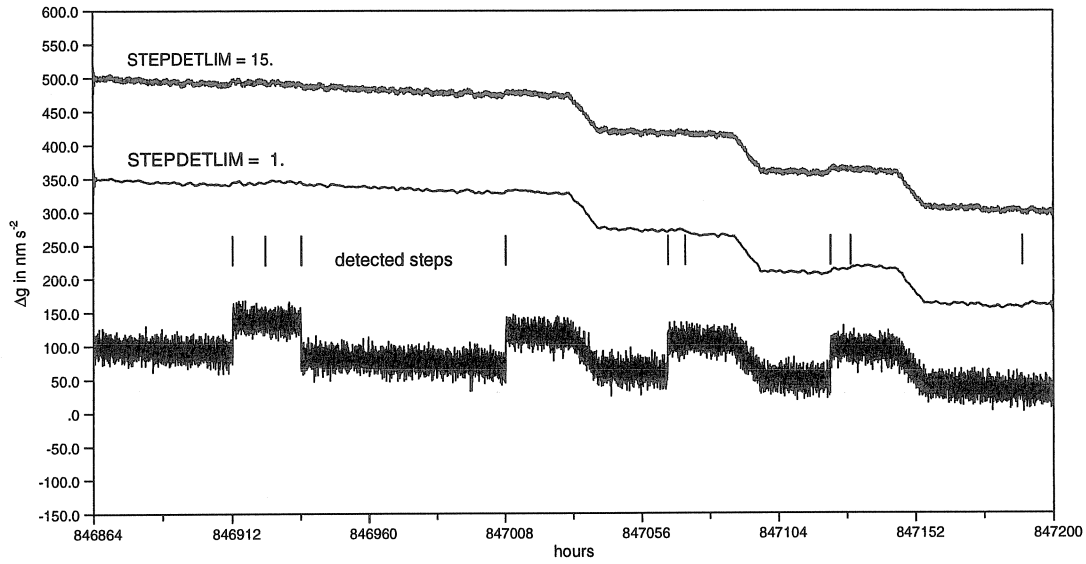

Fig. 6: Results of PRETERNA preprocessing of the noise influenced restkurve of the synthetic observations presented in fig. 5

The synthetic data were processed with the PRETERNA program. With a threshold of 15 nm s^{-2} (STEPDETLIM = 15) exactly the 5 large steps were detected and eliminated (fig. 6). Using a very small threshold of 1 nm s^{-2} (STEPDETLIM = 1) 4 additional fictitious steps were detected. With both thresholds not one of the small steps on the rear of the bulges was corrected. Thus the cumulative step function shows a systematic deviation. But this is not only a problem of PRETERNA. Also during visual inspection small steps are difficult to identify and a systematically falsified restkurve may arise.

In practice the PRETERNA program eliminates most of the large steps without problems (fig. 4). But it is not possible to correct steps combined with gaps, as may be seen from fig. 8. Such situations occur if distorted values in the vicinity of steps are cut away and marked with the code for gaps.

5. TT60, Wettzell, 1989 - 1995[1]

The recording apparatus of the IfAG yields gravity data with a sampling rate of approximately 10 sec. The visual inspection of these original 10 sec data is a very time consuming and troublesome job (each year has appr. 3150000 single values). The detection of steps is difficult due to the high noise level at the station Wettzell (fig. 7).

In order to reduce the time required for the handling of the original data, we used the support given by the PRETERNA program. While the despiking was very successful, the destepping led to falsified results. Large steps combined with gaps were not corrected (fig. 8). Small steps led to systematic deviations of the restkurve depending on the applied threshold (fig. 9). No correspondence could be achieved with the results of the visual supported data handling. This concerns the number of steps as well as the shape of the restkurve. In all cases the corrected restkurve drifted away from the

[1] Due to additional preprocessing activities and actualization of the used polar motion data the results given here differ in some cases from those presented during the Bonn meeting.

uncorrected one. Therefore we inactivated the destepping part of the PRETERNA program setting a high threshold. Only large steps were corrected using visual supported procedures.

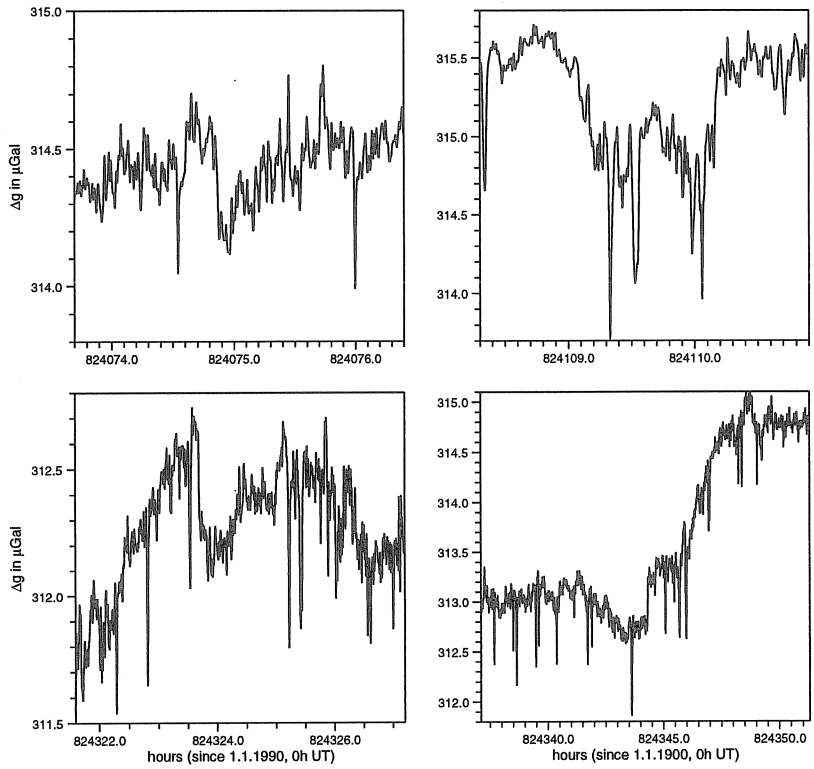

Fig. 7: Sections of the restkurve of TT60, Wettzell (sampling rate 10 s), demonstrating the difficulty to correct steps succesfully

Before the data were analyzed by ETERNA, the gravity effect of the polar motion was subtracted using $\delta = 1.16$. In the tidal analysis the S_a-wave was neglected because the single sections, including the longer ones, were not long enough to get reliable results. At the end of this computation step we got a restkurve broken by gaps and steps into 47 sections as it is shown in fig. 10. This picture is shocking. However a common straight line is to be expected for each section, because we subtracted "all known influences", esp. the influence of polar motions. We can see that after each interrupt (represented by gaps in most cases) the linear drift may alter considerably, also its sign. We have no basis to fit the single sections, neither to a straight line nor to a periodic function. We can only subtract the linear drift of each section separately. The result is a noise-like distribution of residuals. Adding now the influence of the polar motion again, which we have saved before, we get the reflection of the polar motions in the TT60 gravity data, as can be seen in the lower half of fig. 10.

	Annual Constituent	**Chandler Wobble**
Period	365.25	437.29
Gravity effect of Polar Motion	11.607	38.136
Gravity variation	11.411	38.034
δ	1.140 ± 0.0084	**1.157 ± 0.0025**

These data may be fitted by two periodic functions with periods of 1 year exactly and the period of the Chandler wobble, which was estimated for the time span of the gravity time series to 437 days. The amplitudes are 11.411 nm s^{-2} and 38.034 nm s^{-2} respectively (see table above). Fitting the gravity effect of the polar motion in the same way and for the same time section, amplitudes of 11.607 nm s^{-2} and 38.136 nm s^{-2} result. The ratios of these values give tidal gravimetric factors of

$\delta_{Chandler}$ = **1.157 ± 0.0025** for the Chandler period
and δ_{year} = **1.140 ± 0.0084** for the yearly constituent of polar motions.

It has to be taken into account that the annual tidal wave S_a and meteorological influences with yearly period were not eliminated and therefore may disturbe the polar motion in this frequency band.

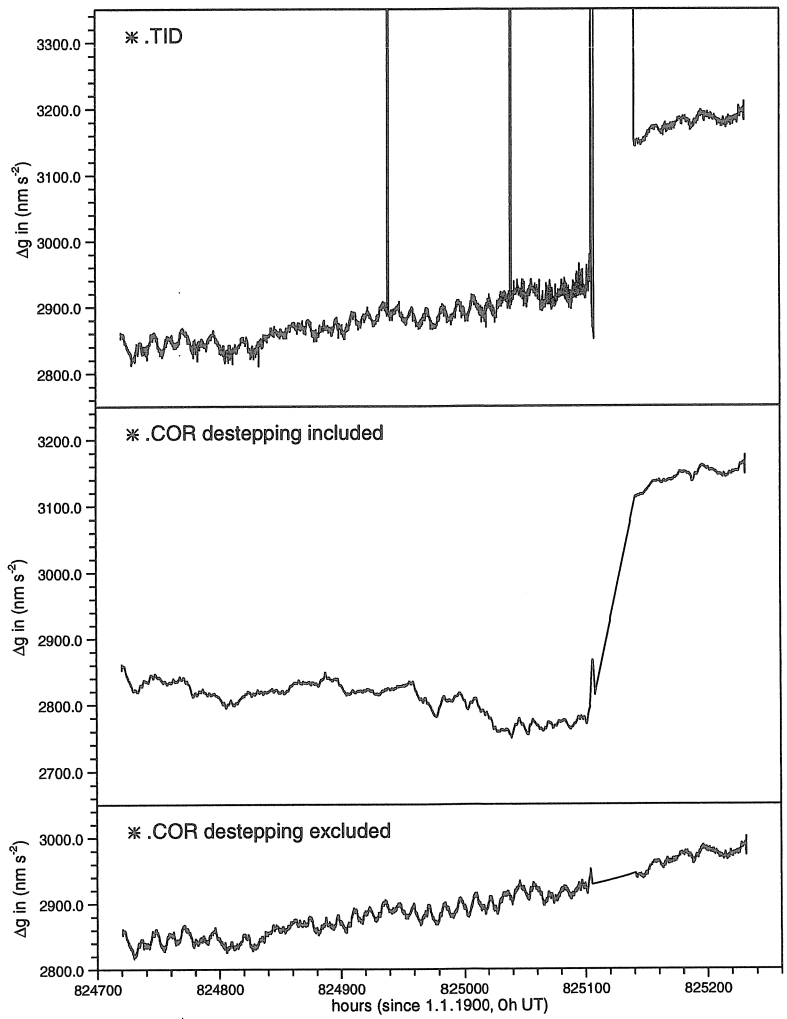

Fig. 8: Restkurve of TT60, Wettzell. This situation of a large step combined with a gap could not successfully corrected by PRETERNA alone (middle). The lower curve is the result of a combination of visual supported preprocessing and PRETERNA.

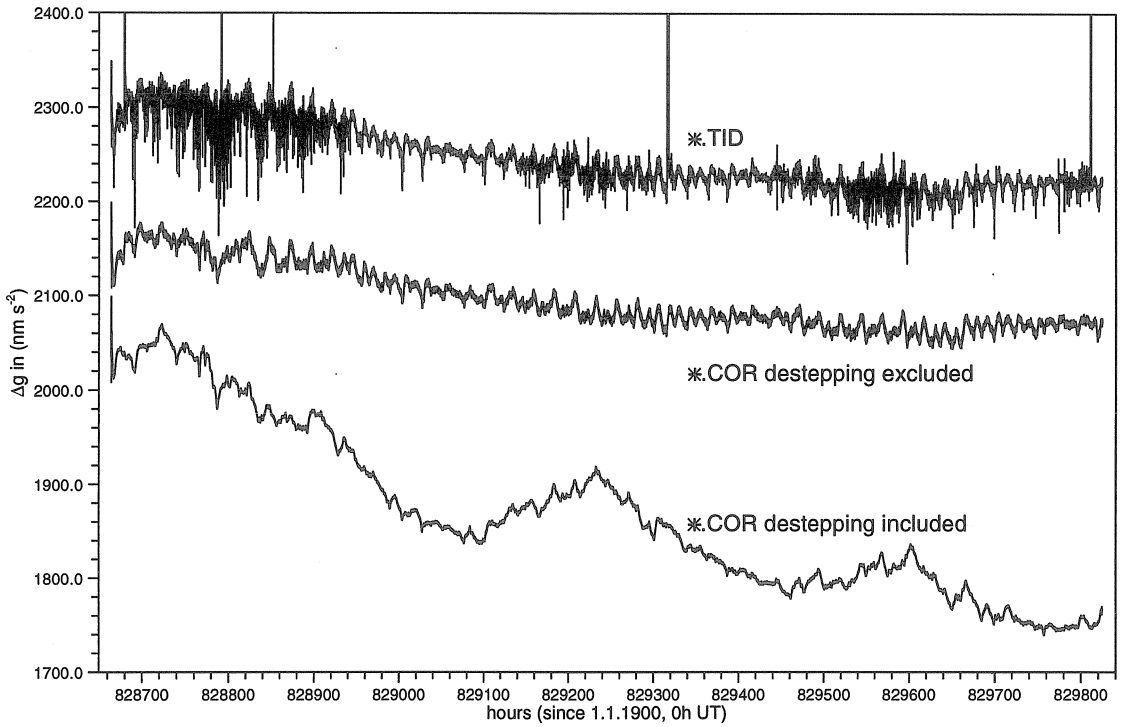

Fig. 9: Restkurve of TT60, Wettzell. This example demonstrates the falsification of the restkurve due to the automatic step correction by PRETERNA (lowermost curve)

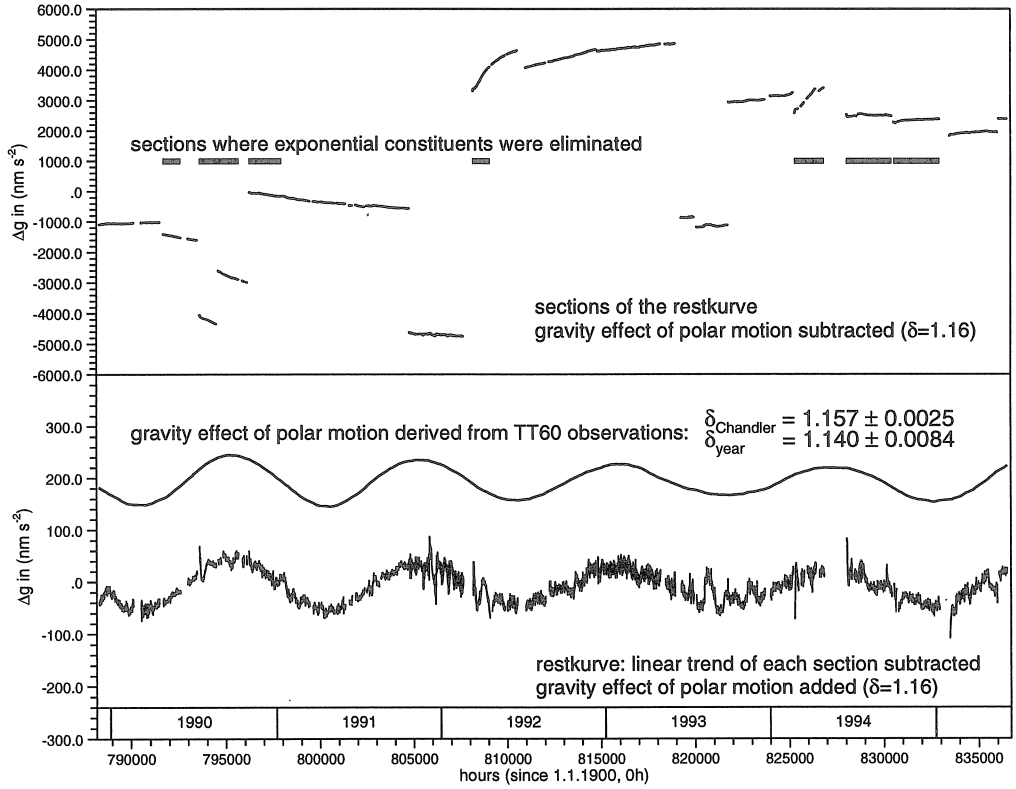

Fig. 10: Final result of TT60, Wettzell, 1989 - 1995 (47 sections). Above: Restkurve (synthetic tides, air pressure effect and gravity effect of polar motion subtracted). Below: Individual drift function subtracted, polar motion effect added again)

6. Final remarks

1. The results of the data recorded between 1989 and 1995 at Wettzell show that it is worth the trouble to evaluate time series over a time span of several years very carefully, even if the data seem to be of low quality, disturbed by numerous gaps, steps, and sections with exponential constituents.
2. To reduce the expenditure of work automatic preprocessing procedures may be a great help. In this context greatest care has to be taken on the elimination of steps.
3. Only greater steps should be corrected. For that purpose only visual supported procedures are suited. Concerning the numerous smaller steps down to some nm s^{-2}, it is the best to ignore them and to hope that they extinguish each other.
4. Concerning future activities, it must be repeated that all efforts have to be made to get time series with continuous parts as long as possible and interruptions as few as possible. Only by this way better and more reliable results may be achieved in the domain of long-term phenomena.
5. Numerical and computational procedures may correct or reduce many deficiencies of the data. But the best basis for good results are reliable data of highest quality. We know that the latter is easier said than done.

References

[1] RICHTER, B.: Das supraleitende Gravimeter. Anwendung, Eichung und Überlegungen zur Weiterentwicklung.
Dt. geod. Komm., R. C, H. 329., Verl. Inst. Angew. Geodäsie, Frankfurt a.M., 1987, 126 S.

[2] WARBURTON, R. J., BRINTON, E. W.: Recent developments in GWR Instruments' superconducting gravimeters.
Proc. Second Workshop: Non Tidal Gravity Changes: Intercomparison between absolute and superconducting gravimeters. Walferdange (Luxembourg), September, 6th to 8th, 1994. Luxembourg 1995, pp. 23 - 56

[3] RICHTER, B., WOLF, P., Otto, G., Wenzel, H.-G., Zürn, W.: Comparison of a cryogenic and a spring gravimeter between 0.2 and 96 cpd at BFO Schiltach.
Marées Terrestres Bull. Inf., **122**, Bruxelles 1995, pp. 9163 - 9162

[4] HARNISCH, M., HARNISCH, G.: Processing of the data from two superconducting gravimeters, recorded in 1990 - 1991 at Richmond (Florida). Some Problems and results.
Marées Terrestres, Bull. Inf., **122**, Bruxelles 1995, pp. 9141 - 9147

[5] WENZEL, H.-G.: PRETERNA - a preprocessor for digitally recorded tidal data.
Marées Terrestres, Bull. Inf., **118**, Bruxelles 1994, pp. 8722 - 8734

[6] WENZEL, H.-G.: Earth tide data processing package ETERNA 3.20
Marées Terrestres, Bull. Inf., **120**, Bruxelles 1994, pp. 9019 - 9022

[7] WENZEL, H.-G.: The nanogal software: Earth tide data processing package ETERNA 3.30
Marées Terrestres, Bull. Inf., **124**, Bruxelles 1996, pp. 9425 - 9439

Comparison of the performances of a broadband seismometer and a superconducting gravimeter in the subseismic frequency band.

Marion Freybourger, Jacques Hinderer

Institut de Physique du Globe de Strasbourg

5 rue René Descartes 67 084 Strasbourg Cedex France

and **Jeannot Trampert**

Department of Theoretical Geophysics

PO Box 80.021 3508 TA Utrecht The Netherlands

Abstract

Superconducting gravimeters and broadband seismometers, vertical component, both measure gravity, but while the first ones are most sensitive to very long period signals (gravity tides with periods longer than six hours), the latter are designed for recording the seismic band (elastic normal modes with periods shorter than one hour). We investigate here the behaviour of a STS-1 broadband seismometer, vertical component (Z), in the spectral band where it is not generally used, with respect to a superconducting gravimeter. More precisely, we compare the French superconducting gravimeter, located at the station J9 near Strasbourg, and the vertical component of a STS-1 seismometer located in a mine at Echery (ECH) in the Vosges, about 70 km away. A power spectral analysis of a one month long record of the two instruments allows the comparison of their noise levels. While for periods shorter than 50 min approximately (i.e. in the seismic band), both instruments exhibit similar noise levels, the STS-1/Z shows clearly higher noise level than the superconducting gravimeter for periods larger than 50 min (i.e. in the subseismic band). The analysis of a two year long record of the STS-1/Z allows to suspect the temperature response of the instrument to be responsible for this higher noise level at low frequencies. It is expected that operating the STS-1 isothermally, or recording on site temperature changes for correction will considerably improve its signal to noise ratio in the subseismic band. In

comparison with recent mean models of low seismic background noise levels, both instruments nevertheless indicate low noise levels at all frequencies.

Key words: superconducting gravimeter, STS-1 broadband seismometer, free oscillations, gravity tides, noise, power spectral densities.

1. Introduction

The purpose of this study is mainly to investigate the sensitivity of the broadband seismometers in the subseismic band (periods longer than one hour). We are particularly interested in the performance of the broadband seismometers Wielandt-Streckeisen STS-1 (Wielandt and Streckeisen, 1982; Wielandt and Steim, 1986) vertical component (Z) in this specific band, whereas they are currently used to study signals of periods under one hour, like the free oscillations of the Earth (see also Pillet et al., 1994 for an evaluation of STS-1 in the tidal domain). We present here a summary of our results that will be published elsewhere in more details (Freybourger et al., 1996).

One of the goals is to check whether the world-wide distribution and the important number of the STS-1/Z could be used to observe some very low amplitude geodynamical phenomena as subseismic modes by stacking techniques. Thus we compare here a broadband seismometer STS-1 with a superconducting gravimeter (SG), which is the instrument currently used in this frequency band. We characterise and compare the superconducting gravimeter located at the site J9 near Strasbourg (GWR Instrument, model TT70) and the broadband seismometer STS-1/Z situated at the site ECH in the Vosges. Both sites are less than 70 km away, a distance sufficiently close so that the gravity signals we are interested in here are comparable in waveforms and amplitude. In the seismic band, we evaluate the quality of the sites in comparison with the very low background noise site (see e.g. Richter et al., 1995) BFO, the Black Forest Observatory, studying the free oscillations of the Earth after the June 9, 1994 Bolivian earthquake. We show the very good

quality of the site ECH (which is an old mine, directly on the bedrock) in this frequency band, with noise levels comparable to those shown by BFO STS-1/Z recordings (Freybourger et al., 1996). On the other hand, the site J9, which is located near the city of Strasbourg and lies on several km of sediments, is quite noisy. We therefore believe that site effects in ECH cannot be responsible for differences in noise level shown by the STS-1/Z with respect to the gravimeter in the subseismic band.

The transfer functions of the different channels of the seismometer used in this study are indicated in figure 1. The POS (Position) channel is directly proportional to acceleration up to a frequency of 1/6 min, while the transfer functions in acceleration of HGLP (High Gain Long Period) and VLP (Very Long Period) channels are linear in frequency with a unit slope up to 1/6 min. On the other hand, we used the TIDE channel of the superconducting gravimeter, which is a low passed filtered gravity output with a cut-off period of 50 s.

We will present here a comparison of the two instruments in the subseismic frequency band (periods longer than one hour), using one month long records (September 1994). We find that the noise levels are clearly weaker for the superconducting gravimeter for periods longer than approximately 50 min. We will then try to explain these results with a two year long record of the STS-1 seismometer at ECH. The influence of temperature variations on the records of the seismometer vertical component is obvious.

2. Comparison in the seismic and subseismic frequency band

We first evaluate the noise levels presented by one month long records of the two instruments (September 1994). Figure 2 shows the power spectral densities (PSD) expressed in μgal^2 / Hz and smoothed by running averages, with respect to the New Low Noise Level (NLNM), the lower limit of the average seismic background noise evaluated by Peterson (1993). At these periods, the PSD noise levels are close to the NLNM for both instruments, indicating relatively low background noise for the sites J9 and ECH with respect to the current global seismic network. But two spectral domains are clearly defined

by the frequency of 0.3 mHz (50 min of period approximately): for frequencies below this limit the ECH STS-1/Z noise level is higher than the J9 SG noise level, while for frequencies higher than 0.3 mHz both instruments present similar noise levels. Notice that a correction for atmospheric pressure effects on gravity has not been computed, as no pressure recording was done then at ECH. Such a correction would have significantly lowered the noise levels for both records (Crossley et al., 1995; Zürn and Widmer, 1995).

3. Temperature influence on ECH STS-1/Z records

In order to investigate further the origin of the high noise level presented by the STS-1/Z one month long record at periods longer than 50 min, we took two years of recordings (1994-1995) of the ECH STS-1/Z VLP channel (see figure 1). This record is shown in figure 3. We emphasise the fact that it is to our knowledge the first time that such a long STS-1/Z record (VLP channel) is processed.

Two very important phenomena can be noticed on this figure. First of all (top of the figure), we can estimate the linear drift of the instrument, due to the mechanical creep of the spring. This drift is quite dramatic, with about 0.08 µgal / 5 min, which is approximately 16.6 mgal within 2 years (or around 23 µgal per day). In comparison, the superconducting gravimeter at J9 is known to show a linear drift of about 10 µgal per year (Hinderer et al., 1994). The second striking phenomenon (bottom of the figure) is a very large annual variation (approximately 6 mgal peak to peak). Clearly, this variation is linked to the annual temperature change. We essentially see this effect because the seasonal temperature changes are by far the largest. Similar effects probably exist at other frequencies but are smaller if one assumes a coloured type spectrum for the temperature and a simple (linear) instrumental temperature admittance. Unfortunately, it is not possible to investigate furthermore this relationship with temperature, as no recording of this parameter was available at ECH.

The influence of temperature on the STS-1/Z signal is well known and generally observed on the POS channel which is directly proportional to acceleration (figure 1). POS records

are nevertheless complex to use, because they always have to be corrected for numerous "steps" due to the periodic recentering of the boom (D. Rouland, personal communication).

4. Conclusion

The main purpose of this study was to investigate the sensitivity of the broadband seismometers STS-1, vertical component (Z), in the subseismic frequency bands (periods longer than one hour) to check if it would be worthwhile to use the large number and the world wide distribution of seismometers for the detection of very low amplitude subseismic modes by stacking techniques. We compared the behaviour of a superconducting gravimeter and a broadband seismometer STS-1/Z located at two close sites (respectively J9 near Strasbourg and ECH, Echery, distant of less than 70 km). The site effects at ECH should not be a limiting factor in our analysis of the subseismic frequency bands.

A power spectral density analysis of the one month long records allowed us to compare the noise levels of the two instruments both in the seismic and subseismic bands, indicating two spectral domains separated at 50 min period where the instrumental behavior is different. At the highest frequencies, the two instruments exhibit comparable noise levels while at the lowest frequencies, the STS-1/Z clearly shows higher noise levels. A further analysis of a two year long record (in 1994 and 1995) of the STS-1/Z has shown its high sensitivity to temperature variations which is most likely at the origin of the observed high noise levels in the subseismic band.

The important conclusion of this study is therefore to emphasise that on site recording of meteorological parameters (temperature, atmospheric pressure or even hygrometry, as it is usually done in gravimetric observatories) should be routinely done in seismological observatories, which would allow to use broadband seismometers in the subseismic frequency bands. Accurate temperature recordings (up to the mK) should balance the large influence of this parameter on the STS-1/Z records and improve the noise levels (we are currently checking the feasibility of this correction). Recordings of the atmospheric pressure would then enable to correct acceleration signals of the seismometers for the physical effects

of pressure changes (ground deformation and Newtonian attraction of air masses), similarly to standard gravity analysis. Following this study, temperature and pressure recordings have now begun at the site ECH.

Acknowledgements

We are grateful to O. Jensen, W. Zürn, R. Widmer and D. Rouland for numerous interesting discussions.

References

Crossley, D.J., Jensen, O.G. and Hinderer, J., 1995. Effective barometric admittance and gravity residuals, Phys. Earth Planet. Inter., 90: 221-241.

Freybourger, M., Hinderer, J. and Trampert, J., 1996. Comparative study of broadband seismometers STS-1/Z and superconducting gravimeters in the seismic and subseismic frequency bands, Phys. Earth Planet. Inter., submitted.

Hinderer, J., Crossley, D.J. and Xu, H., 1994. A two year comparison between the French and Canadian superconducting gravimeter data, Geophys. J. Int., 116: 252-266.

Peterson, J., 1993. Observations and modelling of seismic background, U. S. Geological Survey Report, 93-322.

Pillet, R., Florsch, N., Hinderer, J. and Rouland, D., 1994. Performance of Wielandt-Streckeisen STS-1 seismometers in the tidal domain - preliminary results, Phys. Earth Planet. Inter., 84: 161-178.

Richter, B., Wenzel, H.G., Zürn, W. and Klopping, F., 1995. From Chandler wobble to free oscillations: comparison of cryogenic gravimeters and other instruments in a wide period range, Phys. Earth Planet. Inter., 91: 131-148.

Wielandt, E. and Streckeisen, G., 1982. The leaf-spring seismometer: design and performance, Bull. Seism. Soc. Am., 66: 987-996.

Wielandt, E. and Steim, J., 1986. A digital very broadband seismograph, Ann. Geophys., 4B, 227.

Zürn, W. and Widmer, R., 1995. A simple method for noise reduction in vertical seismic records below 2 mHz using local barometric pressure, Geophys. Res. Lett., 22: 3537-3540.

Figures captions

Figure 1: Transfer functions in acceleration of the different channels of the ECH broadband seismometer STS-1/Z: HGLP, VLP and POS channels. In the subseismic band (periods longer than one hour or frequencies under 0.3 mHz), the transfer functions of HGLP and VLP channels are linear in frequency, with a unit slope (even up to 2.777 mHz, i.e. from DC to 6 min period). The HGLP channel is used here for the study of the one month records; the VLP channel is used for the study of the two year record.

Figure 2: Power spectral densities (PSD), smoothed by running averages on 50 points, of the one month record (September 1994) from J9 superconducting gravimeter and ECH broadband seismometer STS-1/Z. New Low Noise Model (NLNM) of Peterson (1993) is indicated on this figure as a reference to evaluate noise levels of J9 gravimeter and ECH seismometer during this time interval. Notice the intersection of the curves indicating the highest frequency till which the ECH seismometer noise level is significantly higher than J9 gravimeter noise level (0.34 mHz, i.e. 50 min).

Figure 3: Time fluctuations of the gravity in mgal recorded by ECH broadband seismometer STS-1/Z during the years 1994 and 1995 (2 years, 20 minutes). The signal is presented after deconvolution of the output by the instrument response in acceleration. It shows a very important drift (top) and large amplitude annual variations (bottom) most likely due to seasonal temperature changes.

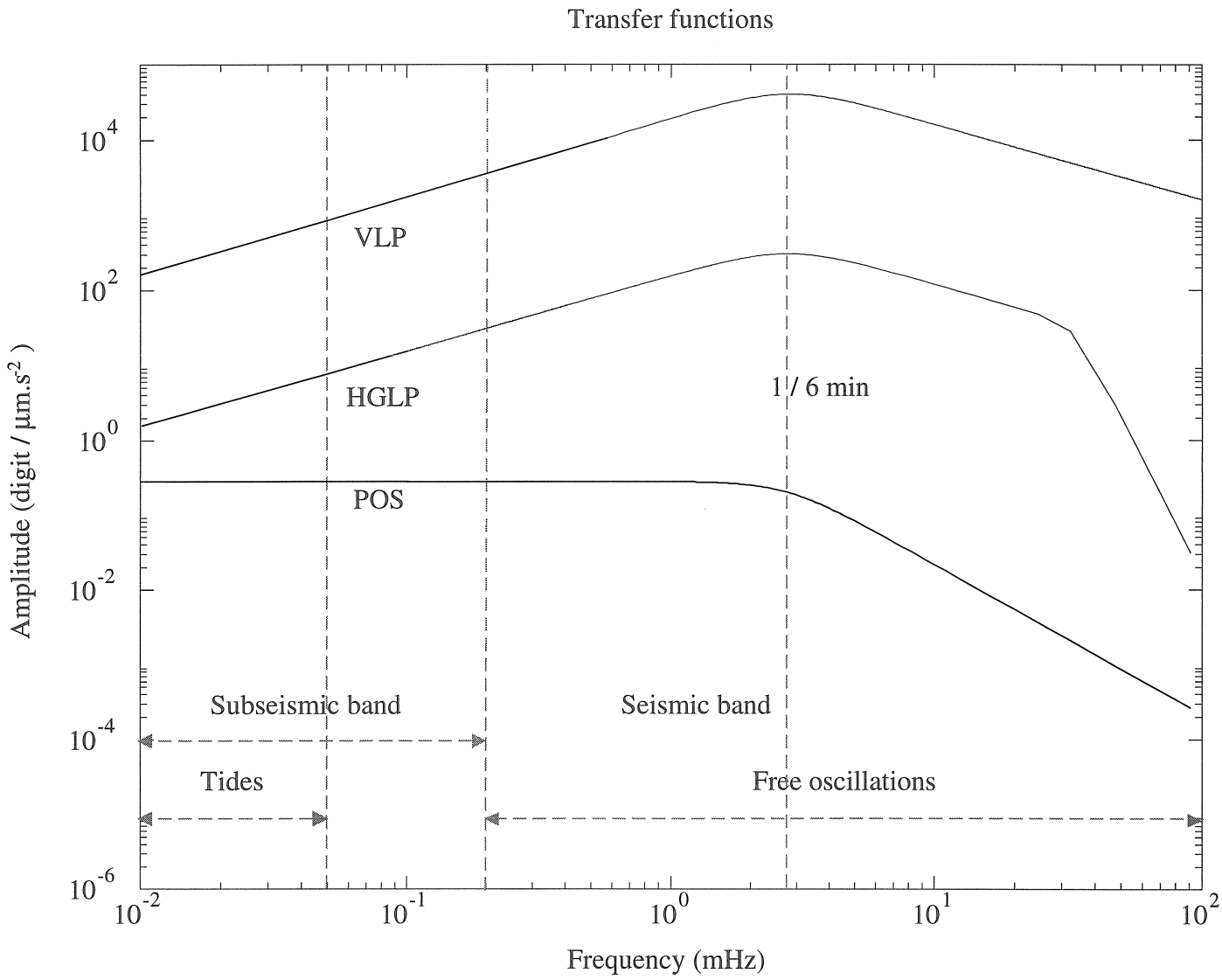
Transfer functions
VLP
HGLP
POS
1 / 6 min
Subseismic band
Seismic band
Tides
Free oscillations
Amplitude (digit / µm.s-2)
Frequency (mHz)
10^4
10^2
10^0
10^-2
10^-4
10^-6
10^-2
10^-1
10^0
10^1
10^2

Figure 1

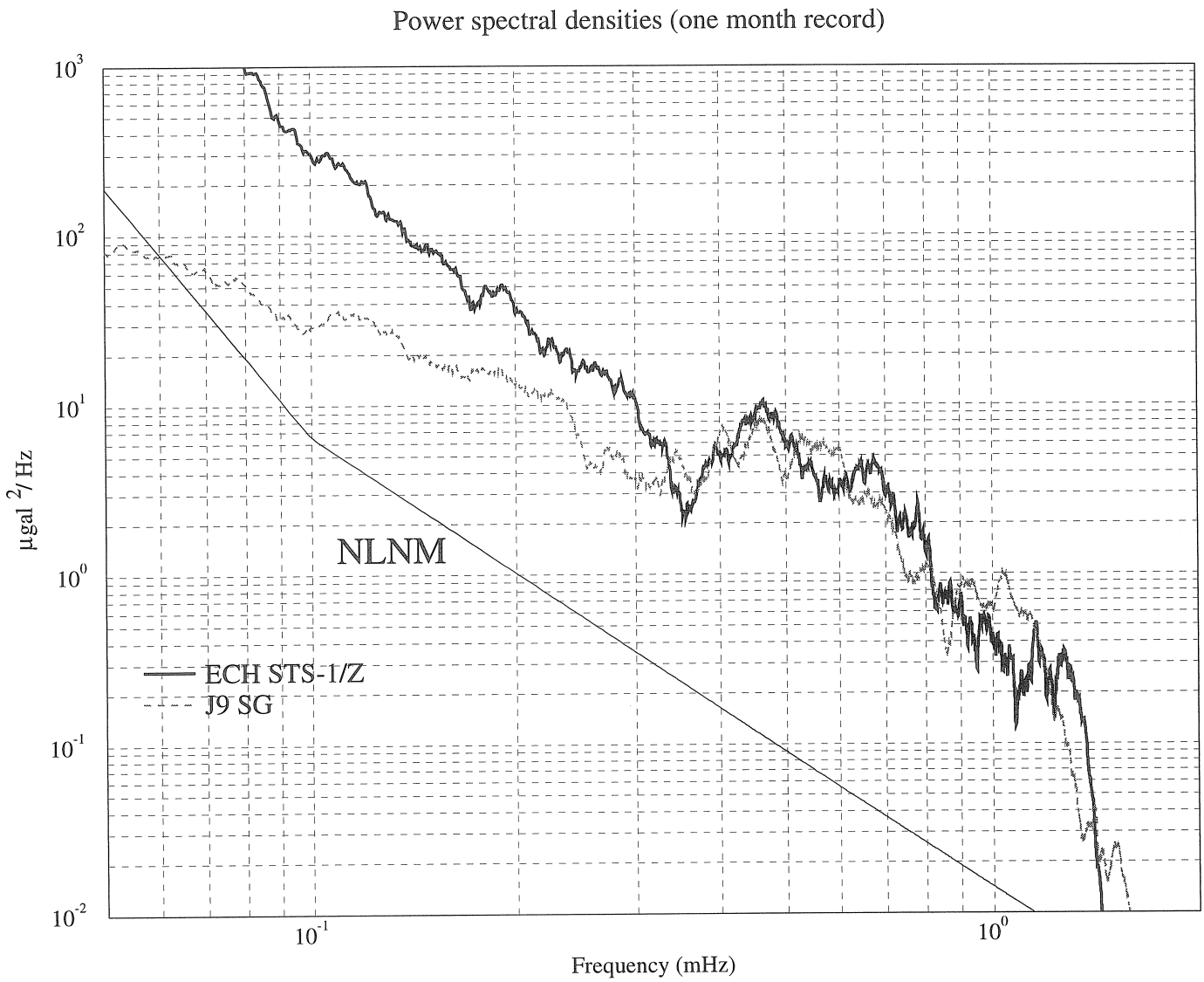
Power spectral densities (one month record)
10^3
10^2
10^1
10^0
10^{-1}
10^{-2}
µgal ^{2}/ Hz
NLNM
ECH STS-1/Z
J9 SG
10^{-1}
10^0
Frequency (mHz)

Figure 2

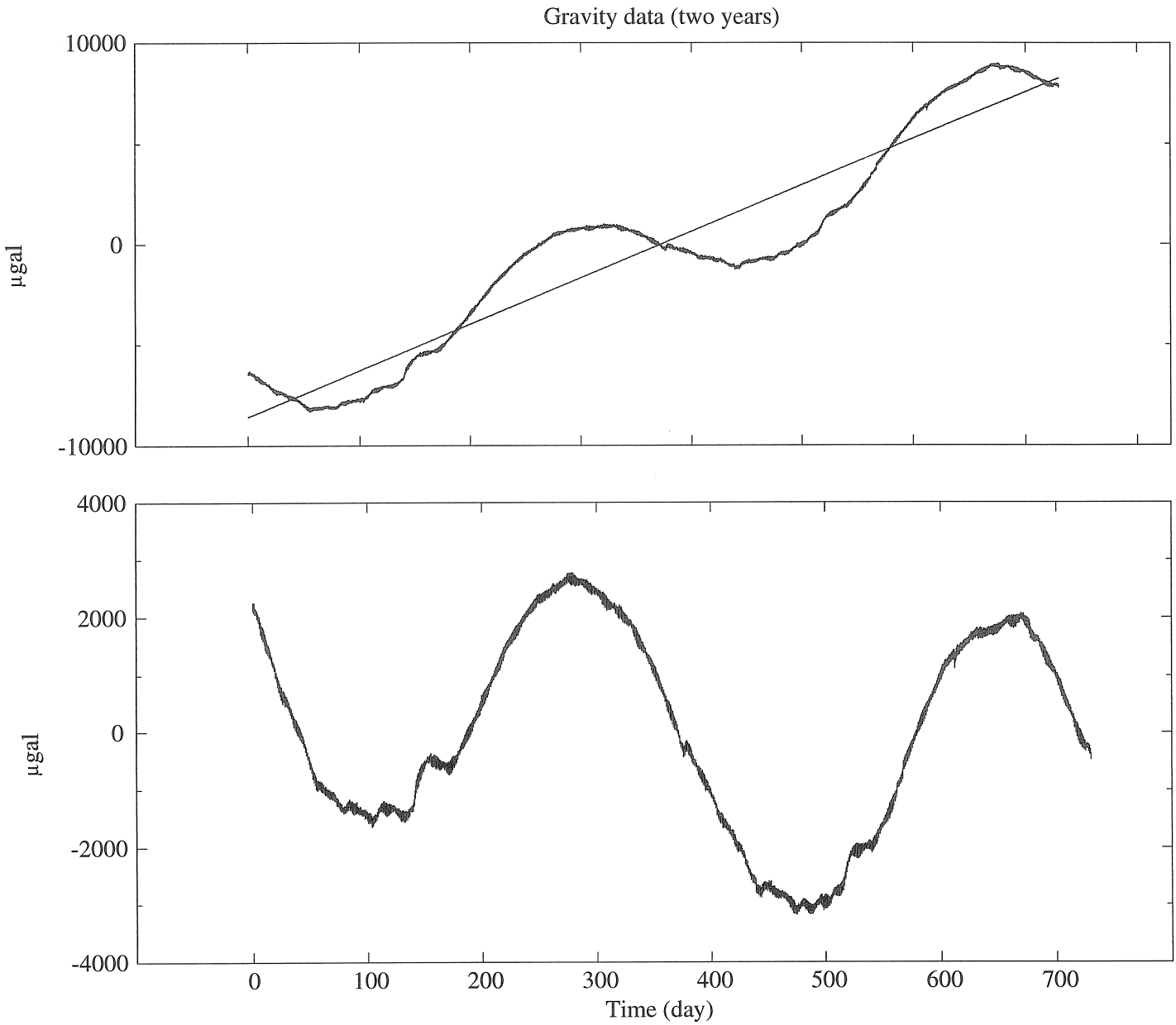
Gravity data (two years)
10000
0
-10000
µgal
4000
2000
0
-2000
-4000
µgal
0
100
200
300
400
500
600
700
Time (day)

Figure 3

Baldi P. *, Casula G.**

The Gravimetric Station of Brasimone

* Department of Physics University of Bologna (Italy)
** National Institute of Geophysics, Roma (Italy)

Abstract.
From 1990 up to now a superconducting gravimeter GWR model TT70 is operating in a laboratory located on the dismissed nuclear power plant of Brasimone, in the Italian Apennines between Bologna and Florence, in the frame of an experiment meant to verify Newton's gravitational law. From July 1995, the gravimeter is involved in the Global Geodynamics Project, and is actually working for high precision tidal analysis and modelling.
In this paper we describe the calibration procedure adopted together with the preliminary results of the tidal analysis performed using the software Eterna 3.20.

Introduction.
Since 1990 the gravimeter GWR T015 is working in different laboratories, in a research center of ENEA (Italian national institute for energy development), located near a lake in the Apennines, 70 Km far from Bologna (Italy, 44° 07' N, 11° 07' E, 845 m above sea level).
The superconducting gravimeter was used in the frame of an experimental program meant to verify the validity of the Newton's law over distances of the order of 10 - 100 m (Achilli et al., 1996).
In 1992 a tidal analysis was performed using a continuative tidal signal relative to a period of five months (Baldi et al., 1995).
From July 1995 the gravimeter is definitively sited in a suitable building in the same area, on the very stable basement of a dismissed nuclear power plant, characterized by a very low noise level.
The set of tidal data (14 month) collected up to now has been analysed using the Eterna 3.2 software.

The Calibration Method.
As well known a superconducting gravimeter converts variations of the local acceleration of gravity in potential differences inside a capacitance bridge, that is an element of the sensing device of the instrument, (Goodkind J.M., 1991). For this reason the gravimeter needs to be calibrated, in other words it is necessary to calculate the calibration constant of the instrument, a factor which converts volts in units (microgal or nm/s^2) of gravity acceleration.
The most used calibration method is the comparison in the same site of the instrument with an absolute gravimeter; using the tidal effect to produce a significant variation of the acceleration of gravity, this approach gives an accuracy of 1% or better, (Hinderer et al., 1991).
In our station a new calibration method is used; it consists in moving a mass of simple geometry (a circular ring with square cross section), along the gravimeter vertical axis, in order to perturb in a known way the gravity field (Achilli et al., 1995), (Varga et al., 1995).
A second mass is placed about ten meters away from the gravimeter, and is connected by means of steel cables and pulleys in such a way to balance the weight of the annular mass, (273.40 +/- 0.010 kg); a little force applied to the cables by an engine servo-controlled by means of a Personal Computer can easily move the calibrating mass (Fig. 1).
The system is improved by adding a wireless digitiser which is able to measure the ring position with an accuracy of 0.1 - 0.2 mm.
Owing to the simple geometry adopted and to the symmetrical distribution of masses, an analytical computation is done to determine the theoretical effect due to the perturbing mass movement.

An erroneous determination of the position of the gravimeter sphere mounted inside a cryostat, is estimated to be well below the precision of the method wich results to be about 0.3%, (Achilli et al., 1995).
Two calibration procedures have been adopted: the calibration signal scan and the peak to peak calibration.
The calibration signal scan consists in moving the calibration mass slowly in a period of about 45 minutes along the gravimeter vertical axis, the following observable quantities are recorded: the mass position, the time and the response of the gravimeter.
A least square adjustment technique is applied to fit the theoretical effect of the mass to the gravimeter response, corrected for the tide and the drift, in order to define the position of maximum and minimum effect due to the mass movement, the position of null effect, corresponding to the sphere center, and a first value of the calibration constant (Fig. 2).
In the peak to peak calibration, moving the mass from the position of maximum to the position of minimum effect in a period of 4 minutes, we produce a calibration square wave (Fig. 3).
The period of the square wave was chosen to be 8 minutes to optimise the computation of the gaps given by the perturbing movement of the mass.
A graphical interactive program written with the aid of the IDL graphical libraries on a VAX 4000-90 computer and a mouse device, allows us to edit in a graphical way the calibration square wave data to eliminate disturbances.
After this operation, a mean value of the data for each peak is computed together with the standard deviation of the mean; this calculation gives about 30 peak values for each calibration session, (about 2 hours).
The calibration constant is obtained by dividing the theoretical peak to peak effect: (6.7311 +/- 0.0001) microgal, by the weighted average of the wave amplitude.
In (Tab. I) the results of calibrations performed in the period 1991-1996 are listed together with their standard deviations.
The gravimeter is equipped with an auxiliary tool, the electrostatic calibrator, allowing the measure of the feedback voltage response to a constant electrostatic force applied to the sphere. The electrostatic calibration allows the monitoring of the time stability of the scale factor to better than 0.01 % (Fig. 4).
Fig. 5 represents the comparison between the ring calibration values and the corresponding electrostatic calibrations related to different coil settings (Achilli et. al, 1995). One can observe a strong linear dipendence of the two values. In Fig. 5 is also shown the value of the calibration obtained from the comparison with the absolute gravimeter of the Istituto of Metrologia G. Colonnetti of Turin which was installed for a period of three days, (10/11/12 May 1994) in the same site (Baldi et al., 1995). The comparison is in agreement with the results of the ring calibration system at a level of 1% or better (see Fig. 6 and Tab. I).

Tidal Analysis.
A set of 14 month of data recorded by the gravimeter GWR T015 were used to perform a tidal analysis using Eterna 3.20 program, written by Professor Wenzel of the Geodetic Institute of the University of Karlsruhe (Wenzel et al., 1993).
Two type of observables were used: the high resolution gravity signal recorded at a rate of 1 sec and the barometric signal recorded at a rate of 20 sec.
The Hr_Grav signal was decimated at 5 seconds rate, filtered and converted to a Preterna format by means of the program Alpha, written by J. Neumeier of the University of Potsdam; the barometric signal was decimated at 1 minutes rate and converted to Preterna format in the same way of the Hr_Grav signal.
The pre-elaboration of the gravimetric and barometric data was performed using Preterna 3.20 program, following the known sequence (Wenzel et al., 1994):

a) Calibration.

b) Graphical editing of the calibrated data and elimination of gross disturbances.
c) Computation of model tide and drift.
d) Graphical editing of the detided data and elimination of steps.
e) Automatic depiking, destepping and degapping.
f) Graphical editing of the previously corrected data and elimination of remaining disturbances.
g) Iteration of the points e) and f) until no more data are corrected by the automatic procedure.
h) Numerical filtering and decimation at 5 minutes sampling interval.
i) Numerical filtering and decimation at 1 hour sampling interval.

The final product of the pre-elaboration with Preterna 3.20 is a file corrected for disturbances, for the barometric pressure effect, using a real single barometric admittance, and for the drift (Fig. 7). This file is prepared in a format fully compatible with the elaboration program Eterna 3.20.
After the pre-elaboration a final run with Eterna was performed to estimate: amplitude, delta factors and phase delay of the main tidal wave using the tidal catalogue of Tamura 1987 (1200 waves), (Tamura , 1987). It was also possible to evaluate a single real pressure admittance (Tab. II).
In table II the values of the amplitudes, delta factors and phase for the main tidal waves are listed together with their RMS errors.
An high pass filter, called Pertsev number 2, was used to reduce the noise (Fig. 8 and 9); in fact in our case we have to point out that the barometric noise is not completely eliminated by using a mean real barometric admittance of -2.712 +/- 0.005 nm/s^2*HPa.
In Fig. 8 and 9 the residuals of the analysis previously described are shown. A standard deviation of the residuals of about 3 nm/s^2 results from the final analysis (Tab. II).

Conclusions.
Since July 1995 the gravimeter GWR T015 is continuously recording the tides in the frame of the GGP Project; the instrument is calibrated by means of a new method based on perturbing in a known way the gravitational field by moving vertically a circular ring and recording the gravimeter response.
A first comparison with an absolute gravimeter was performed in may 1994 to verify the correctness of our calibration approach; the results are in agreement at a level of 1%.
The preliminary tidal analysis performed using the Eterna software shows a standard deviation of residuals of about 3 nm/s^2, which may be due to the mean atmospheric pressure adopted.
In the future we hope to be able to reduce the noise of the non tidal effects by performing a cross spectral analysis of the gravimeter residuals versus the barometric pressure; the calibration will be then verified again with the aid of the two methods described below.

References.
Achilli V., Baldi P., Focardi S., Gasperini P., Palmonari F., Sabadini R., 1991. *The Brasimone experiment: a measurement of the Gravitational constant G in the 10-100 m range of distance.* Proceedings of the Workshop: Non Tidal Gravity Changes. Walferdange, September 1990. Cahiers du Centre Européen de Gèodynamique et de Sèismologie, Vol 3. p. 241-246.

Achilli V., Baldi P., Casula G., Errani M., Focardi S., Guerzoni M., Palmonari F., Ragunì G., 1995. *A calibration system for superconducting gravimeters.* Bulletin Geodesique, Vol. 69, p. 73-80.

Achilli V., Baldi P., Casula G., Errani M., Focardi S., Palmonari F., Pedrielli F., 1996. *A geophysical experiment on the inverse Newton's square law.* Nuovo Cimento, in press.

Baldi P., Casula G., Focardi S., Palmonari F., Cerutti G., De Maria P., and Marson I., 1995. *Intercomparison of IMGC absolute and GWR superconducting gravimeters.* Proceedings of the Symphosium: Gravity and Geoid, Vol. 113, p. 27-36.

Baldi P., Casula G., Focardi S., Palmonari, 1995. *Tidal Analysis of data recorded by a superconducting gravimeter*. Annali di Geofisica, Vol. XXXVIII, n.2, p. 161-166.

Goodkind J.M., 1991. *The superconducting gravimeters: principle of operation, current performance and future prospects.* Proceedings of the Workshop: Non Tidal Gravity Changes. Walferdange,September 1990. Cahiers du Centre Europèen de Gèodynamique et de Sèismologie, Vol 3, p. 81-90.

Hinderer J., Florsch N., Machinen J., Legros H., and Faller J.E., 1991. *On Calibration of a superconducting gravimeter using absolute gravity measurements.* Geophysical Journal International, Vol. 106, p. 491-497.

Tamura Y., 1987. *A harmonic development of the tide - generating potential.* Bullettin d'Information Marèe Terrestres, Vol. 99, p. 6813-6855, Bruxelles, 1987.

Varga P., Hajòsy A. and Csapò G., 1995. *Laboratory calibration of Lacoste-Romberg type gravimeters by using a heavy cylindrical ring*. Geophysical Journal International, Vol. 120, p.745-757.

Wenzel H.G., 1993. *Tidal data processing on a PC.* 12th International Symposium of Earth Tides, Bejing 1993.

Wenzel H.G., 1994. *PRETERNA - a preprocessor for digitally recorded tidal data.* Bullettin d'Information Marèe Terrestres, Vol. 118, p. 8722-8734, Bruxelles, 1994.

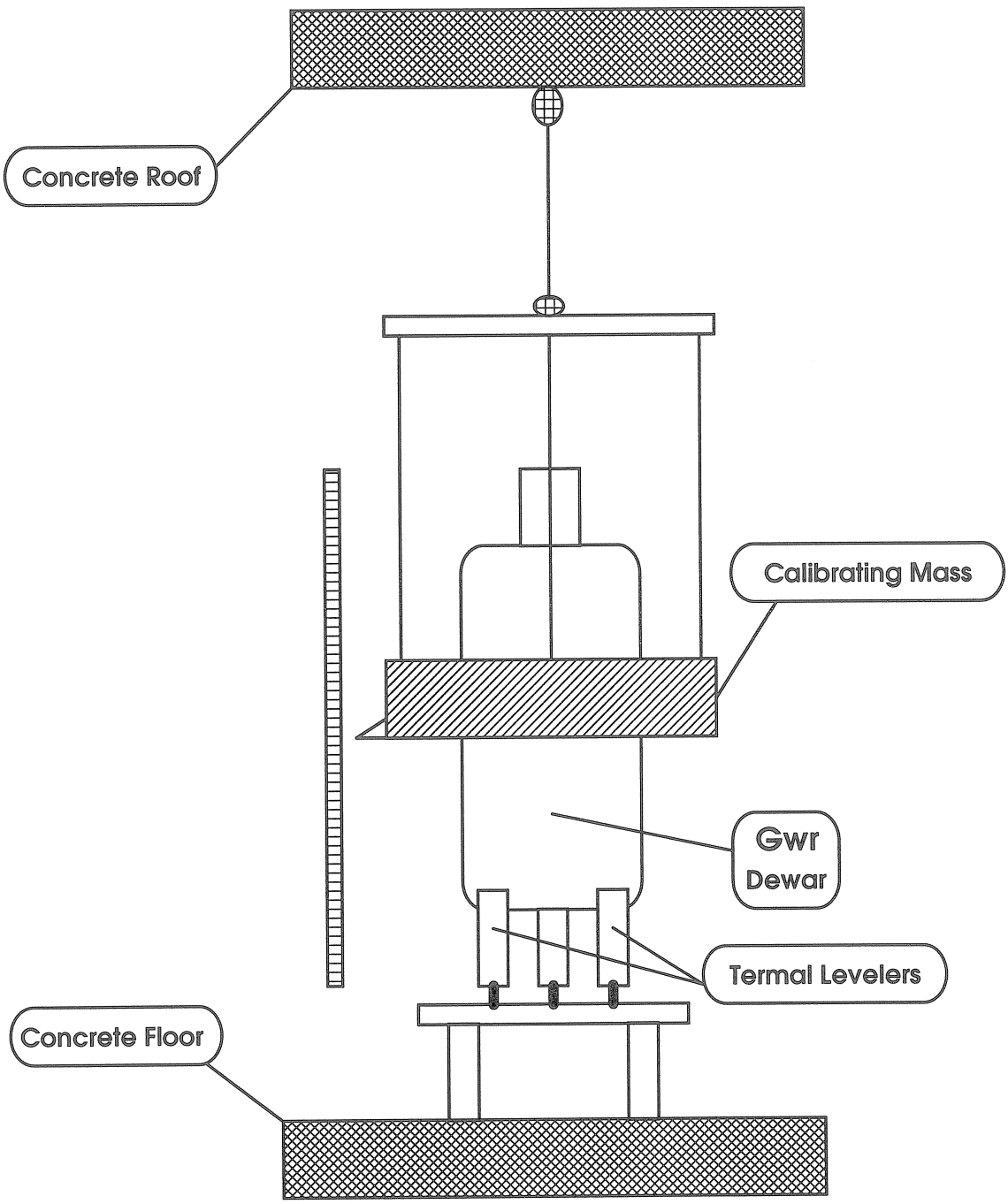

Fig. 1 - Scheme of the ring calibration apparatus.

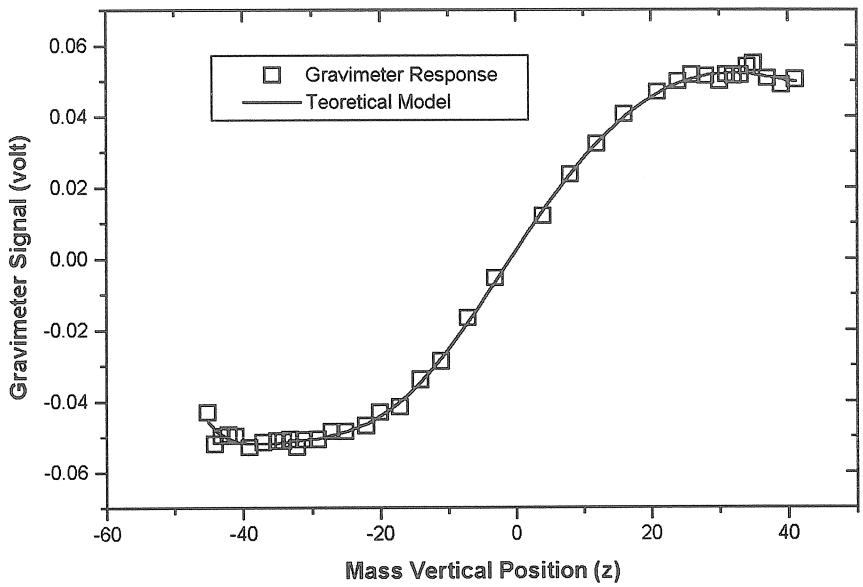

Fig. 2 - Example of Calibration Signal Scan, the response of the gravimeter to a slow motion of the ring along its vertical axis is fitted as a model experiment to the theoretical analytical function, getting: the values of maximum and minimum effect, the position of null effect due to the mass and a first less precise determination of the calibration constant.

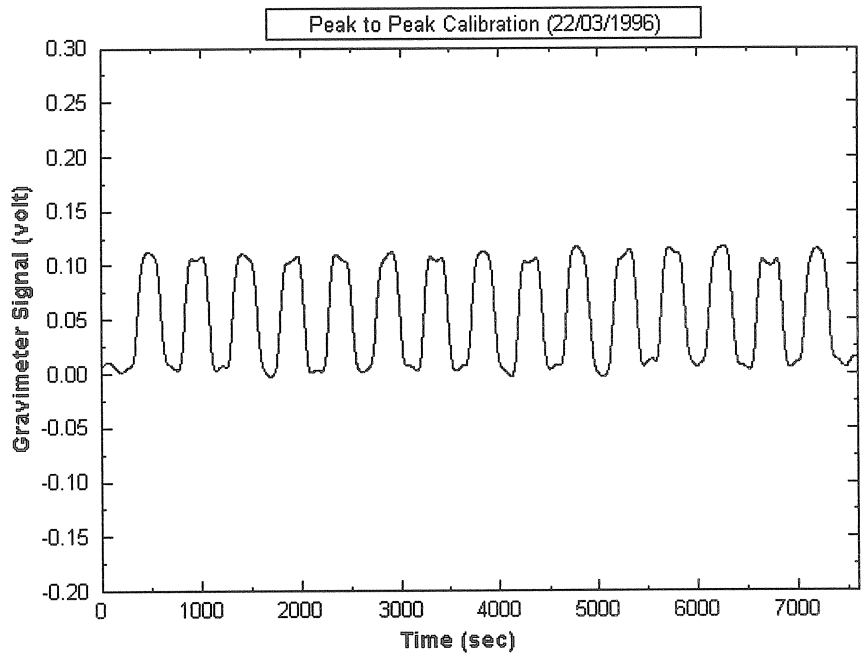

Fig. 3 - Example of peak to peak calibration, the ring is moved from the position of minimum effect to the position of maximum effect in a period of about 8 minutes, and the gravimeter response is recorded.

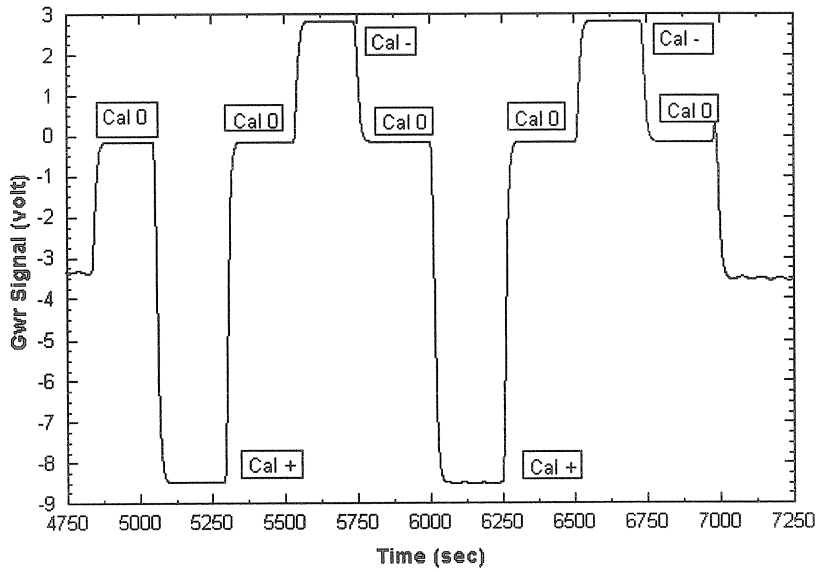

Fig. 4 - Example of electrostatic calibration; a known potential difference of about 5 volt is applied to the capacitance plate of the gravimeter sensor, the response of the gravimeter is recorded and a normalisation factor is computed.

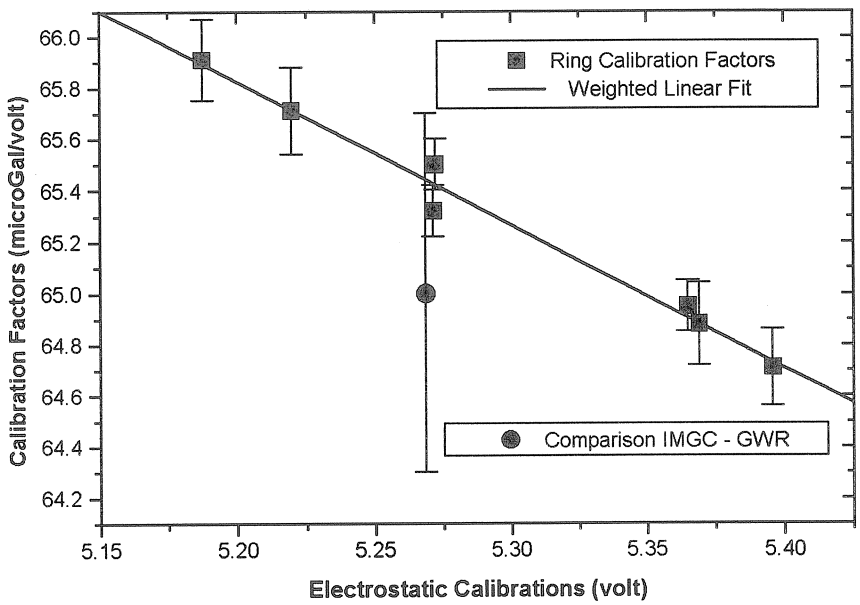

Fig. 5 - Ring calibration factors (squares in the figure) plotted versus the corresponding electrostatic calibrations; a linear trend is observed. Note the value of the calibration obtained from the comparison with the absolute IMGC gravimeter (circle in figure).

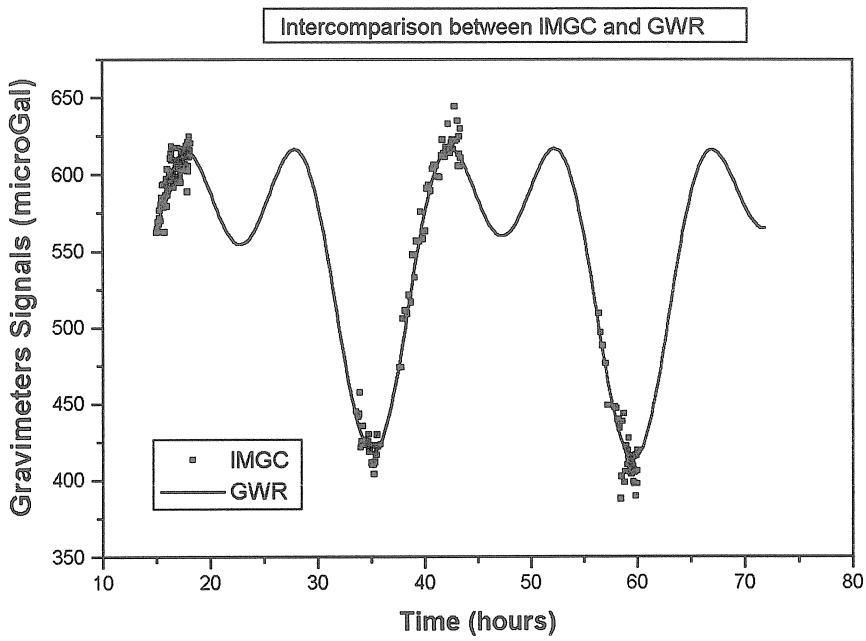

Fig. 6 - Scheme of the calibration for comparison between IMGC absolute and GWR gravimeters; the signal of the superconducting gravimeters (volt) is least square adjusted to the readings of the absolute one (microgal), to calculate the calibration factor of the GWR.

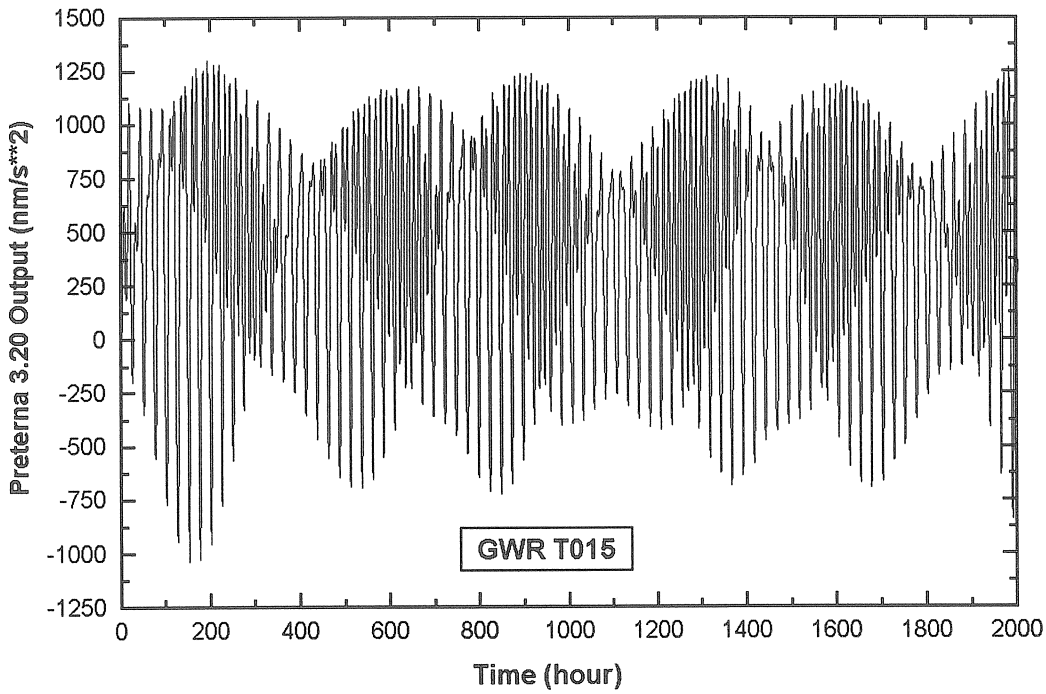

Fig. 7 - Example of data pre-elaborated by means of the Preterna 3.20 program, all spikes, steps and gaps were eliminated at a level of about 3 nm/s^2, the drift was previously corrected using a linear model.

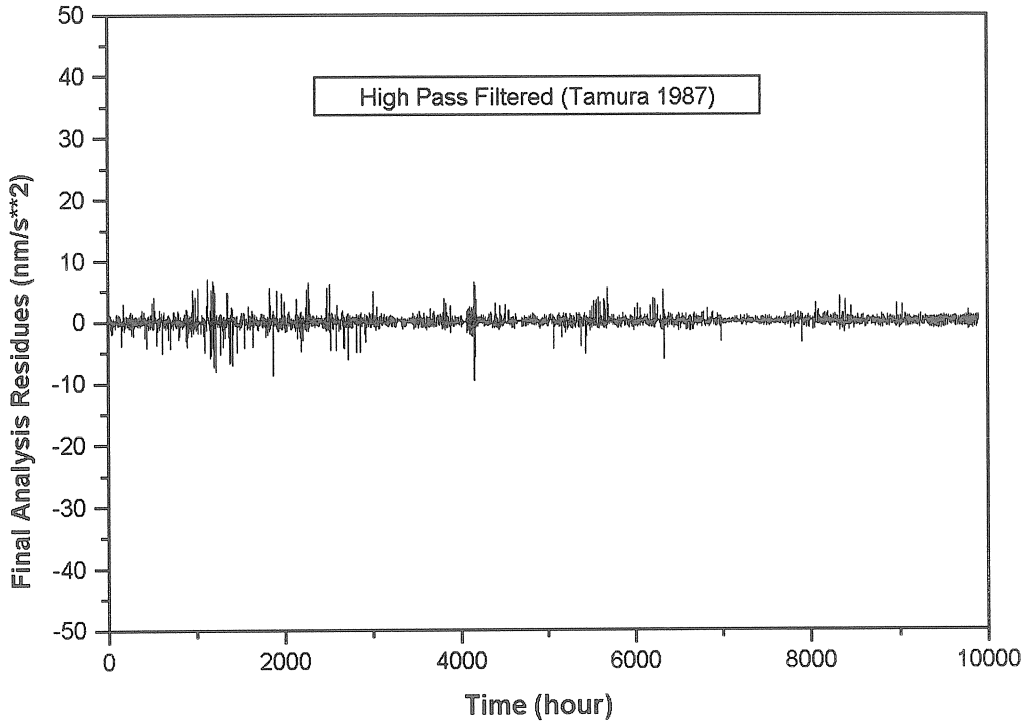

Fig. 8 - Example of HighPass filtered residuals of data analysed with Eterna 3.20 program; a Pertsev number 2 filter was used to reduce atmospheric pressure disturbances.

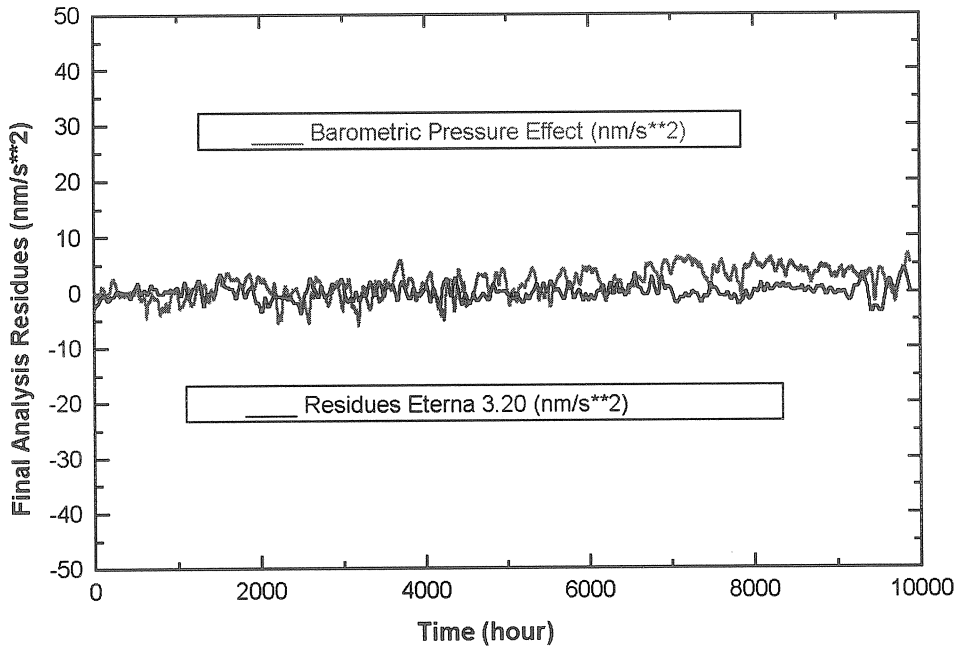

Fig. 9 - Low Pass filtered residuals of a set of 10000 hours of data of the gravimetric station of Brasimone; as can be noted in the figure residuals are still correlated with the barometric pressure.

Period (Year)	Method	Calibration Factors (μgal/volt)	Electrostatic Calibrations (volt)
1991	PSC	65.91 +/- 0.16	5.1875 +/- 0.0009
1992	PSC	65.71 +/- 0.17	5.2198 +/- 0.0003
1993	PSC	65.32 +/- 0.10	5.2715 +/- 0.0003
1994	PSC	65.50 +/- 0.10	5.2722 +/- 0.0003
1995a	PSC	64.95 +/- 0.10	5.3650 +/- 0.0003
1995b	PSC	64.88 +/- 0.18	5.3691 +/- 0.0005
1996	PSC	64.71 +/- 0.15	5.3958 +/- 0.0004

	IMGC Gravimeter		Ring Calibrations	
Date	Drops Number	Calibration Factors (μgal/volt)	Electrostatic Calibration (volt)	Ring Calibration (μgal/volt)
1994-5-9,10,11	166	64.4 +/- 0.5	5.2687 +/- 0.0003	65.26 +/- 0.12
1994-5-10	65	65.0 +/- 0.7		

Tab. I - Results of the ring calibration experiments, of the corresponding electrostatic calibrations and of the calibration for comparison with the IMGC absolute gravimeter.

Tidal Model Computed for the Gravimetric Station of Brasimone Tamura 1987 Catalogue - 1214 Waves					
Wave	Amplitude (nm/s2)	Amplitude Factor δ	RMS	Phase Δφ (°)	RMS
Ssa	16.363	1.21536	0.23570	2.8103	17.4432
Mm	17.461	1.14251	0.01191	0.7619	0.6864
Mf	33.440	1.15578	0.00646	-0.5506	0.3678
Mtm	6.327	1.14222	0.02033	0.7548	1.1687
Q1	68.814	1.15753	0.00115	-0.2259	0.0660
O1	356.570	1.14837	0.00022	-0.3103	0.0129
M1	28.165	1.15337	0.00251	-0.3155	0.1439
P1	165.854	1.14798	0.00040	-0-1955	0.0229
K1	499.034	1.13263	0.00015	-0.0815	0.0086
J1	28.526	1.16206	0.00292	-0.5713	0.1672
OO1	15.214	1.11290	0.00772	-0.4921	0.4423
2N2	13.715	1.15856	0.00326	0.9383	0.1869
N2	87.185	1.17612	0.00068	1.3003	0.0387
M2	456.727	1.17963	0.00012	0.5827	0.0071
L2	12.766	1.16656	0.00285	-0.2871	0.1634
S2	212.537	1.17988	0.00028	-0.5062	0.0160
K2	57.919	1.18276	0.00133	-0.3076	0.0763
M3	5.815	1.06302	0.00319	-0.1434	0.1828
Residuals Standard Deviation = 2.595 (nm/s2) Barometric Pressure Admit.: α = –2.712 +/– 0.005 (nm/s2*HPa)					
Data availability 01/08/1995 - 30/09/1996					

Table II - Tidal Model Computed from data of the gravimetric station of Brasimone using Eterna 3.20 program. Amplitudes , amplitude factors and phases of the main waves of the tidal catalogue of Tamura 1987 are shown.

Atmospheric tide measured by microbarograph

Gyula Mentes and Ildikó P. Eper

Geodetic and Geophysical Research Institute of the Hungarian Academy of Sciences
H-9400 Sopron, Csatkai E. u. 6-8, Hungary

Abstract

The direct and indirect influence of the air pressure variations is well-known on the high precision measurements applied for geodynamical investigations. For a better understanding of this effect a high sensitive microbarograph was developed in the Geodetic and Geophysical Research Institute of the Hungarian Academy of Sciences. In this paper the construction of the instrument is described and some measured data are presented. The results of the measurements prove that the instrument has a high sensitivity and it is also suitable for atmospheric tide measurements.

1. Introduction

Earth tide measurements are influenced by several environmental disturbances that must be taken into account before these records are used to obtain information on physical properties or geodynamics of the solid Earth. One of such phenomena is the barometric pressure variation on the surface. The influence of pressure variation on Earth tide measurements - gravitational and other types (extensometric, tilt, etc.) - consists of two main parts:

- direct attraction of the atmospheric mass,

- indirect effect due to elastic deformation of the Earth which causes change in gravity due to vertical displacement of the Earth's crust and due to redistribution inside the Earth.

The dominant part is the direct attraction. According to investigations the total effect of air pressure variations cause a gravity response of 0.3-0.4 μGal/mbar in the case of local pressure fluctuations (responsible for a part of the random fluctuations of gravity records) while the response to the global atmospheric tides is significantly larger (0.66 μGal/mbar for

S_1 and 0.47 μGal/mbar for S_2, for the two main pressure tide waves) according to the results published by Warburton and Goodkind [1977].

For these reasons it is very important to correct Earth tide measurements for atmospheric variations. To provide appropriate corrections air tide parameters must be determined for the given location and response effects have to be investigated. In our institute a microbarograph of high sensitivity was developed to record atmospheric pressure.

2. The construction of the microbarograph

The principle of the microbarograph is shown in Fig.1. The pressure sensor is a very sensitive closed diaphragm applied in conventional mechanically recording barometers used for meteorological measurements. The bottom of the closed diaphragm is firmly fixed to a rigid frame. The displacements of the top of the closed diaphragm due to air-pressure variations are sensed by a differential condenser. The moving plate of the transducer is fastened to the middle point of the top of the pressure-sensor diaphragm and the fix plates are fastened to the rigid frame isolated electrically from it. The capacitance changes of the transducer are measured in a bridge circuit amplifying its output signal by means of a carrier-frequency and a D. C. amplifier (Mentes, 1994).

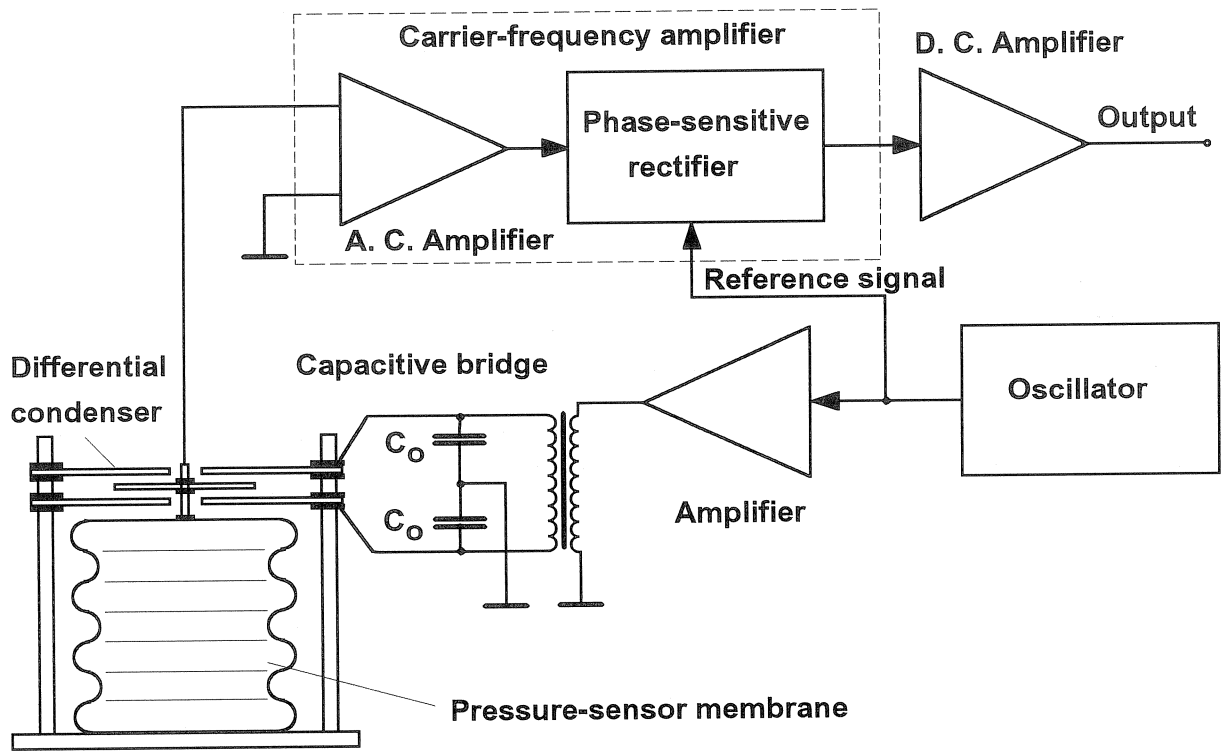

Fig.1. The construction of the high sensitive microbarograph

3. Test of the microbarograph and the first results of the atmospheric tide measurements

The microbarograph was installed at the Geodynamical Observatory of the Geodetic and Geophysical Research Institute of the Hungarian Academy of Sciences in Sopron for recording the air pressure variations in the vicinity of the long quartz tube extensometer. The annual temperature variation in the recording room is less than 0.1 °C. The constant temperature is very important because the sensor membrane of the microbarograph is very sensitive to the temperature variations.

Since 1992 several series of experimental analogous records have been carried out. The calibration of the instrument was made simultaneously with recording the atmospheric tide. For the calibration a conventional high precision pointer barometer was used and its pressure values were regularly compared with the signal of the microbarograph. From the calibration a mean sensitivity of 110.913 mV/mbar was obtained. The highest linearity error of the instrument in the investigated measurement range (approx.38 mbar) is less than 1.5% (0.53 mbar). The instrument must have a lower linearity error because one part of the errors arises from the calibration method. In the future we shall develop a pressure chamber for a regular in-situ calibration of the instrument during the recording.

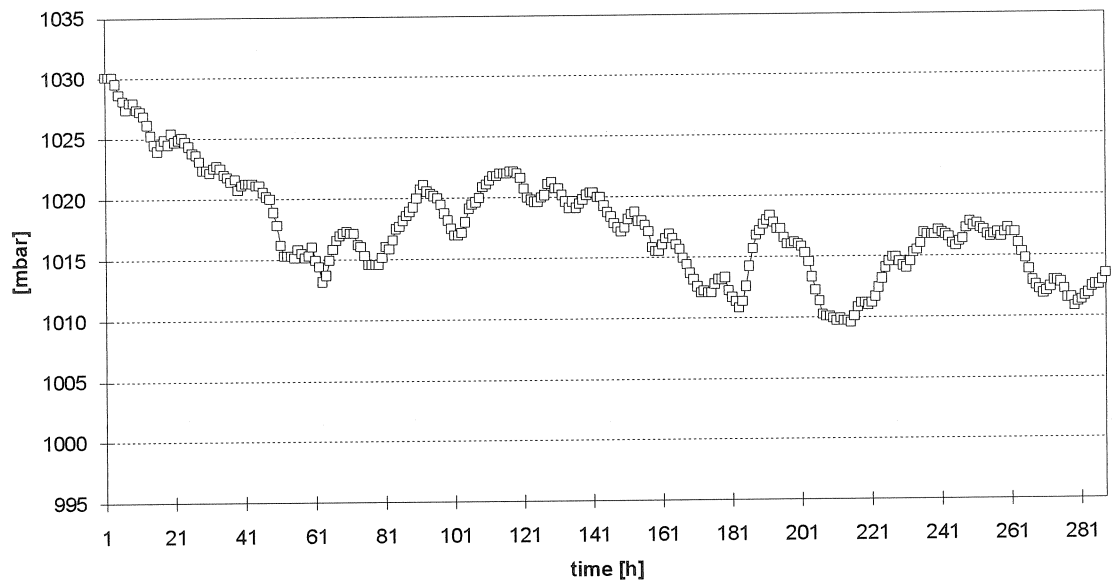

Fig. 2. Air pressure recorded by the microbarograph in the time interval 20.05.92. - 01.06.92.

From the recorded data three continuous data series are shown in Figs 2 - 4. There are small periodic oscillations in the Earth's atmospheric pressure variations . These worldwide coherent waves are excited thermally and gravitationally, where the gravitational part is in general much weaker. One type of air tide waves is solar waves driven thermally with

frequencies of one solar day and integer multiples ($S_1(p)$, $S_2(p)$, $S_3(p)$, $S_4(p)$). In this case the most important sources of excitation are the insolation and the absorption by ozon and water vapor. The other type is the lunar air tide waves with frequencies of one lunar day having significantly smaller amplitudes.

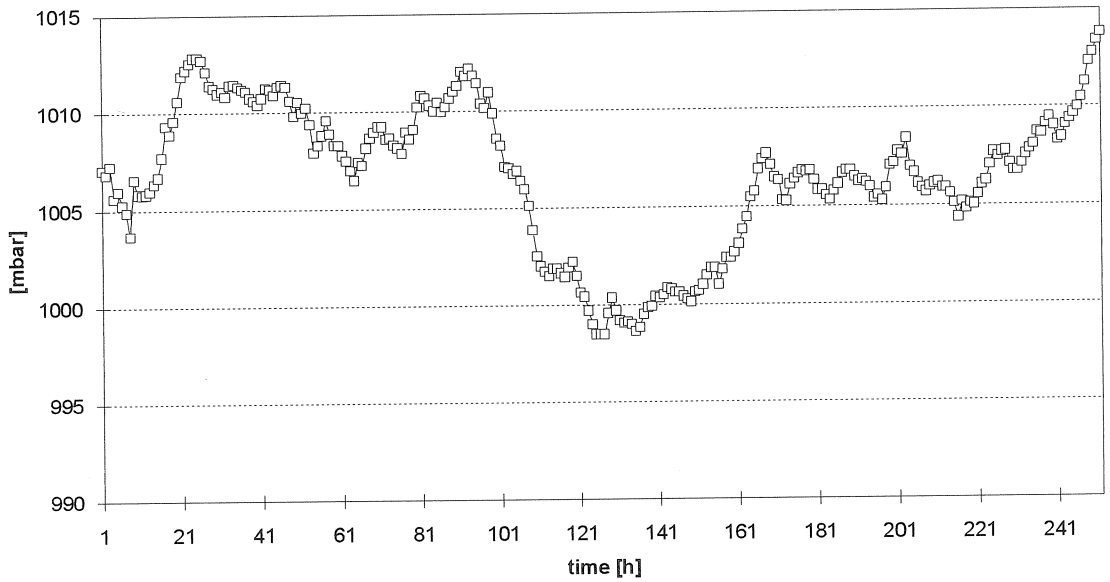

Fig. 3. Air pressure recorded by the microbarograph in the time interval 03.06.92. - 13.06.92.

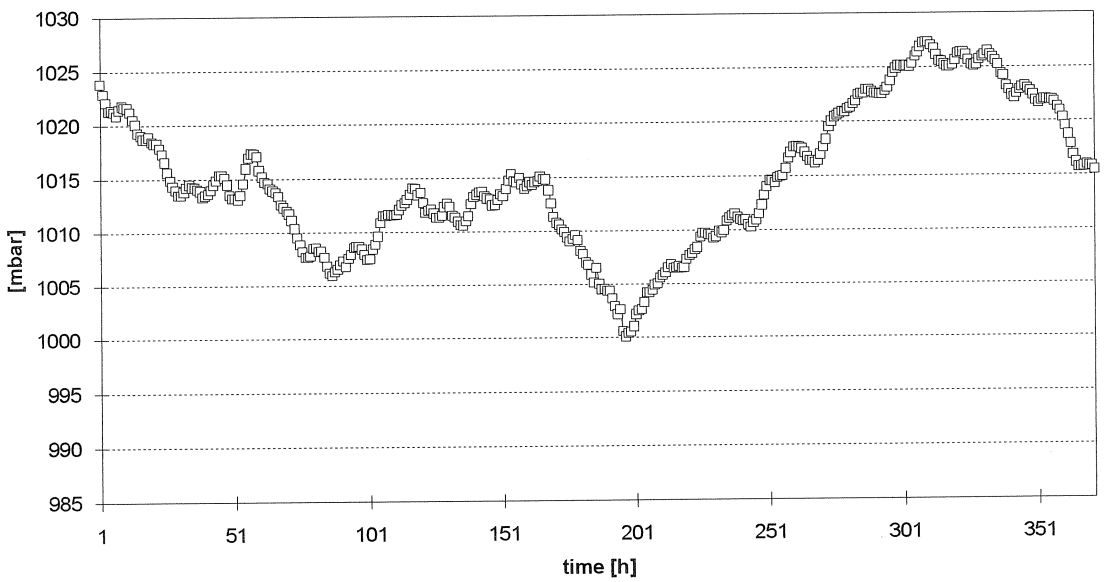

Fig. 4. Air pressure recorded by the microbarograph in the time interval 15.06.92. - 30.06.92.

The main components of the measured barometric tidal variations are the solar semidiurnal (dominant) and diurnal waves. The S-type waves are larger at equatorial regions, than at middle latitudes. They reach an amplitude of approx. 0.4 mbar.

The Fourier representation of the raw data series was produced to detect atmospheric tidal variations covered by much larger pressure changes caused by weather system variations (Figs 5-7.). Diurnal, semidiurnal, terdiurnal oscillations are indicated by spectral peaks. To enhance the tidal speaks in the spectrum the raw data were filtered by a moving average filter which replaces each hourly recorded raw data by the average calculated of the data being in question and of 12-12 data before and after it. The Fourier spectra of the three filtered data series are shown in Figures 8-10. These latter spectra show the S-type waves more clearly than the ones of the unfiltered data.

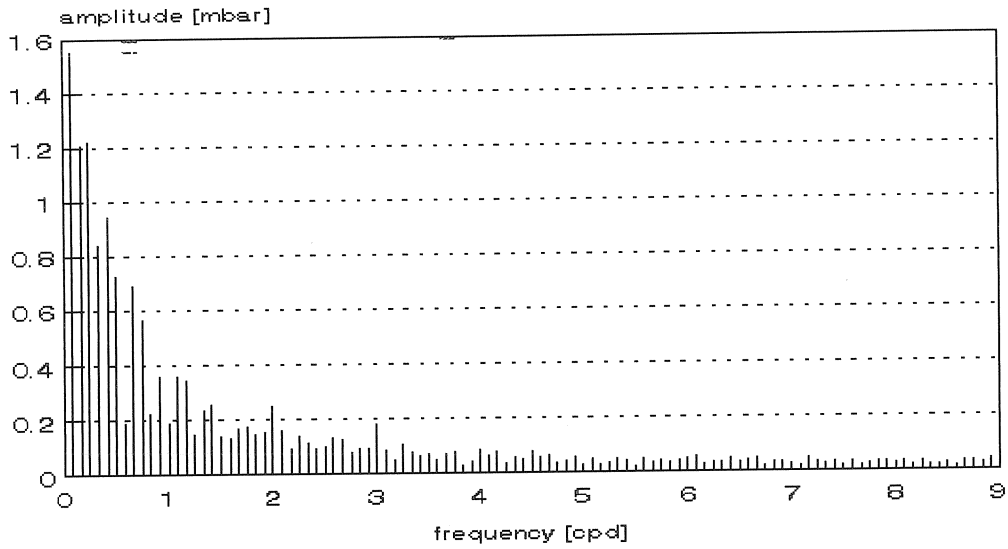

Fig. 5. Amplitude spectrum of the data series from 20.05.92. till 01.06.92.

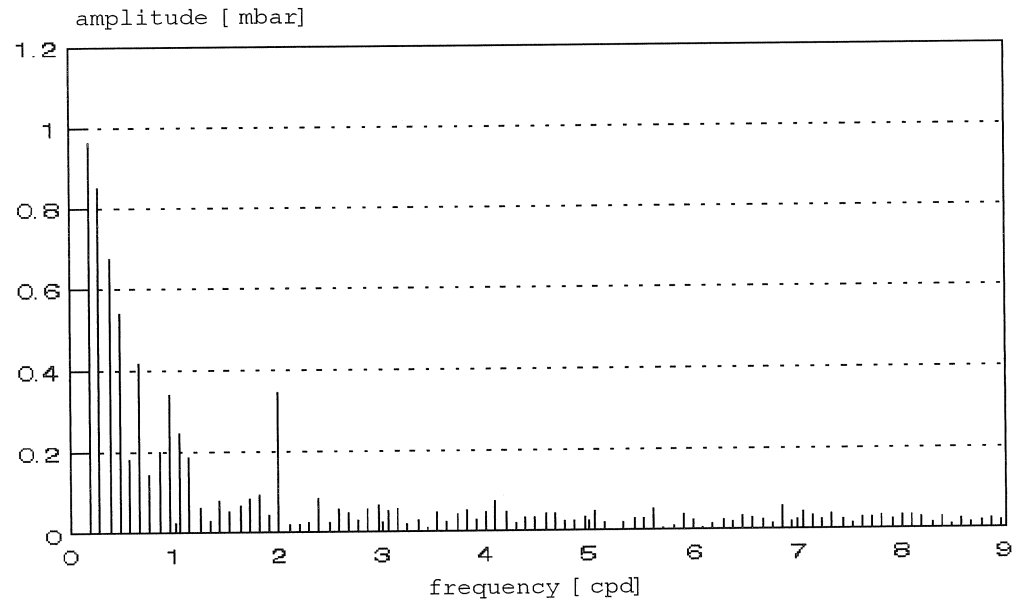

Fig. 6. Amplitude spectrum of the data series from 03.06.92. till 13.06.92.

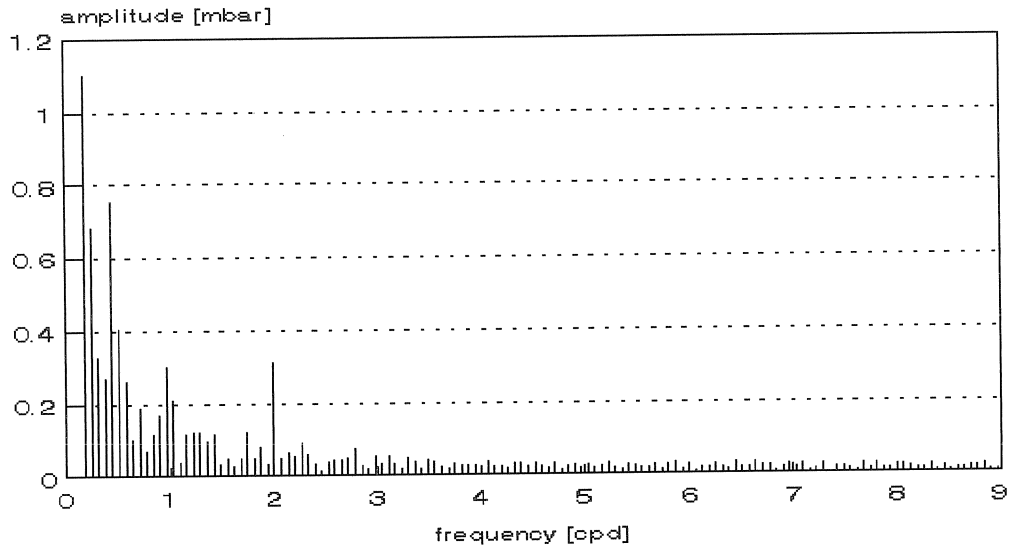

Fig. 7. Amplitude spectrum of the data series from 15.06.92. till 30.06.92.

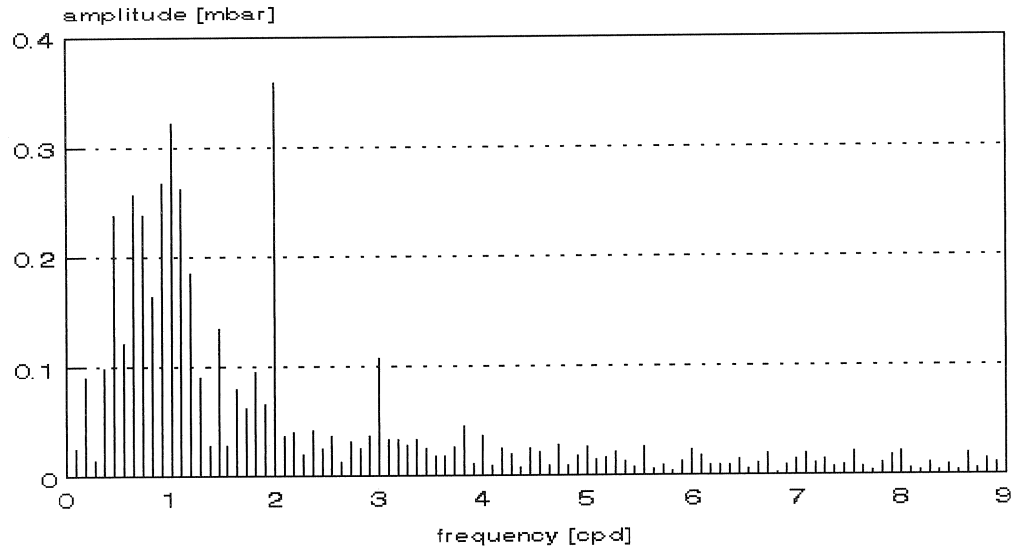

Fig. 8. Amplitude spectrum of the filtered data series from 20.05.92. till 01.06.92.

The difference between the spectra of the filtered and unfiltered data shows how strongly depends the barometric record on the weather, especially on the daily temperature variations. Regarding the construction of the microbarograph it means that the instrument must have a high resolution and a high dynamic range simultaneously because the weather effect is much greater than the tidal one.

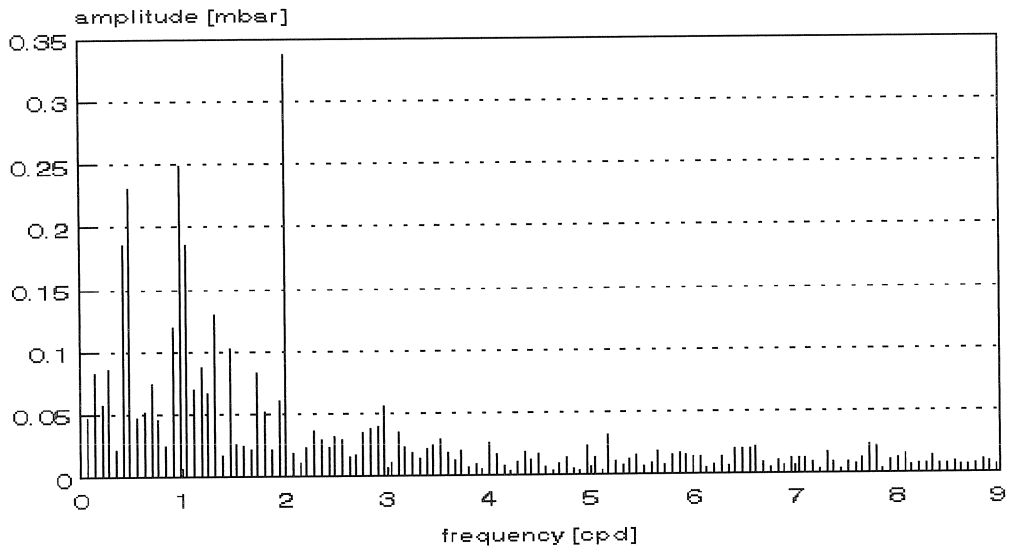

Fig. 9. Amplitude spectrum of the filtered data series from 03.06.92. till 13.06.92.

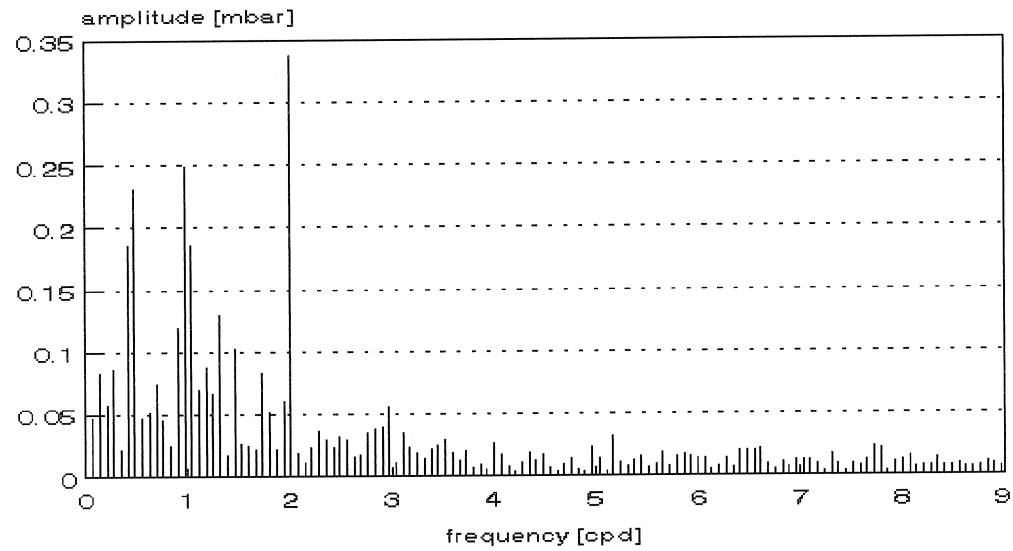

Fig. 10. Amplitude spectrum of the filtered data series from 15.06.92. till 30.06.92.

Table 1. summarizes the amplitudes of the detected S-type main atmospheric tidal waves. In spite of the analyzed short data series the obtained amplitudes of the diurnal (S_1), semidiurnal (S_2) and terdiurnal (S_3) waves approximate rather well the values published by others (Chapman and Lindzen, 1970). The published annual mean amplitude of S_1 is 0.23 - 0.24 mbar and the one of S_2 is 0.41 -0.42 mbar at the latitude of 45°. The air tide has also a seasonal variation. Therefore the mean values of the different type of waves are given in special groupings. For example in the group J-season S_1 is 0.33 -0.34 mbar and S_2 is 0.4 mbar.

Table 1.

Waves	Amplitudes [mbar]			Mean [mbar]	RMS error [mbar]
	Data series 1.	Data series 2.	Data series 3.		
S_1	0.322	0.229	0.249	0.266	0.043
S_2	0.358	0.309	0.337	0.335	0.025
S_3	0.106	0.07	0.057	0.078	0.025

References

Chapman S, Lindzen R S 1970: Atmospheric tides. D. Reidel Publlishing Co.

Mentes Gy 1994:Acta Geod. Geoph. Mont. Hung., 29, 161-177.

Warburton R J, Goodkind J M 1977: J. Geoph. Res., 48, 281-292.

Methods of air pressure reduction tested on Potsdam station

C.Kroner[1], G.Jentzsch[2]

[1] Institut für Geophysik, TU Clausthal,
Arnold–Sommerfeld–Str. 1, D–38678 Clausthal–Zellerfeld, Germany
e–mail: corinna@geowap0.ifg.tu–clausthal.de

[2] Institut für Geowissenschaften, Friedrich–Schiller–Universität Jena,
Burgweg 11, D–07749 Jena, Germany

Abstract

In this paper different methods are used to calculate air pressure reductions for gravity data of the station Potsdam. Both, regression methods as well as attraction/loading models are under consideration. The results are compared in order to give an estimation of the quality of the corrections. As means of comparison the standard deviations of the tidal analysis are taken. We find that the air pressure reduction using atmospheric Green's functions combined with a local regression coefficient yields the best result for Potsdam, but it is not the big improvement hoped for.

1 Data basis

The results of the present work are based upon data from the superconducting gravimeter at Potsdam. This station is taken because it should be sufficiently far from the oceans that air pressure effects are the dominating disturbance, and not effects due to ocean loading. Besides, the possibility exists to get additional hourly recorded air pressure data from several stations around Potsdam.
The data basis consists of hourly gravity and local air pressure data as well as of data (Tab. 1) from the European Centre for Middle Range Weather Forecasts (ECMWF). The results given here are for a time span of one year (92.07.01–93.06.30), but we get analogous results for other and longer time spans.

Table 1: Data from the ECMWF

area	gridding	values per day	time span
Europe	0.5625° x 0.5625°	4	92.07.01–95.06.30
global	2.5° x 2.5°	2	89.01.01–94.12.31

2 Calculation of air pressure reductions

At present there are several suggestions as to correct air pressure effects in tidal records. But up to now no evidence can be given which procedure is the most effective one.
We apply different methods of air pressure reduction commonly used (cp. for Potsdam Dittfeld, 1995; Neumeyer, 1995) to calculate corrections and compare the results. The following methods of air pressure reduction are subject of our investigations:

- reduction with a local regression coefficient;
- reduction with a local and 3 regional regression coefficients;
- correction with an admittance function and
- correction with atmospheric Green's functions (Merriam, 1992) for a regional and a global area combined with a local regression coefficient.

In addition, the correction using the last method is recalculated, but the global contribution is neglected this time. Thus, it is possible to see the influence of global air pressure variations on the gravity data. The proceeding of these calculations is given in Fig. 1. The regional area ranges from $0.4°$ up to $9.0°$ distance from the station. In the area between $0.4°$ and $1.0°$ an air pressure grid of $0.1°$ x $0.1°$ is used in order to take the variations of the Green's functions with the distance better into account. For the zone between $1.0°$ and $9.0°$ data in a $1.0°$ x $1.0°$ grid are used. The outer rectangle in Fig. 1 indicates the global zone that covers all cells with a distance larger than $9.0°$ from the station. For the calculation of the global correction we use air pressure data in a $2.5°$ x $2.5°$ grid. For the computations the assumption is made that the oceans react on air pressure variations like an inverted barometer.

After subtracting the regional and global air pressure correction the regression coefficient between gravity and local air pressure is determined for the area marked by the white square in Fig. 1. This coefficient is necessary because close to the station the air pressure influence is fairly large, the values of the Green's functions vary fast with the distance, and the air pressure data do not have the resolution required for this zone.

3 Comparison of the different air pressure corrections

The quality of the air pressure reductions is estimated by the standard deviations obtained from tidal analyses. The analyses are carried out using ETERNA 3.20 (Wenzel, 1994). A drift elimination is done and the errors are estimated by the Fourier amplitude spectrum of the residuals. The results for the different methods

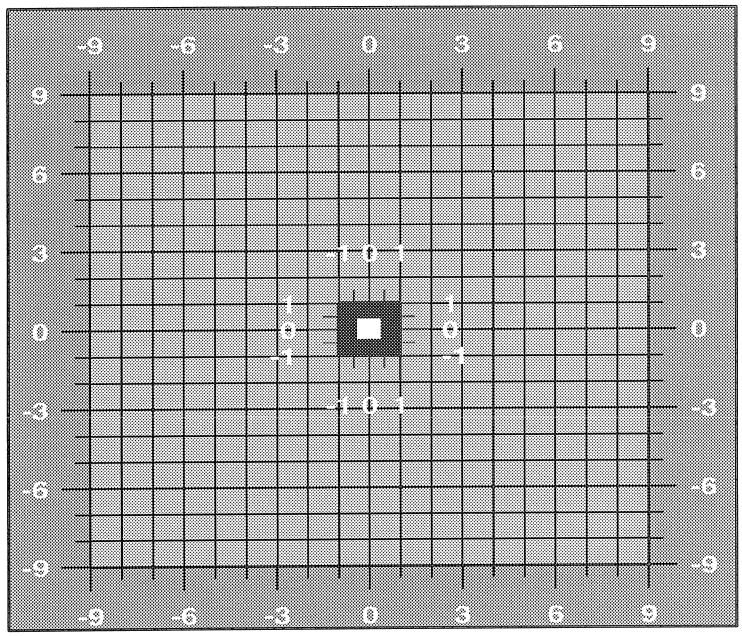

Figure 1: Diagram for the calculation of the air pressure correction using atmospheric Green's functions

applied are examplarily summarized in Tab. 2. The standard deviations obtained are refered to the results yielding after the correction with a local regression coefficient as this method is the mostly used one. The sign indicates whether the respective standard deviation is smaller $(-)$ or larger $(+)$ than the reference standard deviation. From Tab. 2 it becomes obvious that the correction calculated with atmospheric Green's functions and a local regression coefficient yields the best result compared to the other reductions applied. Even the global air pressure variations produce a small but visible contribution, if it is not considered the errors become slightly larger.

The air pressure reduction obtained from the calculations with atmospheric Green's functions combined with a local regression coefficient is given in Fig. 2. At the top the detided gravity data are given (amplitude factor $\delta = 1.16$), below the air pressure reduction and at the bottom the air pressure corrected gravity residuals are shown. As expected a great deal of the signal contents in the gravity is due to air pressure effects. The resulting residuals have a peak–to–peak amplitude of 32 nm/s^2. They

Table 2: Difference of the standard deviations of the amplitude factors obtained for Potsdam (92.07.01–93.06.30) after application of different air pressure reductions from the result obtained after the correction with a local reg. coeff.

method	MF [%]	S1 [%]	S2 [%]	M3 [%]	m_0 [%]
correction with 3 reg. coeff.	+2.4	+1.2	−4.0	−0.8	−0.0
correction with an admittance function	+7.7	−8.2	0.0	−1.1	−1.2
correction with Green's functions + local reg. coeff.	−4.5	−11.8	−4.0	−2.8	−7.8
correction with Green's functions without global contr. + local reg. coeff.	−2.8	−11.2	−4.0	−2.0	−7.8

still seem to contain a component with a period of a quarter of a year.

The scale of magnitude of the regional and global air pressure contribution can be estimated from Fig. 3. For the regional contribution a peak–to–peak amplitude of 16 nm/s^2 is found, whereas the global contribution has a peak–to–peak amplitude of 2.5 nm/s^2. This means, the global part not even amounts to $\frac{1}{6}$ of the regional effect, and the two effects together are just $\frac{1}{10}$ of the total air pressure effect. The apparent anti–correlation between the regional contribution and the total air pressure reduction is misleading: the scale of magnitude is different and a closer comparison yields a phase lag between the curves.

To show the differences between the standard air pressure reduction applying a local regression coefficient and the more laborous method with atmospheric Green's functions and a regression coefficient, the correction using the latter method is subtracted from the standard correction (Fig. 4). The function thus obtained shows a peak–to–peak amplitude of 9 nm/s^2. This is a rather small amplitude but sufficient to affect the tidal analysis. The Fourier amplitude spectrum indicates at which frequencies differences occur: at the frequencies of solar waves and in the low–frequency range, hence at those frequencies where better corrections are necessary.
From the Fourier amplitude spectrum of the gravity residuals (Fig. 5) it becomes clear that the data still contain signals, although they partly have amplitudes below 0.2 nm/s^2. Also a quarterly component, already indicated in Fig. 2, with an amplitude of 0.5 nm/s^2 can be detected. A comparison with the spectrum of the local air pressure proves that a part of the remaining gravity signals is not related to air pressure induced effects.

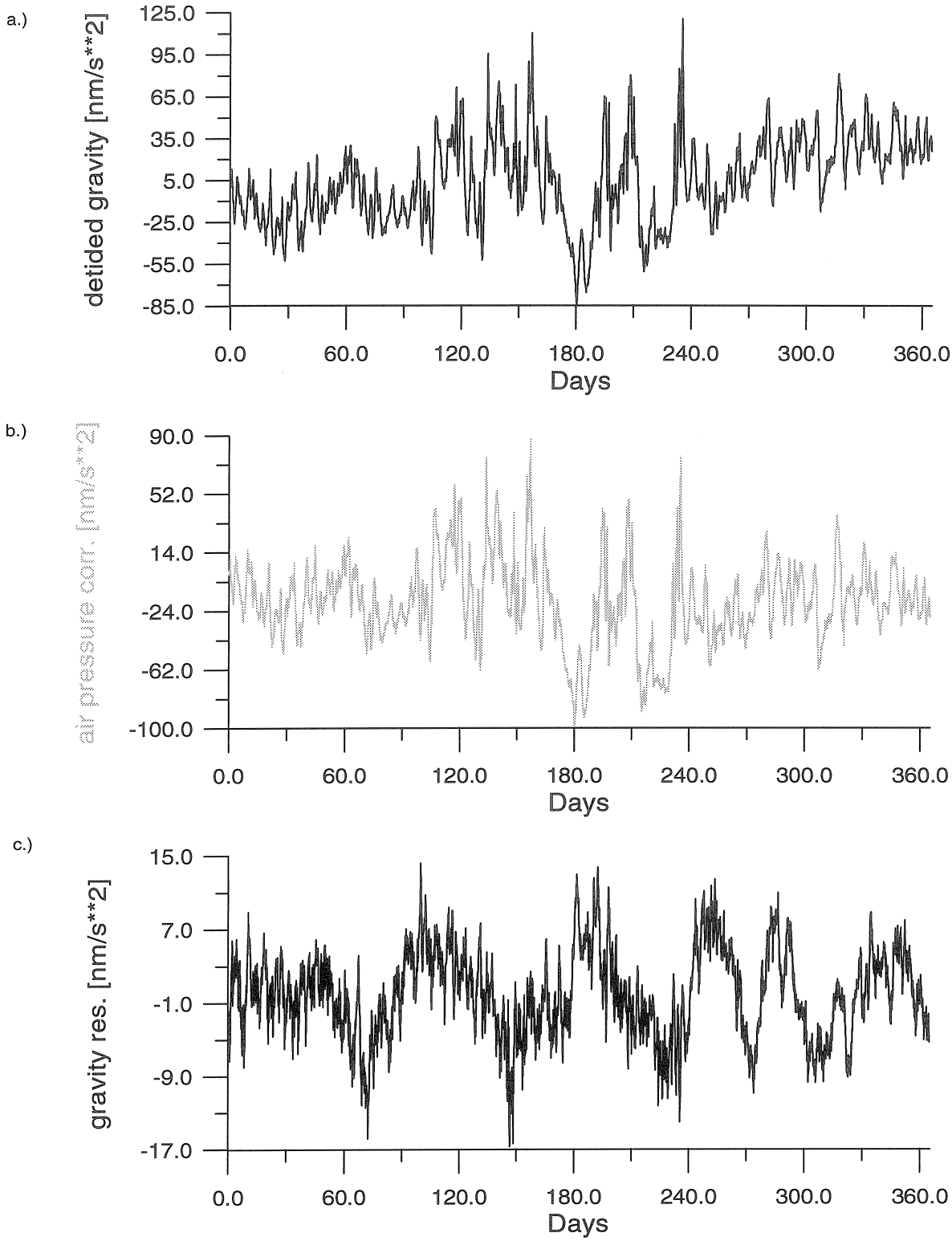

Figure 2: Potsdam, 92.07.01–93.06.30: a.) detided gravity data (δ–factor $= 1.16$), b.) air pressure reduction calculated with atmospheric Green's functions and a local reg. coeff. of -3.08 nm/s^2/hPa, and c.) gravity residuals after air pressure reduction

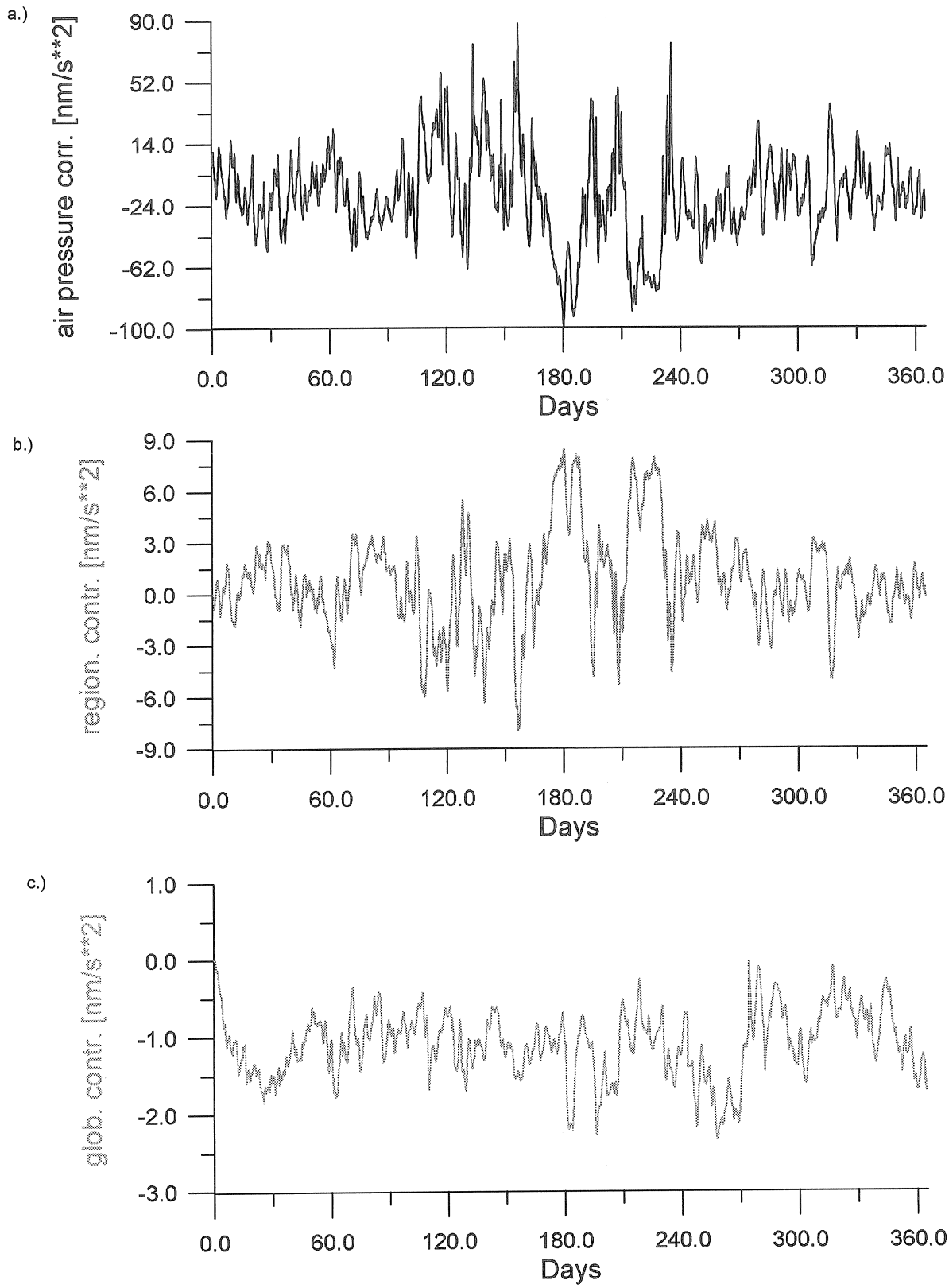

Figure 3: Potsdam, 92.07.01–93.06.30: air pressure correction calculated with atm. Green's functions and a local reg. coeff. of -3.08 nm/s^2/hPa; a.) total air pressure reduction, b.) regional contribution to the air pressure reduction, and c.) global contribution to the air pressure reduction

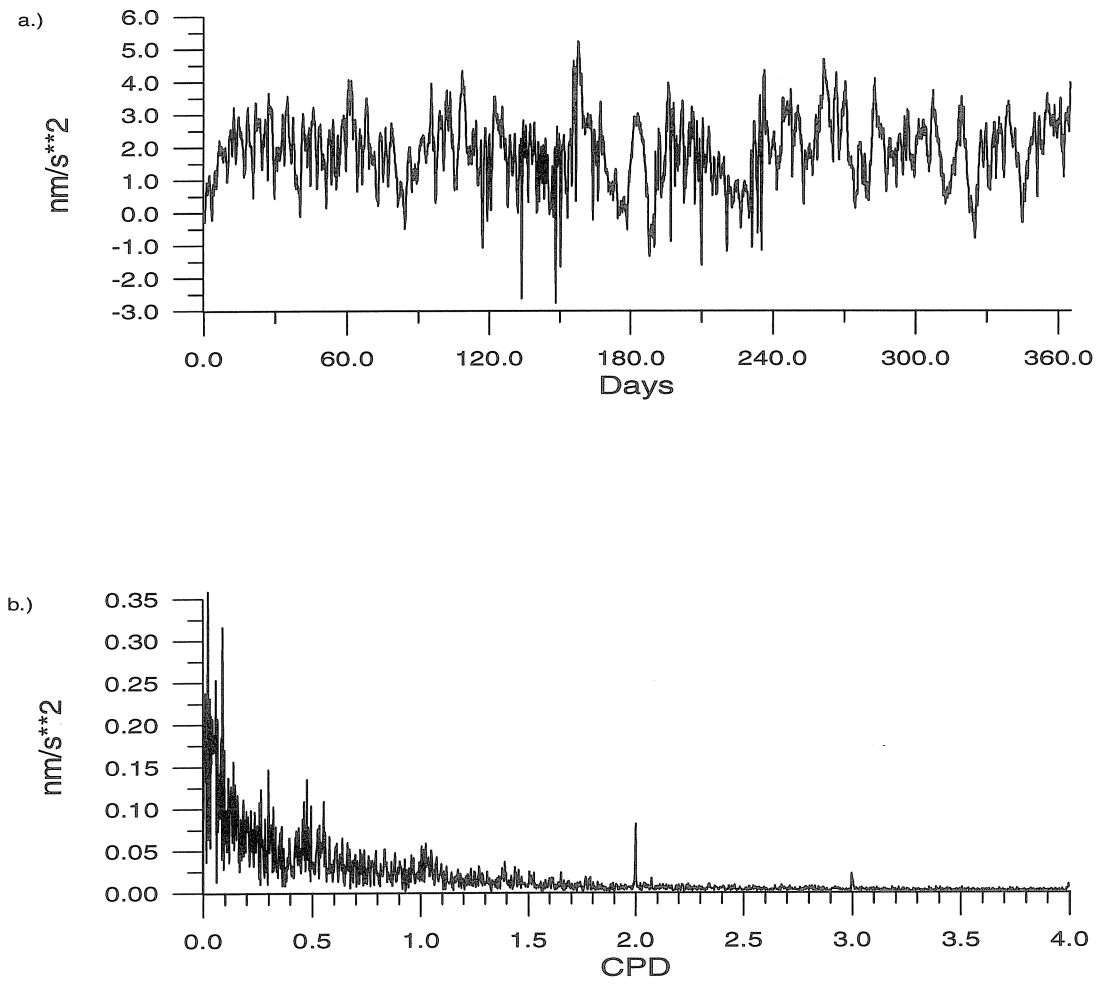

Figure 4: Potsdam, 92.07.01–93.06.30: a.) difference [reduction with a local reg. coeff. of -2.82 nm/s^2/hPa] $-$ [reduction with atm. Green's functions and a local reg. coeff. of-3.08 nm/s^2/hPa], b.) associated Fourier amplitude spectrum

4 Conclusions

From the calculations presented in this paper it emerges that for Potsdam the air pressure correction using atmospheric Green's functions combined with a local regression coefficient leads to an improved air pressure reduction compared to other methods applied. The influence of regional and global air pressure variations is visible in the analysis but nonetheless this extensive method does not yield the big improvement hoped for.

Future investigations should deal with the verification whether comparable results can

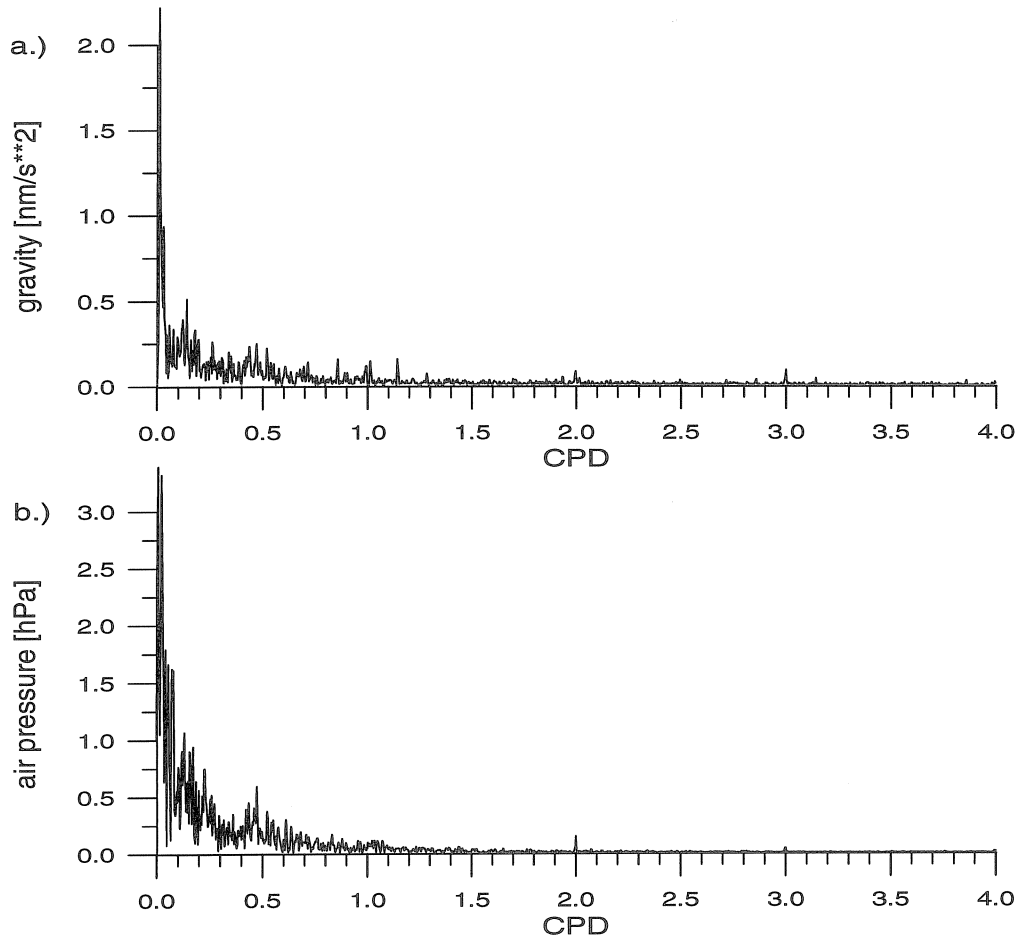

Figure 5: Fourier amplitude spectrum, Potsdam, 92.07.01–93.06.30: a.) gravity residuals after air pressure reduction with atm. Green's functions and a local reg. coeff. of -3.08 nm/s^2/hPa, b.) local air pressure

be obtained for other gravimetric stations, and to which extent the data basis has an influence on the calculated correction. In addition, it ought to be checked whether mean regional and global air pressure reductions are sufficient for the correction of the regional and global air pressure contributions.

Acknowledgements

We kindly thank Dr. J. Neumeyer and H.–J. Dittfeld for making the gravity and air pressure data from Potsdam available to us. We are also obliged to the German Research Society (Deutsche Forschungsgemeinschaft) for the financial support of this study.

References

Dittfeld, H.–J., 1995: *Nontidal features in the SG–record at Potsdam.*– Proc. Sec. Workshop on 'Nontidal gravity changes, Intercomparison between absolute and superconducting gravimeters', Sept. 6th to 8th, 1994, 79–88

Merriam, J. B., 1992: *Atmospheric pressure and gravity.*– Geophys. J. Int., **109**, 488–500

Neumeyer, J., 1995: *Frequency dependent atmospheric pressure correction on gravity variations by means of cross spectral analysis.*– Bulletin d'Informations des Marées Terrestres, **122**, 9212–9220

Wenzel,H.–G., 1994: *Earth tide data processing package ETERNA 3.20.*– Bulletin d'Informations des Marées Terrestres, **120**, 9019–9022

Tidal gravity measurements within the MOTIVE[1] project

by

H.-J. Dittfeld[2], B. Engen[3], G. Jentzsch[4], F. Madsen[5], P.Knudsen[5], M. Ramatschi[6], K. Røthing[3], and P. Schwintzer[2]

Abstract

Near the coast, ocean tidal loading causes vertical deformations in the order of 1 to 10 cm. To benefit from the accuracy of air-borne and space geodetic methods station corrections have to be applied. Models for local corrections are not available yet; therefore tidal gravity measurements were started at fiducial sites around the Norwegian-Greenland Sea and in Westgreenland in order to provide corrections for the dynamic part of the coordinates of the sites. The measurements started in summer 1993 at Scoresbysund / Eastgreenland for a one year record. The following stations were Narsarsuaq at the southern end of Greenland, and Thule in the Northwest. In parallel the station Tromsø, Northnorway, was used in 1994/95. Now our two gravimeters operate in Godhavn / Westgreenland and Stavanger / Westnorway.

The first results show strong tidal anomalies due to ocean loading. Applying a standard local crust loading computations revealed that the vertical deformation is in the order of centimeters, as expected.

1. Introduction

The basic concept of our investigations was already described by Engen et al. (1995a). There, we discussed the need for corrections in relation to the space born and aircraft based observations of the earth especially concerning the changes of the Greenland ice cap at fiducial sites related to kinematic GPS. With regard to the accuracy of these measurements the time variation of the coordinates of the reference stations must be determined. Since ocean tide models for the shelf areas

---

1: MOTIVE: MOnitoring TIdal Variations for Exploitation of Earth Observation Data

2: GeoForschungsZentrum Potsdam, Telegrafenberg A17, D - 14473 Potsdam

3: Statens Kartverk, N - 3500 Hønefoss

4: Institut für Geowissenschaften, Friedrich - Schiller - Universität Jena, Burgweg 11, D - 07749 Jena

5: Kort- og Matrikelstyrelsen, Geodesiavd., Rentemestervej, DK-2400 København NV

6: Institut für Geophysik, TU Clausthal Arnold - Sommerfeld - Str. 1, D - 38678 Clausthal - Zellerfeld

North of 60° to 65° are not available with the required precision measurements of the gravity tides is necessary.

On the other hand, from these measurements boundary conditions can be derived for the validation and improvement of ocean tide models.

First results were discussed by Jentzsch et al. (1994; 1995), and Engen et al. (1995b). In the present paper a short progress report is given. For more information we refer to our earlier papers cited above.

2. Stations and data

Up to now we use two LaCoste & Romberg gravimeters in parallel: The earthtide meter ET 18 in Greenland (responsible: Jentzsch / Ramatschi), and two G - meters (consecutively: G - 995F, G - 087F, and G - 858F; responsible: Dittfeld / Schwintzer) in Norway. The measurements started in Scoresbysund / Eastgreenland in July 1993. After completion of a one year record the gravimeter was moved to Narsarsuaq (1994 - 1995) in the South. The components of the recording equipment and the installations are discussed by Jentzsch et al. (1994; 1995). In autumn 1994, a parallel record started in Tromsø / Northnorway (Oct. 1994 - April 1995). The following stations were Thule / Northwest Greenland (1995 - 1996) and Stavanger / Westnorway. In September 1996 the gravimeter ET 18 was moved to Godhavn / Westgreenland, whereas the G - meter in Stavanger was exchanged to fit other commitments. Because some instrumental problems caused some gaps now the gravimeter G - 858F is still in Stavanger. Tab. 2.1 gives the coordinates of the stations.

Table 2.1. Coordinates of the stations in Greenland and Norway; elevation in meter.

	Scoresby-sund	Narsarsuaq	Thule	Godhavn	Tromsø	Stavanger
N-latitude	70.4850	61.1607	76.3216	69.2511	69.6625	59.0176
longitude	21.9531 W	45.4222 W	68.4272 W	53.5253 W	18.9394 E	5.5984 E
elevation	65	22	61	25	103	55

The station Tromsø is situated on the island named Tromsø near the city. The gravimeter was installed in a temperature stabilized hut on the grounds of the 'Tromsø Satellite Station' (TTS) close to the PRARE - station and the GPS antenna. The equipment consists of an aluminum box that contains the gravimeter and a stabilized heating system. Through holes in the box the gravimeter stood directly on the bed rock.

About 10 km north from Stavanger the second Norwegian station is installed in a concrete bunker on the peninsula Randaberg. This place contains a PRARE station, too. Here, the room is heated, and the gravimeter sits on bed rock covered by the stabilized aluminum box.

In order to control the calibration of our ET 18 prior and after the transports between the stations we carried out parallel records with our G - 979F. These records were performed before removing the station and directly after installation at the new place. It could be shown that the calibration can be checked on the 0.3 % level by parallel recording over three to five days at each station (Jentzsch et al., 1995; Engen et al., 1995b).

The data obtained up to now are quite good as far as the noise levels are concerned. Tab. 2.2 gives the observed noise levels for the main tidal bands (Godhavn: first 67 days only). The residual tidal vectors are given in Tab. 2.3: They show the strong ocean loading effect. The results for Scoresbysund and for Narsarsuaq are based on the total record; therefore the values are slightly different to the earlier published figures.

Table 2.2. Noise levels at the different stations for the two main tidal bands: Values are given in µGal (corresponding to 10 nm/s²).

tidal band	Scoresby-sund	Narsarsuaq	Thule	Godhavn	Tromsø	Stavanger
diurnal	**0.0292**	**0.0536**	**0.0686**	**0.0414**	**0.0850**	**0.0239**
semi-diurnal	**0.0125**	**0.0271**	**0.0381**	**0.0112**	**0.0316**	**0.0098**

3. Determination of vertical deformation

The vertical deformation cannot be computed simply from the tidal residuals. The loading vector contains both the deformation and the Newtonian attraction due to the load. The separation requires model computations on the basis of a local ocean tide model and a local crust / mantle model. These computations were carried out applying the algorithm of Farrell (1972; comp. Jentzsch, 1995).

Since all the stations are very close to the coast special care has to be taken regarding the digitization of the coastlines in the vicinity. Usually we use a 1' x 1' - grid in the near distance, which is widened to 10' x 10', and farther away the grid of the available ocean tidal chart is adapted. In order to reduce the work some algorithms were programmed to read out the ocean cells and to interpolate the data. These programs were tested for O1, M2, and partly for S2 at the stations Scoresbysund and Narsarsuaq. Up to now we only used the maps of Schwiderski (1979a/b) and Flather (1976) to test the software. For the area close to the station available tide gauge results were used to construct the local tidal chart.

It was already shown by Jentzsch et al. (1995) that it is not possible to explain the observed residuals simply by applying global tidal charts. Tab. 3.1 gives the model values for Scoresbysund, and Tab. 3.2 contains the comparison of different models for Narsarsuaq. Here, the effect of amplitude and phase variations of the local cells was tested to prove the sensitivity of the modelizations.

Table 2.3. Tidal residual vectors obtained from the analyses: Only values for O1 and M2 are given in µGal (corresponding to 10 nm/s²). The values for Thule, Godhavn and Stavanger are still preliminary.

	O1		M2	
	amplitude [µGal]	phase [°]	amplitude [µGal]	phase [°]
Scoresbysund	1.130 ± 0.022	144.42 ± 5.69	2.234 ± 0.012	-146.85 ± 0.30
Narsarsuaq	0.696 ± 0.042	99.03 ± 3.44	4.477 ± 0.026	12.02 ± 0.33
Thule	0.361 ± 0.062	7.17 ± 9.82	2.912 ± 0.036	-149.48 ± 0.70
Godhavn	0.755 ± 0.041	48.47 ± 3.14	3.864 ± 0.011	- 48.49 ± 0.17
Tromsø	0.574 ± 0.097	138.24 ± 8.49	4.449 ± 0.026	125.35 ± 0.41
Stavanger	0.490 ± 0.027	112.42 ± 3.18	0.194 ± 0.011	-175.66 ± 3.37

Table 3.1. Scoresbysund: Computed load vectors for the models of Schwiderski (global, 1° x 1°) - **SCH** - and a combined model Schwiderski (global) and Flather (Northatlantic ocean) - **SCH/FL** -; Newtonian attraction and elastic deformation are given separately.

constituent	Newtonian		elastic		total	
	[µGal]	[°]	[µGal]	[°]	[µGal]	[°]
O1 - SCH	0.111	-169.8	0.494	140.1	0.571	149.1
O1 - SCH/FL	0.042	- 58.1	0.183	121.0	0.141	120.7
M2 - SCH	0.083	- 4.4	0.187	- 42.6	0.257	- 31.2
M2 - SCH/FL	0.559	- 81.6	0.826	-105.8	1.355	- 96.1

In the case of O1 the comparison of observed and modeled load vector reveals for Scoresbysund a fairly good fit in the phase but a misfit of 50 % in amplitude, if Schwiderski's chart is used. If this chart is replaced by Flather's model for the Northatlantic ocean the misfit of the amplitude is increased to about 90 %, and the phase difference is also bigger. This is astonishing because Flather's model even covers the fjord area of the Scoresbysund.

For M2 the results are opposite: Schiderski's global model only explains about 10 % of the amplitude with a phase difference of more than 100 °, whereas Flather's model explains about 60 % of the amplitude with a reduced phase difference.

The different loading amplitudes for M2 and O1 are due to the fact that in the Northatlantic ocean the amplitude of O1 is smaller compared to M2: The effects of distant oceans surmount local loading. Therefore, we find a better fit of Schwiderski's global O1 model compared to the combination with Flather's, although Flather's grid covers a great part of the Scoresbysund fjord area. Since it does not fit well in that area, the whole result is deteriorated.

In case of constituent M2 it is just vice versa: Since the amplitudes in the Northatlantic ocean are bigger the regional / local contributions are bigger as well. Therefore, the computed load vector (SCH) does not fit as good as the vector of the combined model (SCH/FL). But still the result is not at all satisfying. This points to the necessity to model the local shelf areas separately.

The sensitivity of the modelization is demonstrated for Narsarsuaq: Again, the M2 amplitude is much bigger than the one of O1; the ratios are about 6.4 (observed) and ≈ 8 (computed - SCH). The amplification of the amplitudes of the neighboring cells by 10 % increases the Newtonian contribution at about the same ratio; the phase shift of 10 ° affects the Newtonian part as well, whereas in both cases the elastic contribution is much less affected. The reason for the small effect on the elastic deformation may be found in the fairly thin crust we used. Therefore, the elastic response includes a wider area where the global values were not changed.

Table 3.2. Narsarsuaq: Computed load vectors for the global model of Schwiderski (global, 1° x 1°) - **SCH** - and modified models with amplitudes and phases of local cells changed by plus 10 % and plus 10°, respectively, as well as local cells replaced by values derived from tide gauge data - **SCH/TG** - ; Newtonian attraction and elastic deformation are given separately.

constituent	Newtonian		elastic		total	
	[µGal]	[°]	[µGal]	[°]	[µGal]	[°]
O1 - SCH	**0.560**	**100.3**	**0.480**	**111.3**	**1.035**	**105.4**
+ 10 %	**0.609**	**100.8**	**0.489**	**111.3**	**1.093**	**105.5**
+ 10 °	**0.550**	**109.1**	**0.479**	**113.3**	**1.028**	**111.0**
SCH/TG	**0.599**	**142.5**	**0.474**	**118.0**	**1.049**	**131.7**
M2 - SCH	**5.284**	**1.3**	**2.966**	**8.4**	**8.235**	**3.8**
+ 10 %	**5.742**	**1.4**	**3.055**	**8.6**	**8.781**	**3.9**
+ 10 °	**5.254**	**10.0**	**2.947**	**11.5**	**8.201**	**10.6**
SCH/TG	**4.305**	**97.6**	**4.425**	**25.7**	**5.559**	**73.1**

For the Norwegian stations table 3.3 gives the computed load vectors for different ocean tidal charts. It is obvious that the computed values have little relation to the observed values. In the case of Tromsø the observed loading amplitude of M2 is up to 20 times bigger than the computed amplitude, and the phases are all too small. Similar results are found for O1 at both stations and for M2 at Stavanger; since the amplitudes are considerably smaller the net effect is smaller as well. The scatter of the computed phases is remarkable.

Table 3.3. Computed loading effects for Tromsø and Stavanger using different ocean tidal models (computed by O. Francis, ICET).

	O1		M2	
	amplitude [µGal]	phase [°]	amplitude [µGal]	phase [°]
Tromsø - *obs*	0.574 ± 0.097	138.24 ± 8.49	4.449 ± 0.026	125.35 ± 0.41
Schwiderski	0.525	162.0	0.225	100.0
CSR3.0	0.997	173.2	0.377	101.2
FRS952	0.831	169.1	0.305	94.3
ORI	0.514	165.5	0.208	116.7
ORI96	0.671	171.1	0.319	101.8
Stavanger - *obs*	0.490 ± 0.027	112.42 ± 3.18	0.194 ± 0.011	- 175.66 ± 3.37
Schwiderski	0.052	4.2	0.041	- 122.1
CSR3.0	0.086	173.2	0.043	149.6
FRS952	0.065	165.8	0.042	123.3
ORI	0.076	52.8	0.110	- 179.5
ORI96	0.061	- 9.3	0.034	- 158.1

The pure vertical deformation is derived from the elastic part of the loading signal. This corresponds to the free air gradient in gravity: This means that 3 µGal are equivalent to 1 cm vertical deformation. Since we have a harmonic signal the total effect is twice that value.

To compute the total signal it is necessary to sum up all load vectors of the different tidal constituents. Because we only have tidal charts for the main tidal constituents (three to four in the two main tidal bands) we have to use the amplitude ratios of the body tides to include the minor tidal waves assuming that the resonance pattern is the same. As a rough estimation of the maximum vertical deformation we can take the value of M2 as about 40 % of the semidiurnal effect and an effect of the diurnal tides in the order of less than half of M2: This leads to a maximum peak-to-peak deformation for our stations in the order of 5 cm.

5. Discussion

All the existing and planned fiducial sites on Greenland and Northern Europe for monitoring global change are close to the ocean. Therefore, deformations of the crust by ocean tidal loading provide a strong time dependent part of the station coordinates. This disturbing signal cannot be corrected applying existing models because these models are global rather than local ones.

Therefore it is not astonishing that the parameters of the main tidal waves obtained vary considerably from the theoretical value of about 1.16. This leads to tidal residuals that can be allocated to the influence of ocean tidal loading. The observed residual vectors summed up show amplitudes in the order of up to 10 µGal. The comparison to the computed values reveals that due to the strong phase differences the usually applied correction on the basis of the available maps would be wrong by more than 10 µGal. Since close to the station the elastic part of the loading effect covers up to 90% of the total load of the local seas the resulting systematic error for the elevation is at least between 1 and 5 centimeters. Thus, the errors in the loading model would cause differences that are in the order of the accuracy of the kinematic GPS as anticipated by several authors.

The application of current ocean tidal models requires the careful digitization of the coastal lines near the stations. Than the given amplitudes and phases have to be fitted to the grid by interpolation. Therefore, this process cannot be done in an automatic way: It has to be repeated for every new station.

For more details, especially the map showing the station distribution and examples of records we refer to our earlier papers.

6. Acknowledgments

Niels Andersen of KMS was responsible for the reconnaissance of the station in Scoresbysund and all the necessary preparations that provided a good start of the measurements. The measurements fully depended on the careful maintenance of the gravimeter and the recording system by the local staff Ib Lorentzen and Tore Andreassen in Scoresbysund and Ulrik Poulsen in Narsarsuaq, Majbritt Didriksen and Uffe Baerentsen at Thule, Leif Skytte and Mogens Fredegaard at Godhavn. In Norway, H. Pflug helped to install the gravimeters; maintenance was provided by Björnar Hansen in Tromsø and Trigve Veggeland in Stavanger.

We thank the DGFI, München, and the Institute for Geodesy and Photogrammetry, TU Berlin, for providing gravimeters. The development of the recording system was carried out in cooperation with M. Liebing, who also took part in the installation work at Scoresbysund. Christina Friedrich and C. Düsing digitized the maps and started the loading computations. Olivier Francis, ICET, Brussels, provided the loading data compiled in Tab. 3.3.

All this is gratefully acknowledged.

7. References

Engen, B., G. Jentzsch, F. Madsen, and P. Schwintzer, 1995a. NATURE: North Atlantic Tides Under Research - Tidal gravity measurements around the Norwegian Greenland Sea -. Proc. 12th Int. Symp. Earth Tides, Beijing, August 1993, Science Press, Beijing, 451-461.

Engen, B., K. Røthing, G. Jentzsch, M. Ramatschi, F. Madsen, P. Knudsen, P. Schwintzer, and H.J. Dittfeld, 1995b. The NATURE-Project: Tidal gravity measurements around the Nowegian-Greenland Sea (abstract). Anales Geophysicae, Suppl. I, p. C159.

Farrell, W.E., 1972. Deformation of the earth by surface loads. Rev. Geophys. Space Phys., 10, 761-797.

Flather, R.A., 1976. A tidal model of the north-west European continental shelf. Mem. Soc. roy. des Sci. Liege, 6th series, 10, 141-164.

Jentzsch, G., M. Ramatschi, and F. Madsen, 1994. Tidal gravity measurements on Greenland: First results from the station Scoresbysund. Proc. 12th Meeting of the Nordic Geodetic Comm., Ullensvang, June 1994, 164 - 173.

Jentzsch, G., M. Ramatschi, and F. Madsen, 1995. Tidal gravity measurements on Greenland. Bulletin d'Information Marees Terrestres, 122, 9239-9248.

Jentzsch, G., 1995. Auflastgezeiten. In: Wilhelm, H. und W. Zürn (Eds.), DGG - Seminar 'Gezeiten', Oberwolfach, 17.-21.10.1994. Deutsche Geophysikalische Gesellschaft, Sonderband II, 1995, 227 S.

Schwiderski, E.W., 1979a. Ocean tides, part I: Global tidal equations. Marine Geodesy, 3, 161.

Schwiderski, E.W., 1979b. Ocean tides, part II: A hydrographical interpolation model. Marine Geodesy, 3, 219.

ADMITT - a Program for Determination of the Atmospheric Pressure Admittance

Jürgen Neumeyer and Hartmut Pflug

GeoForschungsZentrum Potsdam (GFZ), Div.1 "Kinematics and Dynamics of the Earth"
Telegrafenberg A17, D-14473 Potsdam, Germany, E-mail neum@gfz-potsdam.de

Summary

A short introduction of the atmospheric pressure effect on gravity data is given. By means of the cross spectral analysis the frequency dependent atmospheric pressure admittance is calculated. This is an improvement of the atmospheric pressure correction on gravity data compared with the widely used single admittance computed in the time domain by the regression analysis. The ADMITT program is using the standard PRETERNA format with gravity and atmospheric pressure data as input file. The output of the program delivers the amplitude and phase spectrum as graphical display. Additionally the admittance function is written in an output file. This can be used for gravity data correction.

1. Introduction

Atmospheric pressure variations are one of the important perturbation sources in high accuracy gravity observations. Variations of 50 hPa cause gravity changes of 150 nm/s^2, if we assume a single atmospheric pressure admittance of - 3 nm/s^2 per hPa. The atmosphere causes three effects: (1) the gravitational effect (direct attraction of the atmospheric mass), (2) the deformation effect (change in gravity due to vertical displacement of the gravimeter on the deformed Earth) and (3) the change in gravity due to the redistribution of the masses inside the deformed Earth (*Torge 1989 and Sun 1995*). The deformation effect of the order of 1 nm/s^2 per hPa acts in opposite direction to the dominant gravitational effect which is of the order of - 4 nm/s^2 per hPa. Besides the gravity variations, the gravimeter is measuring the sum of these effects due to the atmospheric attraction, surface displacement of the Earth at the gravimeter site, and the mass redistribution inside the Earth. About 90 % of the total effect is caused by atmospheric pressure changes in the local zone within a radius of about 50 km around the station. The remaining 10% are caused by the regional zone (with a radius of about 1000 km around the station) and the global zone (> 1000 km) (*Merriam 1992 and Shi et al. 1993*). The surface displacement is of the order of 20 to 30 mm for regional atmospheric pressure changes of 50 hPa (*Sun 1995*). The period of the atmospheric pressure effect ranges from hours to years. Depending on the location, extension, temporal evolution and magnitude distribution of the atmospheric pressure in the three zones, the admittance is a function of frequency and time.

For precise studies of gravity variations (Earth tides, polar motion, Nearly Diurnal Free Wobble, translational oscillation of the solid core and other effects) the gravity signal must be corrected for the atmospheric pressure effect. The widely used pressure correction is a single admittance computed in the time domain by regression analysis. The regression analysis determines one coefficient for the selected frequency band only. Because of the frequency dependency of the atmospheric pressure effect on gravity, it is necessary to evaluate one coefficient for each frequency. The effective atmospheric pressure admittance is the frequency transfer function between gravity and atmospheric pressure measured at a single station. The recorded gravity data can be corrected for other effects such as ground water table variation near the gravimeter site, polar motion and drift of the instrument before pressure correction. The

effective atmospheric pressure admittance can be determined by the cross spectral analysis. The cross spectral analysis is a method of deriving the frequency response function for a single input - single output model as well as for a multiple input - single output model. The application of the cross spectral method for determination of the frequency dependent atmospheric pressure admittance was first introduced by *Warburton and Goodkind (1977)* and elaborated by *Crossley et al. (1995)* and *Neumeyer (1995).*

2. Algorithm

For a single input - single output model the transfer function H(f) as a function of the frequency can be calculated after *(Bendat and Piersol 1986)* by

$$\hat{H}(f) = \frac{\hat{G}xy(f)}{\hat{G}xx(f)}$$

with the auto spectral density Gxx and the cross spectral density Gxy of the input series x_n and the output series y_n, sampled at equally spaced time intervals δt and n = 0,1,...N-1. The input series is the atmospheric pressure and the output series is the gravity. For evaluation of Gxx and Gxy the data records x_n and y_n must be divided into nb blocks each consisting of N data values. The block size N should be a power of 2, then one can use the faster Cooley - Tukey procedure of Fast Fourier Transform (FFT) calculation. If needed to suppress side - lobe leakage, the data values in each block can be tapered by applying an appropriate window. The program allows three options: no window, Hanning window, and cosine window operating over 10% at the beginning and 10% at the end of the data blocks.

The averaged one - sided raw auto spectral density estimates from the nb blocks of data can be calculated by the Fast Fourier Transform according to the formula

$$\hat{G}xx_k = \frac{2}{nb \cdot N} \sum_i |FFT(x_{k,i})|^2$$

with i = 0,1,...,nb -1 and k = 0,1,...N/2. The frequency is calculated by

$$f_k = \frac{k}{N \cdot \delta t}$$

The averaged raw cross spectral density estimates from the nb blocks of data can be calculated by the formula

$$\hat{G}xy_k = \frac{2}{nb \cdot N} \sum_i (FFT(x_{k,i}))^* \cdot FFT(y_{k,i})$$

The first term is the complex conjugate of the Fourier Transform of the record x_n and the second term the Fourier transform of the record y_n.

3. Program description

The ADMITT - program is written in C language and the executable file is running under the operating system DOS. The PRETERNA - file format is used as input file *(Wenzel 1994)* for gravity and corresponding atmospheric pressure data (Fig.1). Besides the input file the program needs an in-file

```
date          time          gravity          atm. pressure
C*****************************************************************************
yyyymmdd      hhmmss        g.gggggg         p.pppppp
```

Fig 1 PRETERNA - file format

with all processing parameters. Figure 2 shows the necessary parameters (bold face). Suitable block sizes are in the range of 120 to 480 records sampled at 60 minute intervals over 5 to 20 days. Other sampling rates and block sizes are possible. If the selected block size is not a power of 2, the block size for FFT calculation is automatically enlarged to the next power of 2 by zero values. The size of the input file is limited by the operating memory of the computer. A memory of 528 k allows precessing of 24000 records. During operation the program is displaying the working parameters as shown in Fig. 3. The incomplete blocks are not used for processing. An incomplete block can arise at the end of the data or as a result of data gaps. The atmospheric pressure admittance is graphically displayed as amplitude and phase spectrum (Fig. 4). Additionally an output file is produced (Fig 5) with numerical values of frequency, amplitude and phase. This output file can be used for correction of the gravity data. This may be performed in the frequency domain using FFT techniques or time domain using convolution methods.

```
# Ini-file for program ADMITT
#
# Lines starting with "#" are ignored
# Lines with more than 80 characters are not allowed
#
data_file: C:\"directory"\"file name"  - "comments"
# Processing parameters
start_date_time : 19920701 010300 - "comments"
stop_date_time : 19931126 231500  - "comments"
block_size [records] : 240  - "comments"
sampling_rate [minutes] : 60  - "comments"
# 0 = no window, 1 = Hanning window, 2 = cos - window over 10% of the data blocks
window : 1  - "comments"
```

Fig. 2 Ini-file for program ADMITT

Working Parameters
start_date_time : 19920701 010300
stop_date_time : 19931126 231500
block_size : 240 records
sampling_rate : 60 min
window : 1
number of data records : 12336
number of blocks : 52
incomplete blocks : block 52 with 96 records
data reading: finished
number of processing blocks: 51
block_size for FFT set to 256

Fig.3 Display of working parameters

Atmospheric Pressure Admittance

Frequency [cpd]	*Amplitude [nm/s^2 per hPa]*	*Phase [deg]*
0.0937	*-2.037*	*1.913*
0.1875	*-2.679*	*1.767*
.....	.....	.....
12.0000	*-3.808*	*0.000*

Fig. 5 Output file

4. References

Bendat J. S. Piersol A. G. (1986) Random Data - Analysis and Measurement Procedures, A Wiley-Interscience Publication JOHN WILEY & SONS, New York, Chichester, Brisbane, Toronto, Singapore

Crossley D. J. Jensen O.G. Hinderer J. (1995) Effective barometric admittance and gravity residuals. Phys. Earth Planet. Int., 90, 221-241

Merriam J. B. (1992) Atmospheric pressure and gravity. Geophys. J. Int., 109, 488-500

Neumeyer J. (1995) Frequency dependent atmospheric pressure correction on gravity variations by means of cross spectral analysis. Marees Terrestres Bulletin d´Informationes, Bruxelles, 122, 9212-9220

Shi P. Segava J. Fokuda Y. (1993) Effects of Atmospheric Pressure on the Gravity Changes Measured by a Superconducting Gravimeter. Journal of the Geodetic Society of Japan, No.3, Vol. 39, 293 -311

Torge W. (1989) Gravimetry; de Gruyter, Berlin, New York

Sun H.-P. (1995) Static Deformation and Gravity Changes at the Earth's Surface due to the Atmospheric Pressure. Observatoire Royal des Belgique, Serie Geophysique N° Hors-Serie, Bruxelles

Warburton R. J. Goodkind J. M. (1977) The influence of barometric - pressure variations on gravity. Geophys. J. R. astr. Soc., 48, 281-292

Wenzel H.-G. (1994) PRETERNA - a preprocessor for digitally recorded tidal data. Marees Terrestres Bulletin d´Informationes Bruxelles, 118, 8724-8734

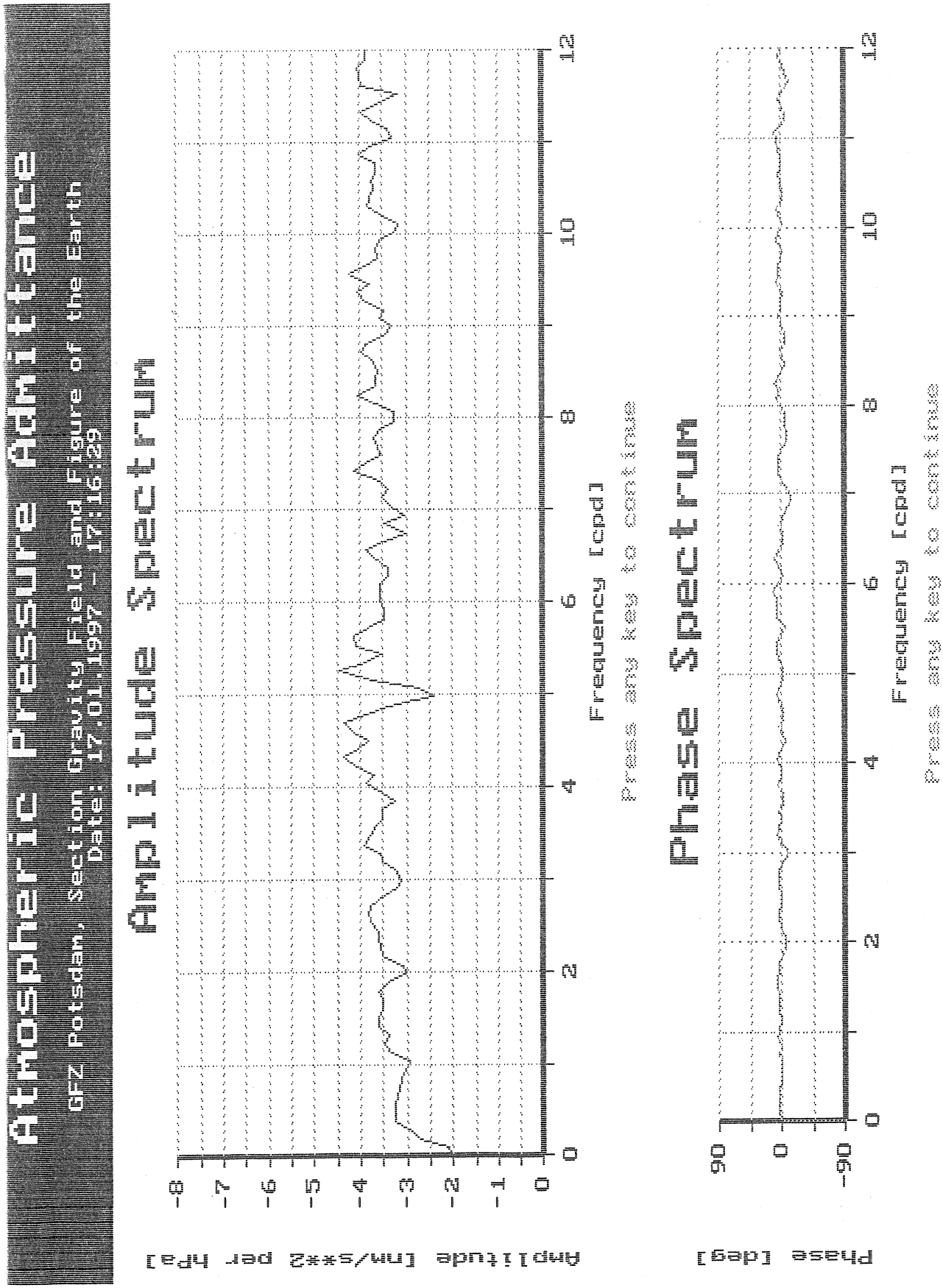

Fig. 4 Graphical display of atmospheric pressure admittance (Amplitude and Phase Spectrum)